VERIFICATION OF A MATHEMATICAL MODEL FOR LAYERED T-BEAMS

M. L. Kuo

M. E. Criswell

J. R. Goodman

J. Bodig

E. G. Thompson

M. D. Vanderbilt

Structural Research Report No. 10
Civil Engineering Department
Colorado State University
Fort Collins, Colorado 80521

March 1974

ABSTRACT

VERIFICATION OF A MATHEMATICAL MODEL FOR LAYERED T-BEAMS

An experimental program and the verification of a mathematical model for layered T-beams, developed assuming small deflection theory and including effects of interlayer slip, are described in this report. This research is a part of an overall program to develop a verified analysis procedure for wood joist floor systems.

After a description of the construction and load-testing of 14 two- and three-layered T-beams, a brief discussion on the mechanical properties of the materials used is given. The deflections observed in the loading tests are then compared with the predicted deflections given by the mathematical model, which used a finite element solution technique. These comparisons for the fourteen T-beams, including two- and three-layered systems, formed the primary basis for the verification of the mathematical model. Test results provided by a manufacturer of joist systems were also compared to the mathematical model. Good agreement between the observed and theoretical values were obtained for all tests. These favorable results show the validity of this general layered beam theory.

Min-Lung Kuo
Civil Engineering Department
Colorado State University
Fort Collins, Colorado 80521
February, 1974

TABLE OF CONTENTS

TABLE OF CONTENTS (Continued)

LIST OF TABLES

LIST OF FIGURES

LIST OF FIGURES (Continued)

CHAPTER 1

INTRODUCTION

1.1 Objective

The high demand of housing is an obvious consequence of increasing population and rising consumer expectations. It is estimated that wood and wood-based products form about 75 percent of the material used in residential housing construction. A small savings in consumption of wood products will reduce the total construction cost of housing by a sizeable amount.

Current methods of design of wood joist floor systems are based on an overly simplified piece-by-piece approach. The contribution of the sheathing flange and connectors to the overall stiffness of the total system is generally ignored. Hence, floors built using the present design usually have excessive strength. This overdesign results in an inefficient and uneconomical use of materials.

Researchers at Colorado State University organized a team under the sponsorship of the National Science Foundation in 1971 to determine the consequences of this limitation in the current design procedure. The overall objective of this study was to develop and verify a mathematical model of wood floor systems considering the floor as a multilayer structural system incorporating interlayer slip, connector properties, sheathing material properties, and discontinuities of the individual sheathing layers. The long range goal is to develop a complete and rational analysis and a unified design procedure for layered beam systems. The objective of the phase of the study reported herein was to construct and test T-beam specimens, consisting of two joists and one or more sheathing layers atop the joists, and to use

the data obtained to verify a developed mathematical model. Results from a mathematical model using a finite element solution technique are compared with the experimentally-observed deflections for T-beam specimens having widely varied properties in order to show the validity of the mathematical model.

The interrelationship between the various tasks of the investigation are shown in the following block diagram:

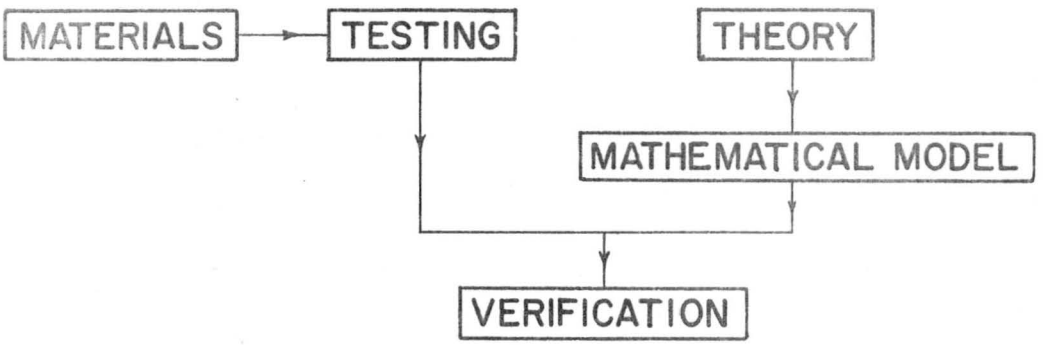

1.2 Scope

A description of the construction, the loading tests, and results from 14 T-beams are included in this report. The materials and member sizes used in the specimens were varied to reasonably represent the many possible joist species, spacings, and sizes; sheathing properties and dimensions; and connector types and spacings. The T-beams constructed and tested included both two- and three-layered systems, i.e., one- and two-layers of sheathing in addition to the joist layer.

A brief literature review is presented in the next section to give a more comprehensive understanding of the development of the layered beam theory. A complete description of the testing equipment, selection of materials, general construction and the testing procedure used in

this study are given in Chapter 2. The material properties, including MOE (modulus of elasticity) values determined by the Wood Science Laboratory and during construction, along with the slip moduli of the nails and glue, are treated in Chapter 3. Chapter 4 contains a comprehensive description of the experimental behavior of the T-beams. The effects of connectors, joints and gaps in the sheathing and the number of sheathing layers are discussed.

A brief description of the mathematical model and the solution methods used, along with a comparison of experimental results and theory are included in Chapter 5. Experimental results from the T-beam tests reported in earlier chapters and from uniformly-loaded T-beam specimens tested by others were used to demonstrate the validity of the general mathematical model for layered T-beams. A summary of the report and the resulting conclusions are given in Chapter 6.

Appendices include data on material properties, specimen configurations, experimental test results, comparison of experimental and theoretical load-deflection curves for all specimens, and information on the computer program used to produce the theoretical results.

1.3 Literature Review

Layered systems of various materials are used extensively in engineering applications. The most common applications are seen in wood flooring system, stressed-skin panels used in prefabricated building units, and other systems such as builtup and laminated beams,

plates, and shells. Problems often arise when analyzing such systems because any assumption of rigid layer interconnection neglects the important presence of interlayer slip. If the layers are joined together with a stiff adhesive, as in the construction of laminated wood and plastics or spot welding in metal assemblies, the interconnection between layers may possibly be nearly rigid. But for layers fastened with nails or elastomeric glues, as in most in-place wood construction, the assumption of rigid interconnection between layers is invalid. The behaviors of layered systems vary considerably, with the degree of connection between the layers provided by the different connectors and the resulting interlayer movement having a very large effect.

The deflections of beams with layers not rigidly connected have received increasing attention from researchers. Many of the important papers resulting from these efforts are summarized below.

In an early theoretical development, Clark (6)* presented a theory for layered systems fastened by rigid connectors. He assumed that connectors such as rivets or spot welds were perfectly rigid, but slip could occur in the intervals between connectors. Thus, his method assumes the layered beams are fastened by rigid connectors at discrete points.

Granholm (10) developed a theory for layered beam systems including the effect of interlayer slip. Pleshkov (24) also analyzed a multilayered beam system with interlayer slip. Their theories assume a constant connector spacing, a uniformly distributed

---

* Number in parentheses refer to the references listed starting on p. 94.

connector effect, and a linear relationship between the connector force and its displacement.

Newmark, Seiss and Viest (20) studied the problem of incomplete interaction between the steel girder and concrete slab of a composite T-beam. Their assumptions are essentially the same as those made by Granholm.

A method based on sandwich theory for beam was developed by Norris, Erickson and Kommers (21) and extended by Kuenzi and Wilkinson (17). This method assumes that a layer of low shear rigidity exists between the layers.

Experimental work on layered beams has been reported by Hoyle (13), who also compared his results with the predictions of the Kuenzi-Wilkinson formula. In his study, four different adhesives with a wide range of shear modulus values were used to laminate twenty two-layered beams composed of approximately 1 x 2 in. clear Douglas fir lumber. Computed deflections generally exceeded those measured.

Hoyle (14) has also presented results from I-beams bonded with elastomeric adhesives. The four beams used consisted of 1 x 2 in. webs and 1 x 3 in. flanges bonded together with three different elastomeric adhesives (low, medium, and high shear modulus values) and one rigid adhesive (phenol-resorcinol-formaldehyde) to form the I-beams. At the design load level, test results showed that the flange-to-web slip along the length of span at the support ranged from 0.002 in. for rigid adhesive to 0.047 in. for the low shear modulus adhesive. Even for the low shear modulus adhesive, the bonded I-beam did show some degree of composite action.

Amana and Booth (1) have presented theoretical studies of stiffened orthotropic plates for single rib T-beams, and both double rib and multiple rib stressed-skin panels. The concept of effective plate width was introduced to account for the nonuniform distribution of stresses in the flanges. The solutions developed for the stressed-skin panels recognize the contribution of the plate to the overall stiffness of the component and consider the slip between the skin and the ribs. Five stressed-skin models were fabricated and tested. Test results showed good agreement between experimental and theoretical deflections (2).

A general theory for layered beams with interlayer slip was formulated by Goodman (8, 9). He developed the governing equation for deflections of a layered beam system with three layers having the same dimensions and symmetrical mechanical properties. The assumptions used include continuous shear connection, linear distribution of strain within each layer, and an interlayer slip proportional to the transmitted load. Nine experiments using layered wood beams were included to verify the theory presented. Excellent agreement between the measured and theoretical values was obtained for this test series.

The governing equation for this system, as reported by Goodman, for three layers having the same modulus of elasticity:

$$3\,EI\,\frac{d^4y}{dx^4} - \frac{kn}{SEA}\,(EI_s\,\frac{d^2y}{dx^2} + M) = -\,\frac{d^2M}{dx^2} \qquad (1.1)$$

where

E = the modulus of elasticity of the material, lb/in.^{2},

I = the moment of inertia of each layer about its own neutral axis, in.^{4},

I_s = the moment of inertia of the rigidly connected section, $in.^4$,

M = the external moment, lb-in.,

A = cross section area of each layer, $in.^2$,

S = the spacing between connector rows along the beam length, in.,

k = the connector modulus per connector, lb/in.,

n = the number of connectors per row,

y = beam deflection, in.,

x = beam length, in.

The governing equations developed by Granholm, Pleshkov, and Newmark et al., can be shown to be identical to that presented by Goodman by substituting appropriate terms into the constants.

As a part of the Colorado State University project, Ko (16) has extended the general theory to include layered beams with a single axis of symmetry and an arbitrary number of layers fastened with mechanical connectors. His study is based on the following assumptions, which are equivalent to those made earlier by Goodman (8, 9):

1. The shear connection between layers is continuous along the length; i.e., discrete deformable connections are assumed to be replaced by a continuous shear connection.
2. The amount of slip at a connector is directly proportional to the load.
3. The distribution of strain through the depth of a given individual layer is linear.
4. At every section of a beam, each layer deflects the same amount and no buckling of the layers occurs.

5. Shear deformations are neglected.

6. Friction between the layers is negligible.

Fig. 1.1 shows a five layered system, the strain distributions within the layers, and the notation for force and moment components used by Ko in his formulation of the m layered beam system.

Applying equations of static equilibrium to the free body diagram in Fig. 1.1(d) yields

$$\text{from } \sum F_x = 0 \qquad \sum_{i}^{m} \frac{dF_i}{dx} = 0 \tag{1.2}$$

By combining the results from $\sum F_y = 0$ and $\sum M = 0$, and assumption 4 outlined above yields

$$\sum_{1}^{m} EI_i \frac{d^4y}{dx^4} - \sum_{1}^{m} r_i \frac{d^2F_i}{dx^2} = q \tag{1.3}$$

For an m layered system there are m+1 unknowns (m values for F and one value for y) and therefore m+1 equations are needed to find these unknown quantities. Equations (1.2) and (1.3) provide two of these equations. Other equations must come from the slip relationships. By applying the assumptions outlined above, the slip relationship for the adjacent layers was derived as the following expression:

$$-\left(\frac{S}{kn}\right)_{i,i+1} \frac{d^2F_i}{dx^2} = \frac{F_{i+1}}{EA^*_{i+1}} - \frac{F_i}{EA^*_i} + C_{i,i+1} \frac{d^2y}{dx^2} \tag{1.4}$$

where

$$C_{i,i+1} = \frac{1}{2}(h_i + h_{i+1})$$

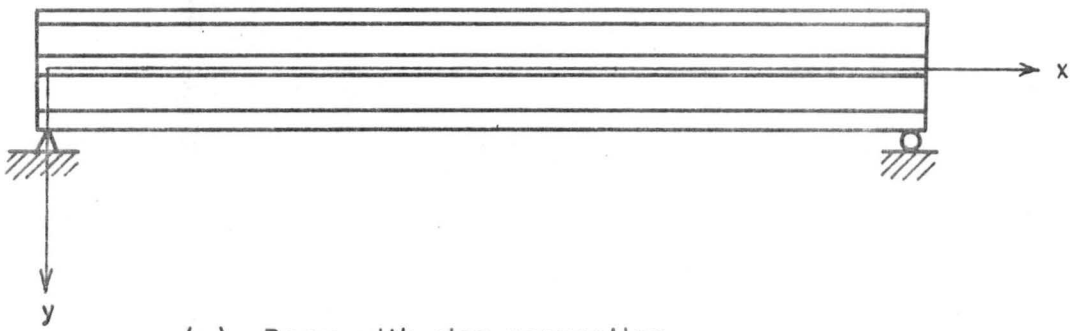

(a). Beam with sign convention

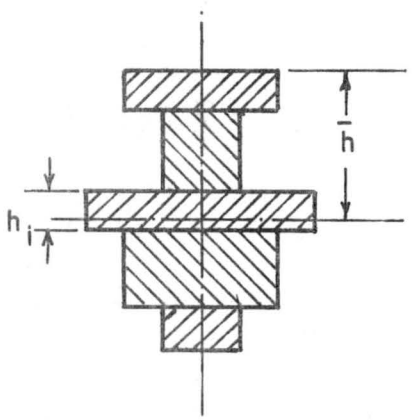

(b). Cross-section

(c). Strain distribution

FIGURE I.1 FIVE LAYERED EXAMPLE OF m LAYERED SYSTEM

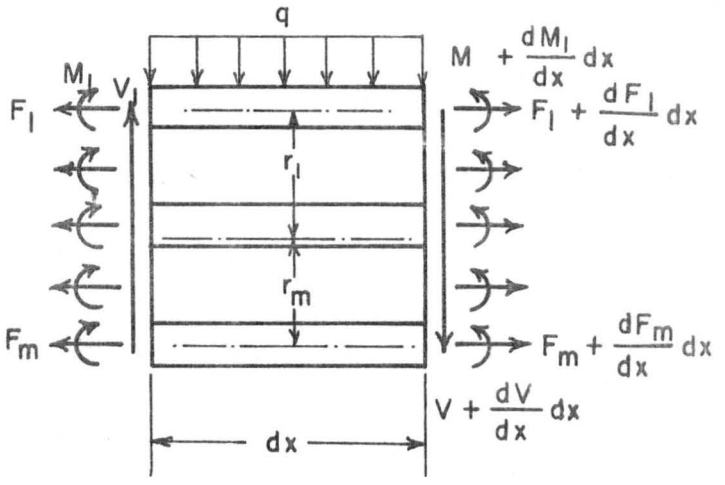

(d). Beam element

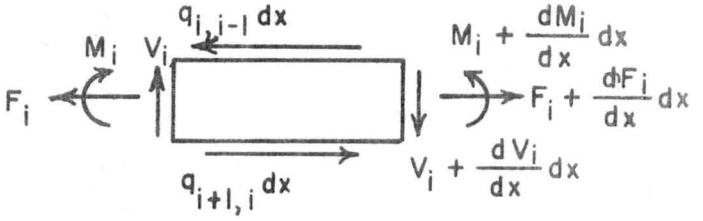

(e). i^{th} layer element

FIGURE 1.1 – CONTINUED

Nomenclature used in Equations (1.2) through (1.4) and not previously defined include:

h_i = thickness of the i^{th} layer, in.,

r_i = the distance from the centroid of the transformed cross-section to the centroid of the i^{th} layer, in.,

F_i = axial force in the i^{th} layer, lb.,

A^*_i = transformed area of the i^{th} layer, $in.^2$

Subscripts i,i+1 refer to properties along the boundary between the i^{th} and the $i+1^{th}$ layer.

Equations (1.2), (1.3) and (1.4) provide a system of m+1 equations for the m+1 unknowns and represent the governing set of equations for an m layered system.

The governing equations can be solved by incorporating the known boundary conditions and then using either closed form solutions or numerical solutions. In his report, Ko has shown examples using both finite difference and closed form solution techniques applied to two- and three-layered systems.

Rose (25) has presented test results for glued and nailed T-beams. In his work, eleven T-beams consisting of Douglas fir plywood and lumber were fabricated. The T-beams were constructed using either glued or nailed connections with glued or nonglued T & G (tongue-and-groove) sheathing joints. The test results showed that the increase in stiffness for the T-beams with respect to that of the joist alone was about 20 percent for unglued T & G joint and about 50 percent for glued T & G joint.

CHAPTER 2

TESTING EQUIPMENT AND PROCEDURE

2.1 Description of Testing Equipment

2.1.1 Introduction

Facilities used for the structural testing are located in the Structural Engineering Laboratory at the Engineering Research Center on the CSU Foothills Campus west of Fort Collins. A 55 kip-capacity MTS hydraulic actuator and its associated control equipment were used to load all the T-beams included in this study. Penner (23) has presented an extensive description of these facilities.

A brief description of load capabilities of the loading system is given in Section 2.1.2. Measurement of the joist deflections during the tests is discussed in Section 2.1.3.

2.1.2 Loading System

The MTS closed-loop structural testing system is essentially a self-controlled hydraulic loading system composed of three major components: the power supply, the control console, and the actuator. The actuator is mounted on a movable steel beam which in turn is attached to the supporting frame by trolleys such that the actuator can be quickly moved to any point over the test area (see Fig. 2.1). An elevated reinforced concrete frame supports the floor and T-beam specimens over a 12-foot span and allows widths up to 16 feet. Along the top face of each 16 foot span of the frame, a nominal 2x6 inch Engelmann spruce sill plate was fastened to the concrete frame with bolts. The bottom of the sill plate was grouted with mortar having a thickness of about one quarter inch. The joists of the floor and T-beam specimens rested upon this sill plate.

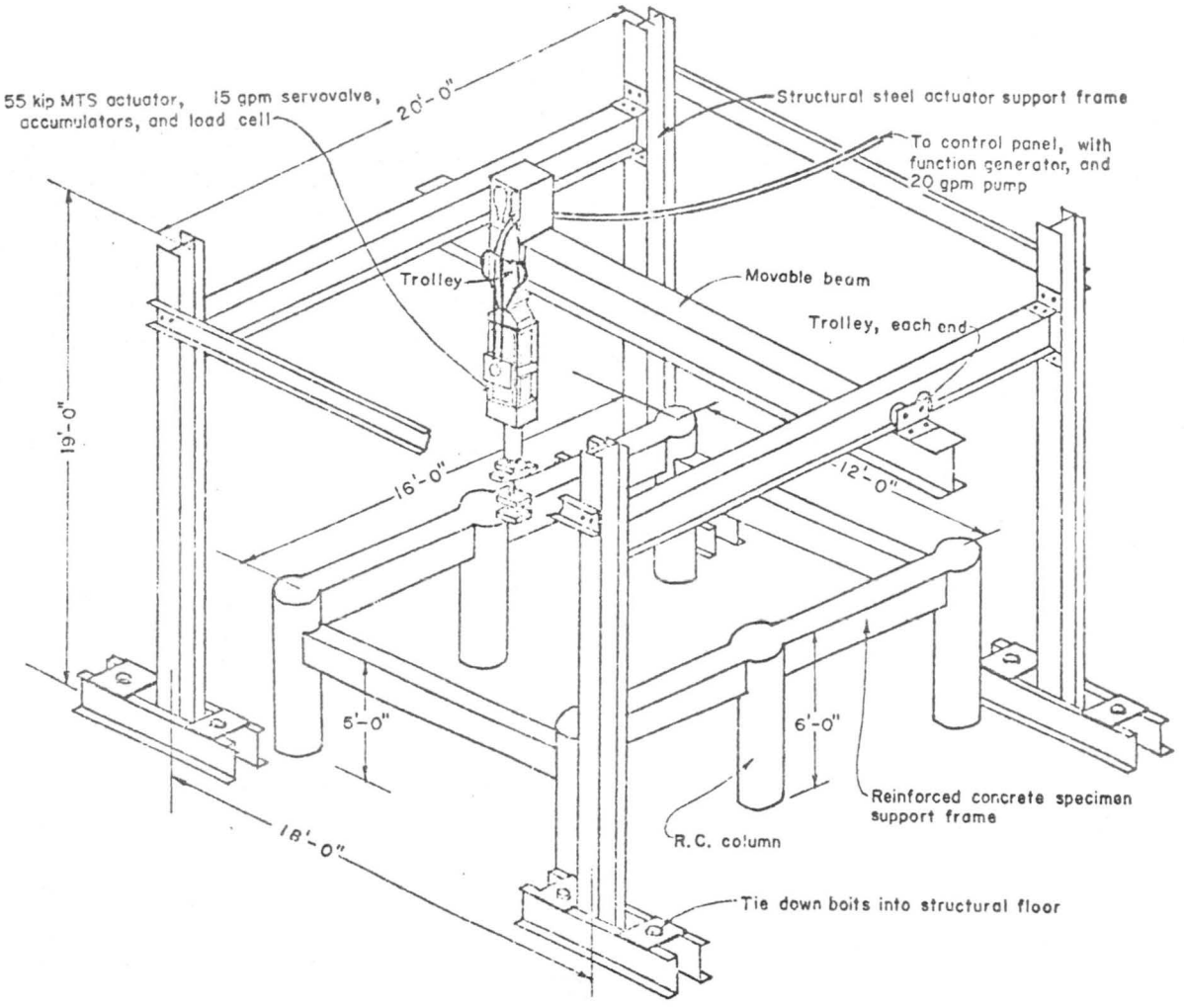

FIGURE 2.1 55 KIP MTS LOADING ACTUATOR AND SUPPORT FRAME

A load cell with a capacity of either 2.5 or 50 kips was mounted on the actuator, depending on the desired load level. The control console can operate the actuator in either a load control or stroke control mode. Besides its static loading capability, a function generator in the console allows cyclic loading with a specific function. Sine, haversine, square, haversquare, and ramp function can be generated.

The ram of the MTS hydraulic loading system applied a concentrated load transmitted onto the specimen through load distribution beam separated from the load cell by a ball bearing. The thickness of the steel pad and the diameter of the ball bearing vary with the load cell capacities.

A twin T-beam configuration was used to obtain the necessary specimen stability. To allow each joist to be equally loaded, the twenty-inch long load distribution beam was used to divide the load and transmit it to each joist through a hinge and 4 by 5 inch steel pads, as shown in Fig. 2.2.

2.1.3 Data Collection

Deflection measurements were obtained at the various load levels using dial gages, surveying level, and LVDT's (linear variable differential transformers) connected to an X-Y plotter.

Dial gages with ranges of one and two inches were used to obtain most of the deflection data in the working load range. The deflection dials were read to the nearest one-thousandths of an inch. They were placed underneath the joist at selected points across the span and were fastened to a punched steel angle attached to a supporting bridge across the span of the test area. A more detailed description

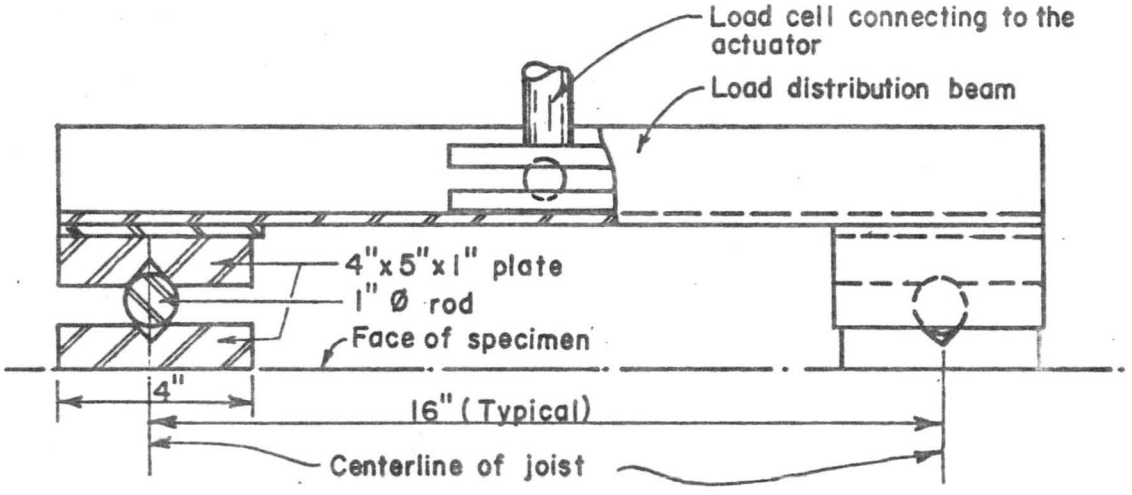

FIGURE 2.2 LOAD DISTRIBUTION APPARATUS

of the dial gages arrangement has been given by Penner (23). Several dial layouts are shown in Fig. 2.3 to indicate the individual gage locations used in the T-beam tests.

For most cases, dial gages were used to measure the deflection within the elastic range. During the test to failure, engineering scales with 50 divisions per inch were attached to the joists at points where deflections were to be measured. A surveying level was used to read the deflection after the application of each load increment.

The LVDT's were used for some tests to obtain a continuous plot of load versus deflection. The LVDT contained within the actuator was used to plot the load-deflection curve to failure for most tests.

2.2 Test Specimens

2.2.1 Description of the Test Specimens

An alphanumeric identifying system was used to describe each specimen. This system was constructed as follows to allow easy recognition of the specimen characteristics:

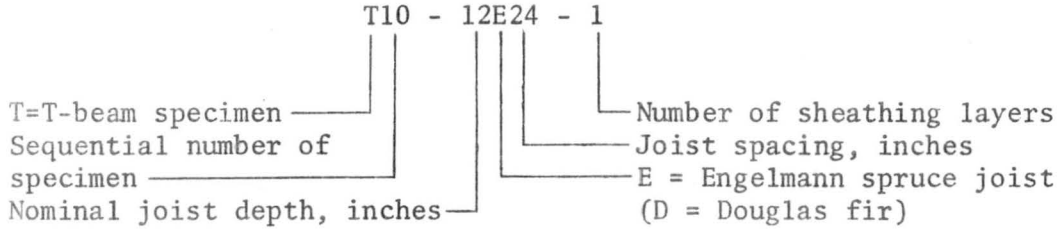

Fourteen T-beams were built and tested. These full size specimens were constructed from joists and plywood sheathing both of either Douglas fir or Engelmann spruce, or from a combination of Douglas fir joists and Engelmann spruce plywood, or vice versa, to

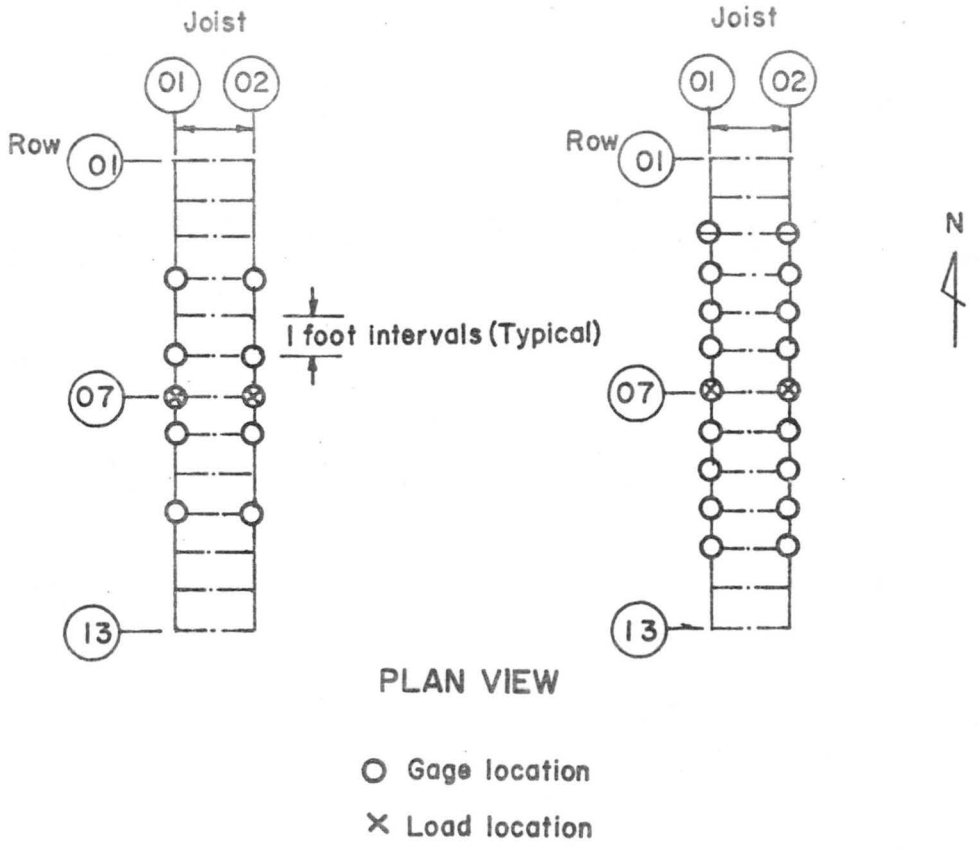

FIGURE 2.3 TYPICAL DIAL GAGE LAYOUTS

form a two-layered T-beam. One-half inch thick particleboard was added to selected two-layered systems in order to form a three-layered system. The nominal dimensions of the joists were 2x8 inches or 2x12 inches with a length of 12 feet and 2 inches. The plywood was 4x8 feet sheets with nominal thicknesses of 1/2 and 3/4 inches. Each piece of joist and sheet of plywood or particleboard was numbered according to the alphanumeric identifying system shown below:

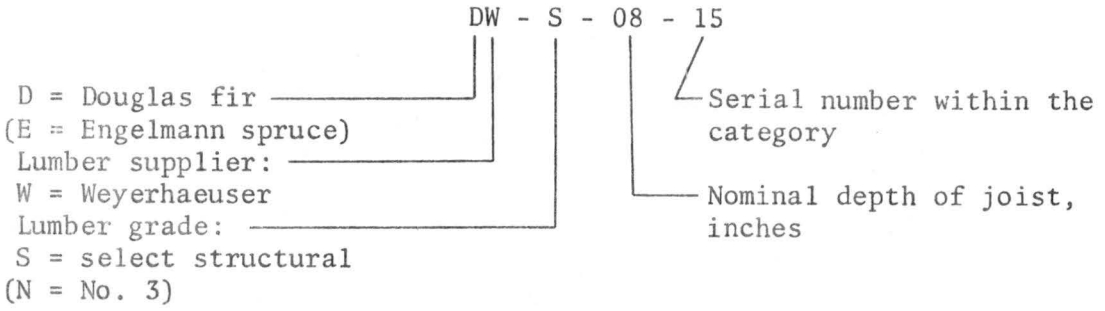

For plywood and particleboard:

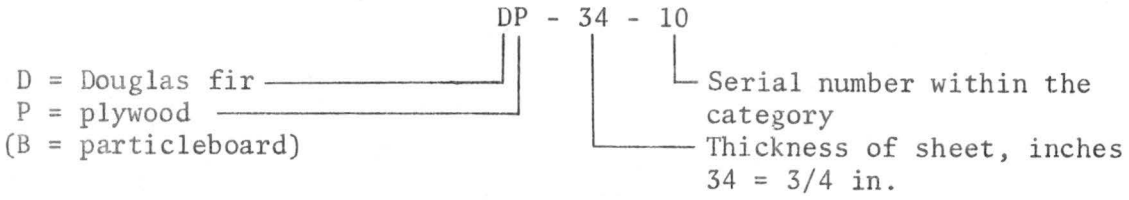

Six- and eight-penny common nails at varying nail spacing (from 2 inches to 8 inches) were used as connectors. An elastomeric glue was also used in the fabrication of some specimens. Joist spacings were 16, 19.2, and 24 inches. A more detailed description of individual specimen configurations will be presented in Chapter 3.

A general numbering system was developed to identify points on the T-beam surface. A location along the joist was specified first by joist number and then by its placement along the joist using the system shown in Fig. 2.4.

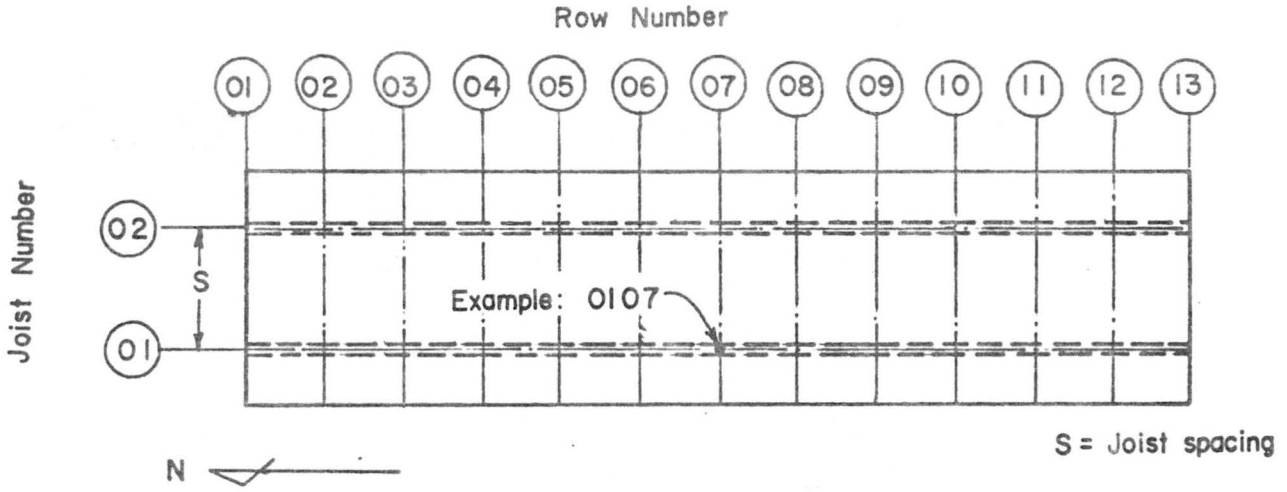

FIGURE 2.4 NUMBERING SYSTEM TO IDENTIFY LOCATIONS ON SPECIMEN

2.2.2 Selection of Materials

Methods of selecting the materials were considered prior to starting the specimen construction. Two schemes were adopted for the selection of joists. In the first method, joists were selected from within a predetermined range of average MOE values using data provided by the Wood Science Laboratory. After these preselected joists were located, the joists found to have excessive crookedness or abnormal cracks or knots were discarded. Joists for most T-beam specimens were selected using this first method. For a few T-beams, random selection was used, i.e., both joists needed were randomly selected from the lumber supply of the desired size, grade, and species without regard to their measured stiffness. Again, excessively crooked or abnormally cracked joists were discarded.

Plywood and particleboard sheets were selected from the top of the supply pile in order as needed.

All joists and sheathing materials were covered with plastic sheets to help maintain a stable moisture content.

2.2.3 General Construction Procedure

The construction procedures for all T-beams were essentially the same. After each joist was selected as described in the previous section, it was marked with a line at its midspan. This was to provide the reference mark for the edgewise MOE test, in which the joist was loaded at the midspan, and to facilitate the attachment of sheathing pieces (see Fig. 2.5). Each joist was then placed edgewise across the concrete frame and seated on the sill plate. Normal house construction practice was followed when placing the joist over the test area. The crowned edge was usually placed upward, and whenever

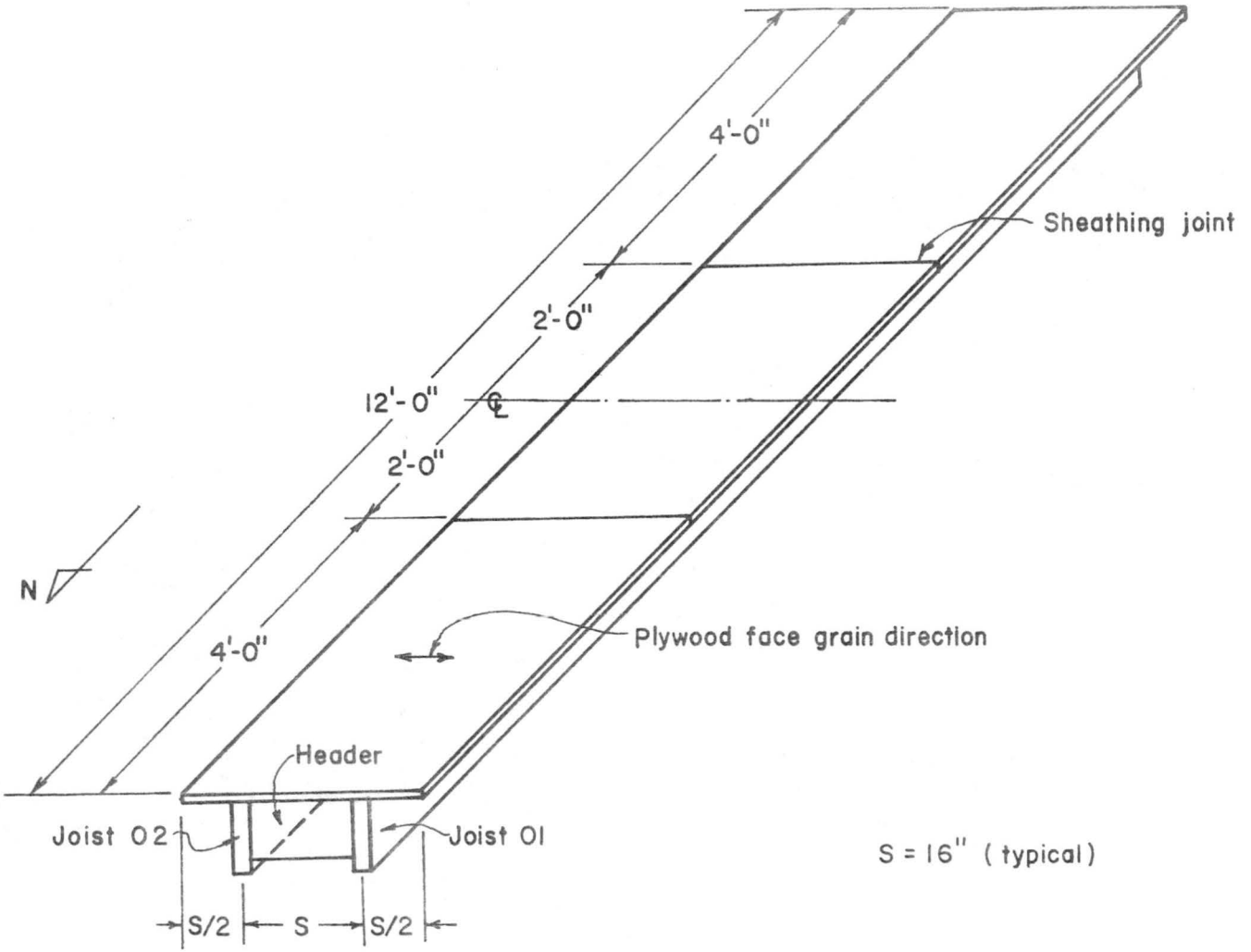

FIGURE 2.5 TYPICAL TWO-LAYERED T-BEAM SYSTEM

a big knot was present at the edge of a joist, it was placed on the top edge in order to prevent early failure when the joist was subjected to loading.

During the edgewise MOE determination (to be discussed in more detail in Chapter 3), the joists were positioned, nailed to the sill plate with six-penny nails, and attached to a short header at both ends of the joist. A 2x6 inch header was used with the 8 inch deep joists, and a 2x8 inch header was used for the deeper 12 inch joist. The joists were toenailed to the sill plate for specimens constructed prior to T7-8D16-1. Starting with this specimen, any end restraint from these nails used to position the joists laterally was eliminated by placing the nails adjacent to but not through the joists. The other construction procedure was the same as those described in detail by Penner (23).

For the two-layered T-beam systems, the plywood was sawed into the required sizes and then placed with the face grain perpendicular to the joists. Eight penny common nails were used to connect the plywood and joist in all nailed specimens. Nail spacings differed from specimen to specimen, ranging from 2 inches to 8 inches apart. One row of nails was used per joist.

An elastomeric glue* was used to connect the plywood to the joist of some specimens. The glue was applied with a caulking gun in two one-quarter inch wide beads placed continuously along the upper joist face. The glue was then spread evenly. After the plywood was placed at the desired position, double-headed common nails were driven into the joist at a spacing of about 8 inches to insure a

---

* Franklin Construction Adhesive

tight contact between the plywood and joist. The glued specimens were allowed to cure about two weeks. The double-headed nails were pulled out immediately before load testing began.

Details of the sheathing joints varied. Usually the tongue-and-groove joints were butted tightly by forcing the unnailed sheathing to the nailed one until the gap was closed at several points along the joint. Small variations of the sheathing edge from a perfectly straight condition resulted in some small gap opening remaining along much of the joint. For some specimens, joints were left with a 1/16 inch wide gap. For others, the joints were glued and tightly butted.

One layer of particleboard was added to several of the two-layered systems to form a three-layered system. The particleboard was selected as described before and sawed into the same sizes as those of the plywood in the two-layered system. The particleboard sheathing joints were staggered from the plywood joints. Six penny common nails were typically used to attach the particleboard. Nail spacings varied from specimen to specimen, with 8 inches spacing most commonly used. Nails were driven through the particleboard and plywood into the joist with the nail spacings staggered from the nails previously driven through the plywood layer, except for T16-8E19.2-2. The special nailing for this specimen, shown in Fig. 2.6, consisted of two rows of nails driven along both edges of the joist and penetrating through the particleboard and plywood layers only.

The location and identification of all joists, plywood, and particleboard used in the test specimens were recorded according to the numbering systems described in the previous section. The specimen configuration, gap locations, and nail spacings are presented in Appendix E.

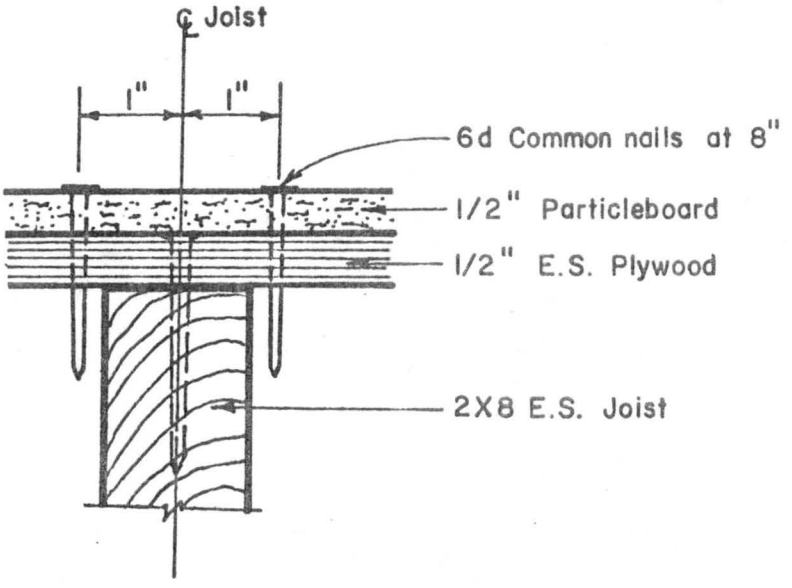

FIGURE 2.6 NAILING ON SPECIMEN T16-8E19.2-2

2.3 Testing Procedure

The general testing procedures used during this study have been more fully discussed by Penner (23). The procedures used differed only in a few details included below from those reported by Penner.

A concentrated load was usually applied at the midspan of the specimen. Load increments of 50, 100, 250, or 500 pounds were used depending on the specimen being tested and the desired final load level. Deflections at selected points along the joist were recorded for every load increment. Service load tests were terminated when the maximum deflection approached, but did not exceed L/360, a 0.4 inch value for the 12 ft span used in this study. The service load tests were repeated up to five times at the same location for selected specimens. The elapsed time between the repeated loadings was about five minutes in most cases. Some load locations other than at the midspan were also included. These locations were usually either 2 feet or 4 feet from the midspan of the T-beam specimens.

Tests including sequential cutting of increasing number of gaps in the sheathing were conducted as follows: After completion of the usual service load level test, the sheathing forming the flange of the T-beam was cut into four foot lengths in the direction perpendicular to the joist using a circular saw adjusted to cut just through the plywood layer. The gap width produced was near 1/8 inch, the thickness of the saw blade. The T-beam was then reloaded at the selected point and deflections again measured. The sheathing was further cut at two foot intervals and load-deflection behavior again determined. This procedure was repeated after cutting the gaps at one foot intervals.

Finally, each specimen was tested to failure with the load applied to the midspan of the specimen. Since the failure load and deflections of the joist were unknown at the time of testing, the 50 kip capacity load cell was installed, and the dial gages beneath the joists were replaced by engineering scales. The use of engineering scales served to preclude possible damage to the gages and allow large deflections to be measured. A concentrated load was applied in 500 pounds increments and the deflections obtained with a surveying level were recorded. The LVDT from the actuator was connected to the X-Y plotter to obtain a continuous load-deflection plot.

A cyclic and sustained load was also used for specimen T13-8D16-1. The first cyclic loading used was a ramp function with the shape shown in Fig. 2.7(a). The period for each cycle was 80 seconds. This load was repeated for 850 cycles, a process taking nearly 19 hours. The second cyclic loading was also a ramp function and had the shape shown in Fig. 2.7(b). The period of this loading, which was repeated for 750 cycles, was 40 seconds.

Observations and sketches of the broken joists were noted after the test to failure for each specimen. Photographs were taken of some specimens to show the failure mode of the T-beam. After the failure test was completed, the specimen was dismantled. Some small samples of the joists and plywood of the specimen were cut, with sizes conforming to the ASTM Standard D 2016-65(5) and sent to the Wood Science Laboratory for moisture content determination.

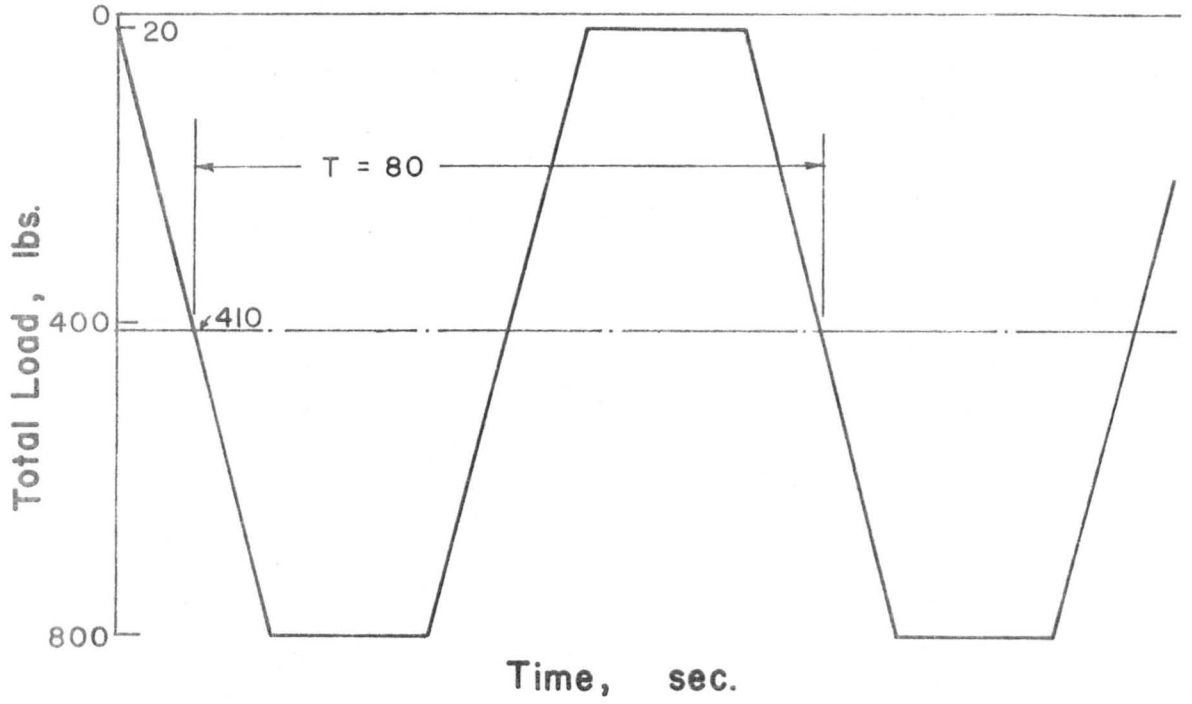

(a). Period = 80 seconds

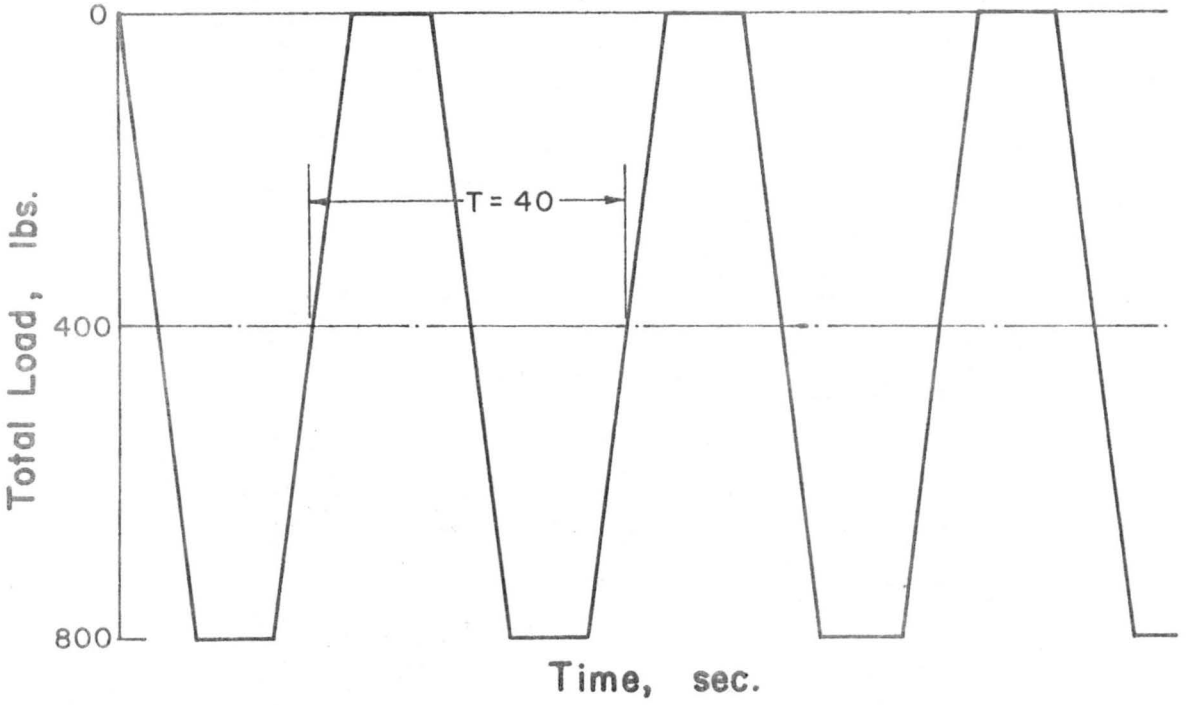

(b). Period = 40 seconds

FIGURE 2.7 RAMP FUNCTION FOR TESTING SPECIMEN T13

CHAPTER 3

MATERIAL AND TEST SPECIMEN PROPERTIES

3.1 Introduction

The most important material properties affecting the deflection of a layered beam of given dimensions are the MOE (modulus of elasticity) values for the materials in each layer and the slip modulus of the connectors. In an isotropic and homogeneous material, the MOE value is theoretically constant. For wood and wood-based products, it is not so because these materials are neither isotropic nor homogeneous. Hence, the MOE value of wood varies from section to section along any given piece of lumber as well as with the direction of loading. Furthermore, MOE values vary from species to species, from one piece of lumber to another within a species, and as a result of many other factors such as grain angle, knot location, and presence of other defects.

Methods for evaluating lumber properties have been studied and standardized by several research institutions and agencies in this country. ASTM Standard D 245-70 specifies a visual grading method for evaluating lumber properties (5). Others combine the visual and machine grading systems (11, 29). In evaluating the stiffness properties of plywood, U.S. Product Standard PS 1-66 (28) specifies a grading system classifying plywood into five groups and assigning each group a design stress.

The characteristics of particleboard are dependent on the geometry of the particles, the type of adhesive, and the manufacturing process used to produce the particleboard. The National Particleboard Association (NPA) currently assigns minimum average MOE values for particleboard ranging from 150,000 psi to 50,000 psi (19).

Methods used in evaluating the MOE of joists and sheathing materials will be discussed in the next section. A discussion of the relationship between flatwise and edgewise MOE of joists is also included.

Nails are the most common mechanical fastener used in housing construction. Although the withdrawal resistance of nails has received considerable study (7,15), information on the forces on nails in a wood floor system at a given loading condition is skimpy and far from conclusive. The increasing use of elastomeric glue in field construction of wood floor systems has drawn much research attention to this material, but verified design methods including the benefits of elastomeric glued systems are not yet available to the designer. Tests to determine slip modulus values for nails and glue are discussed in Section 3.3.

A description, including the configuration and material properties of each T-beam specimen tested in this study is presented in Section 3.4.

3.2 Joist and Sheathing Properties

3.2.1 Flexural MOE Determined by the Wood Science Laboratory

Properties of wood products can differ widely from piece to piece because of the high degree of variation in their mechanical properties. Measurement of the properties of each joist and sheathing element used in the T-beam specimens, rather than properties from samples from each group of materials, was considered necessary to adequately describe the materials in each specimen. This could be done because the determination of MOE values and other elastic constants is easily conducted using nondestructive tests, which allows the use of the materials with known properties in the T-beams.

As a part of the overall research program, joist and sheathing properties were measured at the Wood Science Laboratory located on the Colorado State University campus. Determination of joist properties was performed using a continuous deflection measurement device. The basic operation of this machine entails measuring joist deflection at the center of a span under a constant load and from this deflection, computing MOE. Each piece of dimension lumber was run through the machine in a flatwise position and subjected to a constant load placed at the center of a 3-foot span along the moving piece. This midspan deflection was measured by a LVDT (linear variable differential transformer) and plotted using an X-Y recorder. Each specimen was run through the machine twice, once with each flatwise face loaded, to allow the effects from any warp, twist, or thickness variation present in the joist to be removed. The MOE was then calculated for one foot intervals along the length of the joists. The dimensions of each joist measured at three locations along the joist length were used to compute the moment of inertia. Wolfe (30) has described in more detail the joist flatwise MOE test. A computer program was used to compute the MOE values using the following equation, which includes both bending and shear deflections:

$$\Delta = \frac{\Delta_1 + \Delta_2}{2} = \frac{PL^3}{48EI} + \frac{0.3\ PL}{AG} \qquad (3.1)$$

where

Δ_1 and Δ_2 = deflections for sides 1 and 2, respectively, in.,

Δ = average deflection, in.,

P = load applied at midspan, lb.,

L = span, in.,

E = modulus of elasticity, lb/in^2,

I = moment of inertia, in^4,

A = cross section area, in^2,

G = shear modulus in the plane of lumber thickness, lb/in^2.

Rearranging this expression with the substitution of $I = bh^3/12$, $A = bh$, $G = E/16$, and solving for E gives

$$E = \frac{P(L/h)}{4\Delta b} \left[(L/h)^2 + 19.2\right] \qquad (3.2)$$

where

b = board width, in.,

h = board thickness, in.

Eq. 3.2 was incorporated to a computer program which computed the MOE from the recorded deflection data. The computed MOE value recorded is an average value over each one foot interval. The average MOE values, given as the mean of the values for each one foot interval along each joist used in the test specimens, are listed in Appendix A.

Five groups of sheathing materials were tested to determine their elastic parameters. These groups include 1/2 and 3/4 in. thick Douglas fir plywood, 1/2 and 3/4 in thick Engelmann spruce plywood, and 1/2 in. thick Douglas fir particleboard. The measurement of the parameters and testing procedure for these materials are fully discussed by McLain (18).

The MOE test for the sheathing utilized static bending and was set up as shown in Fig. 3.1. Since the effect of defects along the length of a panel was not thought to be significant, the interval-based MOE was not used. Instead, overall MOE values for both

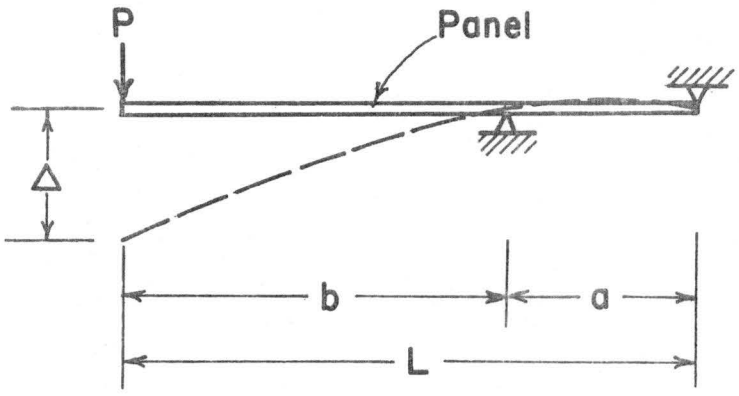

FIGURE 3.1 LOADING CONFIGURATION FOR COMPOSITE PANEL IN STATIC BENDING TEST

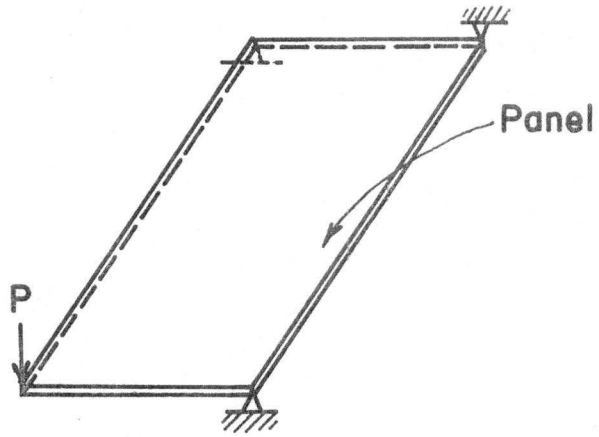

FIGURE 3.2 LOADING CONFIGURATION FOR COMPOSITE PANEL IN SHEAR MODULUS TEST

directions, i.e., parallel and perpendicular to face grain direction were determined.

The mechanical properties of plywood are different for the two principal directions. This results from plywood being made up from several veneers, or thin sheets of wood, glued together with the grain of adjacent veneers at right angles. Because of the orthotropic nature of wood, the mechanical properties of plywood are dependent upon the grain orientation and thicknesses of the individual plies. The properties of the transformed section in each direction must be used to determine the actual MOE values for plywood (3, 18). These transformed section properties must also be considered to determine MOE values valid for bending and for axial loads based on gross section dimensions.

McLain (18) also reported that the ratio of actual thickness to nominal thickness of the 1/2 and 3/4 inch Engelmann spruce plywood was 0.86 and 0.87 respectively, compared to ratios of 0.97 and 0.99 for 3/4 and 1/2 inch Douglas fir plywood. This indicates that the Engelmann spruce sheets had been densified during the manufacturing process, while the Douglas fir panels had negligible change in thickness. The MOE values for Engelmann spruce plywood were computed using thicknesses of 3/8 and 5/8 inches. Values for the Douglas fir panels were based on the given nominal dimensions.

In computing the MOE values, any correction due to Poisson's ratio and shear effects were neglected because these effects were judged to be insignificant for the sheathing materials (18).

Evaluation of the shear modulus, G, was conducted by applying a load at the opposite corners of the panel and supporting the other two corners, as shown in Fig. 3.2.

All panels were tested in both the lengthwise (veneer parallel to the long axis of panel) and crosswise directions. The corresponding MOE and G of each panel used in T-beam tests are listed in Appendix B.

3.2.2 Joist Properties Determined during Specimen Construction

The correlation of flatwise and edgewise MOE has been studied and reported previously (11, 12). A perfect correlation should not be expected since the natural variation, grain angle orientation, and other defects existing in a piece of lumber can easily have different effects for bending about the two directions.

In the T-beam specimen constructions, joists were placed edgewise, as discussed in Chapter 2. Because of this configuration, the MOE determined from the property tests described in Section 3.2.1 can only approximate the true MOE of the joist as used. As noted above, only approximate relationships between flatwise and edgewise MOE are available. Therefore, it was decided to determine the edgewise MOE for each joist as a part of the specimen construction procedure because of the possibility that these MOE values might yield more consistent results when verifying the mathematical model.

Each joist was first placed on edge in the test area. No lateral support was provided along the joist except that provided by the joist resting upon the sill plate. Then a concentrated load was applied at the joist midspan, and the deflection indicated by the dial gage mounted underneath the joist was recorded as described in Chapter 2. At least three load increments of 100 pounds each were usually applied to obtain a load-deflection plot and to determine how linear the data was, see Fig. 3.3. The MOE values due to static bending was computed from the commonly available deflection equations

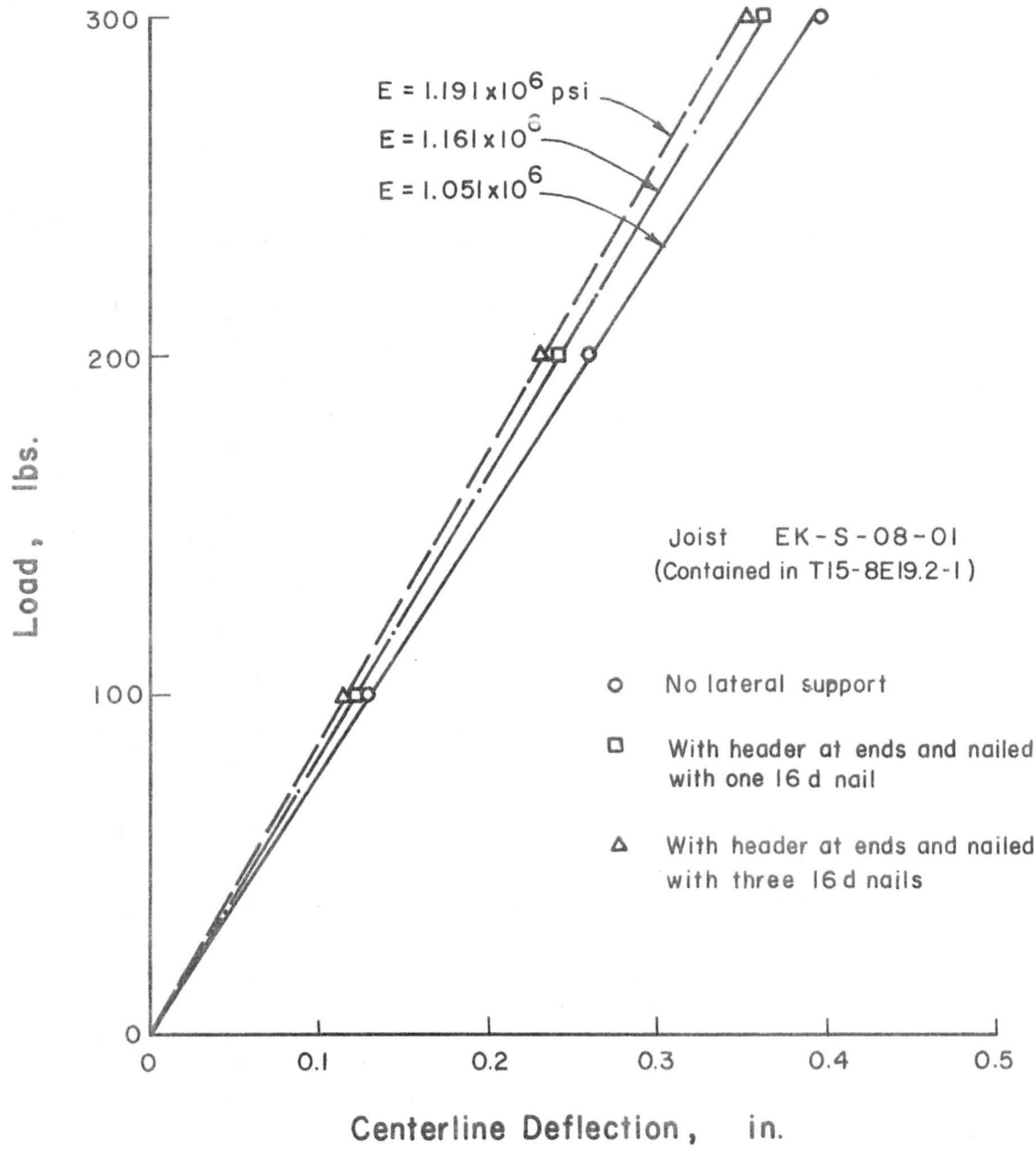

FIGURE 3.3 TYPICAL LOAD-DEFLECTION PLOT FOR JOIST MOE TEST

including only flexural deformations (see Section 5.3 for a discussion of the neglecting of shear deformations).

After the MOE determinations for the laterally unsupported joists were completed, a header joist was attached at both ends of the joists and nailed with a single 16-penny common nail through the mid-depth of each end of the joist, see Fig. 3.4.

The testing procedure just described was again followed. The test was performed for one joist at a time. Finally, two more 16-penny common nails were driven at each joist end, see Fig. 3.4, and the joists were again reloaded. A typical load-deflection plot with and without lateral support is shown in Fig. 3.3.

The relationship between flatwise and edgewise MOE of the joist is discussed in Appendix C.

Joist moisture content during the MOE determinations at the Wood Science Laboratory were measured using an electrical resistance moisture meter. The moisture content ranged from 6.4 to 11.3 percent (23). After each T-beam test, samples of joists and plywood were cut from the test specimen and sent to Wood Science Laboratory for moisture content measurement. A procedure including oven drying and conducted according to ASTM Standard No. D 2016-65 (5) was used. Moisture content of materials from the T-beam test specimens ranged from 5.0 to 7.3 percent for the joists, and from 5.6 to 6.9 percent for the plywood. Since MOE values of the joists used for later mathematical verification were evaluated during the specimen construction and the moisture content of the sheathing appeared to be quite constant, the effect of moisture content changes on the stiffness of the joists and plywood were deemed to be negligible.

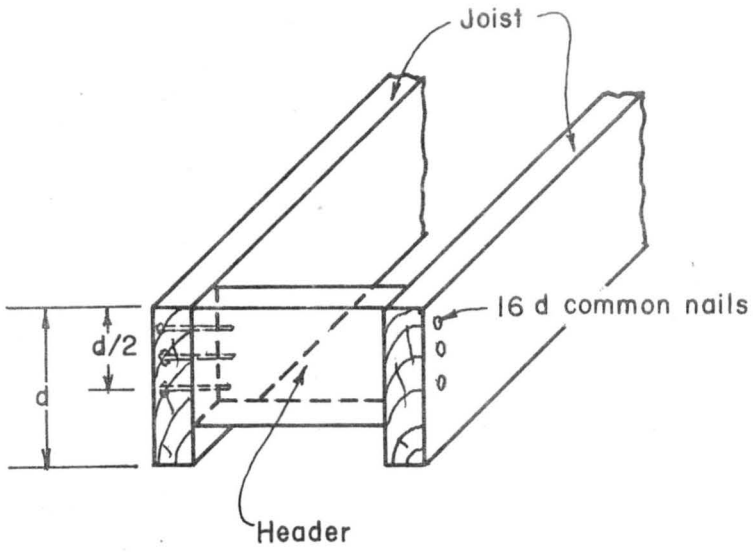

FIGURE 3.4 ATTACHMENT OF HEADER FOR T-BEAM CONSTRUCTION

3.3 Properties of Nail and Glue Slip Moduli

The slip modulus of the connectors is one of the important parameters in the floor system study since it greatly influences the degree of interaction between layers. The interlayer slip effect is a function of the load-slip characteristics of the fastener-wood combination. The slope of the load-slip curve is defined as the slip modulus, k (see Fig. 3.5). Goodman (8) has developed an equation to fit this load-slip curve which has been included by Patterson (22) in his recent work on nail slip modulus conducted as a part of the overall wood joist floor project.

In his study Patterson selected one-foot long 2x8 joist pieces from either Douglas fir or Engelmann spruce as the center member, and used 3/4 inch thick Douglas fir or Engelmann spruce plywood cut into 8x12 in. boards as side members (see Fig. 3.6(a)) to form a double shear test configuration. Eight penny common nails with 2, 4, and 8 nails on each side were used. A series of tests with different combinations of lumber plywood species were conducted to determine the effect of the number of nails in the nail slip test. Specimens with plywood face grain either parallel or perpendicular to the load were included in his study. Test results expressed in terms of slip modulus based on tangent and secant lines at various load levels are listed in Appendix D. A typical load-slip curve is shown in Fig. 3.5.

A group of tests using 1/2 inch thick plywood as side member for the double shear test and with 8-penny nails were also conducted. The load-slip characteristics between particleboard and plywood were determined for 6 penny common nails driven through the plywood and particleboard in two rows, one on each side of the center member,

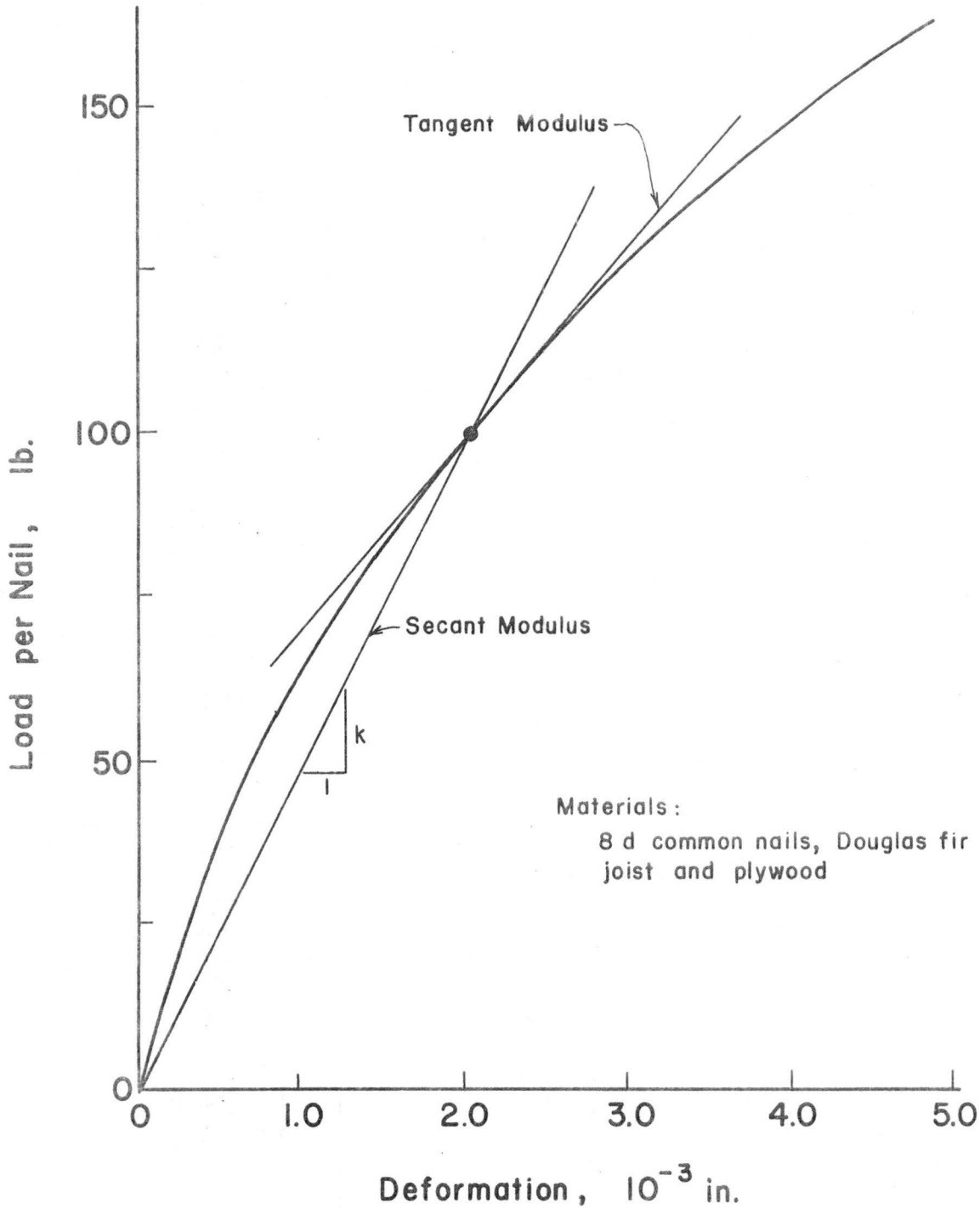

FIGURE 3.5 TYPICAL LOAD-SLIP CURVE

which was attached to the plywood with a rigid glue, see Fig. 3.6b. Test results are shown in Appendix D.

According to Ref. 4, the increasing use of elastomeric adhesives for connecting members in housing construction results from its advantages of easy handling for construction, labor and materials saving, increasing overall stiffness of the structures, prevention of floor squeaks, and many other factors. Because of its importance in the field construction and module home assembly in factory as well, the properties of elastomeric glue were also included for study in this research program.

Specimens used for the slip modulus tests were essentially the same as those used in the nail-slip tests under lateral load described by Patterson (22). The adhesive used matched the adhesive used in the T-beam test specimens included in this study. Test values used in the T-beam studies were obtained as the average value of many individual tests, expressed in terms of slip modulus, lb/in^2 (see Appendix D).

3.4 Layered Beam Specimen Configuration

The individual specimen configurations shown in Appendix E are included to give a clear identification of the materials and configuration of each specimen along with the tests performed on each specimen. Tests of fourteen T-beams are reported in this study. Three test specimens were 3-layered systems; the rest were 2-layered systems.

The identifying mark for each T-beam tested is constructed according to the alphanumeric system described in Chapter 2. Each joist and sheathing were individually identified and their relative positions were noted. Sheathing face grain direction, location and type of joints, and joint conditions in sheathing construction are

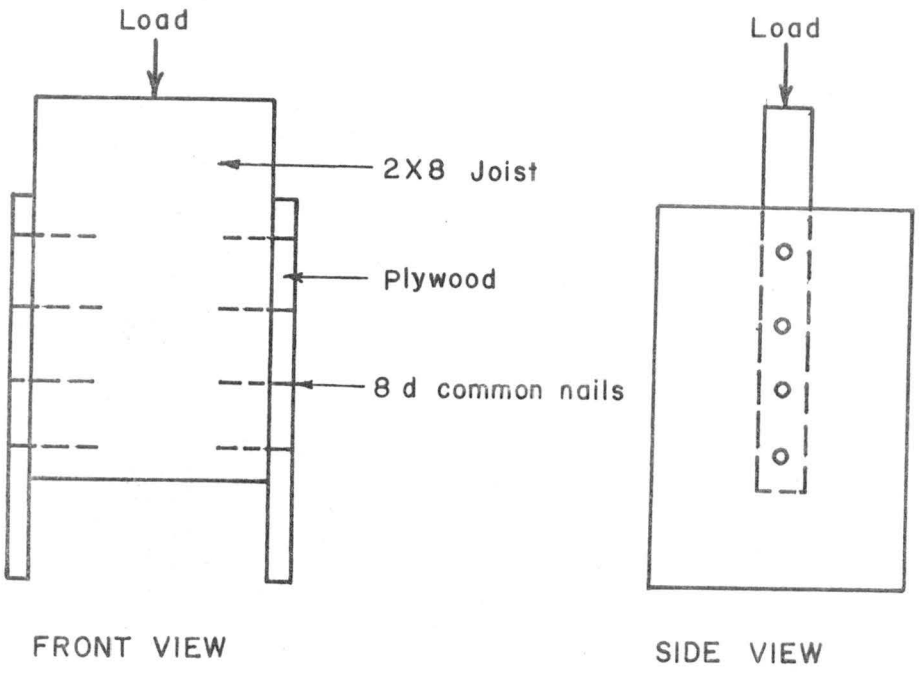

(a). PLYWOOD AND JOIST

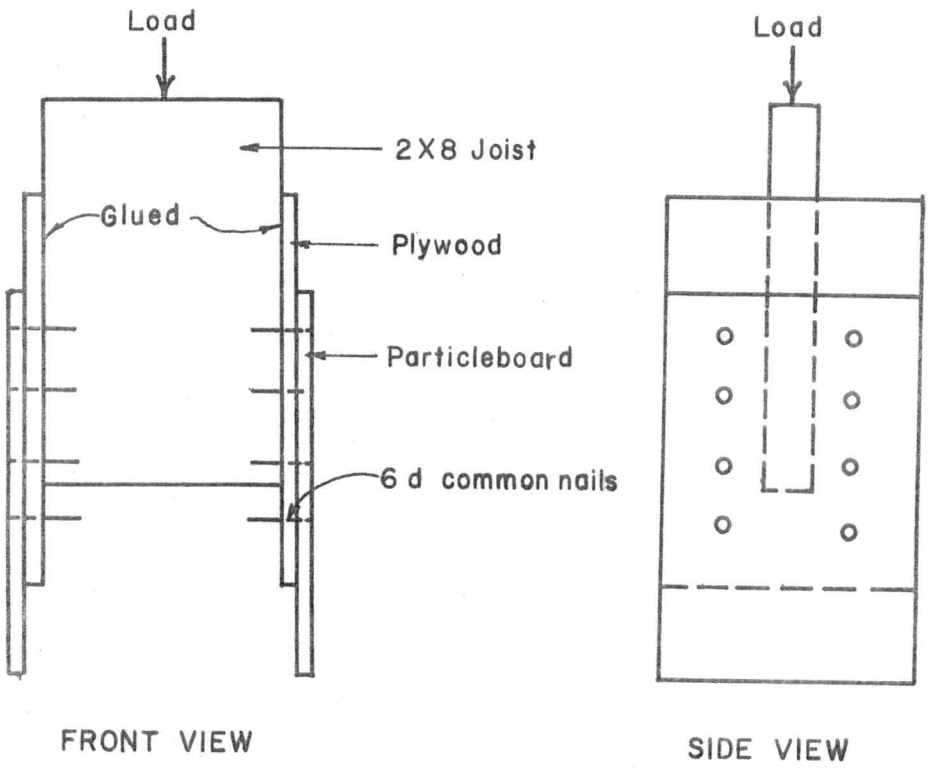

(b). PLYWOOD AND PARTICLEBOARD

FIGURE 3.6 NAIL SLIP MODULUS TEST SPECIMENS

also described. Edgewise MOE of each joist and appropriate MOE values for the sheathing layer(s) are included for the later mathematical model verification.

Types of nails and nail spacing are indicated in the diagrams when nails were used. When glue was used, the manufacturer's name is indicated. The interlayer slip modulus shown for each specimen is the value which was used in the computation of theoretical deflections.

A brief description of test sequence is also presented to indicate the load level, load increment, and load location for each specimen tested. Other information including failure load, cutting gaps, and others are shown wherever applicable to the individual test specimen.

CHAPTER 4

EXPERIMENTAL BEHAVIOR OF T-BEAM

4.1 Introduction

As discussed earlier, the objective of this study was to verify the developed mathematical model for T-beam components by comparing the data from carefully constructed specimens having known material properties with the results predicted by the mathematical model. The results of the verification studies for the mathematical model of the T-beam will be discussed in Chapter 5.

Prior to presenting the verification of the mathematical model, some experimental behavior exhibited by the specimens will be discussed to demonstrate how composite T-beams carry loads and how varying degrees of composite action can be obtained. The experimental behavior described are those observed for specific specimens and are cited as examples of typical behavior. Because most T-beams differed from the other T-beams tested in several respects and the effects of various parameters are often strongly interrelated, only trends rather than more precise quantitative information on how the several variables affect T-beam response can be presented. Parameter studies using the verified mathematical model can better isolate the effects of specific variables.

Many factors affect the deflections of the T-beam specimens. The T-beam behavior is a function of sheathing dimensions and modulus of elasticity, both parallel and perpendicular to the face grain, joist size and modulus of elasticity, sheathing joint conditions, number of sheathing layers, as well as the connector properties. For a T-beam composed of a piece of lumber and one or more layers of

sheathing, the behavior is neither the same as a solid T-beam (equivalent to assuming the connectors have infinite slip modulus) nor the same as two structurally-independent members. The T-beam response between these extremes depends primarily upon the connector properties (see Fig. 4.1). Joist and sheathing dimensions and properties determine how much the fully composite and fully independent behaviors differ.

The effect of the connector types, including nails and elastomeric adhesive, and nail spacing on the overall beam behavior is discussed in Section 4.2. Section 4.3 presents the effect of gaps in the sheathing layers. Results obtained by sequentially testing T-beam specimens with an increasing number of gaps cut in the sheathing perpendicular to the joists are also included.

The effect of the thickness, species, and number of sheathing layers on the T-beam stiffness are treated in Section 4.4. Linear and nonlinear behaviors of the T-beams, modes of failure, and other behaviors are discussed in the last section of this chapter.

4.2 Effect of Connectors

Connectors play an important role in the composite design used in several civil engineering applications. Nails and elastomeric adhesive are the most commonly used connectors in wood housing construction. The latter has been gaining popularity in recent years. Connectors other than nails and elastomeric adhesive are not widely used at present and were not included in the test program.

In this study, specimens were connected using 8-penny common nails as connectors between the plywood and joist layers, as described in Chapter 2. The sheathing and joist layers of four specimens were connected with elastomeric adhesive. Two other specimens included a third layer attached with six-penny cement-coated nails.

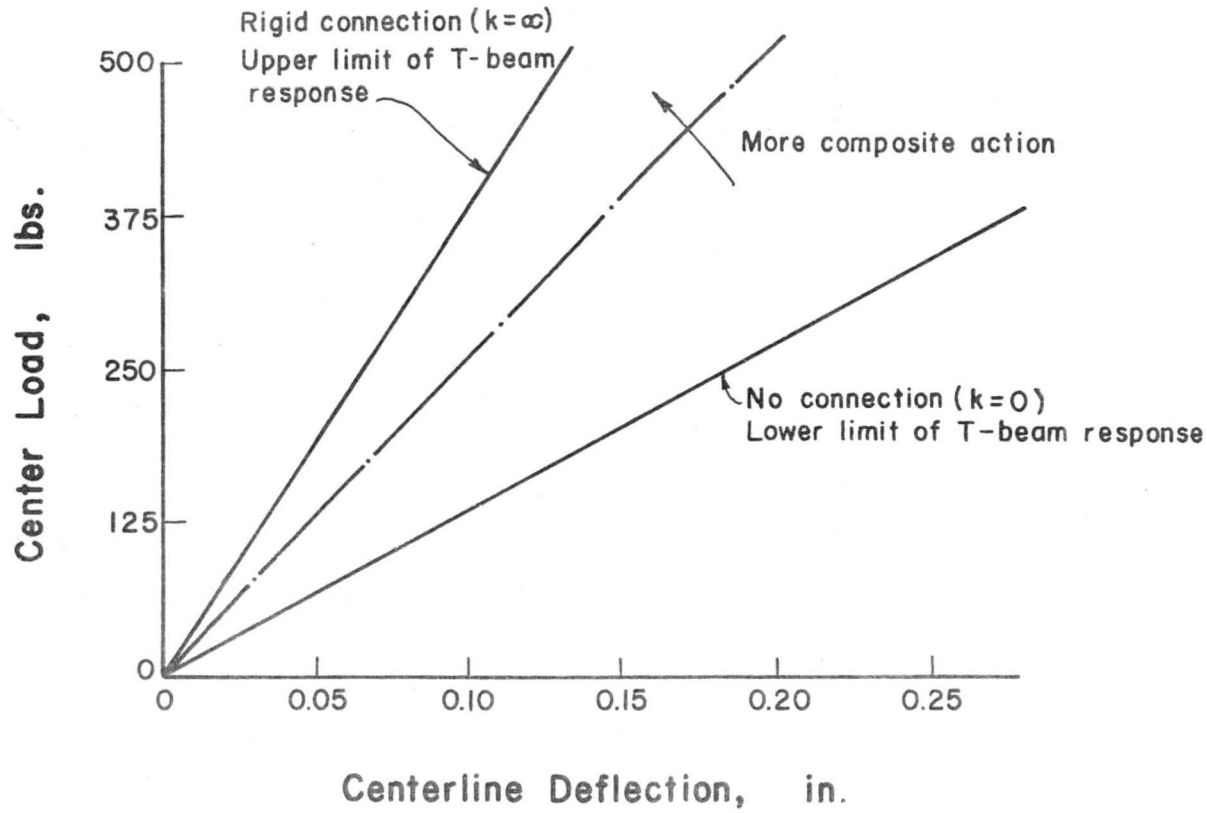

FIGURE 4.1 TYPICAL LAYERED BEAM BEHAVIOR

The spacing of nails along the joist has a significant effect on the overall stiffness of the systems. The observed increase of the system stiffness was roughly inversely proportional to the nail spacing. As shown in Fig. 4.2, the smaller the spacing, the greater the stiffness. The percentages of increased stiffness for specimens nailed at an 8 inch spacing were scattered because of the differences in joist and plywood properties.

The specimens tested with the joist and sheathing glued together showed higher stiffness than those which were nailed. One glued specimen, T8-8D16-1, was nail-glued with 8-penny common nails spaced 8 inches apart. The stiffness of this T-beam was not appreciably greater than the other glued specimen without this nailing.

Most T-beams were constructed with either tightly butted unglued tongue and groove (T & G) sheathing joints or with the T & G joints glued along its length. For the nailed specimens, the increase of stiffness over that for the joists only was considerably higher for the glued T & G joint specimens than for the beams with unglued T & G joints. For the glued specimens, the sheathing joint conditions did not show an appreciable effect. The effect of sheathing joints will be further discussed in Section 4.3.

The tests confirmed that stiffness of a T-beam can be increased appreciably by using glue or more closely spaced nails to increase the shear connection between the layers of the T-beam.

4.3 Effects of Gaps in the Sheathing Layers

Gaps in the sheathing layer(s) are unavoidable in wood construction because of limitations on the sheathing dimensions imposed by the manufacturing process, product standardization, and a

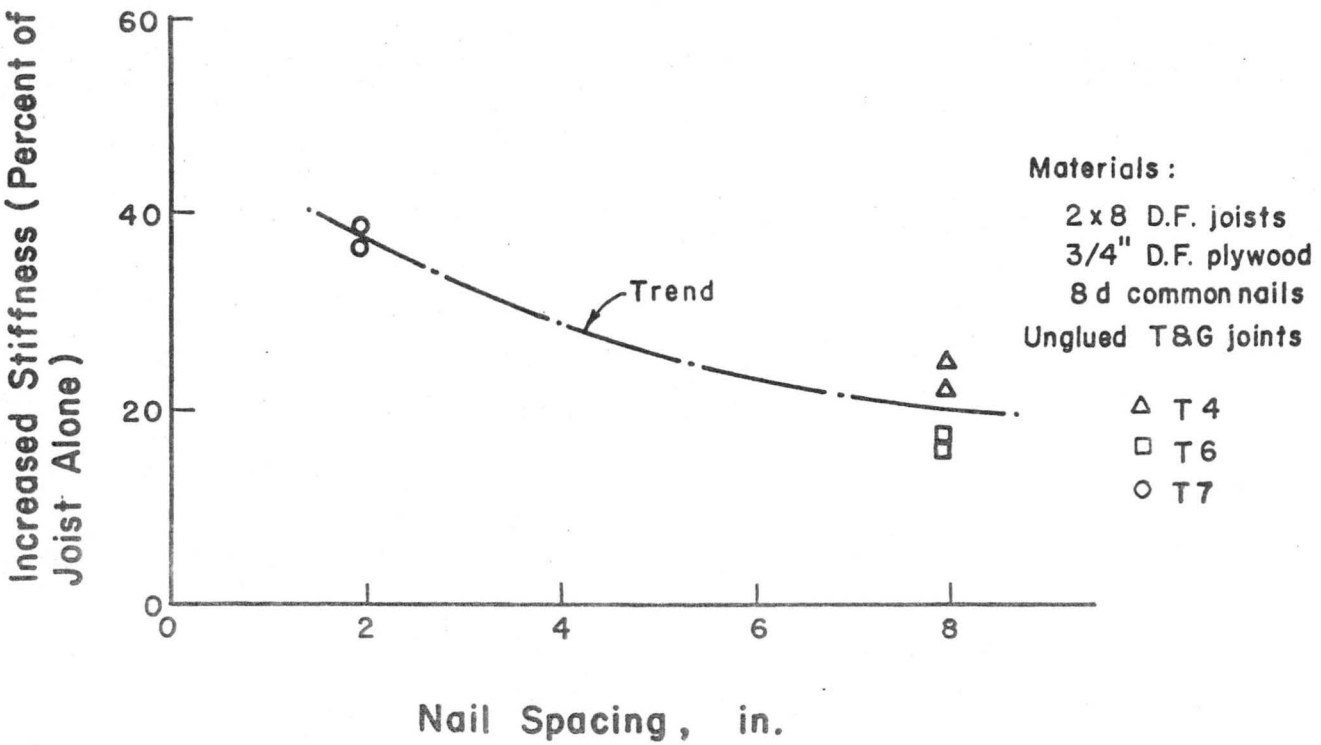

FIGURE 4.2 INCREASE IN STIFFNESS VERSUS NAIL SPACING

need for joints to allow the shrinkage or expansion accompanying changes of temperature or moisture content in the sheathing material. Butt, tongue and groove, shiplap, and other jointing techniques are used in sheathing constructions. Although T & G joints either glued or tightly butted were used in the construction of a majority of test specimens included in this study, some specimens were constructed using joints with open gaps of 1/16 inch.

The presence of gaps in sheathing layer can lower the overall stiffness of T-beams significantly. Local areas of the sheathing including joints constructed with glued or unglued T & G joints were not as stiff as the sheathing material itself; but were, of course, stiffer than when open gaps were used. The treatment of sheathing joints in the verification of mathematical model will be discussed in Chapter 5.

Cutting gaps in the sheathing layer at midspan of a T-beam led to considerably more increase of deflection than did cutting a gap at other locations. For specimen T12-8D16-1, the overall stiffness was reduced by a great amount after a gap at the center was cut, see Fig. 4.3. The sheathing layer of another specimen, T10-12E24-1, was cut at third points (4 foot intervals). The load-deflection behavior of this heavily loaded beam is shown in Fig. 4.4. A gap at the center would be expected to have a larger effect than a gap cut elsewhere because the concentrated load applied at the midspan of the beam with simply supported ends produces greatest moment at midspan. A gap cut at that point results in the total loss of composite action at the most critical location.

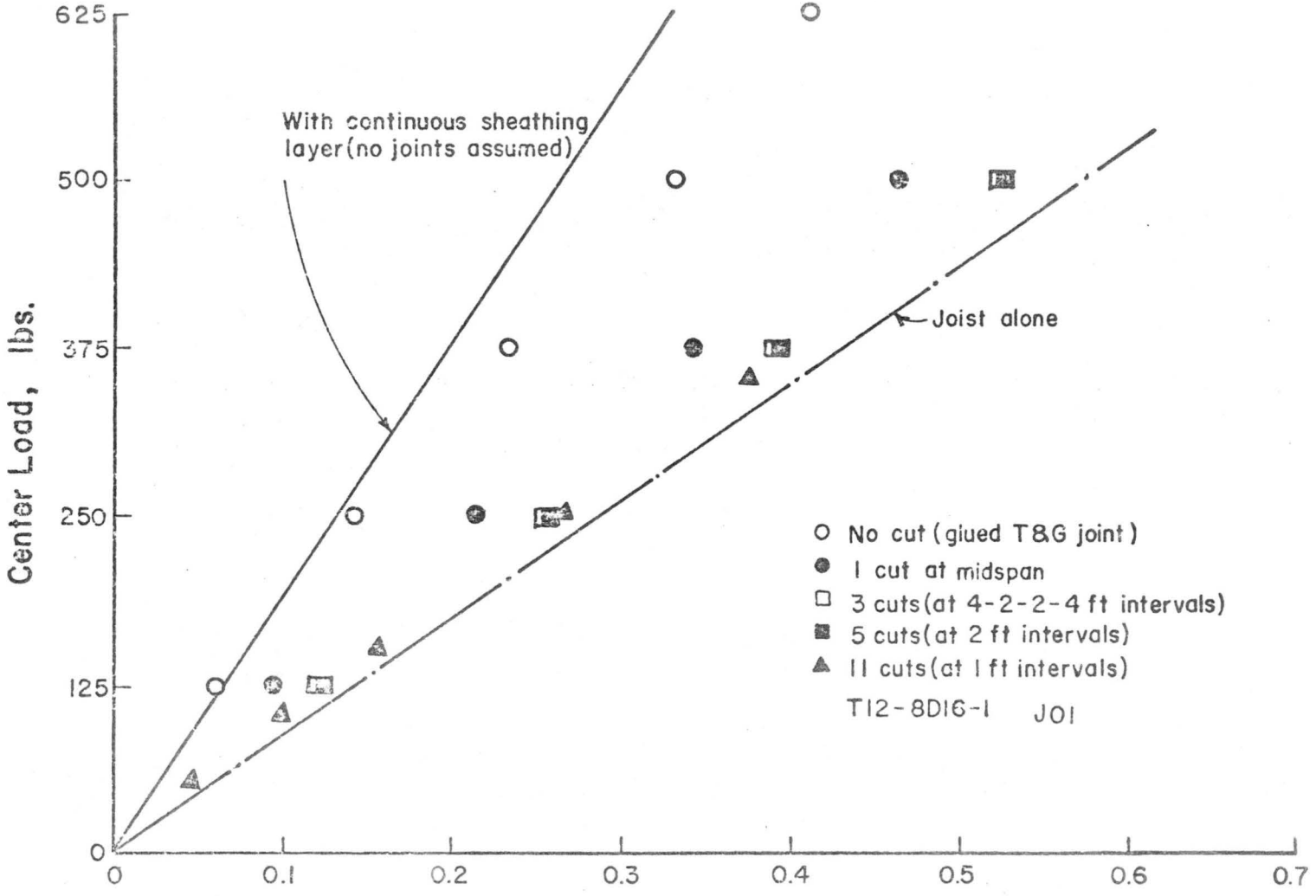

FIGURE 4.3 EFFECT OF CUTTING GAPS ON T-BEAM BEHAVIOR, SPECIMEN T12

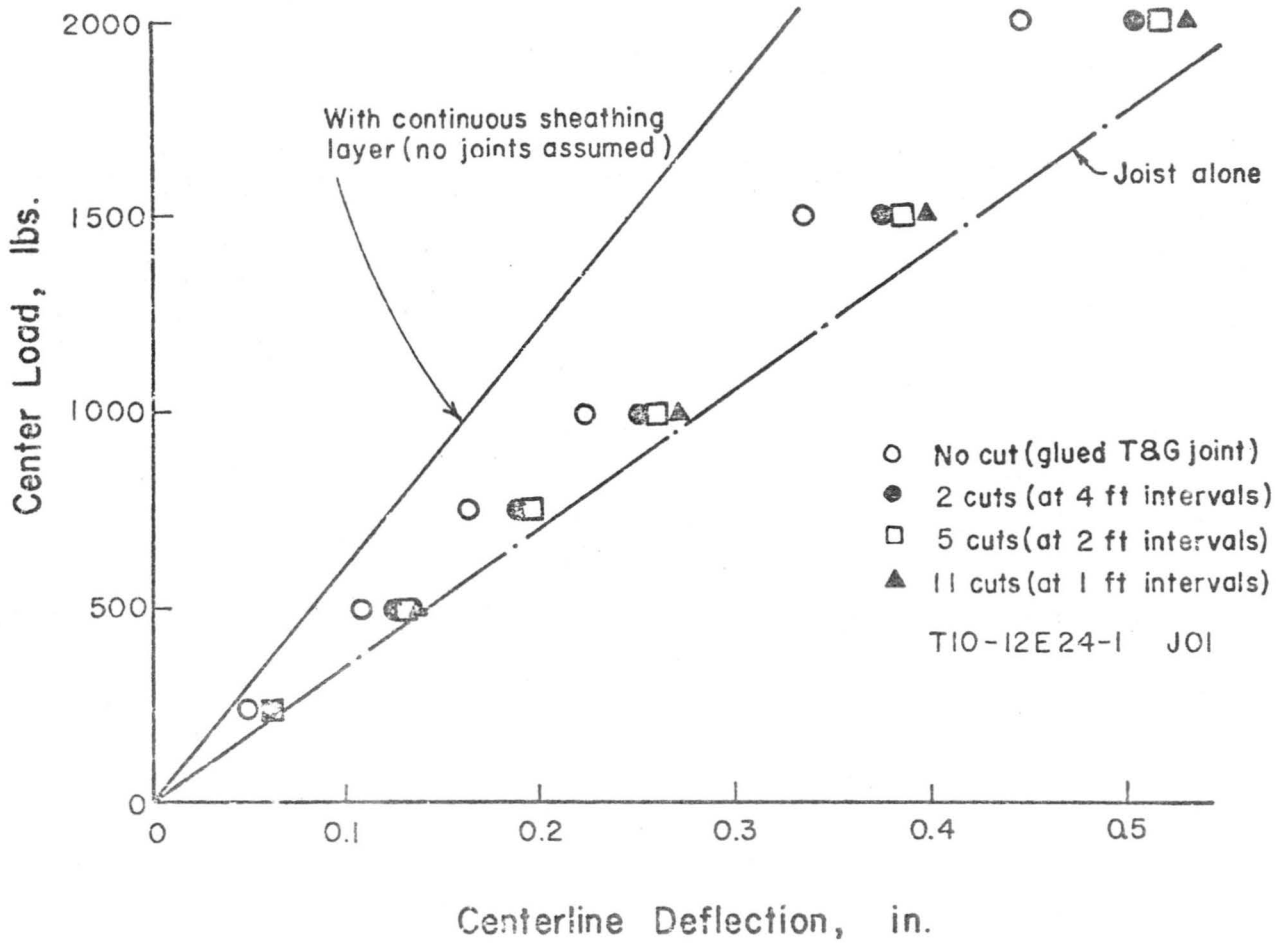

FIGURE 4.4 EFFECT OF CUTTING GAPS ON T-BEAM BEHAVIOR, SPECIMEN T10

The effect of cutting gaps at locations far from the midspan was small. Fig. 4.5 illustrates the much smaller effect when sheathing joints were introduced at a low moment location. These data are from a specimen with the sheathing layer cut only at two feet from both ends and loaded at the midspan. The increase in deflection did not change appreciably from the no gap condition.

The stiffness of the T-beam was gradually reduced as the number of gaps cut in the sheathing was increased. With one foot gap intervals, the stiffness of the T-beam specimens T10 and T12 was close to that of a single joist acting alone, showing that the composite action of T-beam was nearly destroyed.

In the T-beam tests, the gaps of the sheathing layer began to close as the applied loading was increased. Further loading often brought the two edges of the sheathing into contact. This closing of the gaps produced a partial continuity for the sheathing layer. The resulting partial composite action increased the stiffness of the T-beam. With still further increases of the applied load, the contact surface area also increased and produced still more composite action and stiffness for the T-beam. Most T-beams tested having butted sheathing joints displayed this behavior when loaded above the service load level, see Fig. 4.6. When the gap width was increased to 1/8 inch, the beam did not show this kind of behavior because the closing of these wider gaps was not accomplished even at overload levels.

T-beam with glued sheathing joints developed more of their potential stiffness due to composite action than did those having either tightly butted or open gaps.

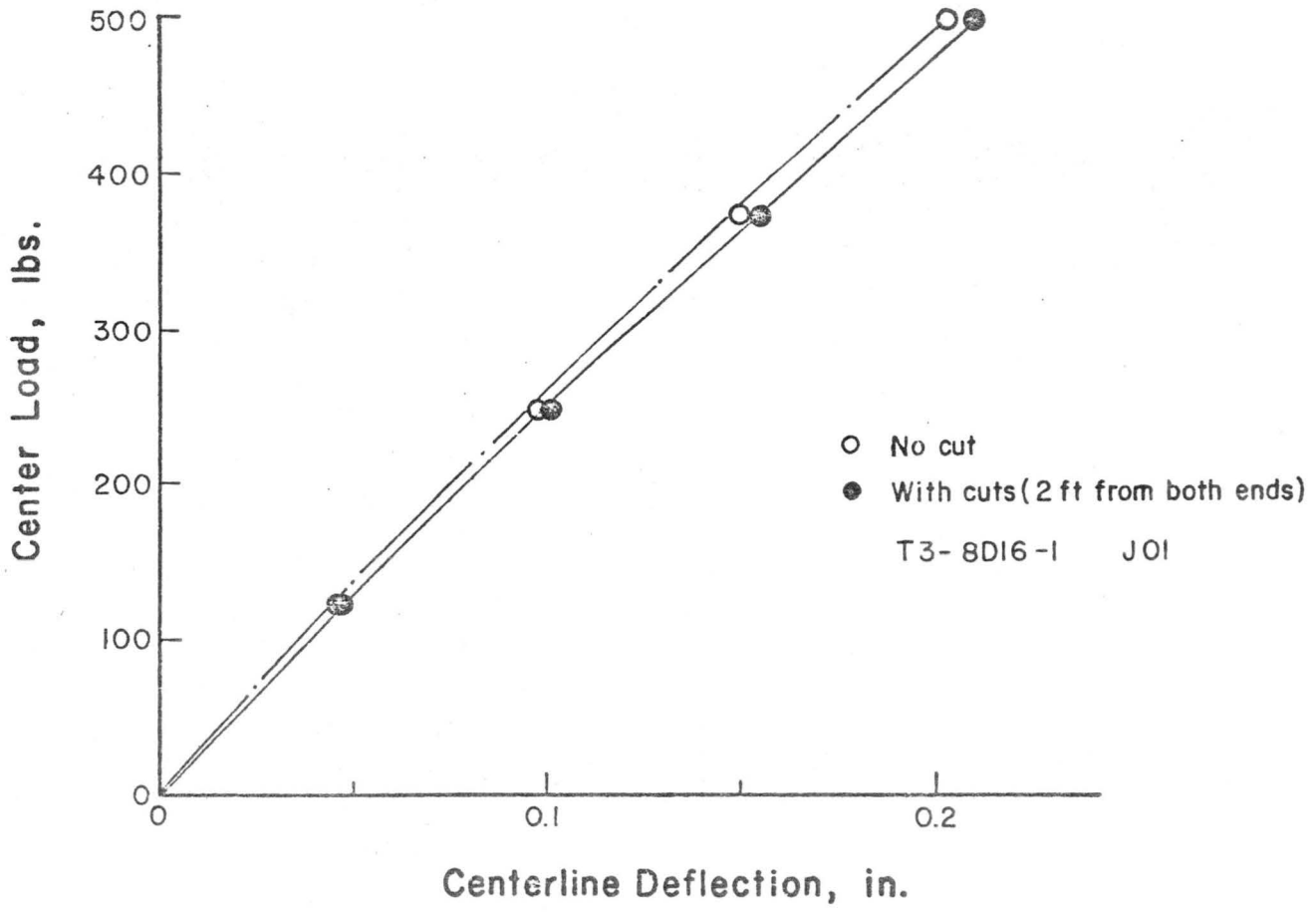

FIGURE 4.5 EFFECT OF CUTTING GAPS ON T-BEAM BEHAVIOR, SPECIMEN T3

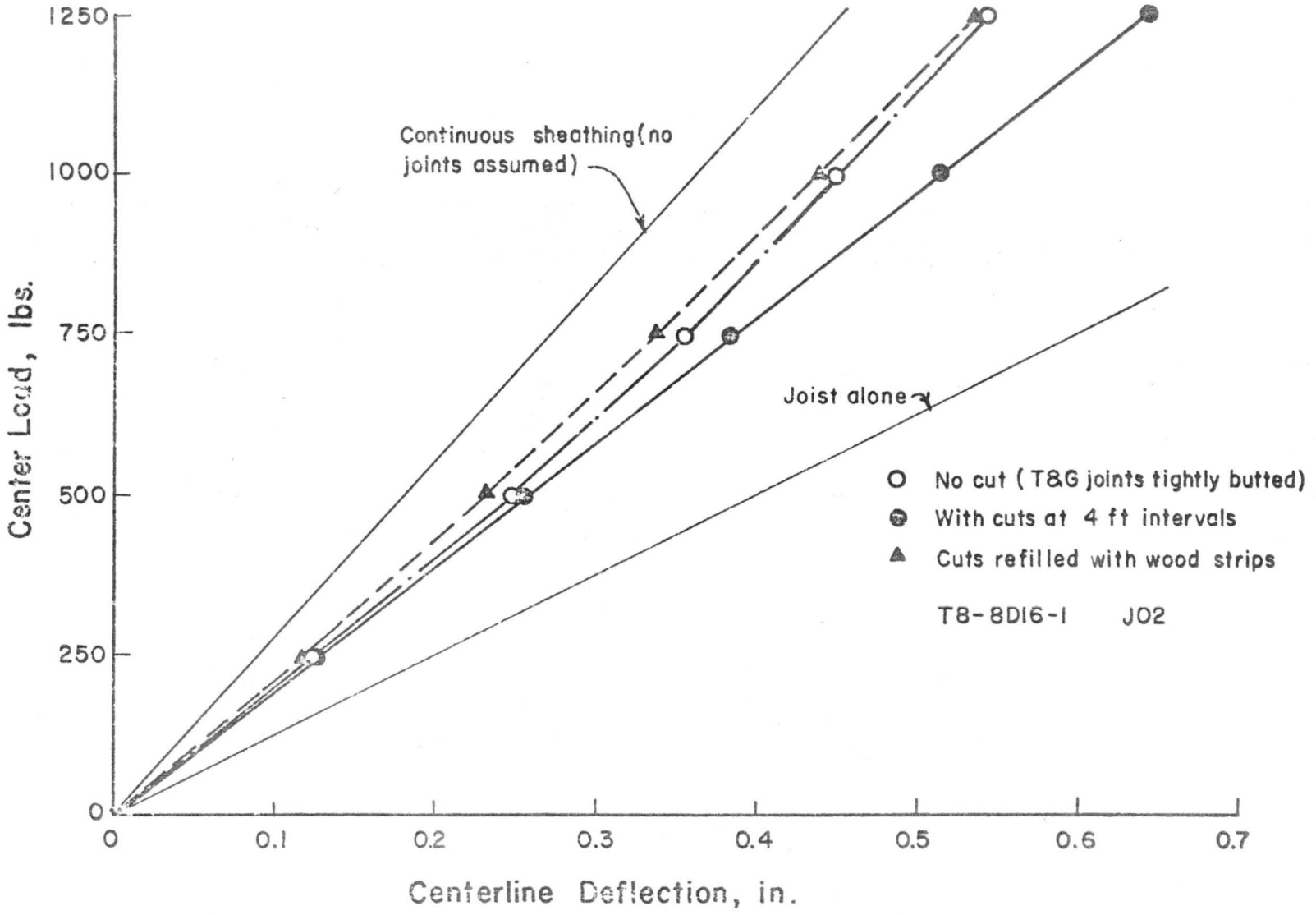

FIGURE 4.6 BEHAVIOR OF T-BEAM WITH SHEATHING GAPS CUT AND REFILLED

4.4 Effect of Sheathing Layers

The modulus of elasticity and dimensions of the sheathing layers are among the many factors known to affect the behavior of a layered beam. For T-beam constructed with large joists having high MOE values, and a thin, weak sheathing layer, such as specimen T14-12D24-1, composed of 2x12 Douglas fir joists and 1/2 inch thick plywood, the increase of overall stiffness compared to joist alone was not appreciable. When the T-beam consisted of smaller joists and a thick, stiff sheathing layer, the conditions for specimen T4-8D16-1 for instance, the increase in overall stiffness was appreciably larger.

The addition of a second sheathing layer (particleboard) to specimens T14, T15 and T16 increased the overall stiffness of these T-beams appreciably over that of the two layer joist-sheathing configuration. These three specimens were constructed with 1/2 inch thick plywood having relatively low MOE values as the first sheathing layer, and with the additional layer being 1/2 inch thick particleboard. Fig. 4.7 presents load-deflection plots for specimen T16 in its two-layer configuration, T16-8E19.2-1, and after the particleboard was added, T16-8E19.2-2. The two-layered system showed a relatively linear behavior while the three-layered system showed a more nonlinear behavior at service load levels.

4.5 Nonlinear Behavior and Mode of Failure

Most T-beams tested exhibited a nonlinear response when subjected to overloading. Some creep under sustained loading was observed. Rate of creep is known to be dependent both upon time and load level. Fig. 4.8 displays the creep deflections observed over a ten minute period for specimens T11-8D16-1 and T12-8D16-1 with total load on the

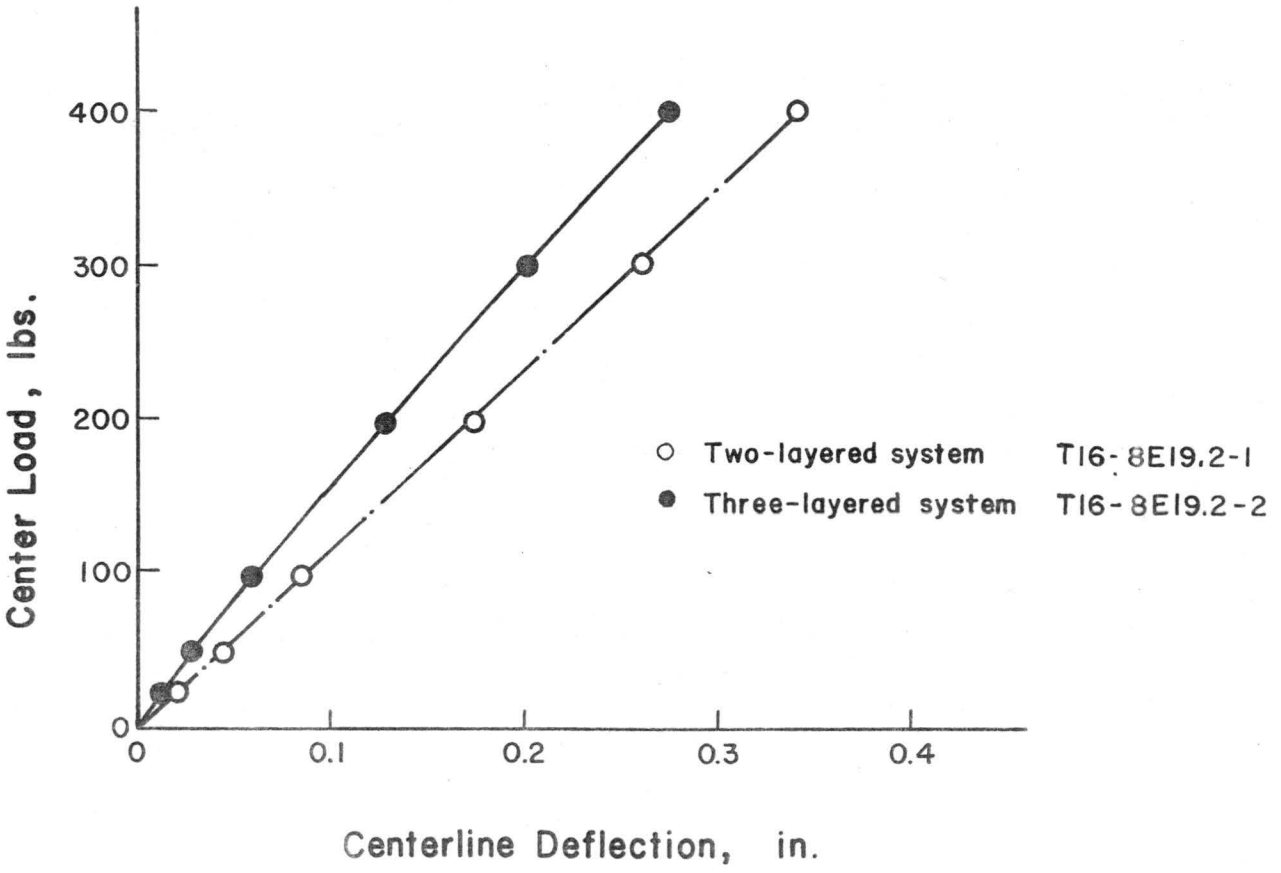

FIGURE 4.7 TYPICAL LOAD-DEFLECTION BEHAVIOR OF TWO- AND THREE-LAYERED T-BEAMS

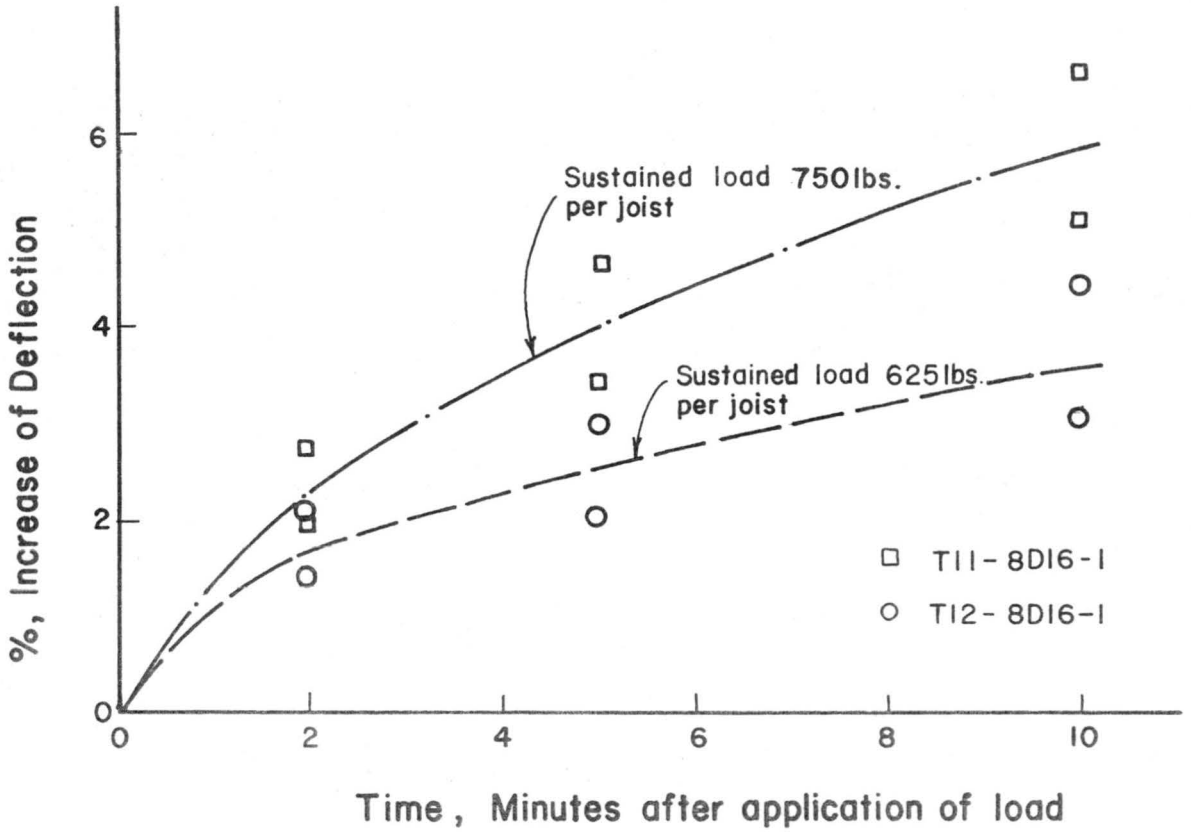

FIGURE 4.8 CREEP AT SUSTAINED LOADING LEVELS

two joists being 1500 pounds and 1250 pounds, respectively for the two T-beams. It should be noted, however, that these load levels are fairly high and above normal working load levels.

These additional time-dependent or creep deflections may account for some of the difference between the computed values and the observed deflections reported in Chapter 5. It should be noted, however, that in the static testing, each loading increment was completed within two minutes or less, thus the creep deflections were minimized and should have been less than 2 percent of measured values in most cases.

Fig. 4.9 displays some hysteresis loops from the loading and unloading of specimen T7-8D16-1. The load during the first cycle only was applied in 250 pounds increments. The horizontal movement of the load-deflection plot shows the inelastic behavior occurring during measurement of the deflections at each load increment, which usually took one to two minutes to complete. A sizable hysteresis loop occurred during the initial unloading and a small residual deflection was observed. This residual deflection was gradually recovered, although only slowly. In the subsequent reloadings and unloadings, the load history remained nearly constant.

Cyclic loading behavior was studied for one T-beam. Specimen T13-8D16-1 was loaded until the center deflection was just over L/360 to obtain the initial load-deflection plot. Then the specimen was subjected to cyclic loading at service load level. The cylic loading induced was the ramp function shown in Fig. 2.7. All load was applied at the midspan of the specimen. After 1600 cycles of loading, deflections were again measured. Load-deflection curves obtained

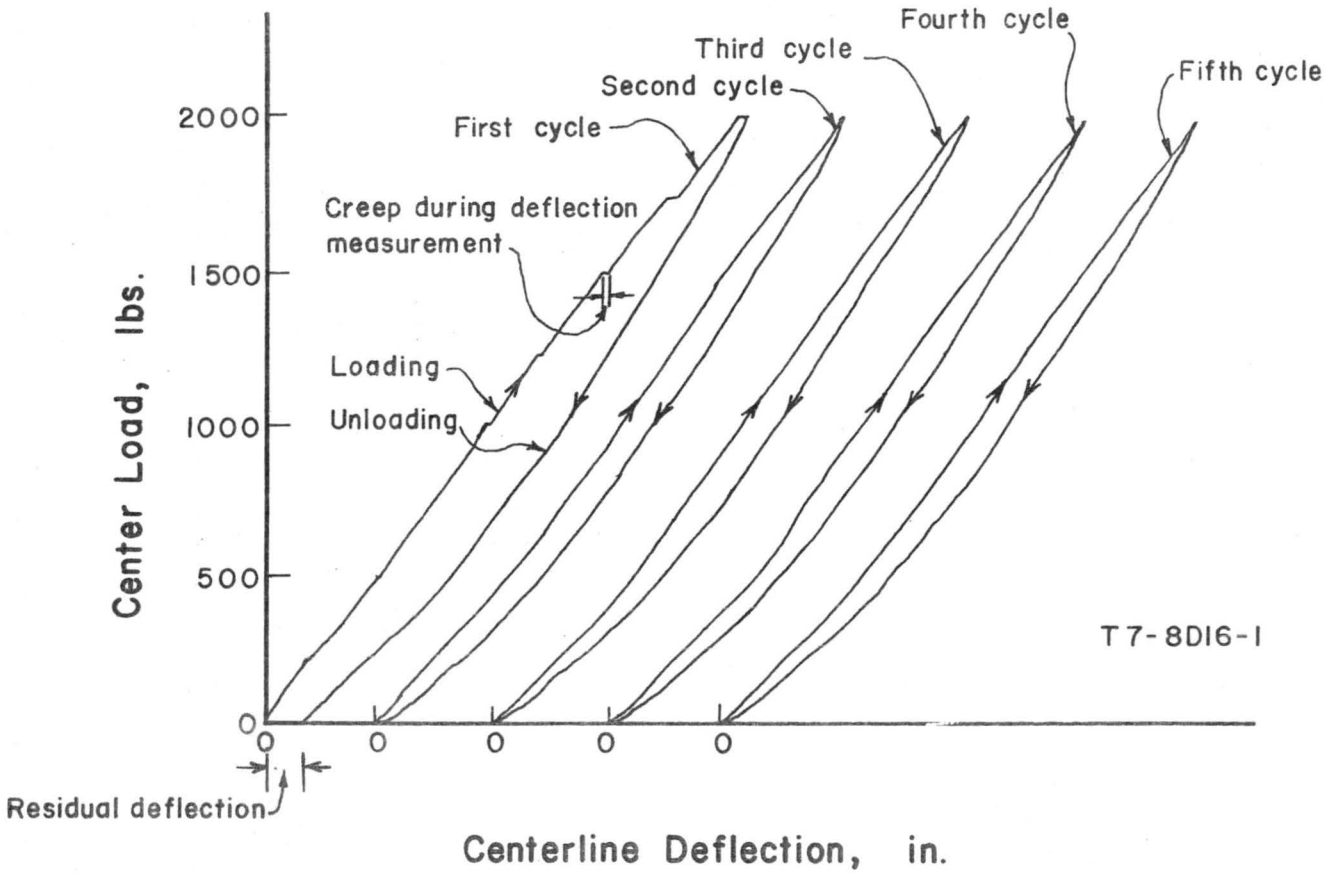

FIGURE 4.9 TYPICAL HYSTERESIS LOOPS FOR T-BEAM SPECIMEN T7

before and after cylic loading are compared in Fig. 4.10. Behavior of this specimen was observed prior to, during, and after the cylic loading. Most nail heads observed were pulled into the plywood about 1/32 to 1/16 in. deep during the prolonged cyclic loading. A more linear load-deflection behavior was obtained after the cylic loading.

Elastic, inelastic behavior and mode of failure of wood floors and T-beams have been presented by Penner (23). A brief additional discussion is added here to aid in the understanding of T-beam behavior.

Fig. 4.11 shows a typical load-deflection plot, obtained with an X-Y recorder and using the deflection detected by the actuator LVDT, when the specimen was tested to failure. As the load increased within and slightly above the service load range the slope became slightly greater. This is believed to have resulted from the closing of the sheathing gaps as discussed in Section 4.3. Creep during the time between load increments increased somewhat at the higher load levels, and nonlinear behavior increased. The nonlinear slip modulus of the nails likely contributed to this behavior, especially where withdrawal forces on the nails were large. The joist began to split for this specimen as the load was increased to 4500 pounds. The splitting propagated as load increased further, and eventually extended through the entire joist depth. Fig. 4.12 illustrates some types of observed joist failures during the overload test.

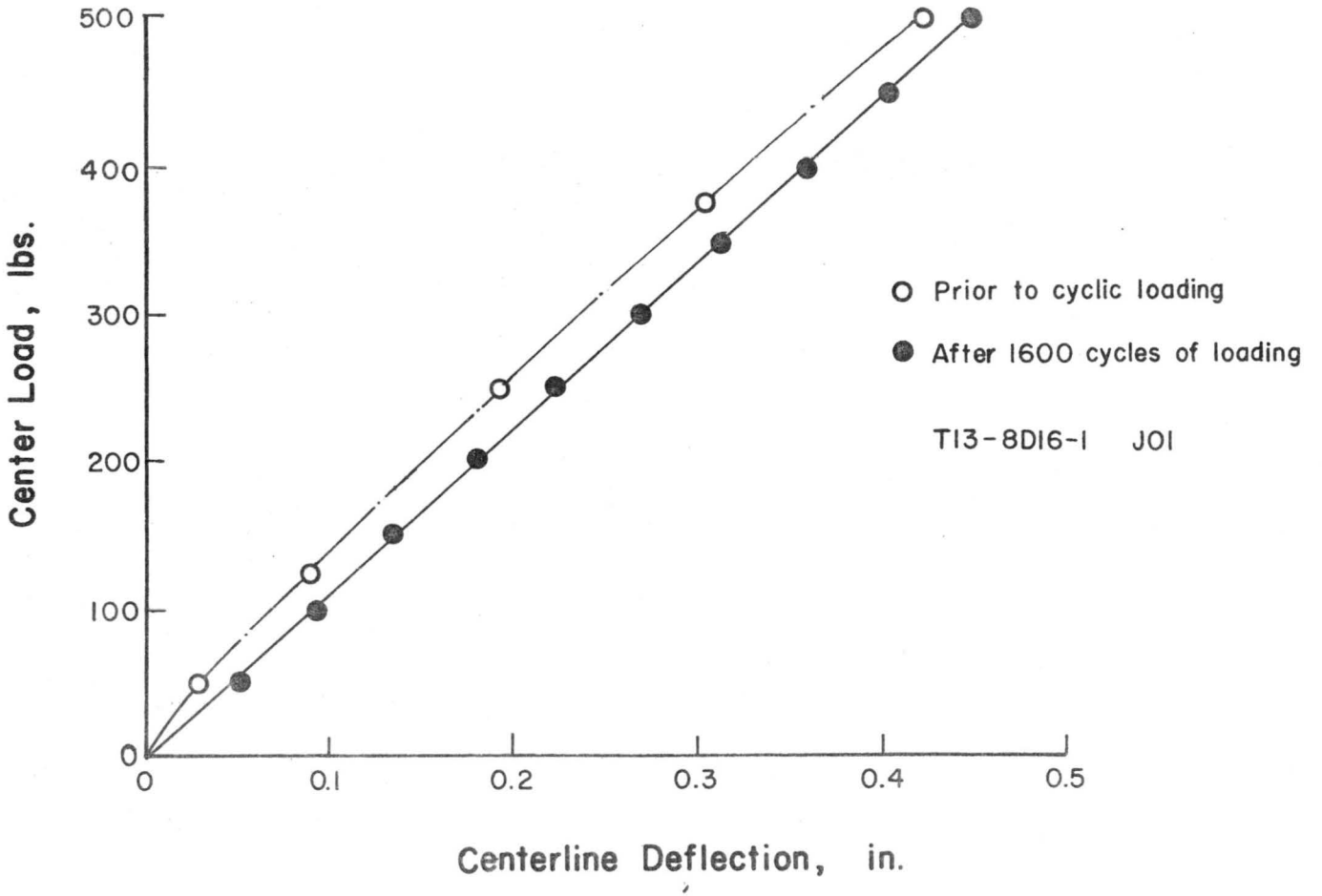

FIGURE 4.10 T-BEAM BEHAVIOR PRIOR TO AND AFTER CYCLIC LOADING

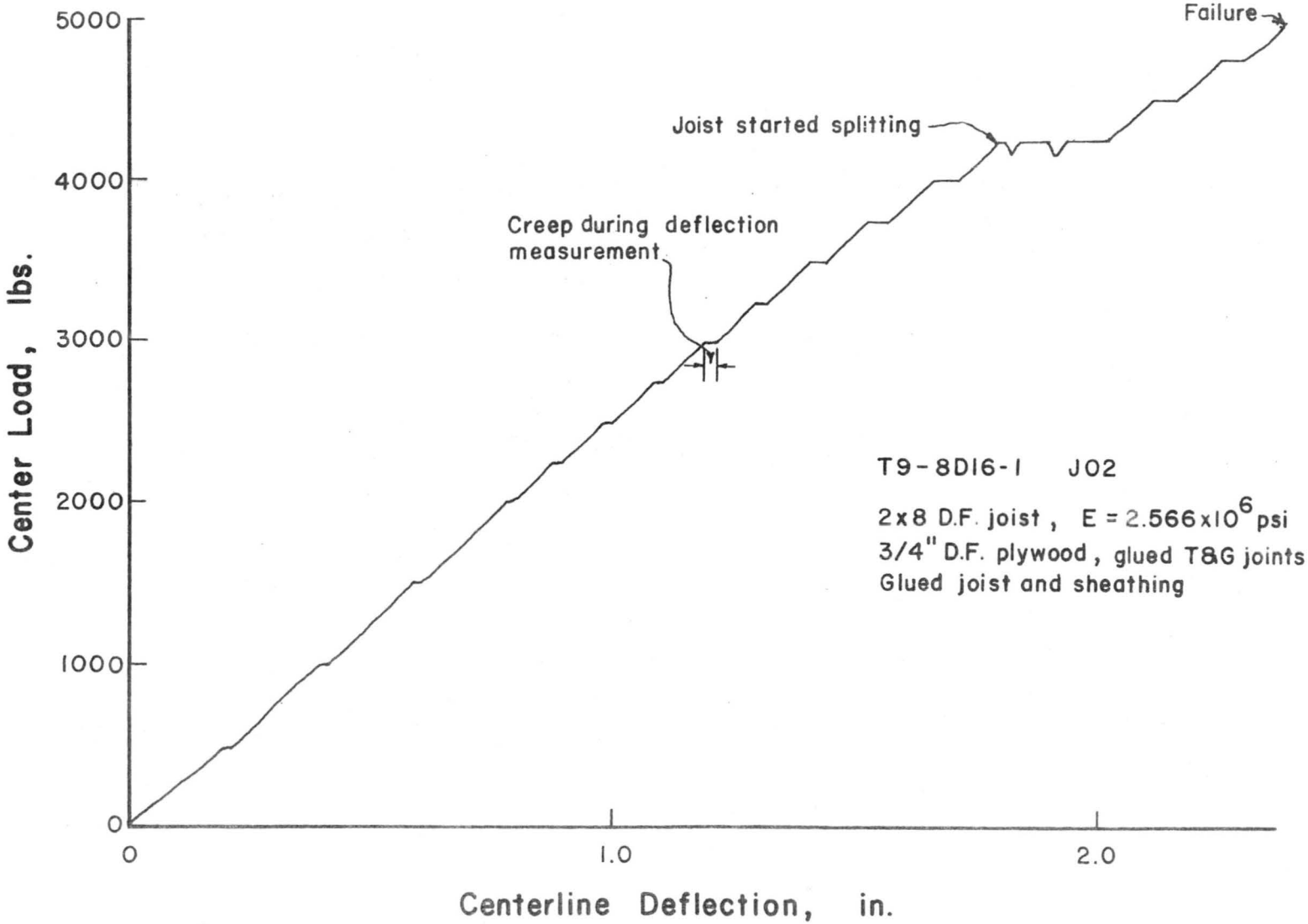

FIGURE 4.11 TYPICAL LOAD-DEFLECTION BEHAVIOR OF A T-BEAM LOADED TO FAILURE

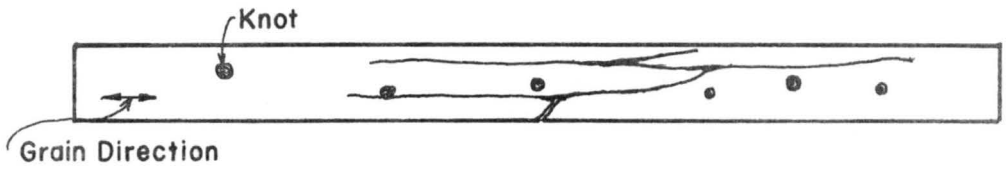

T8-8D16-1 J01

T9-8D16-1 J02

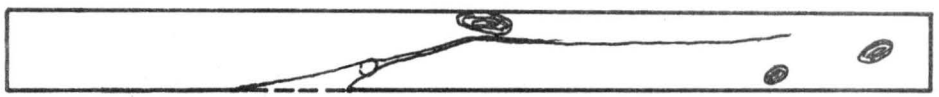

T11-8D16-1 J01

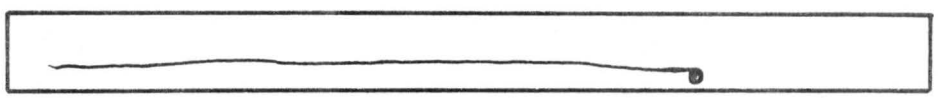

T14-12D24-1 J02

T15-8E19.2-2 J01

T16-8E19.2-2 J02

FIGURE 4.12 TYPICAL FAILURE TYPES OF T-BEAM

CHAPTER 5

VERIFICATION OF THE MATHEMATICAL MODEL FOR T-BEAM BEHAVIOR

5.1 Introduction

The primary purpose for the T-beam tests presented in this report is to provide the necessary data needed for verification of the developed mathematical model. At present the beneficial effect of composite action on the T-beam response is generally ignored in the analysis of such systems. The verification of the mathematical model along with some details of the model are presented in this chapter.

Studies on T-beam and composite action effects presented by several investigators have been reviewed in Chapter 1. Two studies concerned with developing mathematical solutions for computing T-beam deflections have been conducted within overall research effort which includes the T-beam tests reported in the previous chapters. The ability of these two methods to match the experimental T-beam results is presented in this report. The theoretical solution for the mathematical model, based on beam theory with consideration of interlayer slip, was developed by Goodman (8, 9) and extended by Kuo (16). Particular attention was given to two-layered systems with one axis of symmetry. Thompson et al. (27) have expressed this basic mathematical model in a different form using the potential energy theorem. This method uses a finite element solution technique and can include the effect of gaps within the individual layers. The formulation of the above two basic solution techniques for the mathematical model, which forms the basis for the experimental verification, is reviewed in Section 5.2.

The selection of material parameters such as MOE of the joists and sheathing materials, and the slip moduli of connectors used in mathematical verification is presented in Section 5.3.

Deflections measured during the T-beam tests and those computed using the theory are compared in Section 5.4. The mathematical model has also been used to compute the deflections of some composite beams tested by a joist manufacturer. These results are presented to show the validity of the mathematical model for uniformly-loaded T-beams.

5.2 Mathematical Model of T-Beam and its Solution Techniques

The general layered beam theory discussed in Chapter 1 can be specialized to the case of a two-layered beam with one axis of symmetry. The basic assumptions used in developing the beam theory, as outlined in Chapter 1, are small deflections, linearly elastic matierials, linear variation of strains over the depth of each layer, linear slip modulus, negligible shear deformations, and equal curvature of each layer during bending. Fig. 5.1 shows a typical two-layered T-beam, along with some of the notation used for the development of the mathematical model. Two governing equations for this system are given as follows (for more detailed treatments, refer to Goodman (8) and Kuo (16)):

$$\frac{d^2y}{dx^2} = \frac{-M_T + C_{12}F}{E_1I_1 + E_2I_2} \tag{5.1}$$

$$\frac{S}{kn}\frac{d^2F}{dx^2} = \left[\frac{1}{E_1A_1} + \frac{1}{E_2A_2}\right]F + C_{12}\frac{d^2y}{dx^2} \tag{5.2}$$

where E_i = the modulus of elasticity of the i^{th} layer, lb/in^2,

I_i = the moment of inertia of the i^{th} layer about its own neutral axis, in^4,

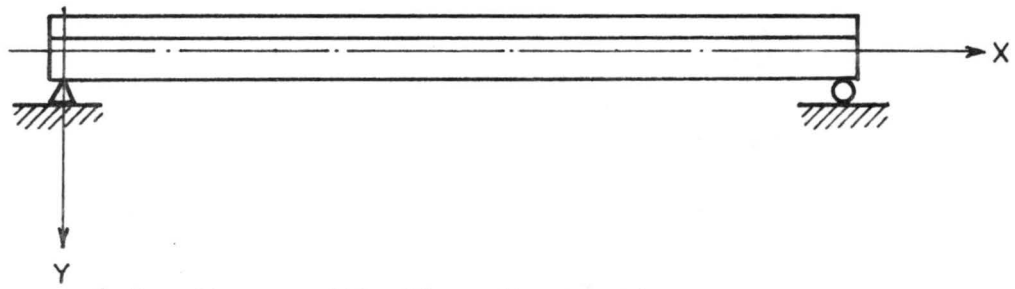

(a). Beam with Sign Convention

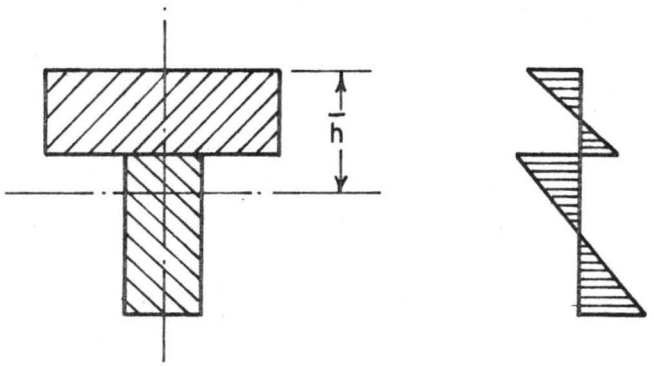

(b). Cross-section

(c). Strain Distribution

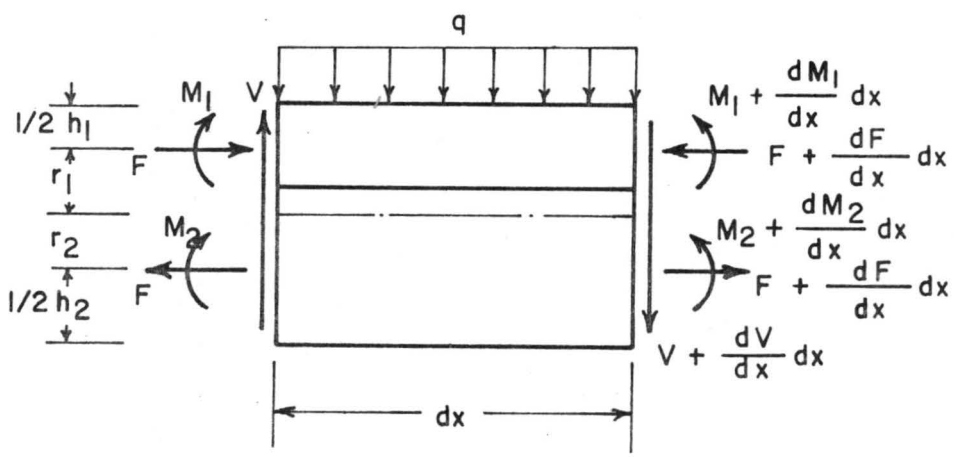

(d). Beam Element

FIGURE 5.1 TWO LAYERED SYSTEM

A_i = cross section area of the i^{th} layer, $in.^2$,

S = the spacing between connector rows along the beam length, in,

k = the connector modulus per connector, lb/in,

n = the number of connectors per row,

M_T = total applied moment, in-lb, $C_{12} = \frac{h_1 + h_2}{2}$.

Solving this system for a beam with a uniform load and applying the boundary conditions for a simply supported beam leads to the following closed form solution for the beam deflections:

$$y = y_s + \frac{1}{C_1} \left[\frac{C_{12}}{E_1I_1 + E_2I_2}\right] F \tag{5.3}$$

where $F = \frac{C_2}{(C_1)^2} q \left[\cosh (\sqrt{C_1}\, x) + \frac{1 - \cosh (\sqrt{C_1}\, L)}{\sinh (\sqrt{C_1}\, L)} \sinh ([\sqrt{C_1}\, x) - 1\right]$

$+ \frac{C_2}{C_1} \frac{q}{2} x (L - x)$ = axial force in each layer.

$$C_1 = \frac{kn}{S} \left(\frac{1}{E_1A_1} + \frac{1}{E_2A_2}\right) \frac{I_s}{I_1 + I_2} ,$$

$$C_2 = \frac{kn}{S} \left[\frac{C_{12}}{E_1I_1 + E_2I_2}\right] ,$$

I_s = the moment of inertia of the rigidly connected section, $in.^4$,

y_s = deflections of the rigidly connected beam.

When computing the theoretical deflections of a beam using this closed form solution, the section properties, connector modulus and spacing must be assumed to be constant along the length of the beam.

To eliminate these restrictions, a finite difference solution technique, which is a numerical approach for solving differential equations directly by approximating the infinitesimal region in a discrete manner, may be used (26). This solution technique leads to a set of simultaneous equations which can be written in the following matrix form (16):

$$[H]\{F\} = \{C_2 L^2 M\} \tag{5.4}$$

where [H] = square matrix combining all finite difference operators,

L = length of the simply-supported beam.

The deflections of a rigidly connected beam, y_s, can be obtained from another set of equations:

$$[R]\ \{y_s\} = \{-\frac{6qL^4}{n^2 EI_s}(1 - z)z\} \tag{5.5}$$

where [R] = square matrix combining all finite difference operators.

z = x/L, $0 \leq z \leq 1$

Once $\{F\}$ and $\{y_s\}$ are solved from Eqs. (5.4) and (5.5), the total beam deflection y can be computed from Eq. (5.3).

The finite difference approximation still assumes continuous layers, i.e., no gaps may exist in the individual layers in the model.

A closed form solution and finite difference approximation for a concentrated load on a simply supported beam can be derived following basically the same procedure. Solution techniques for a three-layered system with uniformly distributed and concentrated load parallel those for a two-layered system (16).

Due to the limitations of these two approaches, a more versatile technique is needed in order to consider the properties displayed by real floors and beams, to allow consideration of more general loading conditions and to include gaps in the sheating.

Thompson et al. (27) have presented such a solution technique: a finite element method using the same mathematical model and basic assumptions utilized by Goodman (8), along with the introduction of potential energy concepts. Energy expressions from the following sources are developed and included in the solution for the layered beam problem:

1. pure bending of each layer,
2. axial elongation of each layer,
3. slip deformation of the connectors between each layer, and
4. external loads on the beam.

By including all the potential energy resulting from the forces above, the total potential energy of an m-layered beam is

$$J = \sum_{i=1}^{m} \int_{o}^{L} \left\{ \tfrac{1}{2} E_i I_i \left(\frac{d^2y}{dx^2}\right)^2 + \tfrac{1}{2} E_i A_i \left(\frac{d^2u}{dx^2}\right)^2 \right\} dx$$

(bending) (axial loads)

$$+ \sum_{i=1}^{m-1} \int_{o}^{L} \left[\tfrac{1}{2} \left(\frac{k_i n_i}{S_i}\right) (u_{i+1} - u_i) - \tfrac{1}{2} (h_{i+1} + h_i) \frac{dy}{dx} \right]^2 dx$$

(slip deformation)

$$- \int_{o}^{L} qy \, dx \qquad (5.6)$$

(external loads)

where J = total energy, in.-lbs.,

u_i = axial displacement in i^{th} layer, in.

The principle of virtual work requires that the potential energy reach a stationary value at the equilibrium position of the layered beam. Using the variational principle, this requirement may be expressed as (δ = variational operator)

$$\delta J = 0 \tag{5.7}$$

The deflection and axial displacements of the layered beam must satisfy Eq. (5.7) and can be approximated with the finite element form of the Rayleigh-Ritz procedure. This allows direct solution of the differential equation using an approximate minimization of the functional (31). Formulation of the finite element solution technique is shown in Appendix F.

The three solution methods discussed above yield nearly identical answers when the limitations of the methods are met. This can be demonstrated by comparing the deflections predicted by each method for the same problem. As an example, consider the two layered beam with the following properties:

Specimen T4-8D16-1, Joist No. 1

Joist E = 2.43×10^6 psi

Plywood E = 5.50×10^5 psi

Slip modulus k = 30,000 lb/in.

Nail spacing 8 inches

Load level 500 lb.

Load at midspan

Number of elements 24

Midspan deflection for this specimen obtained by each method using separate computer programs are listed in Table 5.1, along with a

comparison of the predicted deflections and the central processor (CP) time used for each technique (CDC 6400 computer, 65k core). Because of its closeness to the exact (closed form) solution and its many advantages cited earlier, the finite element method was used to compute the theoretical deflections in all the subsequent verification calculations.

Table 5.1 Comparison of Solution Techniques

Technique	Closed Form	Finite Difference	Finite Element
Centerline Deflection	0.1980"	0.1985"	0.1978"
Error, %	-	0.24	0.10
CP, sec.	13.991	9.534	7.546

5.3 Computation of Deflection Using the Mathematical Model

Geometrical and mechanical properties of the materials used in the T-beam specimens must be known so that the T-beam being analyzed by the mathematical model corresponds to the one tested in the laboratory. Some discussion of this necessary input data is presented here to help illustrate how the theoretical deflections were computed from the mathematical model.

As discussed in Chapter 3, the material properties of each piece of lumber and sheathing were individually determined before and during T-beam construction. Joist dimensions entered were those measured during the determination of flatwise MOE in the Wood Science Laboratory. For the joists, both an edgewise MOE value for each piece and a flatwise MOE value for increments along each joist was available. The edgewise MOE obtained during construction of the specimens and with the

joists in their final configuration, as described in Chapter 3 (three nails driven through the header), was used rather than the flatwise MOE. Since the former were based on the actual orientation of the joist, they are thought to better estimate the actual MOE for the joists as used. The MOE values for the sheathing material, either parallel to or perpendicular to the face grain as needed, were provided by the Wood Science Laboratory.

Shear deformations were neglected in all the MOE values used with the mathematical model. This was desired because the mathematical model currently does not include shear deformations directly. The shear deformations can be included indirectly by entering MOE values also determined neglecting shear deformations, values slightly below the true E values. Negligible errors result if the span to depth ratios, or alternately, the moment to shear ratios, of the materials during the MOE determination and in the T-beam specimen are similar, a condition which was met in these tests.

The MOE values for the joists were assumed to be equal for both bending and axial loading, which is equivalent to assuming the material is homogeneous throughout the joist depth. For the plywood, this condition obviously is not met, and the effect of ply thickness and orientation on the bending and axial stiffness must be recognized.

The modulus of elasticity values reported for the plywood are gross values valid for bending only and based on the moment of inertia of the full measured thicknesses (1/2 in. and 3/4 in. for Douglas fir, 3/8 in. and 5/8 in. for Engelmann spruce). These values are different from those valid for use with the transformed sections. Although modulus of elasticity values based on the transformed sections are often

used for plywood, the analysis programs were set up to receive gross MOE values based on gross section dimensions as input information. A parameter, k*, which converts the gross MOE values valid for bending to gross MOE values valid for axial load, was determined and input into the programs. Further explanation of this parameter k* along with the values computed for the various plywood species and thicknesses are given in Appendix G. MOE values for both the particleboard and plywood differed in the lengthwise and the crosswise direction because of the particle orientation resulting from the production process and the ply orientation, respectively (18). The MOE values of particleboard for bending and for axial loading causing stresses in the same direction were assumed to be equal.

Slip moduli for both nails and elastomeric adhesive, as determined by the Wood Science Laboratory, are tabulated in Appendix D. The actual load-slip curves are nonlinear (see Fig. 3.5), which results in the slip moduli values decreasing at increasing load levels. Because the program assumes a constant slip modulus (an assumption equivalent to linear load-slip behavior), a slip value representative of the conditions at the desired load level must be selected. Some preliminary calculations indicated that a secant moduli up to a load level of between 100 to 150 pounds per nail provided good results in the working load range. Table 5.2 shows the slip moduli of nails and elastomeric adhesive used in the model verification calculations. A load level extending up to the upper end of the working range and corresponding to deflections approaching values near 1/360 of the span was selected as the load levels of most interest and practical importance.

Table 5.2 Values of Slip Modulus, k

Connector	8-d common nails				Adhesive	6-d common nails	
Joist	Douglas fir		Engelmann spruce		D.F., E.S.	------	
Sheathing	D.F.	E.S.	D.F.	E.S.		Particleboard	
						D.F.	E.S.
	lb/in	lb/in	lb/in	lb/in	lb./in./in^2	lb/in	lb/in
k	30,000	30,000	30,000	18,000	16,000	4,000	3,000

Note: These values are for 8 inch nail spacing. Adjustment is made in the values for other nail spacing due to the difference in nail loads.

All parameters used in the computation of deflections for each T-beam are included in the beam configuration diagrams contained in Appendix E.

The division of a typical T-beam into elements for the computation of the deflections by the finite element method is shown in Fig. 5.2.

Significant increases in deflections resulted from the introduction of open gaps in both the experimental studies and in some parameter studies conducted during the development of the finite element program. These observations, along with some obvious inaccuracies which arose when the theoretical deflections were computed with the assumption that the sheathing layers were continuous, showed that the effects of the sheathing joints present in all the specimens were sizable and had to be carefully modeled.

The introduction of a flexible gap was necessary to properly model the glued and tightly butted sheathing joints present in most specimens. For computing deflections from the mathematical model, these joints were assumed to have finite lengths (about 1/16 to 1/8 in) and a low joint stiffness. MOE values for the joints were assumed and good results were obtained with values ranging from 500 psi for tightly butted joints to about 5×10^3 psi for glued joints.

The finite element solution technique is capable of easily handling a true (open) gap resulting from either the joint being left open during construction or the sheathing being sawn later. When such a gap occurs in a given layer, the axial displacement in that layer is no longer continuous and the axial force becomes zero.

Current studies indicate that negligible errors will result, for the beam configurations used, from assuming the entire flange width is effective.

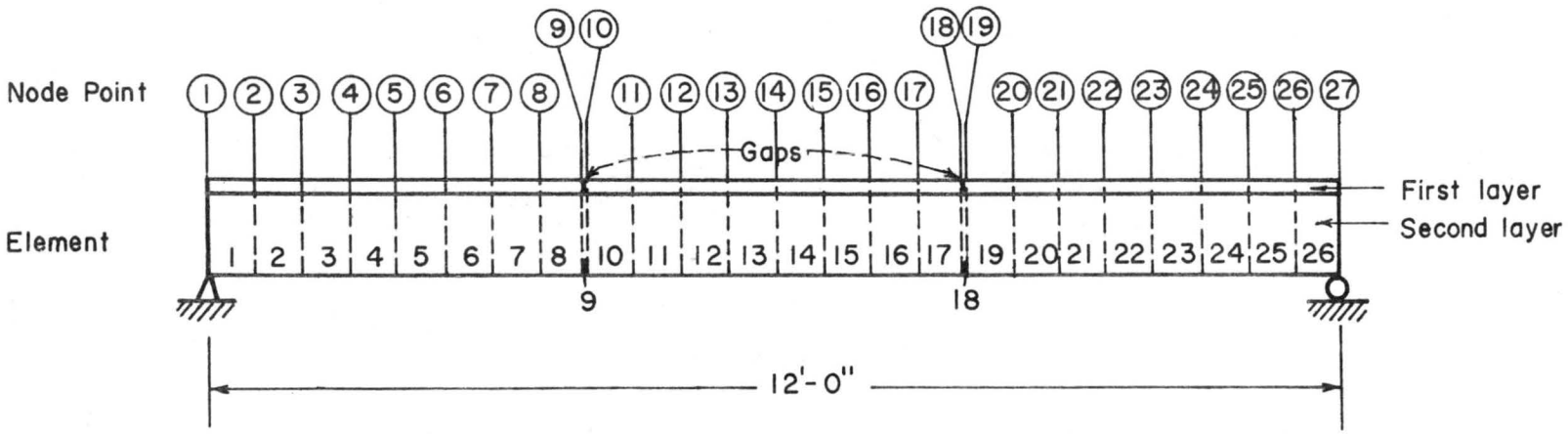

FIGURE 5.2 TYPICAL T-BEAM ELEMENTS USED IN COMPUTER PROGRAM INPUT

5.4 Comparison of Experimental and Theoretical Values

Computed deflections and deflections observed during the experimental program are displayed in Appendix E for fourteen two- and three-layered T-beam specimens. The favorable comparison of these results forms the basis for the verification of the developed mathematical model. The figures in Appendix E include, for each specimen, a load-deflection plot for the midspan of each joist and a deflection profile along the length of one joist for a selected load level. The load was placed at the T-beam midspan and equally shared by the two joists unless otherwise noted. Because specimen T3-8D16-1 was the first T-beam constructed with elastomeric adhesive and served primarily as trial specimen, it was not included in the verification study.

Examples from representative T-beams of the different configurations and fastening methods included in the test program will be discussed at length in this section.

The sizable effect of the sheathing joint conditions can be seen in Fig. 5.3. The T-beams constructed with either glued or tightly butted joints displayed deflections between those calculated using the assumptions of either no gaps or open gaps, as would be expected. The introduction of flexible gaps allowed the deflections of these T-beams to be closely predicted. This is evident from both Fig. 5.3, showing results from Specimen T4 which had tightly butted joints, and from the load deflection plots for other specimens contained in Appendix E.

Results from a typical two-layered nailed T-beam specimen are contained in Fig. 5.4. This specimen, T15-8E19.2-1, was constructed with 2x8 Engelmann spruce joists and 1/2 in thick Engelmann spruce plywood nailed with 8-penny common nails spaced 8 inches apart.

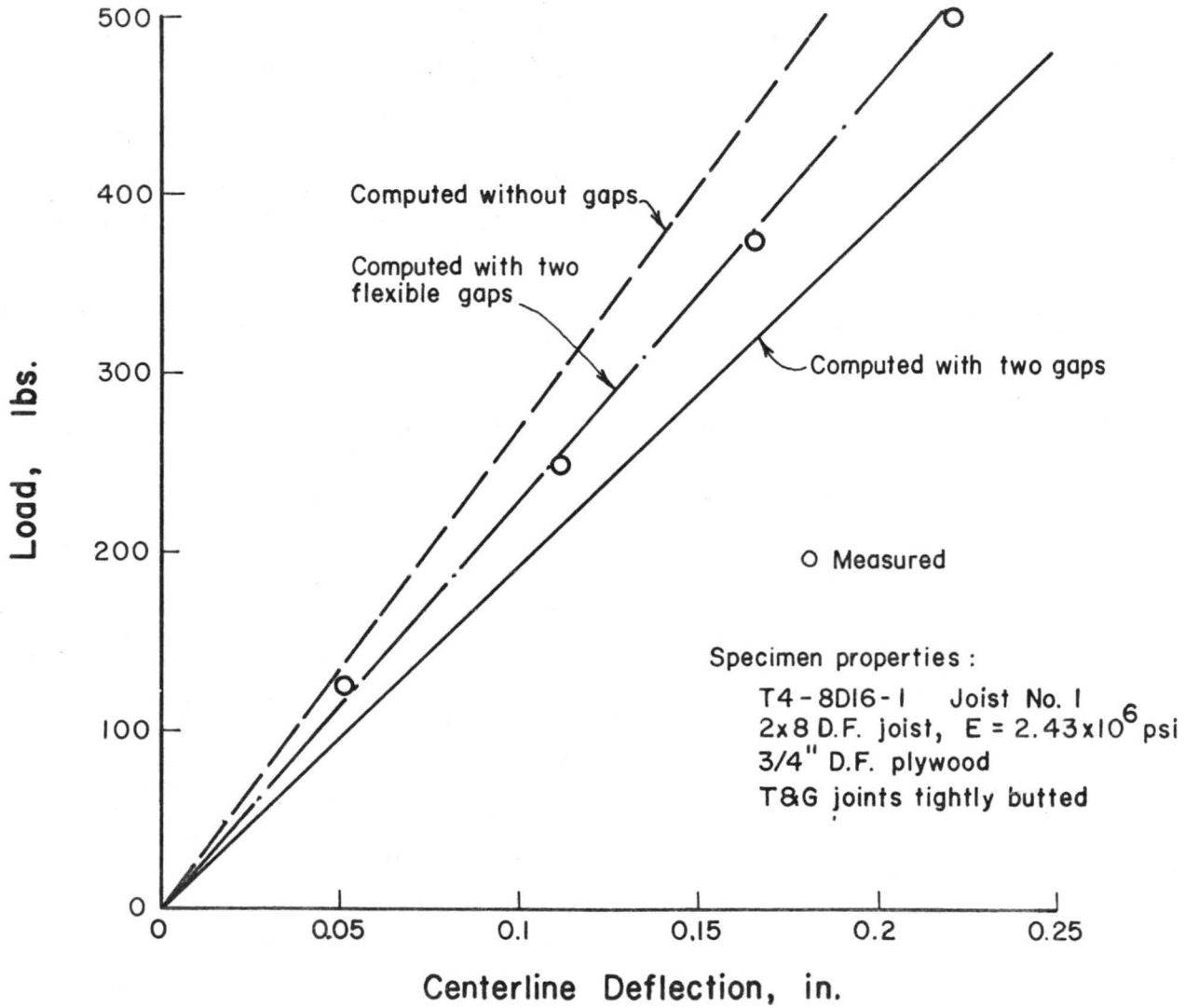

FIGURE 5.3 TYPICAL LOAD-DEFLECTION BEHAVIOR OF T-BEAM WITH SHEATHING JOINTS

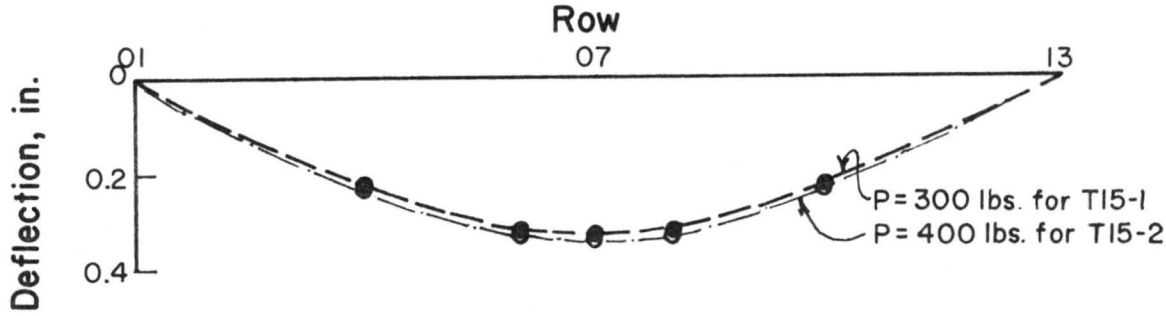

(a). Deflection Profile - Load at Midspan

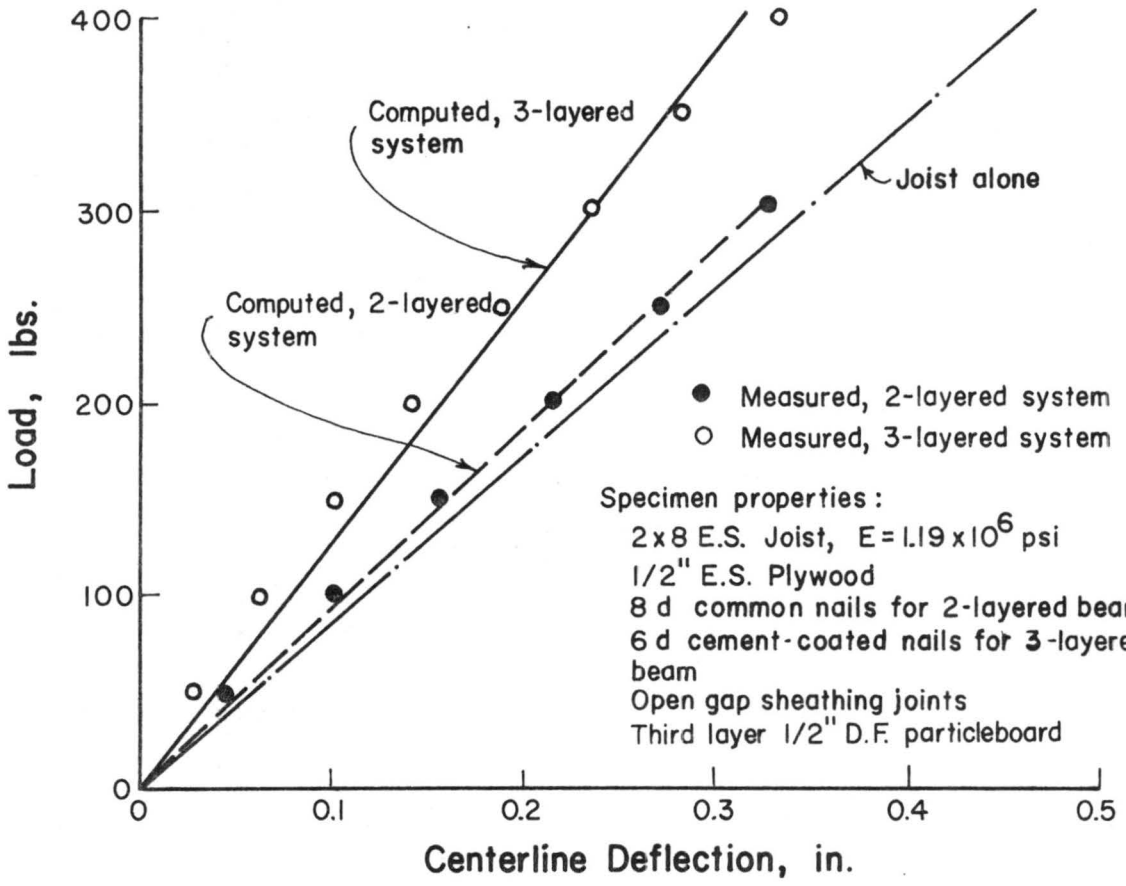

(b). Load deflection Behavior

FIGURE 5.4 EXAMPLE OF BEAM VERIFICATION
JOIST NO. 1 T15-8E19.2-1 & T15-8E19.2-2

Sheathing joints were left open with a 1/16 in. gap. In the working load tests, this specimen was loaded at midspan up to a maximum total applied load of 600 pounds (300 pounds per joist) in 100 pound load increments. The load-deflection plot shows good agreement between the measured and predicted values in the working load range. The predicted values slightly overestimate the deflections at lower load levels and underestimate the observed values at higher load levels. The small differences are thought to have resulted from the changing connector slip modulus, which decreases at higher load levels and thus results in a smaller degree of composite action. The deflection profile presented shows good agreement between the computed and measured deflections not only at midspan but along the length of the beam.

A 1/2 in Douglas fir particleboard was added to this specimen to form a three-layered system. This specimen, now designated as T15-8E19.2-2, was again loaded at midspan up to a maximum total applied load of 800 pounds. The nonlinear behavior was more distinct than for the two-layered system. This may have resulted from the effect of the low slip modulus value for the nails in the particleboard layer. The predicted values at $\Delta \doteq L/500$ gave good results close to the measured deflections.

The sheathing-joist surface of several T-beams were connected with an elastomeric adhesive. Specimen T9-8D16-1 was a typical glued T-beam and was composed of 2x8 Douglas fir joists and 3/4 in thick Douglas fir plywood. Sheathing joints located at third points of the span were T&G tightly butted joints. The specimen was loaded at mid-span with 500 pound load increments to a total load of 2000 pounds. The two joists shared this load equally. Fig. 5.5 shows the load

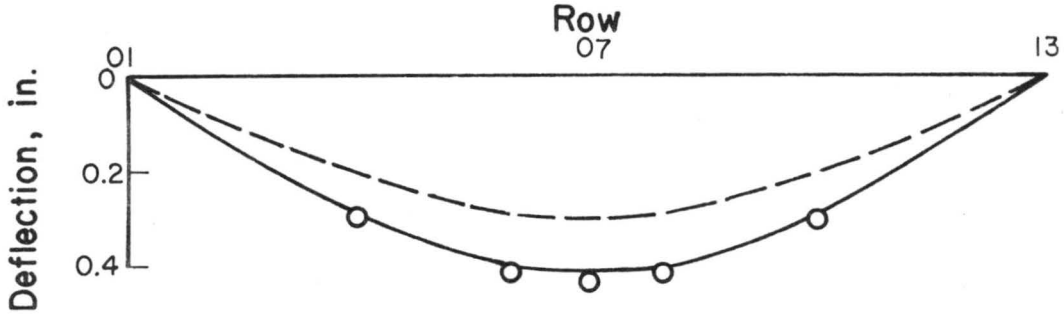

(a). Deflection Profile at 1000 lbs. Load at Midspan

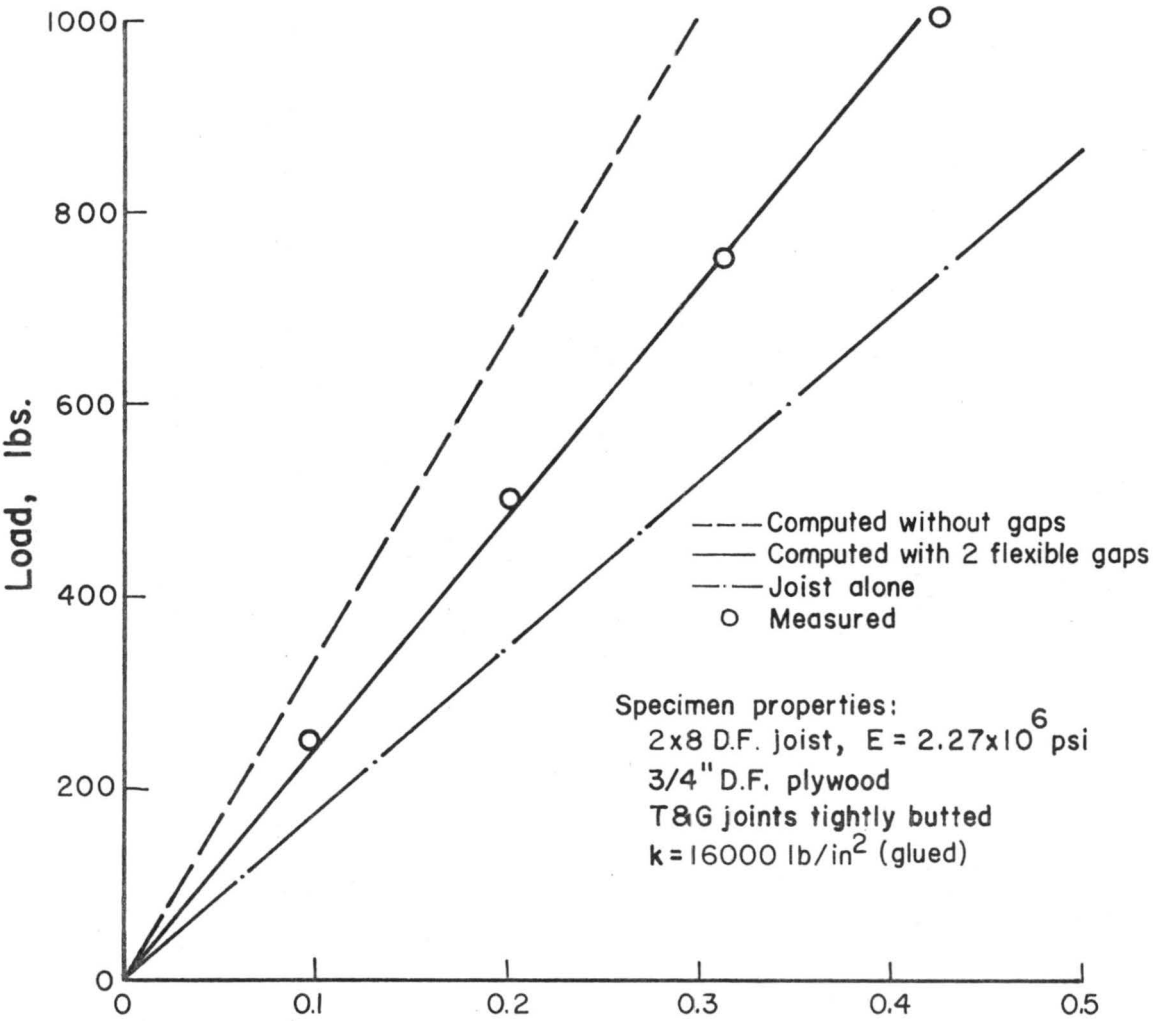

(b). Load-deflection Behavior

FIGURE 5.5 EXAMPLE OF BEAM VERIFICATION
T9-8D16-1 JOIST NO. 1

deflection behavior of this beam. Again, the predicted deflections are slightly greater than the measured values at low load values and less at the higher end of the load range. In general, good agreement was obtained both for the center load-deflection behavior and the deflection profile of the beam. Further underestimation of deflections for loads beyond the working load range would be expected because of the nonlinear effect of the slip modulus of the adhesive used.

To illustrate further the use of the mathematical model and the ability of the solution technique to approximate various sheathing joint conditions, the deflections observed for Specimen T12-8D16-1 were compared to those of the computed results. This specimen was tested several times after successively cutting additional joints in the sheathing layer perpendicular to the joists at desired intervals. The specimen was tested first without any gaps in addition to the two flexible joints between the four foot wide sheathing elements. The sheathing was then cut at midspan and the T-beam reloaded. This procedure was repeated until the gaps were located at one foot intervals. All loads were applied at the midspan of the specimen and were shared equally by each joist.

For clarity, Fig. 5.6 shows only some selected experimental and computed results obtained for Specimen T12-8D16-1. The predicted values again exhibit the underestimation of the deflections beyond the working load range and overestimation at low load levels for both the uncut and with one cut at midspan cases. For the five cuts case, the predicted deflections agreed closely with the measured results even at overload conditions. For this extreme case of many gaps, the load applied may be considered to be carried primarily by joist alone. The effect of composite action was minimal.

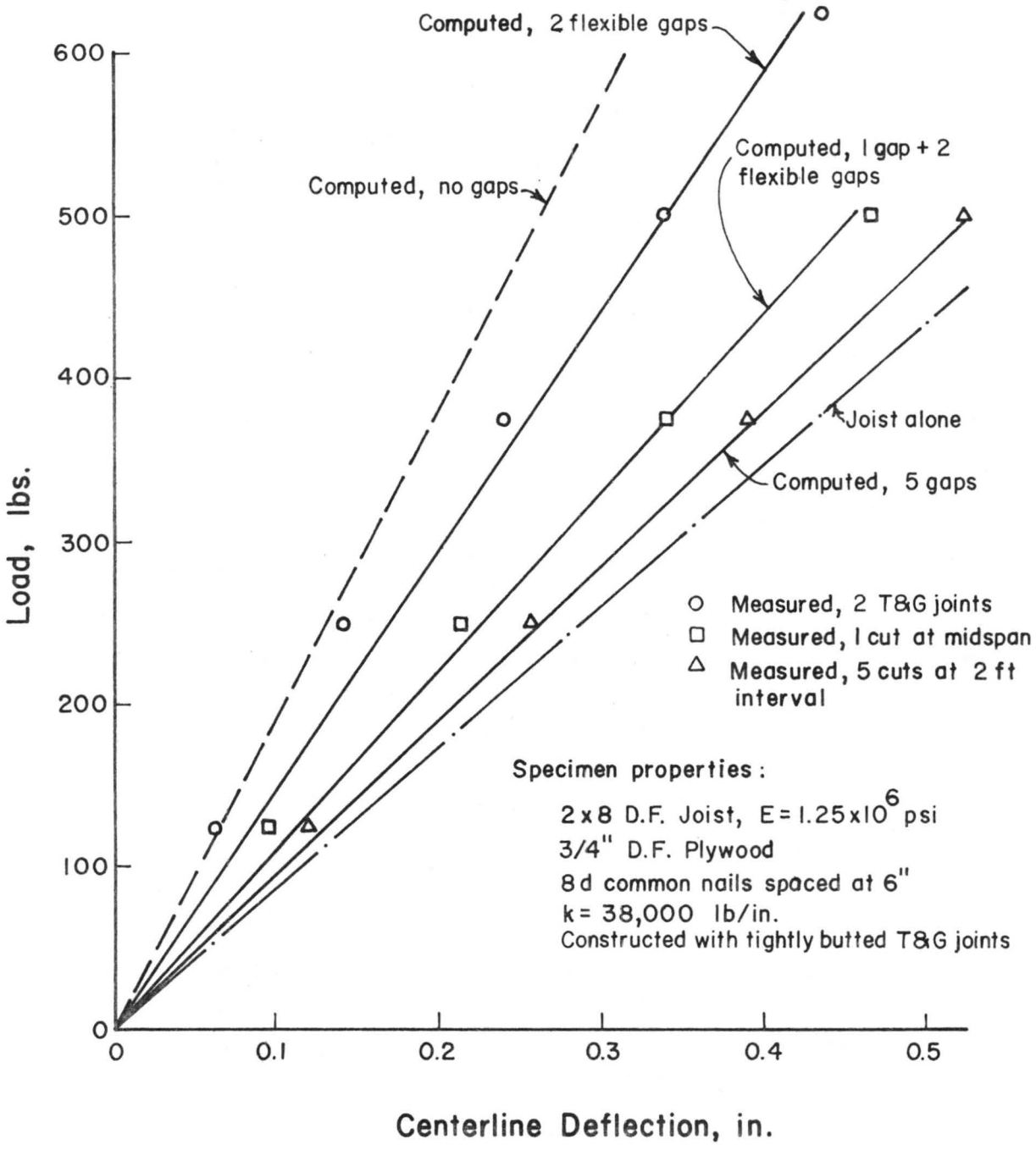

FIGURE 5.6 EXAMPLE OF BEAM VERIFICATION
T12-8D16-1 JOIST NO. 1

For clarity, deflections for only joist 1 of the twin-joist T-beams has been shown in the examples of beam verification illustrated above. For deflection behavior of the other joist, see Appendix E.

Table 5.3 shows the comparison of the computed and measured deflections along the length of one joist in Specimen T15, T9, and T12, the three T-beams discussed above. The computed and observed centerline deflections agree within 3 percent in those three two-layered specimens.

Table 5.4 shows the comparison of predicted and observed midspan deflections for all T-beam specimens tested. The comparisons are based on conditions corresponding to an experimental midspan deflection of near L/500. The corresponding load level for each specimen is also shown. The last column shows the ratio of computed to observed deflections. Good agreement was generally obtained, with the predicted deflection averaging within 4 percent of the observed values.

To demonstrate the ability of the mathematical model and analysis procedures to also predict the deflections of uniformly loaded beams, the model was used to compute deflections of some layered system tests conducted by others. Data from tests conducted by a joist manufacturer, including member properties and load-deflection results were released for this purpose by the manufacturer. Geometry and properties used in obtaining the numerical computations and the results of these comparisons are contained in Appendix H.

The joist element of these composite beams was an I-beam with 1.5x2.3 inch laminated flanges connected with a rigid glue to a 3/8 in. thick plywood web. A layer of 5/8 in thick plywood served as a sheathing layer. The beam configuration and the testing setup are

TABLE 5.3 COMPARISON OF MEASURED AND PREDICTED DEFLECTIONS FOR T-BEAMS ILLUSTRATED

Specimen		Row No. (dial gage location along the beam length)					Remark
		4	6	7	8	10	
T15-8E19.2-1	Measured, in	0.223	0.314	0.327	0.316	0.225	Loaded at mid span at 300 lbs. load
	Predicted, in	0.219	0.305	0.318	0.305	0.219	
	Differences, %	1.8	2.9	2.7	3.5	2.7	
T15-8E19.2-2	Measured, in	0.226	0.321	0.335	0.328	0.232	Loaded at mid span at 400 lbs. load
	Predicted, in	0.217	0.302	0.313	0.302	0.217	
	Differences, %	4.0	5.9	6.5	7.9	6.5	
T9-8D16-1	Measured, in	0.293	0.411	0 427	0.414	0.303	Loaded at mid span at 1000 lbs. load
	Predicted, in	0.289	0.401	0.416	0.401	0.289	
	Differences, %	1.4	2.4	2.6	3.1	4.6	
T12-8D16-1	Measured, in	0.236	0.327	0.340	0.326	0.232	Loaded at mid span at 500 lbs. load, No cut
	Predicted, in	0.234	0.328	0.342	0.328	0.234	
	Differences, %	0.8	0.3	0.6	0.6	1.0	
T12-8D16-1	Measured, in	0.228	0.325	0.340	0.323	0.224	Loaded at mid span at 375 lbs. load, 1 cut at centerline
	Predicted, in	0.227	0.326	0.341	0.326	0.227	
	Differences, %	0.4	0.3	0.3	0.9	1.3	
T12-8D16-1	Measured, in	0.270	0.375	0.391	0.373	0.267	Loaded at mid span at 375 lbs load, 5 cuts at 2 foot intervals
	Predicted, in	0.274	0.382	0.398	0.382	0.274	
	Differences, %	1.5	1.9	1.8	2.4	2.6	

TABLE 5.4 COMPARISON OF MEASURED AND PREDICTED MIDSPAN DEFLECTIONS FOR ALL T-BEAMS TESTED

Specimen	Joist No.	Load Level (lbs.)	Observed Deflection Δm (in.)	Computed Deflection Δc (in.)	Δc/Δm	Remarks
T4-8D16-1	1	500	.232	0.258	1.11	2 flexible
	2	500	.309	0.361	1.17	gaps
T4-8D16-1	1	500	.262	0.262	1.00	2 open gaps
	2	500	.353	0.349	0.99	2 open gaps
T5-8D16-1	1	500	.338	0.332	0.98	2 open gaps
	2	500	.354	0.341	0.96	2 open gaps
T6-8D16-1	1	640	0.300	0.280	0.93	2 flexible
	2	640	0.282	0.288	1.02	gaps
T7-8D16-1	1	770	0.300	0.300	1.00	2 flexible
	2	770	0.282	0.306	1.08	gaps
T8--8D16-1	1	750	0.373	0.364	0.98	2 flexible
	2	750	0.352	0.378	1.07	gaps
T8-8D16-1	1	750	0.399	0.370	0.93	2 open gaps
	2	750	0.386	0.384	0.99	2 open gaps
T9-8D16-1	1	750	0.314	0.312	0.99	2 flexible
	2	750	0.317	0.302	0.95	gaps
T9-8D16-1	1	750	0.336	0.317	0.95	2 open gaps
	2	750	0.340	0.307	0.91	2 open gaps
T10-12E24-1	1	1000	0.215	0.194	0.90	2 flexible
	2	1000	0.197	0.194	0.98	gaps
T10-12E24-1	1	1000	0.252	0.253	1.00	2 open gaps
	2	1000	0.242	0.253	1.04	2 open gaps
T10-12E24-1	1	1000	0.259	0.272	1.05	5 open gaps
	2	1000	0.253	0.271	1.07	5 open gaps
11-8D16-1	1	375	0.371	0.361	0.97	1 open gap
	2	375	0.348	0.353	1.01	at centerline
T12-8D16-1	1	500	0.322	0.342	1.06	2 flexible
	2	500	0.316	0.316	1.00	gaps
T12-8D16-1	1	375	0.340	0.341	1.00	1 open gap at
	2	375	0.325	0.313	0.96	centerline
T12-8D16-1	1	375	0.390	0.386	0.99	3 open gaps
	2	375	0.362	0.353	0.98	3 open gaps
T12-8D16-1	1	375	0.391	0.398	1.02	5 open gaps
	2	375	0.386	0.364	0.94	5 open gaps
T13-8D16-1	1	375	0.307	0.288	0.94	2 open gaps
	2	375	0.346	0.337	0.97	2 open gaps
T14-12D24-1	1	1000	0.184	0.181	0.98	2 open gaps
	2	1000	0.205	0.194	0.95	2 open gaps

TABLE 5.4 (Continued)

Specimen	Joist No.	Load Level (lbs.)	Observed Deflection Δm (in.)	Computed Deflection Δc (in.)	Δc/Δm	Remarks
T14-12D24-2	1	1000	0.154	0.157	1.02	3 open gaps
	2	1000	0.167	0.166	0.99	3 open gaps
T15-8E19.2-1	1	300	0.327	0.318	0.97	2 open gaps
	2	300	0.332	0.319	0.96	2 open gaps
T15-8E19.2-2	1	400	0.335	0.313	0.94	5 open gaps
	2	400	0.318	0.314	0.99	5 open gaps
T16-8E19.2-1	1	400	0.339	0.351	1.04	2 flexible
	2	400	0.368	0.384	1.04	gaps
T16-8E19.2-2	1	500	0.357	0.367	1.03	3 flexible
	2	500	0.392	0.396	1.01	gaps

shown in Fig. 5.7. Pieces of plywood 12x48 inches in size were placed with the grain face direction perpendicular to the joist. The plywood and I-section layers were connected with either 8-penny nails at 12 inch spacing or were both nailed and glued with an elastomeric adhesive*. The tongue and groove joints were glued in the glued-nailed specimens only.

To simulate the uniformly distributed loading case desired, loads were applied at 12 inch intervals using one-inch diameter hydraulic cylinder, each loading a six-inch diameter plate. The beam was simply supported at both ends by a 4 inch long bearing pad resting atop a roller. Lateral supports were placed at several points along the beam to prevent lateral movement.

Fig. 5.8 shows the load-deflection behavior of the manufacturer's specimen No. 1. The specimen was constructed with a 20 in deep I-beam 24 feet in length. The sheathing was nailed to the I-joist and contained tightly-butted tongue and groove joints. The beam behavior was inbetween the computed deflections with gaps and without gaps in the sheathing layer.

For both the T-beams tested as a part of this project and for one available series of beams tested by others, the deflections computed with the developed mathematical model were generally very close to those observed during tests of the actual specimen. These favorable comparisons demonstrate the validity of the mathematical model and show that the behavior of non-rigidly connected composite beams can now be closely predicted over a wide range of conditions.

---

*Franklin Construction Adhesive

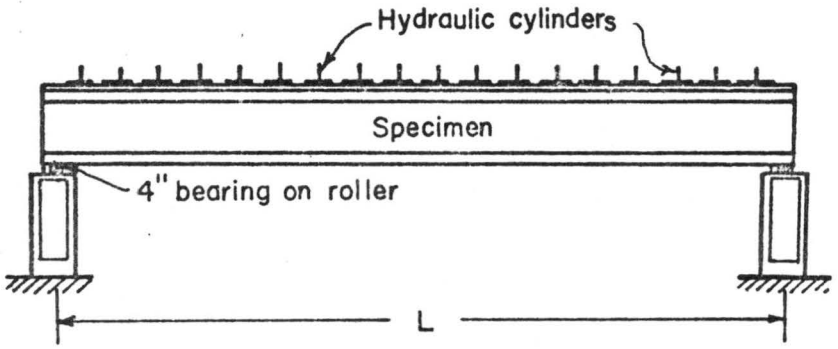

(a). Loading Setup

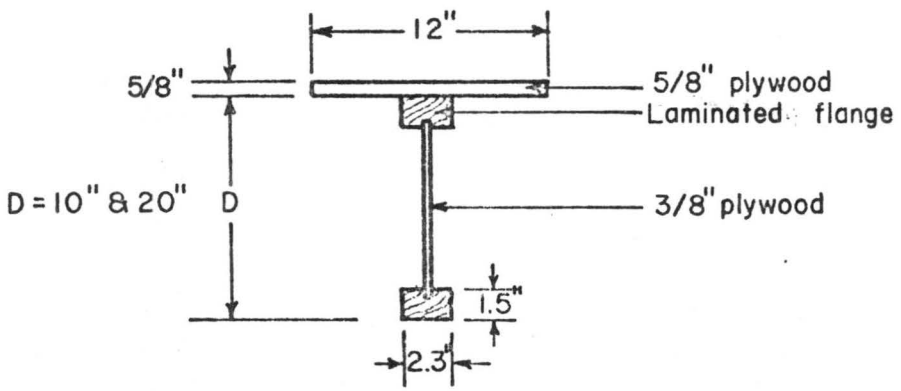

(b). Cross Section

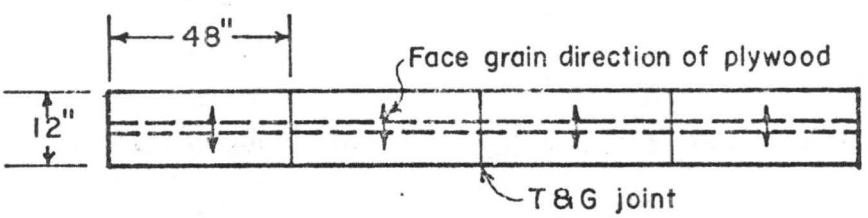

(c). Top View

FIGURE 5.7 CONFIGURATION OF T-BEAMS USING MANUFACTURED JOISTS

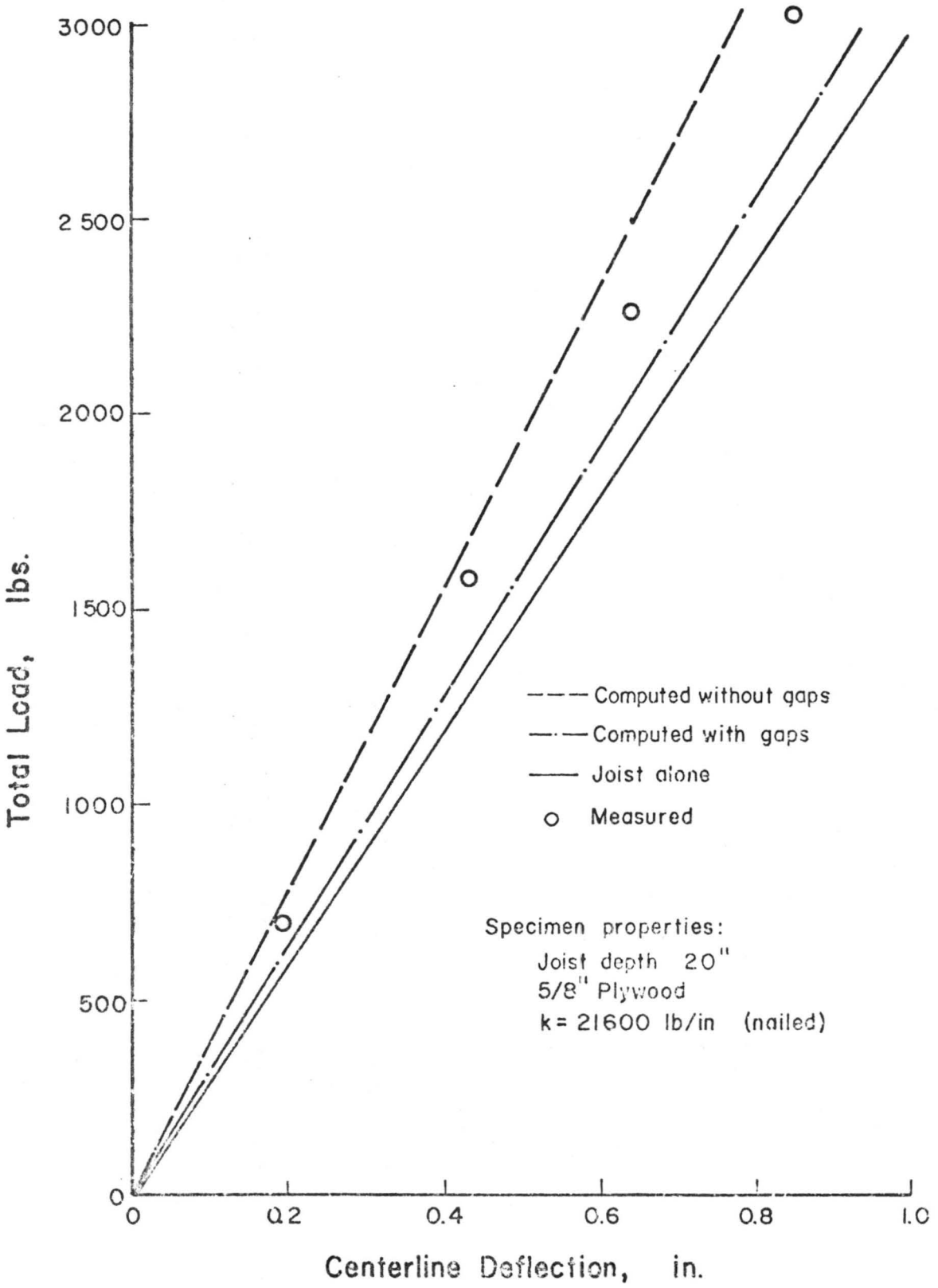

FIGURE 5.8 EXAMPLE OF BEAM VERIFICATION
MANUFACTURER'S SPECIMEN NO. 1

CHAPTER 6

SUMMARY AND CONCLUSIONS

A brief discussion on the development of the mathematical model to predict the deflections of wood joist T-beam systems has been presented. This model is based on a small deflection theory for layered beams with interlayer slip considered. A finite element solution technique developed during the overall research effort on joist floor systems was used in this project to compute the theoretical deflections for two and three layered systems with variable material properties along the length of the beam.

Fourteen twin T-beams were constructed and tested to allow experimental demonstration of the validity of this mathematical model. This verification was the primary objective of the research effort described in this report. The T-beams were built from pieces of lumber and sheathing material having known material properties. Properties for each piece were individually determined by the Wood Science Laboratory at the Colorado State University campus. The joist modulus of elasticity values were also determined during the specimen construction. For these tests, the joists were bent about their strong axis, as they would be loaded in the T-beam configuration, rather than about the weak axis (flatwise bending) as was used at the Wood Science Laboratory. Of the T-beams constructed and tested, eleven T-beams were two-layered systems and three were three-layered systems. Most T-beams were constructed with nails connecting the joist and sheathing layers, while selected T-beams were connected with elastomeric adhesive.

A concentrated load within the working load range was applied at the midspan of the beam for most cases. Deflections were obtained from dial deflection gages mounted underneath the joists at selected locations. Loadings other than at midspan were applied for selected specimens.

Verification of the developed mathematical model was achieved by the favorable comparison between the measured deflections and those computed from the mathematical model using the known T-beam geometry and material properties. To further verify this mathematical model, results from tests conducted by a joist manufacturer and using uniform loading were compared with those computed from this mathematical model.

In general, test results showed good agreement with the predicted values from the mathematical model for loads in the working load range. The predicted values for some specimens with glued and nonglued tongue and groove sheathing joints deviated some from the experimental results. These differences were believed to have resulted primarily from the unknown but varying tightness of the sheathing joints. To model the effects of these joints, short finite elements with low modulus of elasticity values were used in the mathematical model. Further studies on the behavior of sheathing joints are necessary to allow the properties of the sheathing joints to be better defined and more accurately entered into the model.

The predicted deflection values slightly underestimated most test results at overload levels. This resulted from the linear model not being able to follow the nonlinear response of the T-beams resulting primarily from the decreasing slip modulus of the connectors with increasing load. Modification of the mathematical model to include

nonlinear load-slip characteristics is recommended and would result in theoretical values which better match the experimental results over a wide range of load levels, including overloads.

Other effects which could be responsible for a small portion of the deviation between theoretical and observed deflections arise from practical difficulties in precisely defining, for use in the analysis programs, the specimen properties at the time of testing. Among these are effects arising from small dimensional changes due to temperature or moisture content changes in the wood, localized defects in the materials, and the restraints at the T-beam supports. Errors resulting from assuming a fully effective flange are thought to be small.

In conclusion, the verification studies demonstrated that the developed mathematical model for multilayered beams with interlayer slip closely predicts the load-deflection behavior of two- and three-layer T-beams over a wide range of specimen configurations and material properties for loads in the range of interest in working load design procedures. This verification of the model now opens the way for further development and use of the model to more realistically analyze and design wood joist structural systems with the composite nature being properly recognized. This rational analysis procedure, when fully developed, will allow more economical design and more efficient use of materials.

REFERENCES

1. Amana, E. J. and Booth, L. G., "Theoretical and Experimental Studies on Nailed and Glued Plywood Stressed-Skin Components: Part I. Theoretical Study" Journal of the Institute of Wood Science, Vol. 4, No. 19, September 1967.

2. Amana, E. J. and Booth, L. G., "Theoretical and Experimental Studies on Nailed and Glued Plywood Stressed-Skin Components: Part II. Experimental Study" Journal of the Institute of Wood Science, Vol. 4, No. 20, April 1967.

3. American Plywood Association, "Plywood Design Specification," 1970.

4. American Plywood Association, "Plywood Construction Systems for Commercial and Industrial Buildings," General Information, APA, August 1971.

5. American Society for Testing and Materials, 1972 Annual Book of ASTM Standards, part 16, "Structural Sandwich Construction; Wood; Adhesives," ASTM, Philadelphia, Pa., 1972.

6. Clark, L. G., "Deflections of Laminated Beams," Transactions, American Society of Civil Engineers, Vol. 119, 1954.

7. Foschi, R. O., "The Load-Slip Characteristics of Nails," Department of the Environment, Canadian Forestry Service, Western Forest Products Laboratory, Vancouver, British Columbia, 1969.

8. Goodman, J. R., "Layered Wood Systems with Interlayer Slip," Ph.D. Dissertation, University of California, Berkeley, 1967.

9. Goodman, J. R., and Popov, E. P., "Layered Beam Systems with Interlayer Slip," Journal of Structural Division, American Society of Civil Engineering, Vol. 94, No. ST 11, November 1968.

10. Granholm, H., "Om Sammansatta Balkar Och Pelare Med Sarkilo Hansyn Till Spikade Trakonstrukioner" ("On Composite Beams and Columns with Particular Regard to Nailed Timber Structures"), Chalmers Tekniska Hogskoas Handlingar, No. 88, 1949.

11. Hilbrand, H. C. and Miller, D. G., "Machine Grading Theory and Practice," Forest Products Journal, Vol. 16, Nos. 11 and 12, Nov. and Dec. 1966.

12. Hoeber, G. F., "A Study of Modulus of Elasticity and Modulus of Rapture in Douglas-Fir Dimension Lumber," Unpublished Report of the Research Dept. Potlach Forests Inc., Lewiston, Idaho, 1966.

13. Hoyle, R. J. Jr., "Deflections of Twenty Experimental Wood Beams Using Design Method of Kuenzi and Wilkinson," Unpublished report, Washington State University, College of Engineering Research Division, September 1972.

REFERENCES (Continued)

14. Hoyle, R. J. Jr., "Behavior of Wood I-beams Bonded with Elastomeric Adhesive," Bulletin 328, College of Engineering Research Division, Washington State University, Pullman, Washington, 1973.

15. Kennedy, D. E., "Research on Mechanical Fasteners for Residential Construction in Canada," Publication No. 1071, Department of Forestry, Canada 1964.

16. Ko, M. F., "Layered Beam Systems with Interlayer Slip," M.S. Thesis, Colorado State University, Fort Collins, Colorado, December 1972.

17. Kuenzi, E. W. and Wilkinson, T. L., "Composite Beams -- Effect of Adhesive on Fastener Rigidity," USDA Forest Service Research Paper FPL 152, 1971.

18. McLain, T. E., "Nondestructive Evaluation of Full Size Wood Composite Panels," M.S. Thesis, Colorado State University, Fort Collins, Colorado, May 1973.

19. National Particleboard Association, "Particleboard Design and Use Manual," AIA file No. 23-L, 1967.

20. Newmark, N. M., Seiss, C. P., and Viest, I. M., "Tests and Analysis of Composite Beams with Incomplete Interaction," Proceedings, Society for Experimental Stress Analysis, Vol. 19, No. 1, 1951.

21. Norris, C. B., Erickson, W. S., and Kommers, Wm. J., "Flexural Rigidity of a Rectangular Strip of Sandwich Construction -- Comparison between Mathematical Analysis and Results of Tests," Forest Products Laboratory Report 1505A, May 1952.

22. Patterson, D. W., "Nailed Wood Joist under Lateral Loads," M.S. Thesis, Colorado State University, Fort Collins, Colorado, April 1973.

23. Penner, B. G., "Experimental Behavior of Wood Flooring Systems," M.S. Thesis, Colorado State University, Fort Collins, Colorado, December 1972.

24. Pleshkov, P. F., Teoriia Rashceta Depeviannykh (Theoretical Studies of Composite Wood Structures), Moscow, 1952.

25. Rose, J. D., "Field-Glued Plywood Floor Tests," Report 118, American Plywood Association Laboratory, Revised, May 1970.

26. Salvadori, M. G. and Baron, M. L., Numerical Methods in Engineering, 2nd ed., Prentice-Hall, Englewood Cliffs, N.J., 1961.

27. Thompson, E. G., Goodman, J. R., and Vanderbilt, M.D., "Analysis of Layered Wood Systems with Gaps at Joints," To be published.

28. U. S. Department of Commerce, "U. S. Product Standard PSI-66 for Softwood Plywood -- Construction and Industrial," 1971.

29. Western Wood Products Association, Western Woods Use Book, WWPA, Portland, Oregon, 1973.

30. Wolfe, R. W., "Upgrading of Dimension Lumber by Finger Jointing," M.S. Thesis, Colorado State University, Fort Collins, Colorado, May 1972.

31. Zienkiewicz, O. C., The Finite Element Method in Engineering Science, McGraw-Hill Publishing Company, London, 1971.

APPENDIX A

PROPERTIES OF JOISTS

APPENDIX A PROPERTIES OF JOISTS

Specimen No.	Joist No.	Joist Dimension		*Average Flat-wise MOE 10^6 psi	**Edgewise MOE 10^6 psi		
		w in	h in		No lat. supp.	With Header 1 nail	With Header 3-nail
T3-8D16-1	DW-S-08-33	1.495	7.153	1.938	2.402		2.320
	DW-S-08-39	1.475	7.190	1.964	1.850		1.811
T4-8D16-1	DW-S-08-37	1.468	7.145	1.766	2.206		2.429
	DW-S-08-43	1.488	7.210	1.696	2.131		2.269
T5-8D16-1	DW-S-08-27	1.490	7.137	1.481	1.656		1.847
	DW-S-08-34	1.491	7.163	1.448	1.765		1.774
T6-8D16-1	DW-S-08-15	1.468	7.187	1.799	2.181		2.330
	DW-S-08-23	1.475	7.092	1.798	2.062		2.349
T7-8D16-1	DW-S-08-45	1.503	7.209	1.787	1.883		2.141
	DW-S-08-58	1.478	7.170	1.791	2.027		2.152
T8-8D16-1	DW-S-08-22	1.476	7.251	1.739	1.757	1.628	1.805
	DW-S-08-29	1.429	7.195	1.793	1.879	1.535	1.744
T9-8D16-1	DW-S-08-12	1.496	7.217	1.880	1.981	2.074	2.269
	DW-S-08-05	1.443	7.130	1.830	2.395	2.478	2.566
T10-12E24-1	EC-S-12-05	1.492	11.210	1.068	1.124	1.076	1.269

APPENDIX A (Continued)

Specimen No.	Joist No.	Joist Dimension w in	Joist Dimension h in	*Average Flat-wise MOE 10^6 psi	**Edgewise MOE 10^6 psi No lat. supp.	**Edgewise MOE 10^6 psi With Header 1 nail	**Edgewise MOE 10^6 psi With Header 3-nail
T10-12E24-1	EC-S-12-04	1.503	11.205	.988	1.243	1.217	1.261
T11-8D16-1	DW-N-08-52	1.500	7.231	.853	.929	.968	.975
	DW-N-08-47	1.480	7.092	.933	.993	1.074	1.088
T12-8D16-1	DW-N-08-51	1.480	7.048	.838	1.178	1.249	1.249
	DW-N-08-55	1.491	7.232	.937	1.222	1.261	1.261
T13-8D16-1	DW-N-08-21	1.494	7.226	1.174	1.357		1.342
	DW-N-08-49	1.496	7.268	1.021	1.055		1.077
T14-12D24-1	DW-S-12-21	1.488	11.115	1.296	1.740	1.845	1.883
	DW-S-12-23	1.507	11.156	1.290	1.586	1.667	1.715
T15-8E19.2-1	EK-S-08-01	1.494	7.139	.769	1.051	1.161	1.191
	EK-S-08-09	1.500	7.197	.781	1.054	1.106	1.151
T16-8E19.2-1	EC-S-08-06	1.454	7.115	1.033	1.425		1.500
	EK-N-08-13	1.465	7.091	1.026	1.261		1.261

*Determined by the Wood Science Laboratory. Refer to Section 3.2.1 for description of tests.

**Determined during the specimen construction. Refer to Section 3.2.2 for description of tests.

APPENDIX B

PROPERTIES OF SHEATHING

APPENDIX B PROPERTIES OF SHEATHING*

Specimen No.	Sheet No.	Nominal Dimension	$E_{\parallel}$** 10^6 psi	$E_{\perp}$** 10^5 psi	G 10^5 psi	Grade
T3-8D16-1	DP-34-27	4'x8'x3/4"	1.341	4.870	0.7870	Tongue and groove, STD-INT
	DP-34-28	4'x8'x3/4"	1.133	5.418	0.8184	Tongue and groove, STD-INT
T4-8D16-1	DP-34-25	4'x8'x3/4"	1.283	5.5 0	0.8829	Tongue and groove, STD-INT
T5-8D16-1	DP-34-21	4'x8'x3/4"	1.499	5.390	0.8613	Tongue and groove, STD-INT
T6-8D16-1	DP-34-20	4'x8'x3/4"	1.249	6.008	0.8872	Tongue and groove, STD-INT
T7-8D16-1	DP-34-22	4'x8'x3/4"	1.369	5.300	0.8641	Tongue and groove, STD-INT
T8-8D16-1	DP-34-17	4'x8'x3/4"	1.243	4.912	0.8901	Tongue and groove, STD-INT
T9-8D16-1	DP-34-18	4'x8'x3/4"	1.270	5.352	0.8389	Tongue and groove, STD-INT
T10-12E24-1	DP-34-10	4'x8'x3/4"	1.235	5.463	0.8025	Tongue and groove, STD-INT
	DP-34-13	4'x8'x3/4"	1.513	5.516	0.9863	Tongue and groove, STD-INT
T11-8D16-1	DP-34-8	4'x8'x3/4"	1.247	5.326	0.7421	Tongue and groove, STD-INT
T12-8D16-1	DP-34-12	4'x8'x3/4"	1.513	5.581	0.8251	Tongue and groove, STD-INT
T13-8D16-1	EP-58-28	4'x8'x3/4"	1.281	4.323	0.9537	Tongue and groove, STD-INT (exterior glue)
T14-12D-24-1	DP-12-02	4'x8'x1/2"	1.721	2.563	1.351	STD-INT (intermed. glue)
	DP-12-03	4'x8'x1/2"	1.664	2.236	1.504	STD-INT (intermed. glue)
T14-12D-24-2	DB-12-19	4'x8'x1/2"	.5782	4.494	1.719	Floor underlayment
	DB-12-20	4'x8'x1/2"	.5837	4.367	1.806	Floor underlayment
T15-8E19.2-1	EP-12-02	4'x8'x1/2"	1.411	2.221	2.224	STD-INT (exterior glue)
	EP-12-03	4'x8'x1/2"	1.390	2.157	2.246	STD-INT (exterior glue)

APPENDIX B* (Continued)

Specimen No.	Sheet No.	Nominal Dimension	$E_{\parallel}$** 10^6 psi	$E_{\perp}$** 10^5 psi	G 10^5 psi	Grade
T15-8E19.2-2	DB-12-19	4'x8'x1/2"	.5782	4.494	1.719	Floor underlayment
	DB-12-20	4'x8'x1/2"	.5837	4.367	1.806	Floor underlayment
	DB-12-21	4'x8'x1/2"	.5447	4.290	1.702	Floor underlayment
T16-8E19.2-1	EP-12-03	4'x8'x1/2"	1.390	2.157	2.246	STD-INT (exterior glue)
	EP-12-04	4'x8'x1/2"	1.360	2.287	2.058	STD-INT (exterior glue)
T16-8E19.2-2	DB-12-7	4'x8'x1/2"	.4486	3.331	1.773	Floor underlayment
	DB-12-10	4'x8'x1/2"	.4869	3.808	1.657	Floor underlayment

* See Section 3.2.1 for description of testing procedure.
**E values are valid for bending and based on gross section dimensions, see Section 5.
$\parallel$ = Face grain parallel to bending; $\perp$ = Face grain perpendicular to bending.

APPENDIX C

STATISTICAL ANALYSIS OF FLATWISE AND EDGEWISE MOE OF JOISTS

APPENDIX C

STATISTICAL ANALYSIS OF FLATWISE AND EDGEWISE MOE OF JOISTS

Correlation coefficients were computed and analyses of variance carried out to determine the degree of relationship between flatwise and edgewise MOE values. A simple linear regression analysis of edgewise MOE (Y) on flatwise MOE (X) was also computed such that the edgewise MOE can be predicted if the flatwise MOE is given. Table C.1 shows a summary of the regression analysis including the regression equations, F values, and coefficient of correlation (r)* for 2x8 and 2x12 Douglas fir and Engelmann spruce joists used in the construction of both T-beam and floor system specimens.

Scatter diagrams, Fig. C.1 through Fig. C.7, show the edgewise MOE versus flatwise MOE of joists at different end conditions. The regression lines and their corresponding equations are also shown in the diagrams. The flatwise MOE values used were corrected for shear deformations, while those resulting from edgewise loadings were not.

Results from previous studies on the relationship between flatwise and edgewise MOE values are available. The r value for flatwise versus edgewise MOE values reported in Hoerber's work (12) is 0.82. Hilbrand and Miller's found an average value of 0.85 (11). These are about the same magnitudes as shown in Table C.1.

*Coefficient of correlation, r, is the measure of the degree of linear dependence of Y on X. An r value of 1 indicates a perfect linear dependence with Y increasing with X, while r = 0 indicates no detectable linear dependence.

TABLE C.1. SUMMARY OF REGRESSION ANALYSIS FOR EDGEWISE MOE (Y) ON FLATWISE MOE (X)

Joist Type	End Condition	Regression Equation	d.f.*	F	r	Sig. at $\alpha = 0.05$
2x8 Douglas fir	A	$Y = 0.423 \times 10^6$ psi$+0.912X$	50	88.35	0.802	yes
	B	$Y = 0.873 \times 10^6 + 0.700X$	27	23.18	0.687	yes
	C	$Y = 0.435 \times 10^6 + 0.945X$	72	99.12	0.763	yes
2x8 Engelmann spruce	A	$Y = 0.223 \times 10^6 + 0.920X$	34	61.82	0.807	yes
	B	$Y = 0.455 \times 10^6 + 0.771X$	15	70.20	0.913	yes
	C	$Y = 0.348 \times 10^6 + 0.874X$	28	43.52	0.786	yes
2x12 Douglas fir	A	$Y = 1.048 \times 10^6 + 2.090X$	10	17.21	0.810	yes
	B	$Y = -1.977 \times 10^6 + 2.931X$	8	27.94	0.894	yes
	C	$Y = -2.245 \times 10^6 + 3.160X$	8	47.00	0.933	yes
2x12 Engelmann spruce	C	$Y = 0.346 \times 10^6 + 0.932X$	12	12.86	0.734	yes

Note:

End condition A = no lateral support along the joist
B = with header attached at ends and driven one 16 d nail at mid-depth of the joist end
C = with header attached at ends and driven three 16 d nails

*degree of freedom

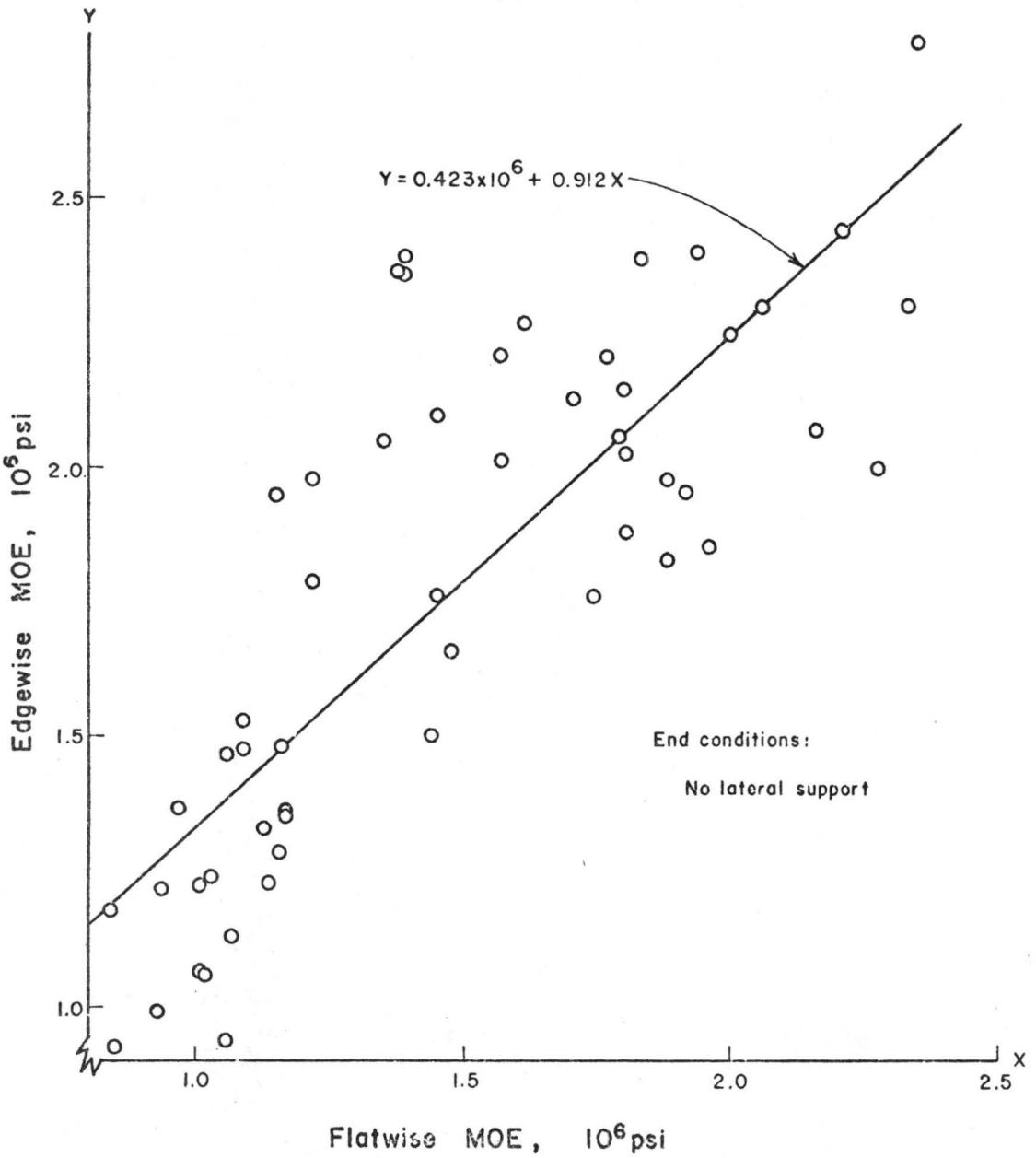

FIGURE C.1 EDGEWISE MOE VS. FLATWISE MOE FOR 2x8 DOUGLAS FIR JOIST

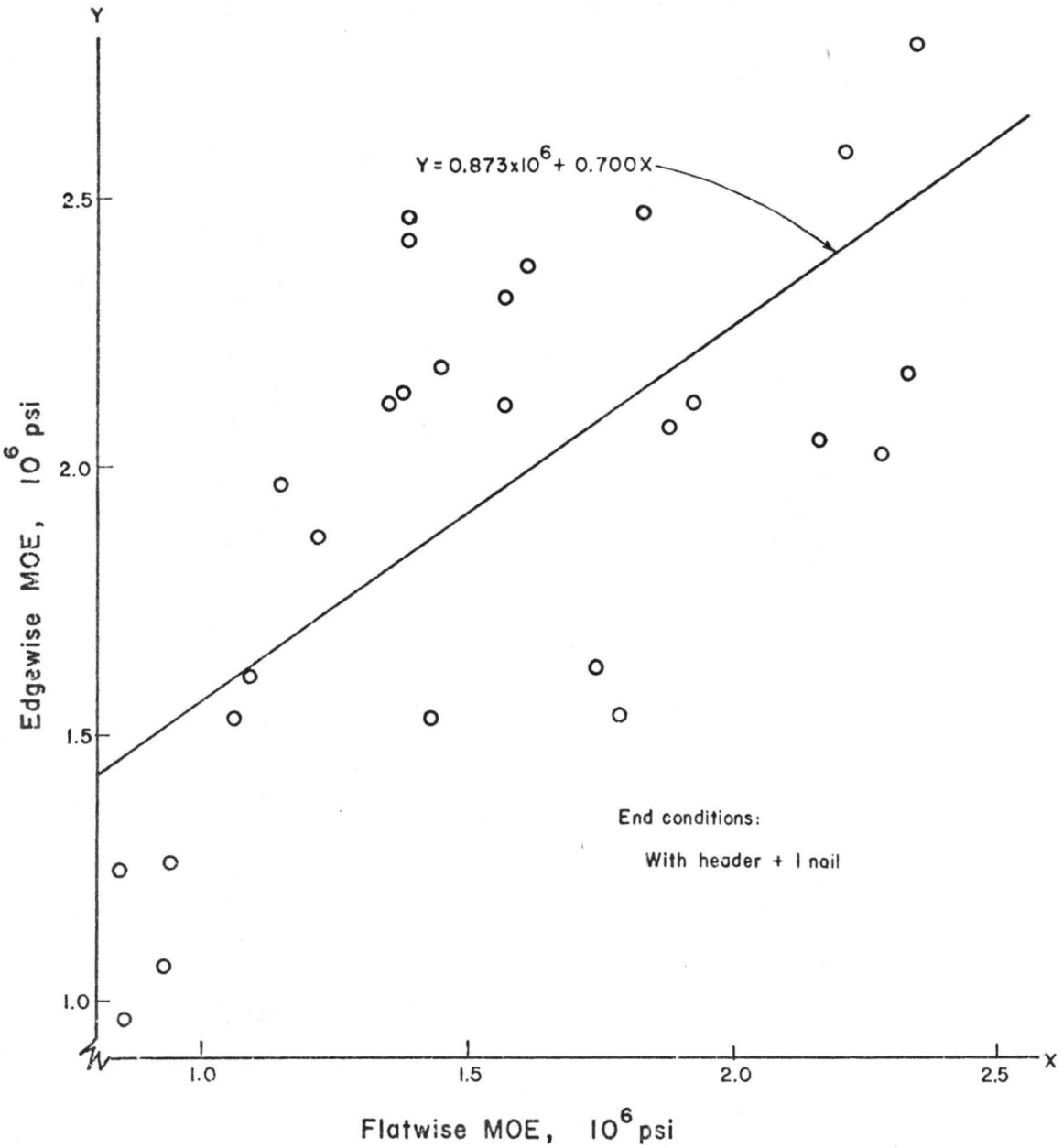

FIGURE C.2 EDGEWISE MOE VS. FLATWISE MOE FOR 2x8 DOUGLAS FIR JOIST

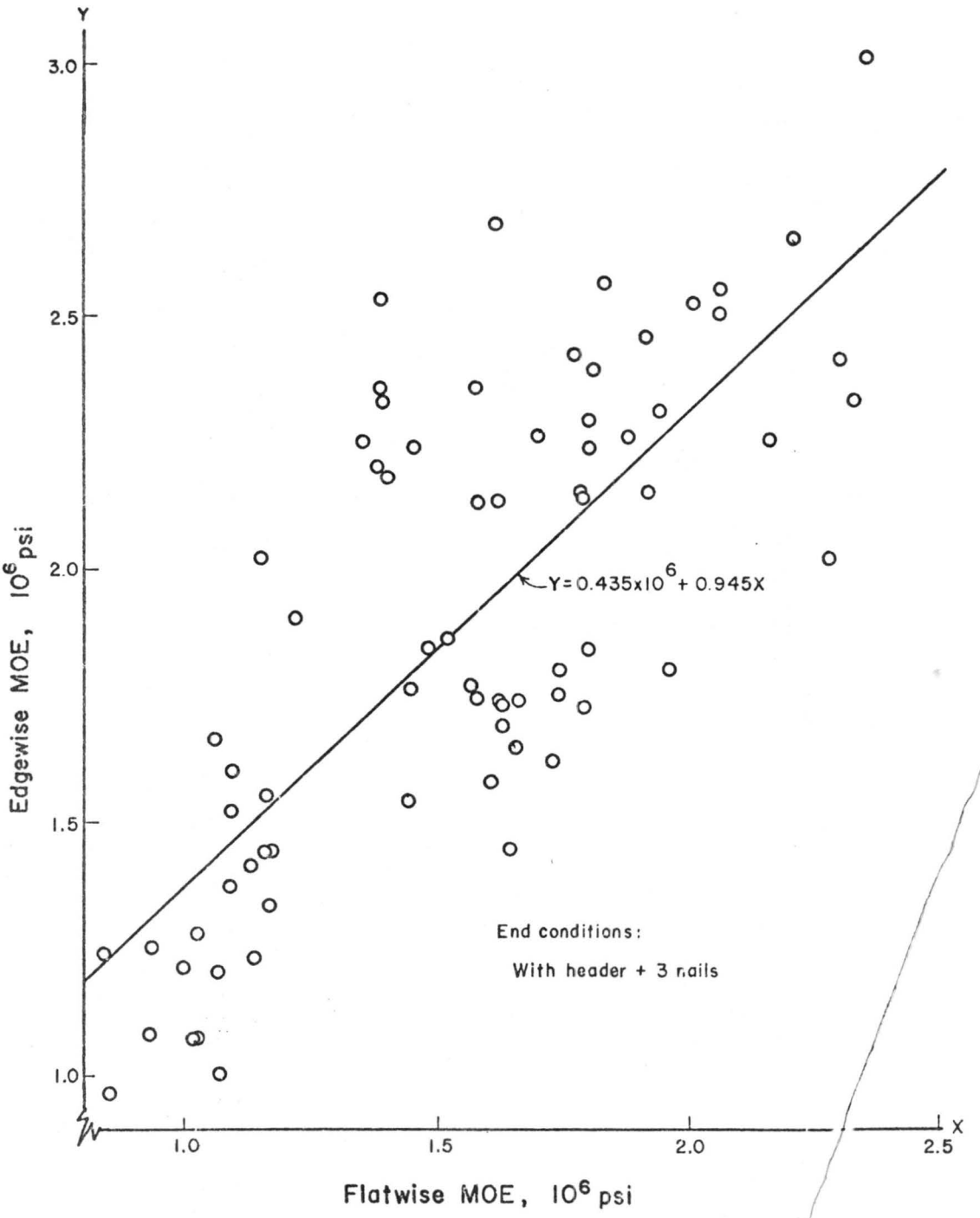

FIGURE C.3 EDGEWISE MOE VS. FLATWISE MOE FOR 2x8 DOUGLAS FIR JOIST

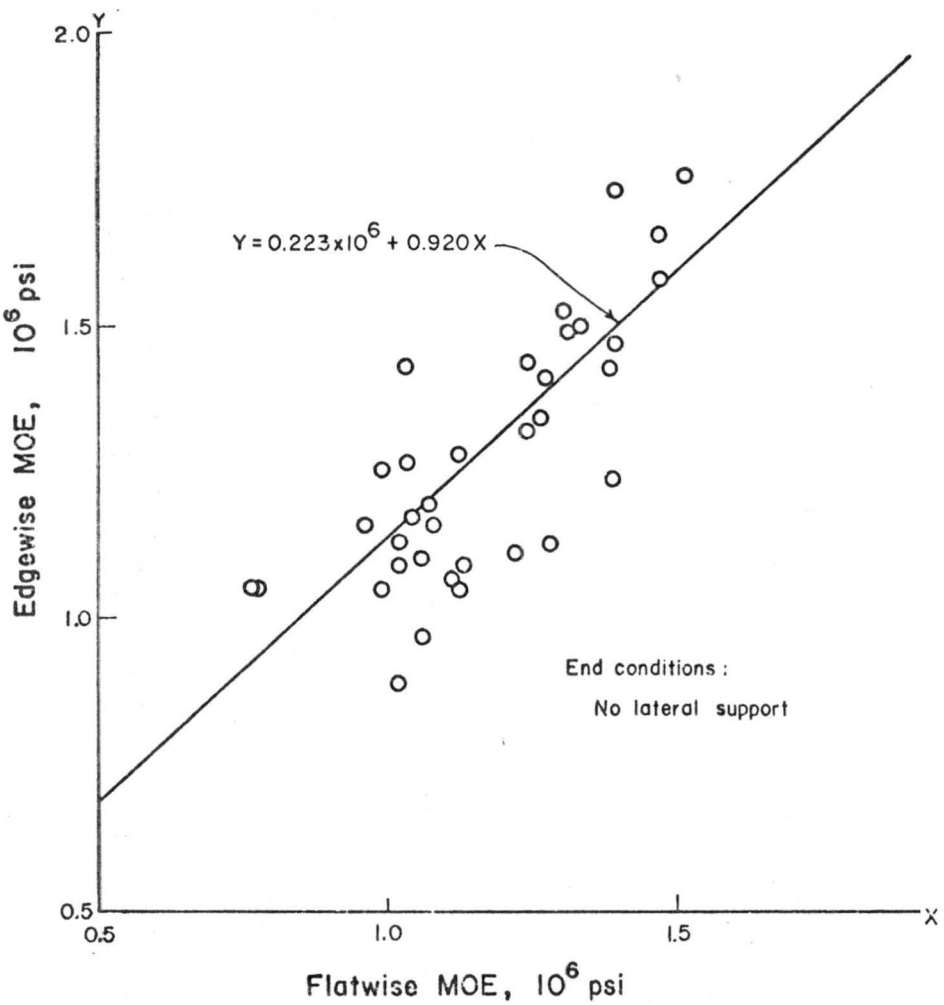

FIGURE C.4 EDGEWISE MOE VS. FLATWISE MOE FOR 2x8 ENGELMAN SPRUCE JOIST

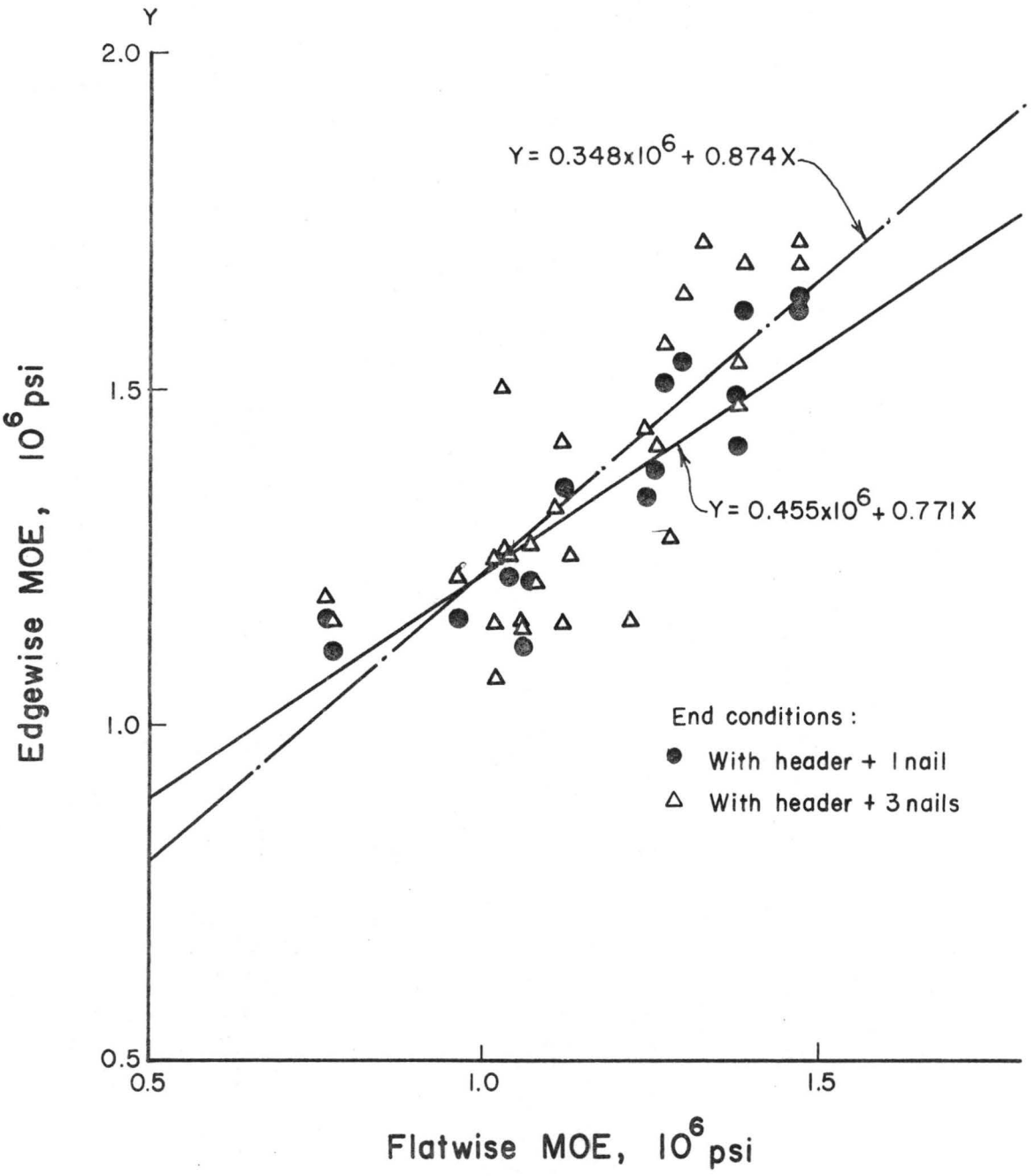

FIGURE C.5 EDGEWISE MOE VS. FLATWISE MOE FOR 2x8 ENGELMANN SPRUCE JOIST

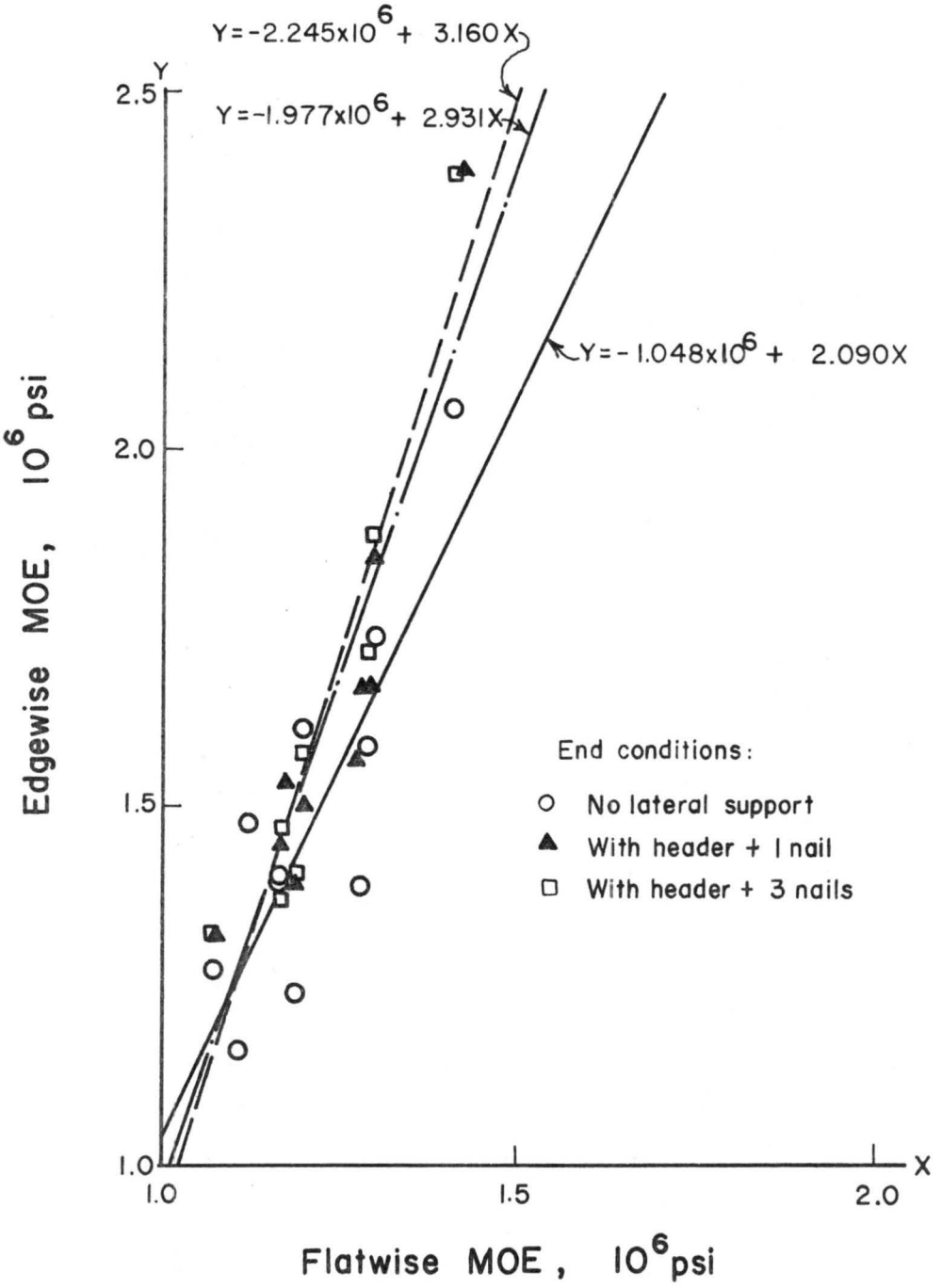

FIGURE C.6 EDGEWISE MOE VS. FLATWISE MOE FOR 2x12 DOUGLAS FIR JOIST

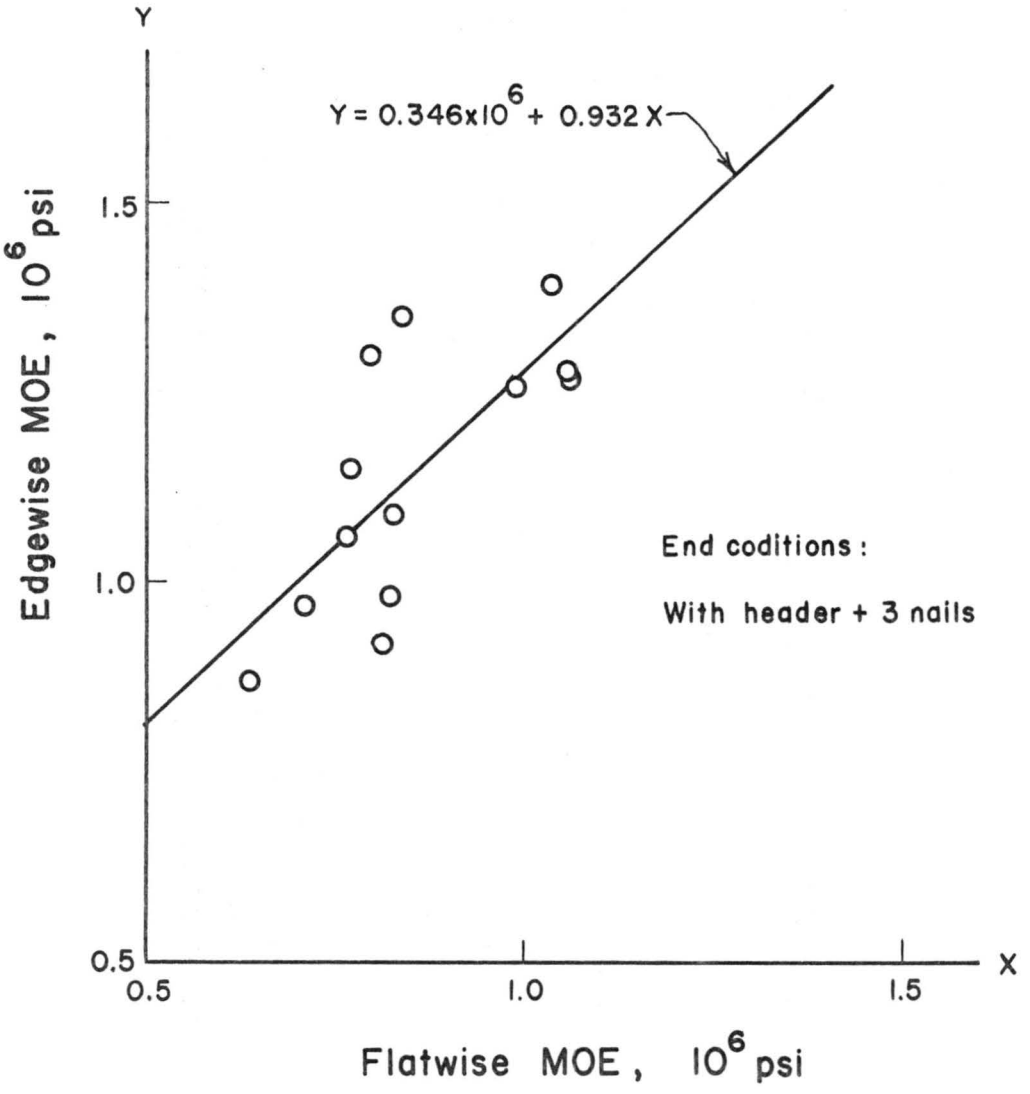

FIGURE C.7 EDGEWISE MOE VS. FLATWISE MOE FOR 2x12 ENGELMANN SPRUCE JOIST

APPENDIX D

AVERAGE CONNECTOR SLIP MODULI VALUES

APPENDIX D AVERAGE CONNECTOR SLIP MODULI VALUES

Load Level lb.	Douglas fir Joist Douglas fir Plywood Parallel to veneer	Douglas fir Joist Douglas fir Plywood Perpendicular to veneer	DF Joist 3/4" DF Plywood	DF Joist 3/4" ES Plywood	ES Joist 3/4" ES Plywood	ES Joist 3/4" DF Plywood	Joist 1/2" DF Plywood	Joist 1/2" ES Plywood	1/2" DF Particleboard 1/2" DF Plywood	1/2" DF Particleboard 1/2" ES Plywood	DF Joist DF Plywood
	8d cement-coated		8d common						6d common		Glue
	lb/in.		lb/in.						lb/in.		lb/in./in.^{2}
					Average tangent moduli						
KT 25	93,200	3,280	69,800	59,400	36,300	48,000	29,025	32,900	3,920	3,900	46,800
KT 50	58,900	3,540	56,400	33,700	32,500	25,500	15,070	13,800	3,870	3,930	36,700
KT 100	16,200	3,570	27,300	10,500	10,300	14,200	3,300	3,620	3,370	2,340	7,810
KT 150	6,080	2,890	20,000	4,160	3,700	4,900	1,217	2,300	2,460	1,010	2,750
					Average secant moduli						
KS 25	---	---	75,900	56,800	52,700	63,100	29,475	31,120	4,000	3,780	39,400
KS 50	83,400	3,260	73,500	53,700	39,000	45,200	23,900	21,360	3,900	3,810	37,300
KS 100	41,900	3,420	49,200	25,300	23,000	30,100	9,583	8,922	3,780	3,450	24,000
KS 150	---	---	31,200	12,200	11,300	12,800	3,958	4,502	3,480	2,560	8,440

Note: All values from tests conducted by the Wood Science Laboratory, see Section 3.3.

APPENDIX E

SPECIMEN CONFIGURATION AND COMPARISON OF PREDICTED AND OBSERVED DEFLECTIONS

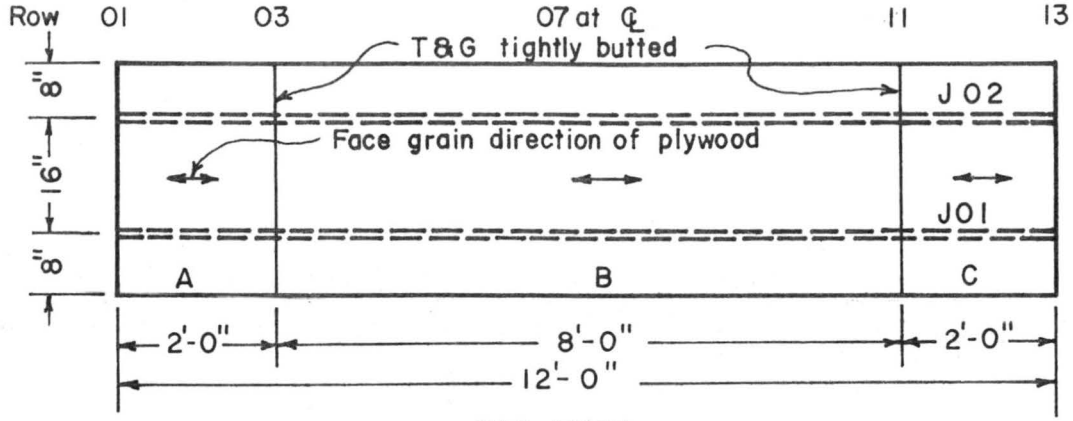

TOP VIEW

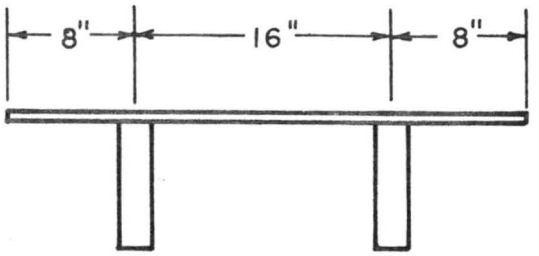

CROSS SECTION

Description of specimen

Joist: 2x8 Douglas fir

J01	DW-S-08-33	$E = 2.32 \times 10^6$ psi
J02	DW-S-08-39	$E = 1.811 \times 10^6$ psi

Sheathing: 3/4" D.F. Plywood

A	DP-34-28	$E_{\perp} = 1.133 \times 10^6$ psi
B	DP-34-27	$E_{\perp} = 1.341 \times 10^6$
C	DP-34-28	

Connector: Franklin Construction Adhesive

Sheathing Joints: T&G tightly butted

Test sequence

1. Loaded at row 07 with ΔP = 250 lb up to P = 1000 lb
2. Loaded at row 09 with loads same in 1
3. Loaded at row 11 with loads same as in 1
4. Cut gaps at rows 03 and 11, repeated test 1.

Fig. E.1 Configuration and Properties of Specimen T3-8D16-1

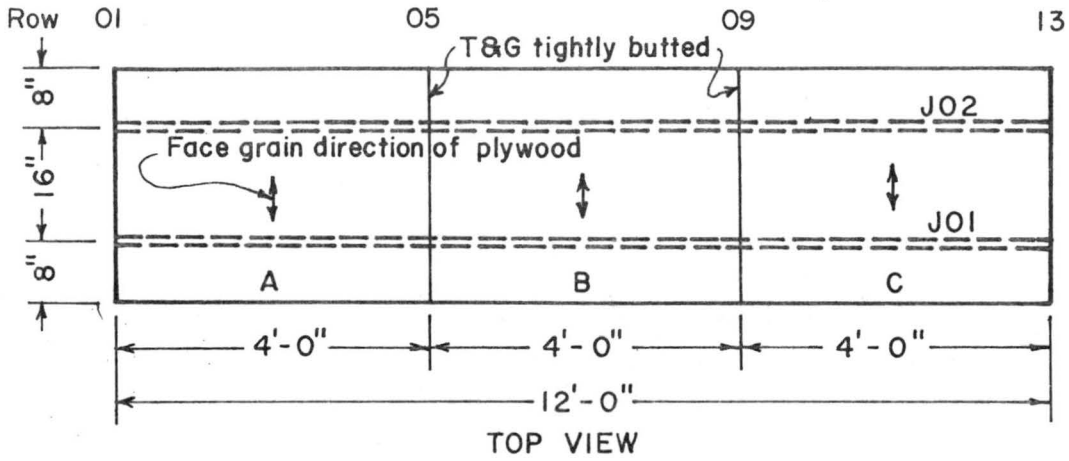

TOP VIEW

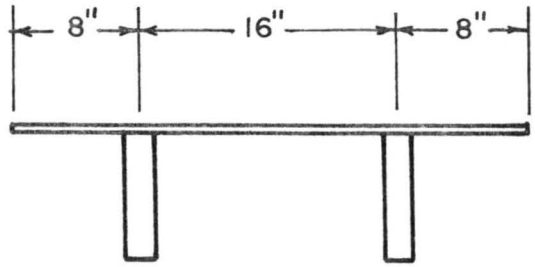

CROSS SECTION

Description of Specimen:

Joist: 2x8 Douglas fir

J01	DW-S-08-37	$E = 2.429 \times 10^6$ psi
J02	DW-S-08-43	$E = 1.694 \times 10^6$ psi

Sheathing: 3/4" D. F. Plywood

A	DP-34-25	$E_{\perp} = 5.50 \times 10^5$ psi
B	DP-34-25	
C	DP-34-25	

Connector: 8-d common nails, spacing @ 8"

Sheathing joints: Tongue & groove, tightly butted.

Slip modulus: k = 30,000 lb/in

Test sequence:

1. Loaded at row 07 with ΔP = 250 lb up to P = 1000
2. Loaded at row 09 with loads same in 1
3. Loaded at row 11 with loads same in 1
4. Cut gaps at rows 05 and 09; repeated tests 1, 2 and 3
5. Failure test: loaded at row 07; J02 failed at P = 4000 lbs.

Fig. E.2 Configuration and Properties of Specimen T4-8D16-1

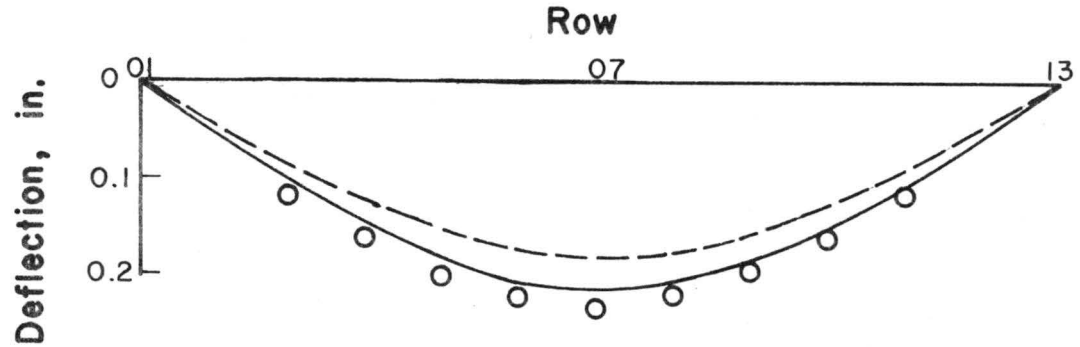

(a). Deflection Profile at 500 lbs. Load at Midspan

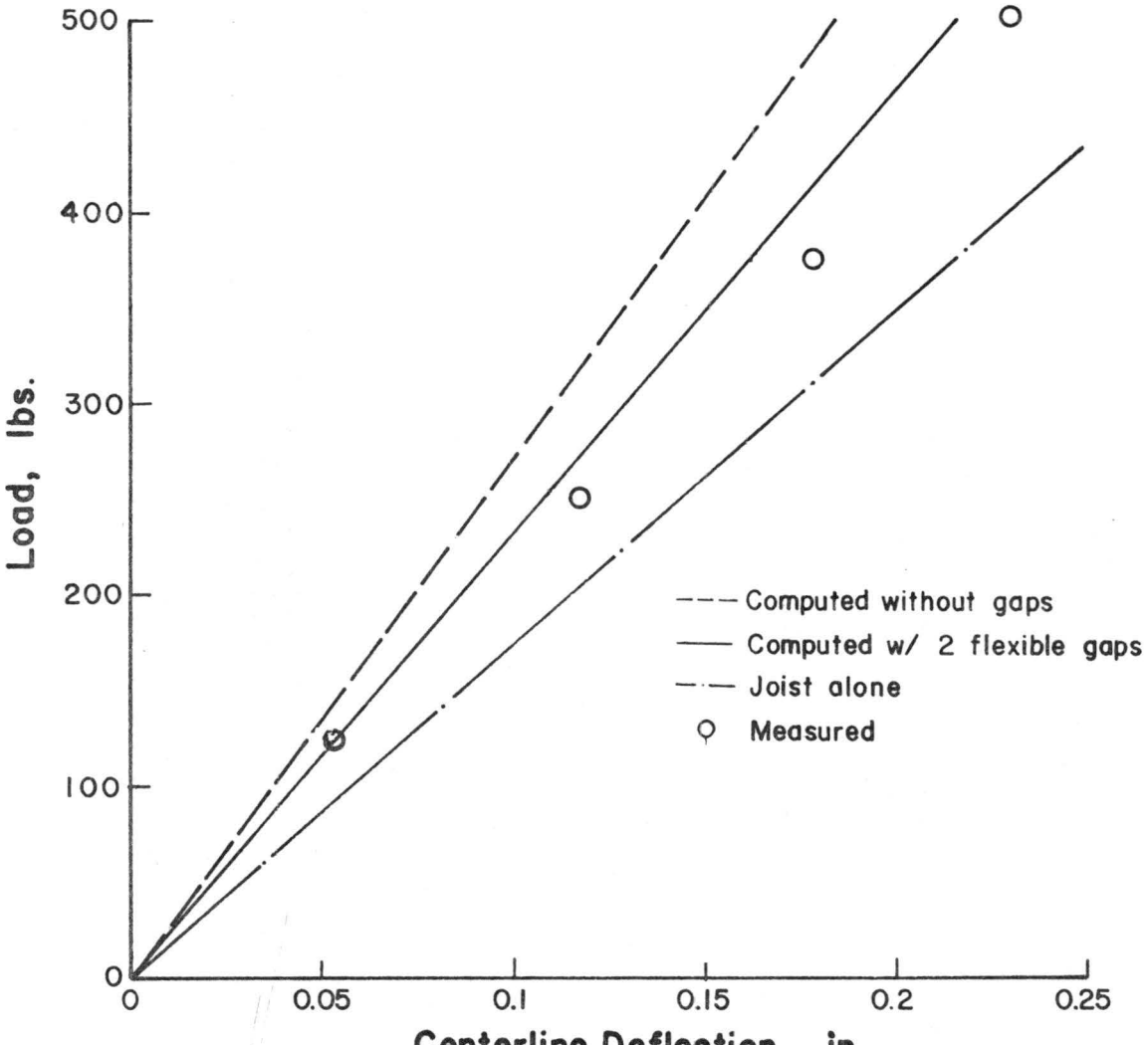

(b). Load-Deflection Behavior

Figure E.3. Beam Verification - T4-8D16-1 J01 with Butted T&G Joints

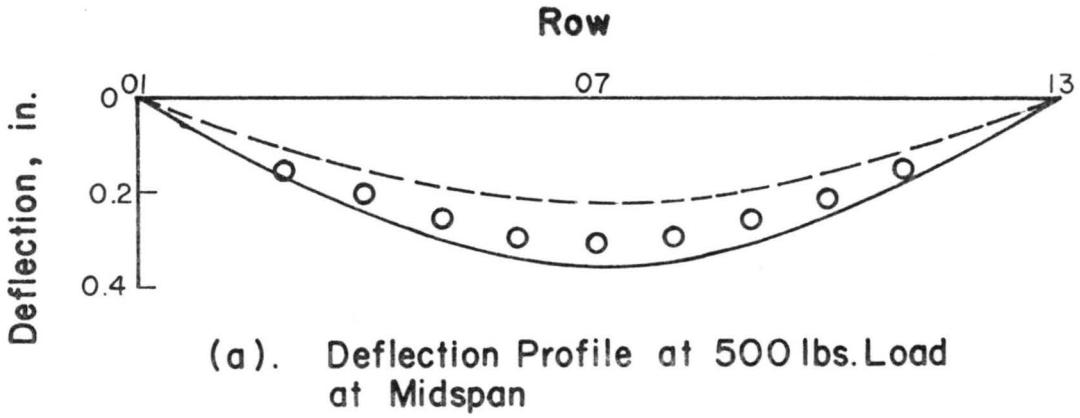

(a). Deflection Profile at 500 lbs. Load at Midspan

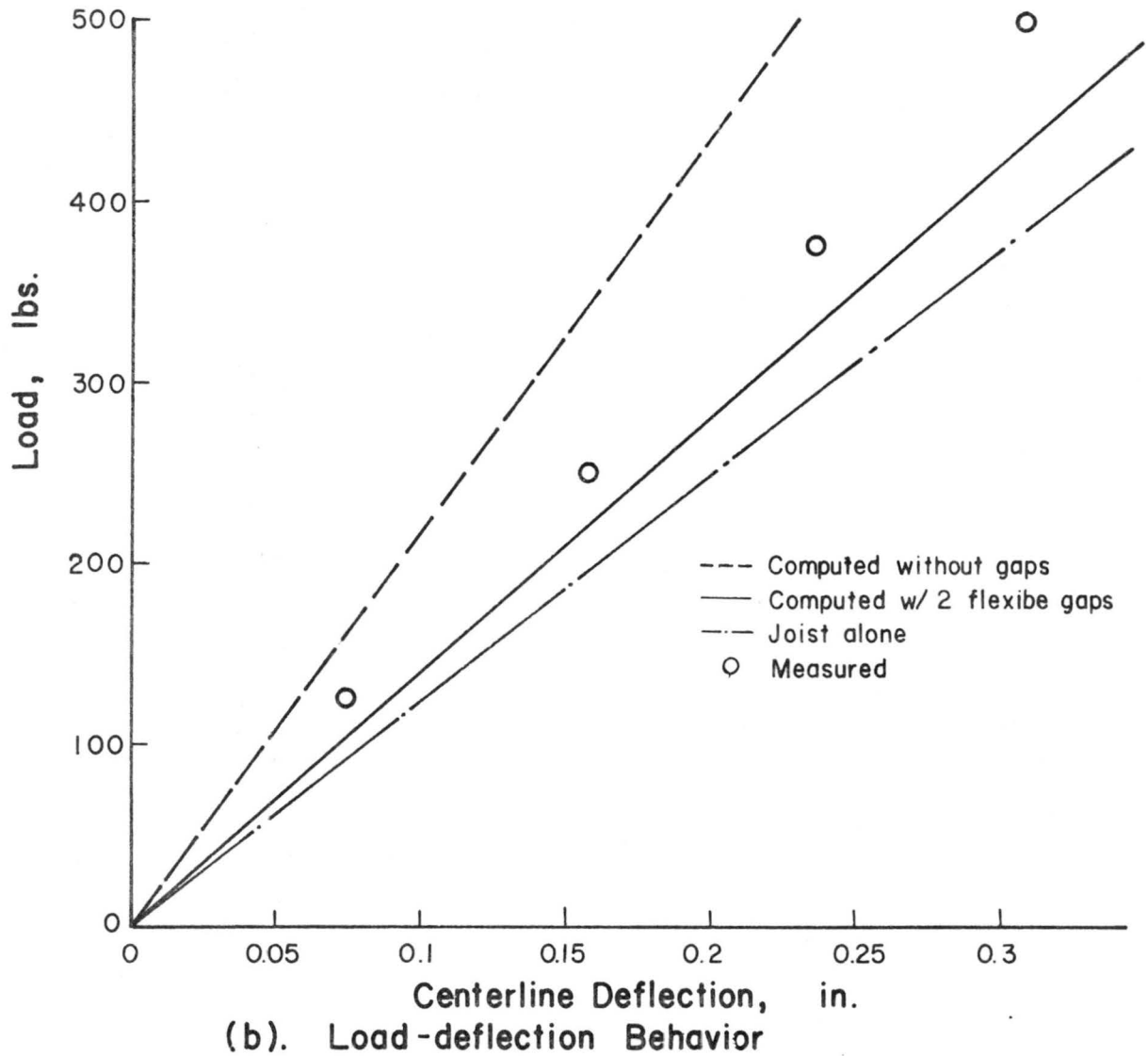

(b). Load-deflection Behavior

Figure E.4. Beam Verification - T4-8D16-1 JO2 with Butted T&G Joints

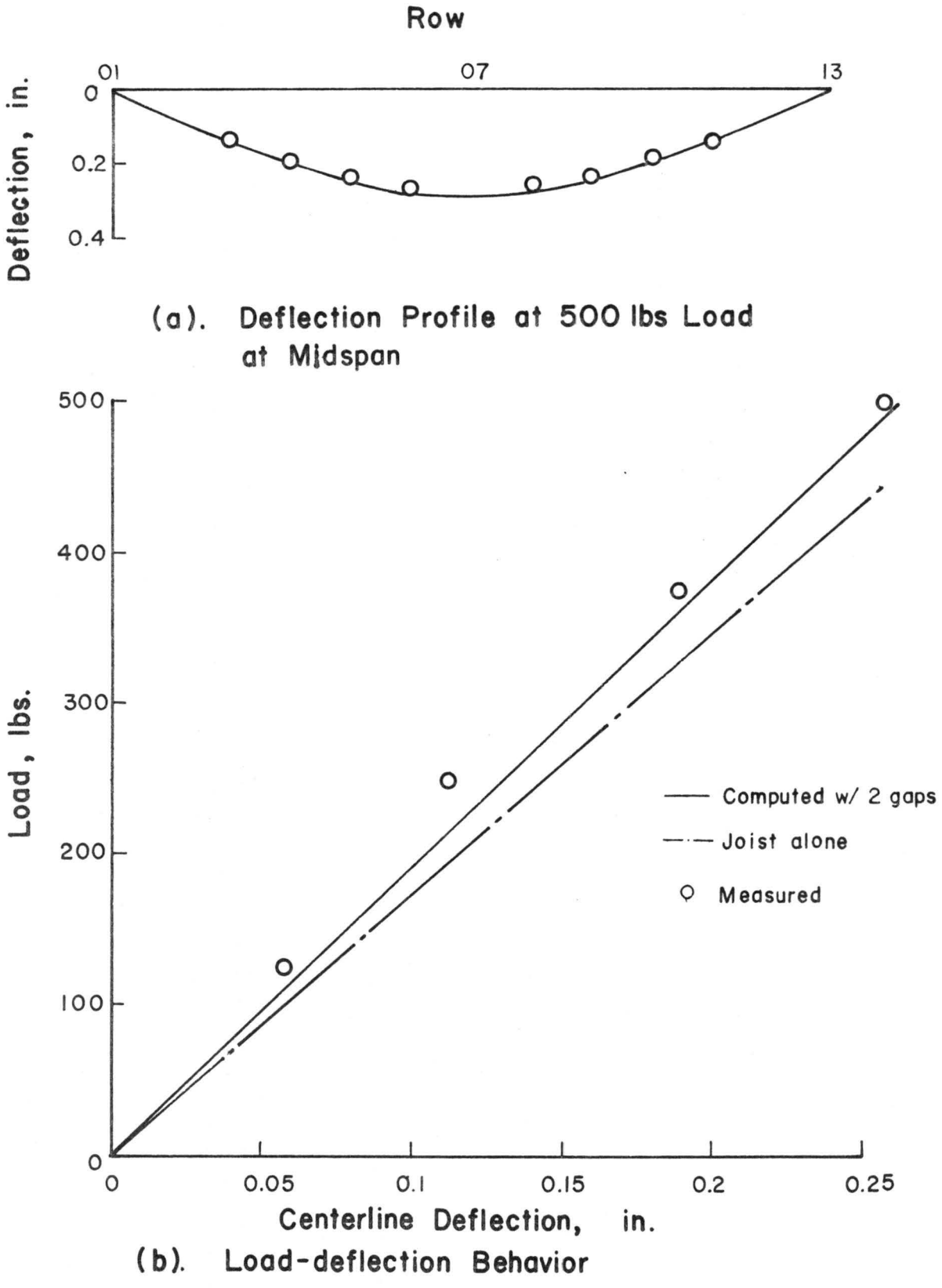

Figure E.5. Beam Verification - T4-8D16-1
J01 with Gaps

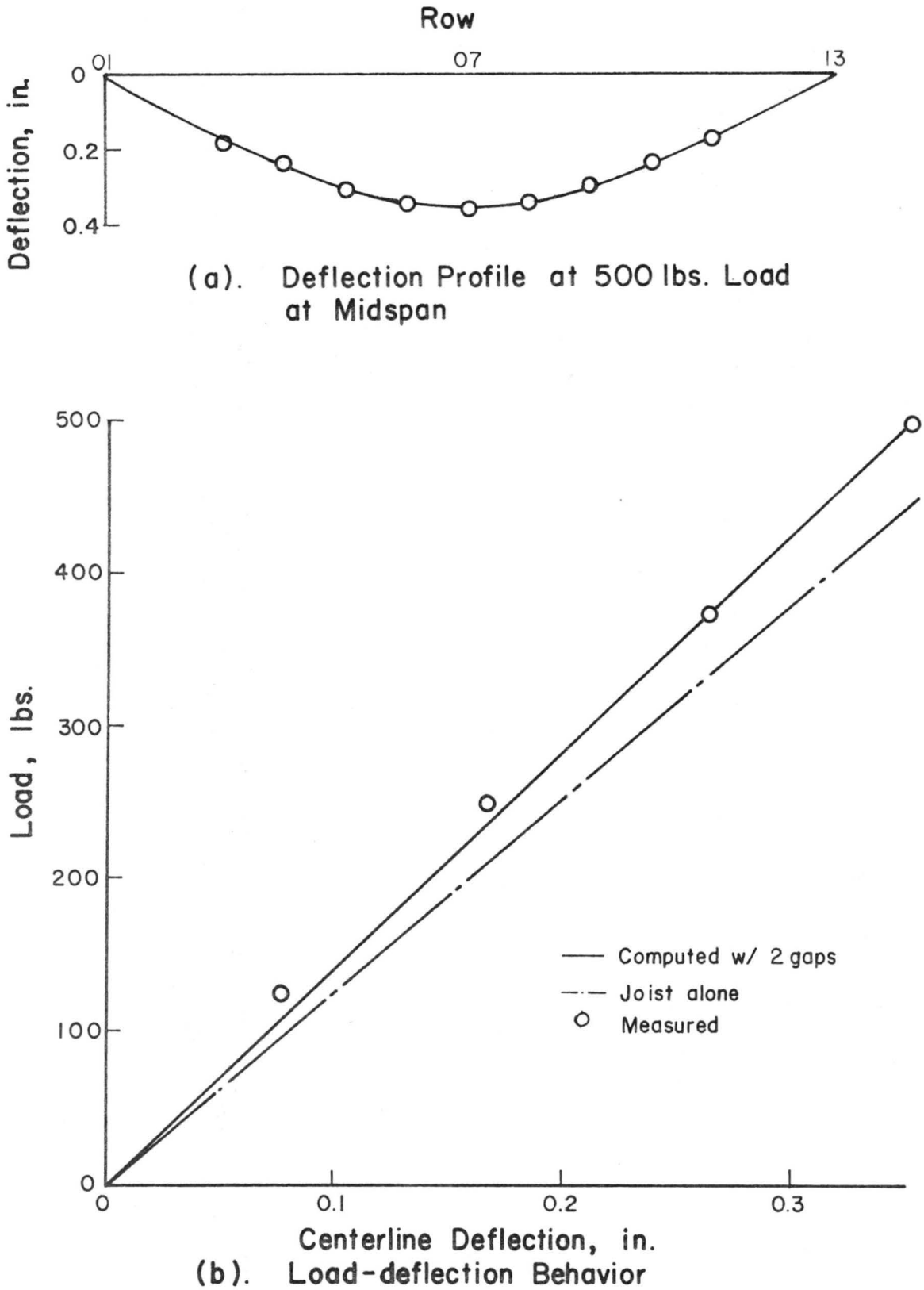

Figure E.6. Beam Verification - T4-8D16-1
J02 with Gaps

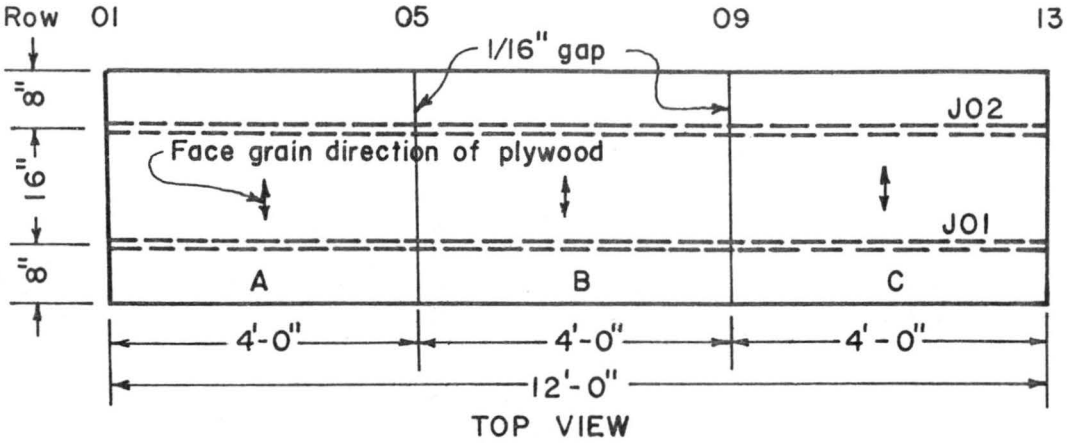

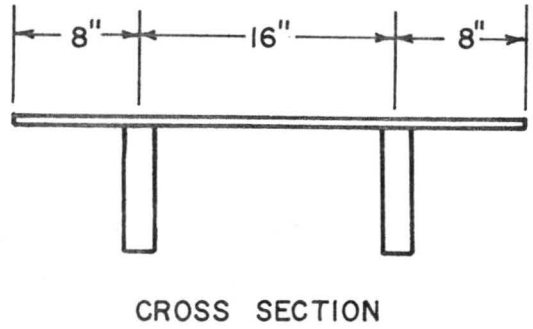

Description of specimen:

Joist: 2x8 Douglas fir

J01	DW-S-08-27	$E = 1.847 \times 10^6$ psi
J02	DW-S-08-34	$E = 1.774 \times 10^6$

Sheathing: 3/4" D.F. Plywood

A	DP-34-21	$E_{\perp} = 5.39 \times 10^5$ psi
B	DP-34-21	
C	DP-34-21	

Connector: 8-d common nail spacing at 8"

Sheathing Joints: T&G with 1/16" gap

Slip Modulus: k = 30,000 lb/in

Test sequence

1. Loaded at row 07 with ΔP = 250 lb up to P = 1000 lbs.
2. Loaded at row 09 with loads same in 1
3. Loaded at row 11 with loads same in 1
4. Cut gaps at rows 05 and 09; repeated tests from 1 to 3
5. Failure test: P at row 07; J01 failed at P = 5500 lbs.

Fig. E.7 Configuration and Properties of Specimen T5-8D16-1

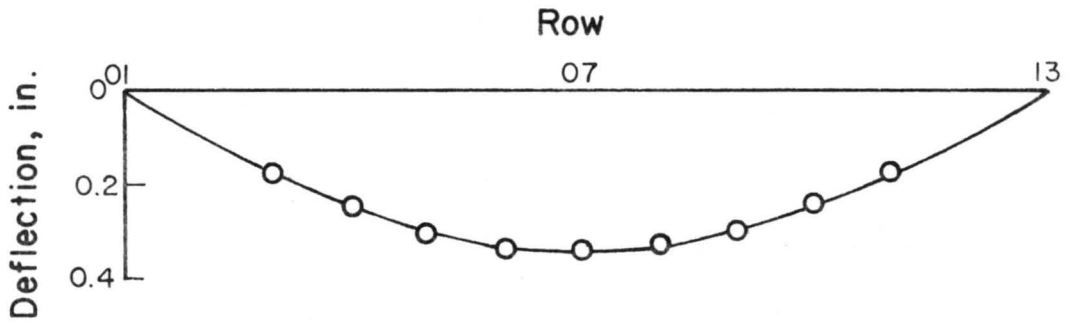

(a). Deflection Profile at 500 lbs. Load at Midspan

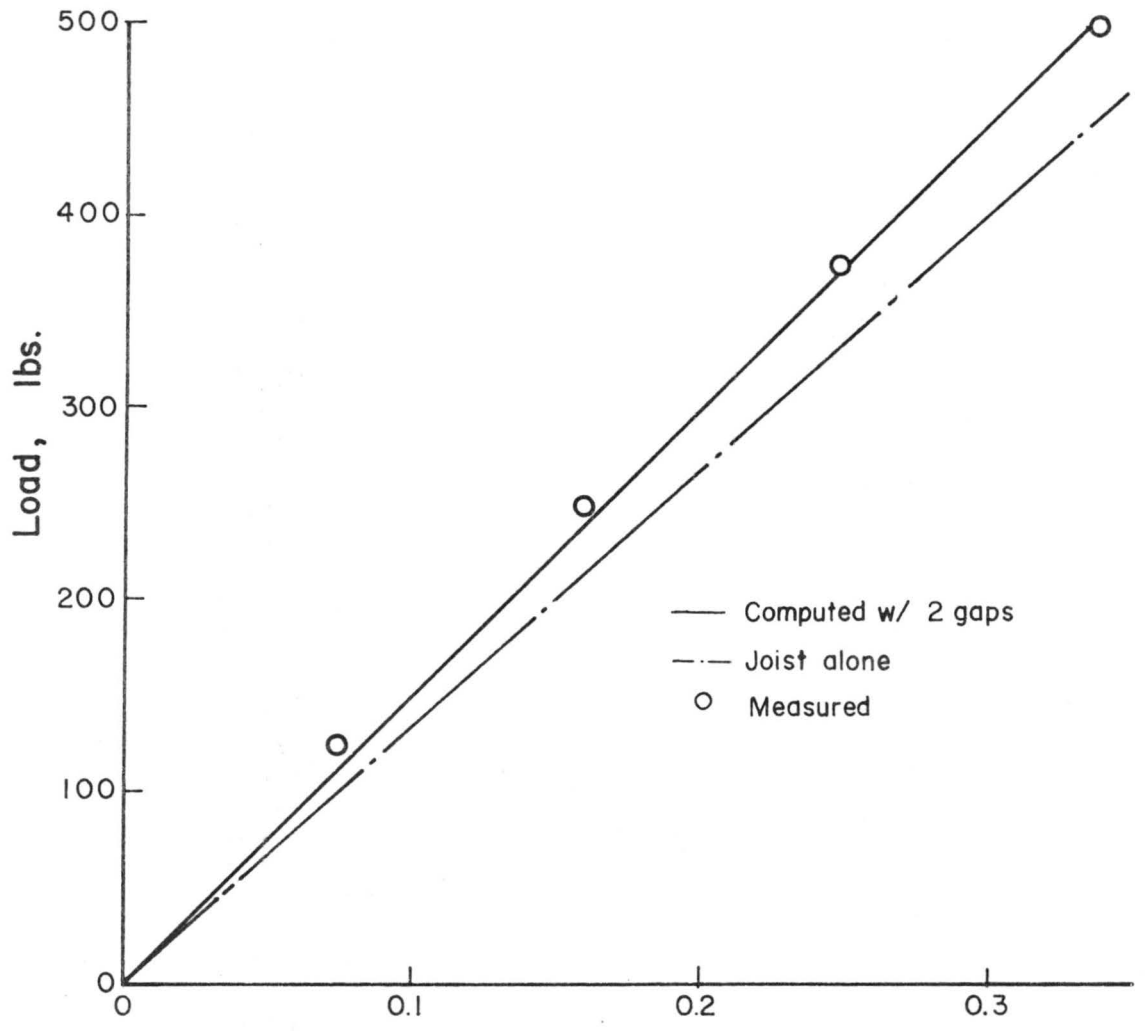

(b). Load-deflection Behavior

Figure E.8. Beam Verification - T5-8D16-1 J01 with Gaps

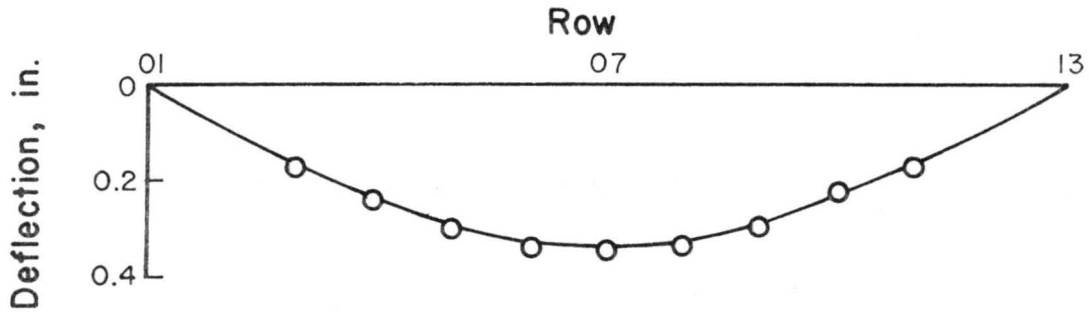

(a). Deflection Profile at 500 lbs. Load at Midspan

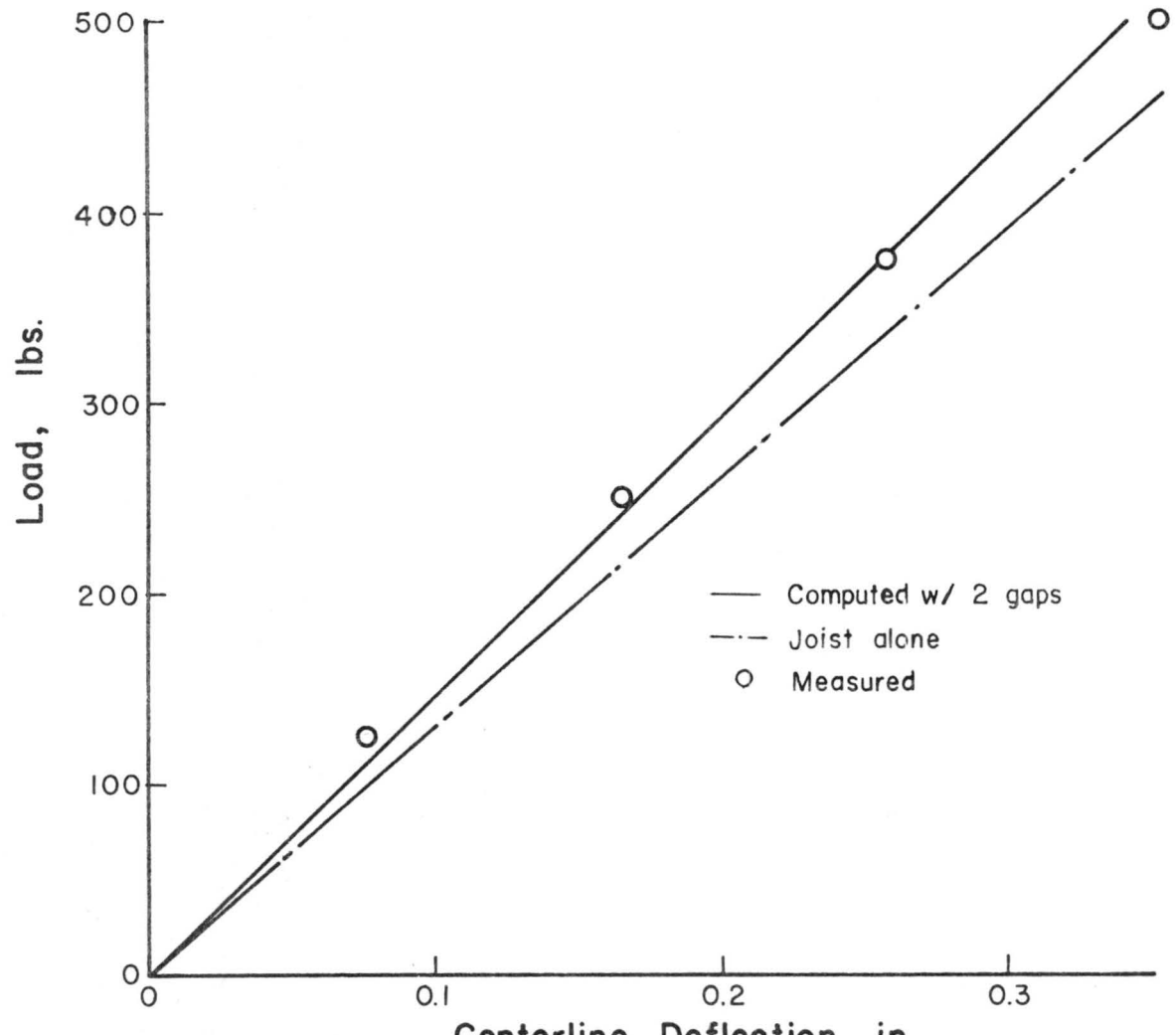

(b). Load-deflection Behavior

Figure E.9. Beam Verification - T5-8D16-1 JO2 with Gaps

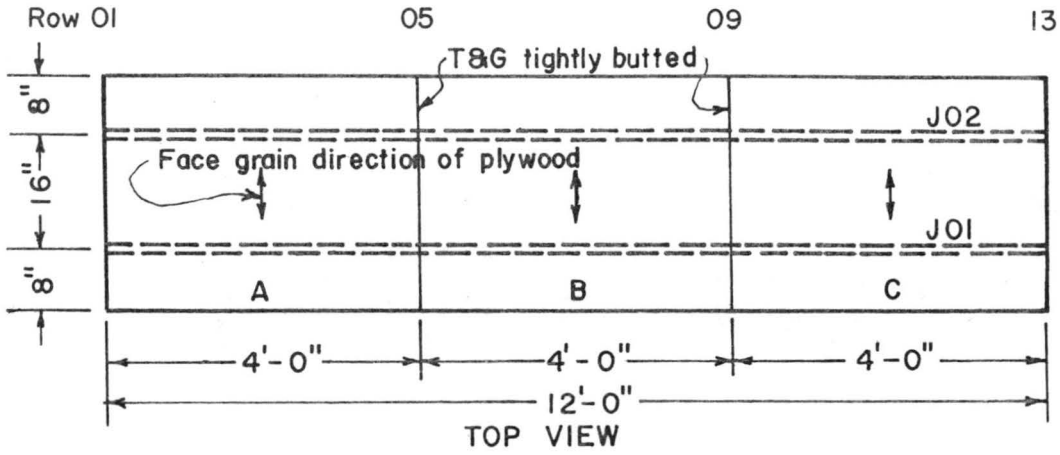

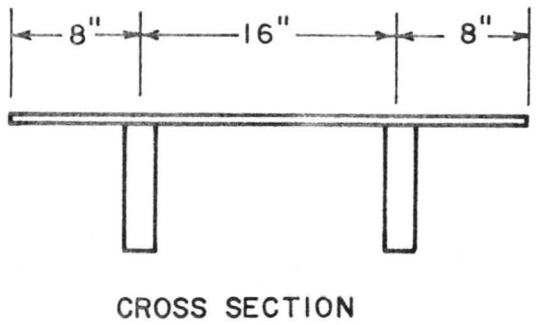

Description of specimen:

Joist: 2x8 Douglas fir

J01	DW-S-08-15	$E = 2.330 \times 10^6$ psi
J02	DW-S-08-23	$E = 2.349 \times 10^6$ psi

Sheathing: 3/4" D.F. Plywood

A	DP-34-20	$E_{\perp} = 6.008 \times 10^5$ psi
B	DP-34-20	
C	DP-34-20	

Connector: 8-d common nails spacing at 8"

Sheathing Joints: T&G tightly butted

Slip Modulus: k = 30,000 lb/in

Test sequence

1. Loaded at row 07 with controlling $\Delta = 0.1$" for each increment, up to $\Delta = 0.4$"
2. Repeated test 1 for five times
3. Failure test with P at row 07; J01 failed at P = 5900 lbs.

Fig. E.10 Configuration and Properties of Specimen T6-8D16-1

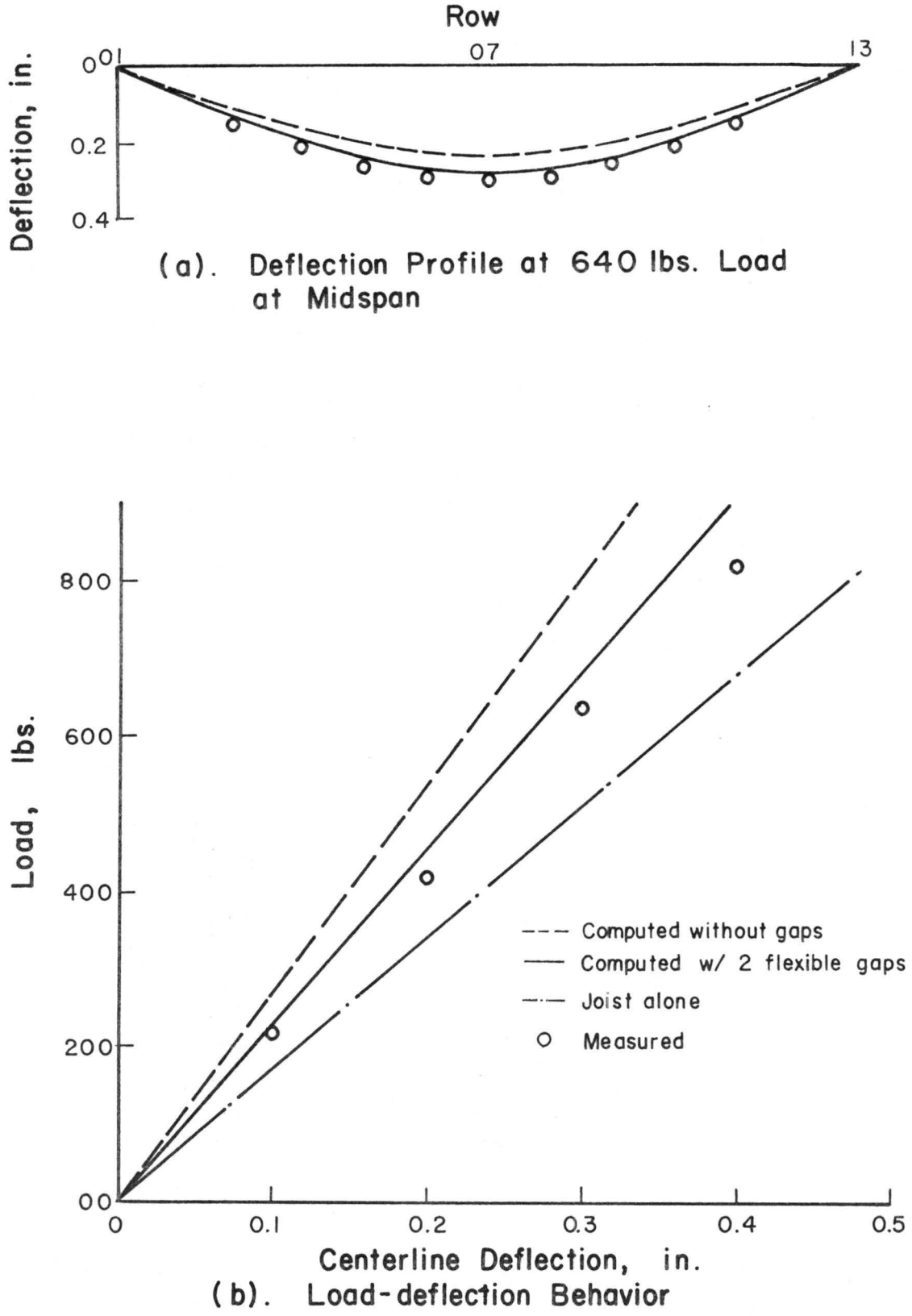

Figure E.11. Beam Verification - T6-8D16-1
J01 with Butted T&G Joints

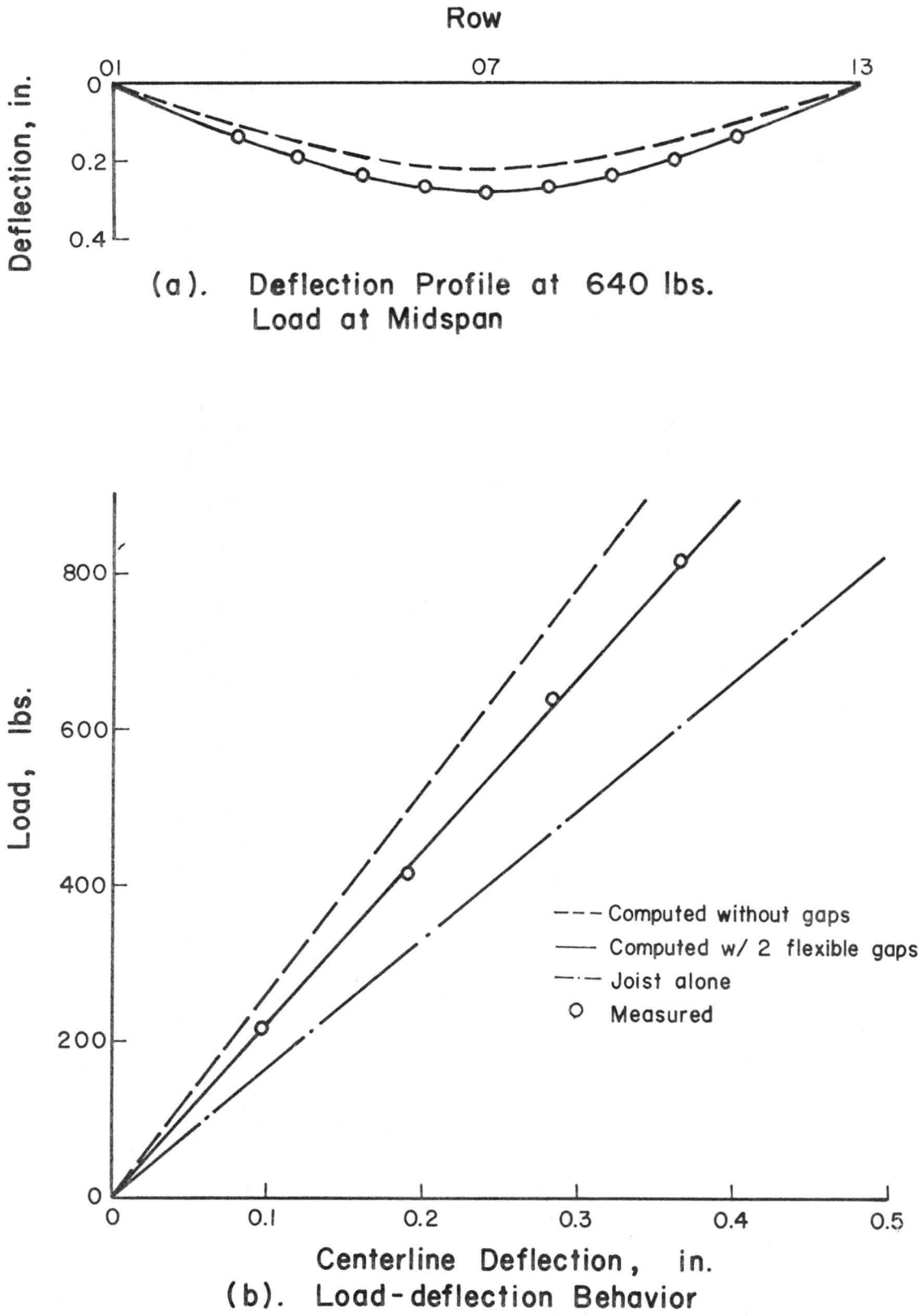

Figure E.12. Beam Verification - T6-8D16-1 JO2 with Butted T&G Joints.

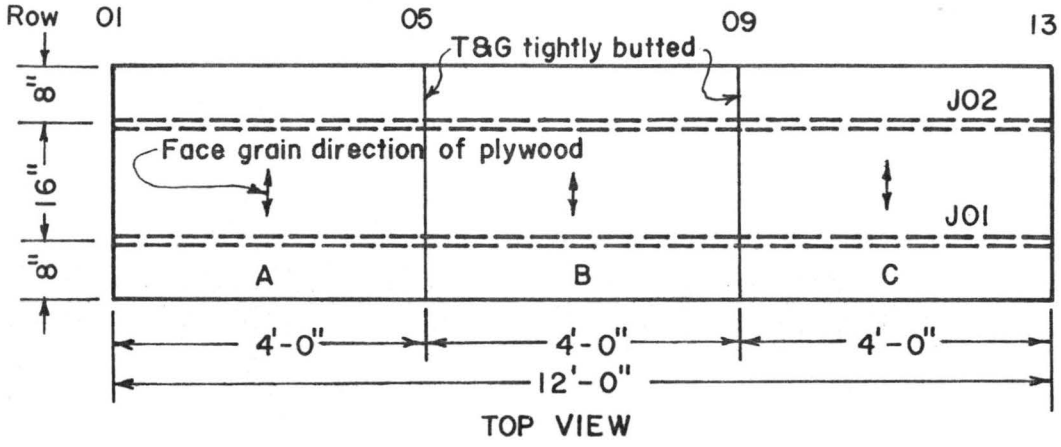

TOP VIEW

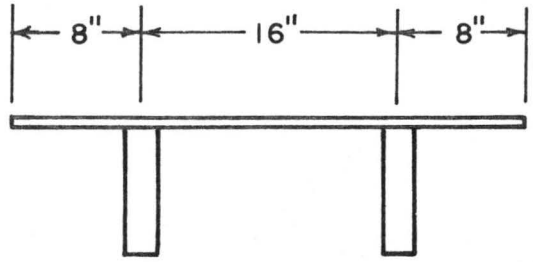

CROSS SECTION

Description of specimen:

Joist: 2x8 Douglas fir

J01	DW-S-08-45	$E = 2.141 \times 10^6$ psi
J02	DW-S-08-58	$E = 2.152 \times 10^6$ psi

Sheathing: 3/4" D.F. Pluwood

A	DP-34-22	$E_{\perp} = 5.30 \times 10^5$ psi
B	DP-34-22	
C	DP-34-22	

Connector: 8-d common nails spacing at 2"

Sheathing Joints: T&G tightly butted

Slip Modulus: k = 50,000 lb/in

Test sequence

1. Loaded at row 07 with controlling $\Delta = 0.1$" for ecach increment, up to $\Delta = 0.4$"
2. Repeated test 1 for five times
3. Failure test with P at row 07; J01 failed at P = 7500 lbs.

Fig. E.13 Configuration and Properties of Specimen T7-8D16-1

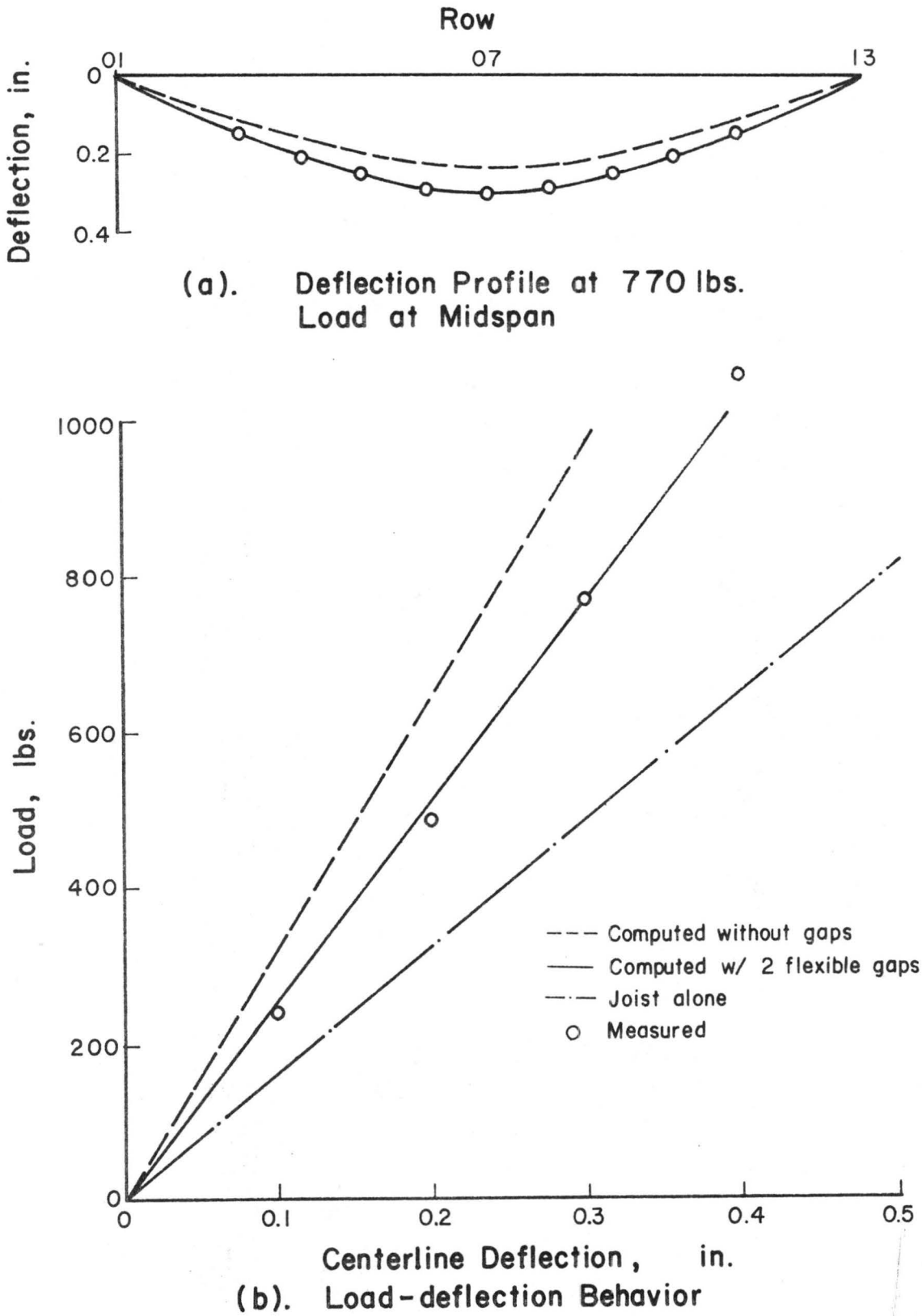

Figure E.14. Beam Verification - T7-8D16-1 JO1 with Butted T&G Joints

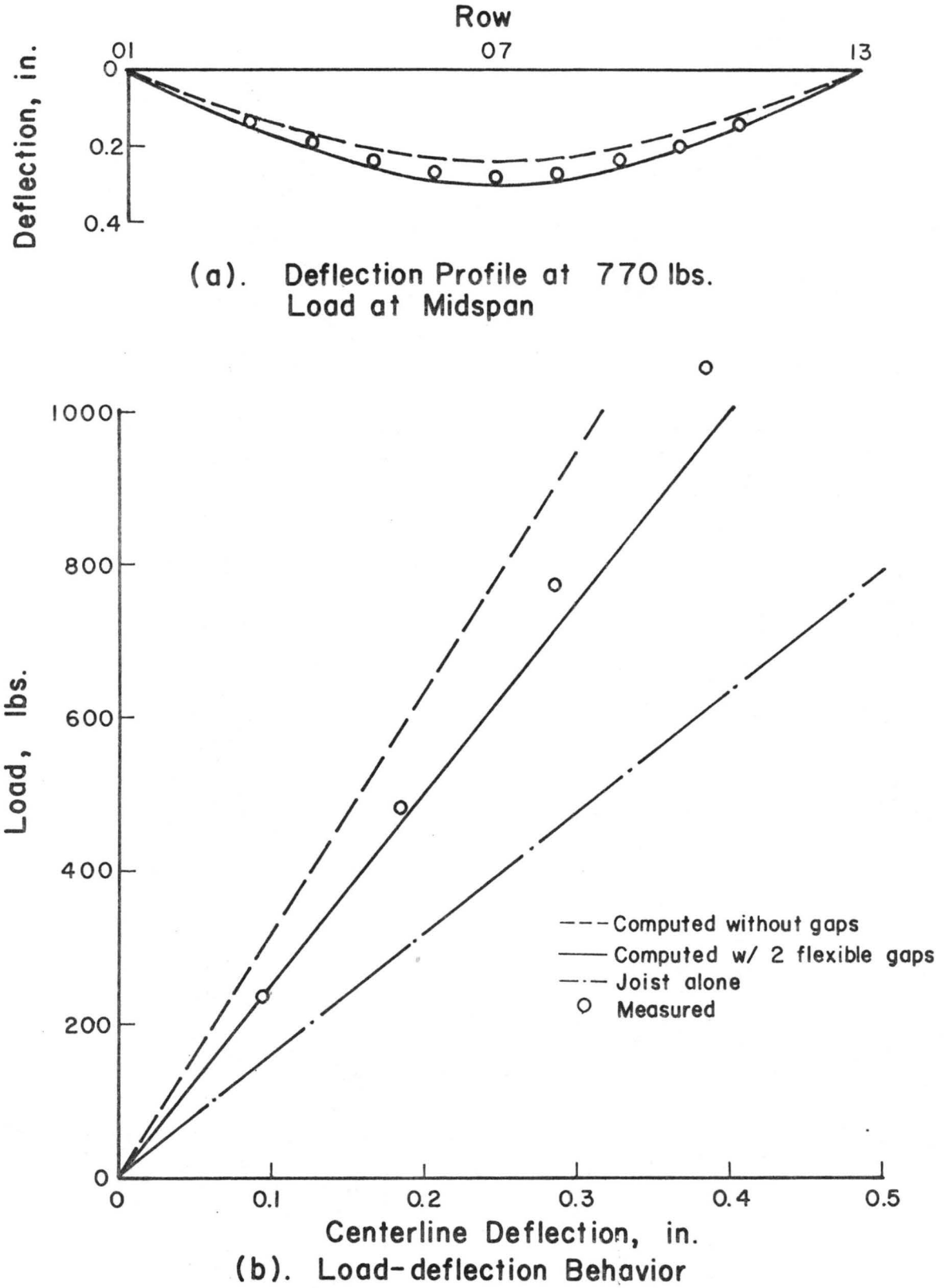

Figure E.15. Beam Verification - T7- 8D16-1
J02 with Butted T&G Joints

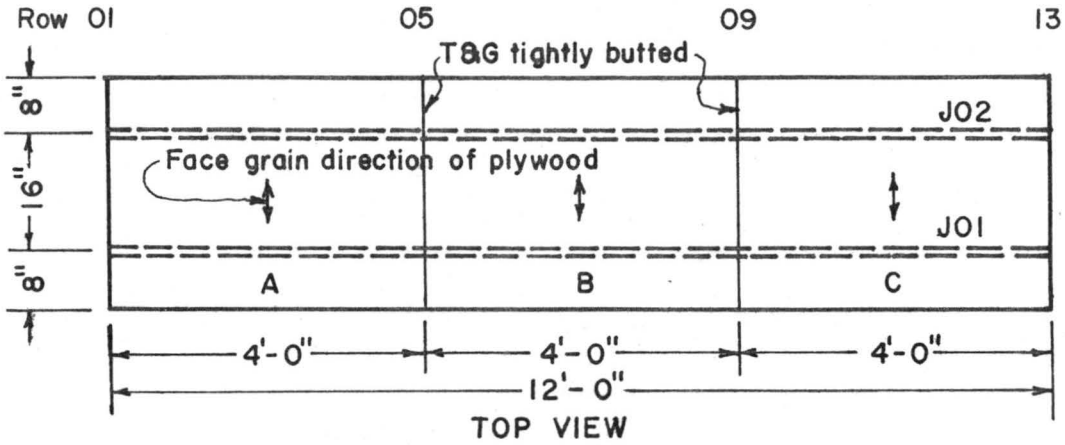

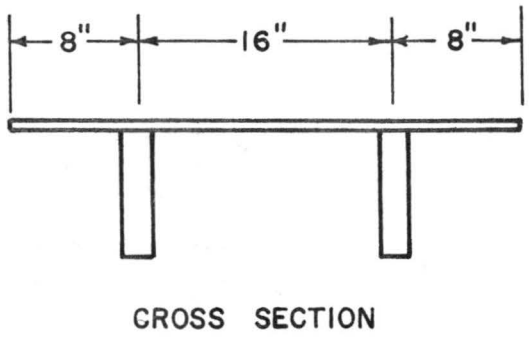

Description of specimen:

Joist: 2x8 Douglas fir

J01	DW-S-08-22	$E = 1.805 \times 10^6$ psi
J02	DW-S-08-29	$E = 1.744 \times 10^6$ psi

Sheathing: 3/4" D.F. Plywood

A	DP-34-17	$E_{\perp} = 4.912 \times 10^5$ psi
B	DP-34-17	
C	DP-34-17	

Connector: Franklin Construction Adhesive and 8d common nails spaced at 8"

Sheathing Joints: T&G tightly butted

Slip Modulus: $k = 16{,}000$ lb/in^2 + 30,000 lb/in

Test sequence

1. Loaded at row 07 with $\Delta P = 500$ lb up to $P = 2500$ lbs
2. Repeated test 1 for three times
3. Cut gaps at rows 05 and 09; repeated test 1
4. Gaps filled with wood strip and repeated test 1
5. Test to failure: P at row 07; J01 failed at $P = 5900$ lbs.

Fig. E.16 Configuration and Properties of Specimen T8-8D16-1

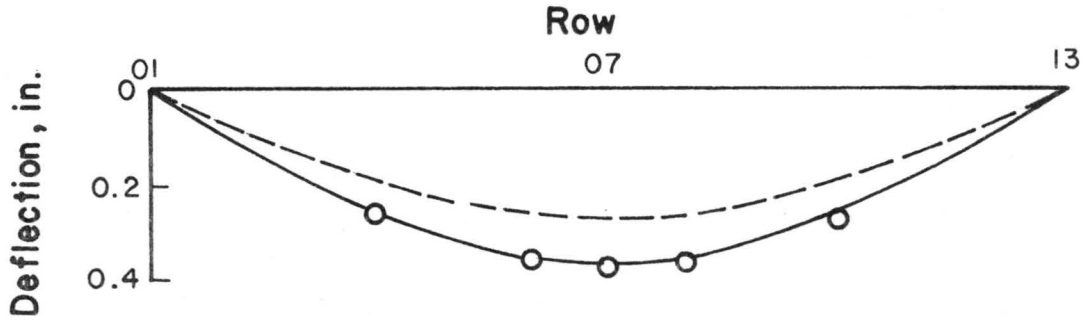

(a). Deflection Profile at 750 lbs. Load at Midspan

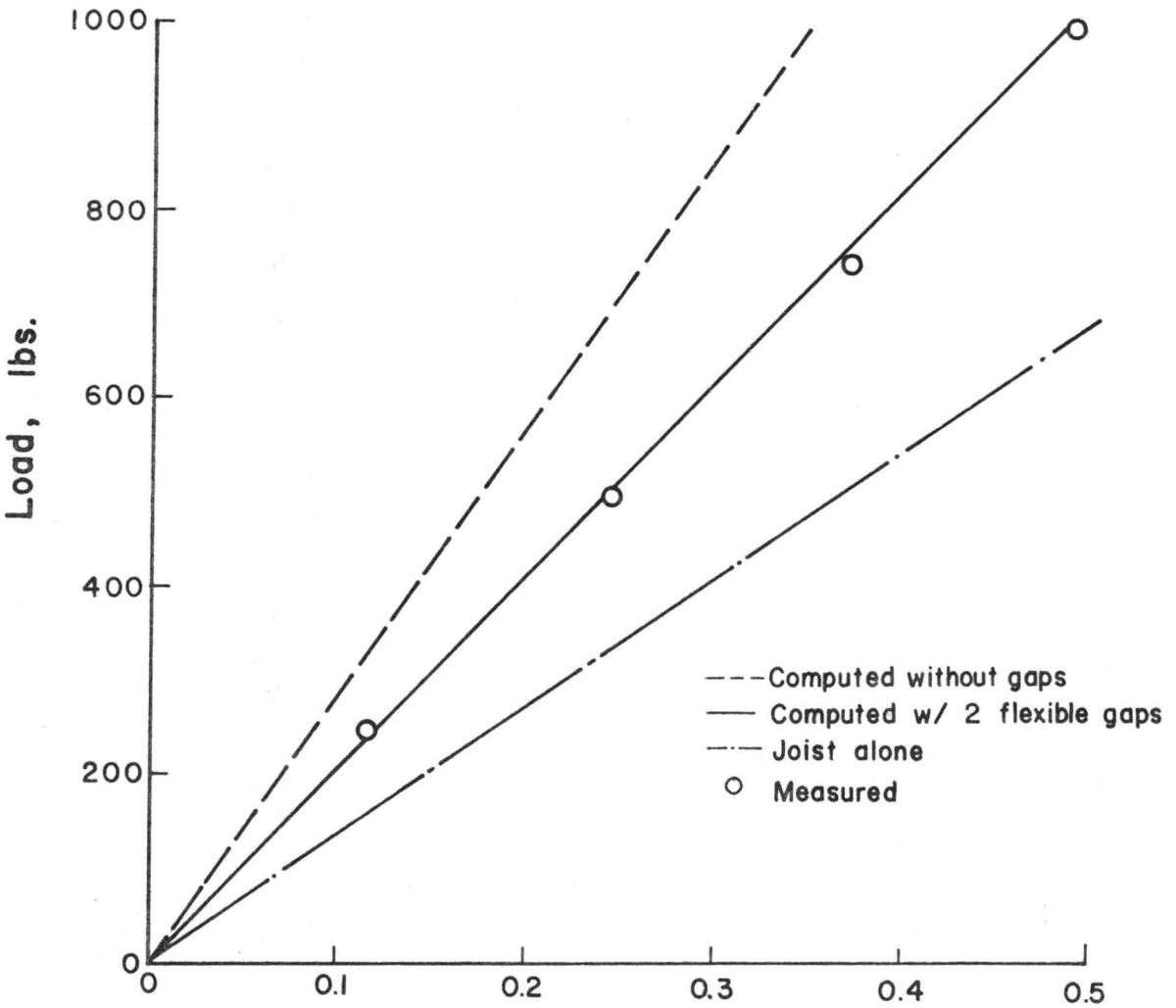

(b). Load-deflection Behavior

Figure E.17. Beam Verification - T8-8D16-1 JO1 with Butted T&G Joints

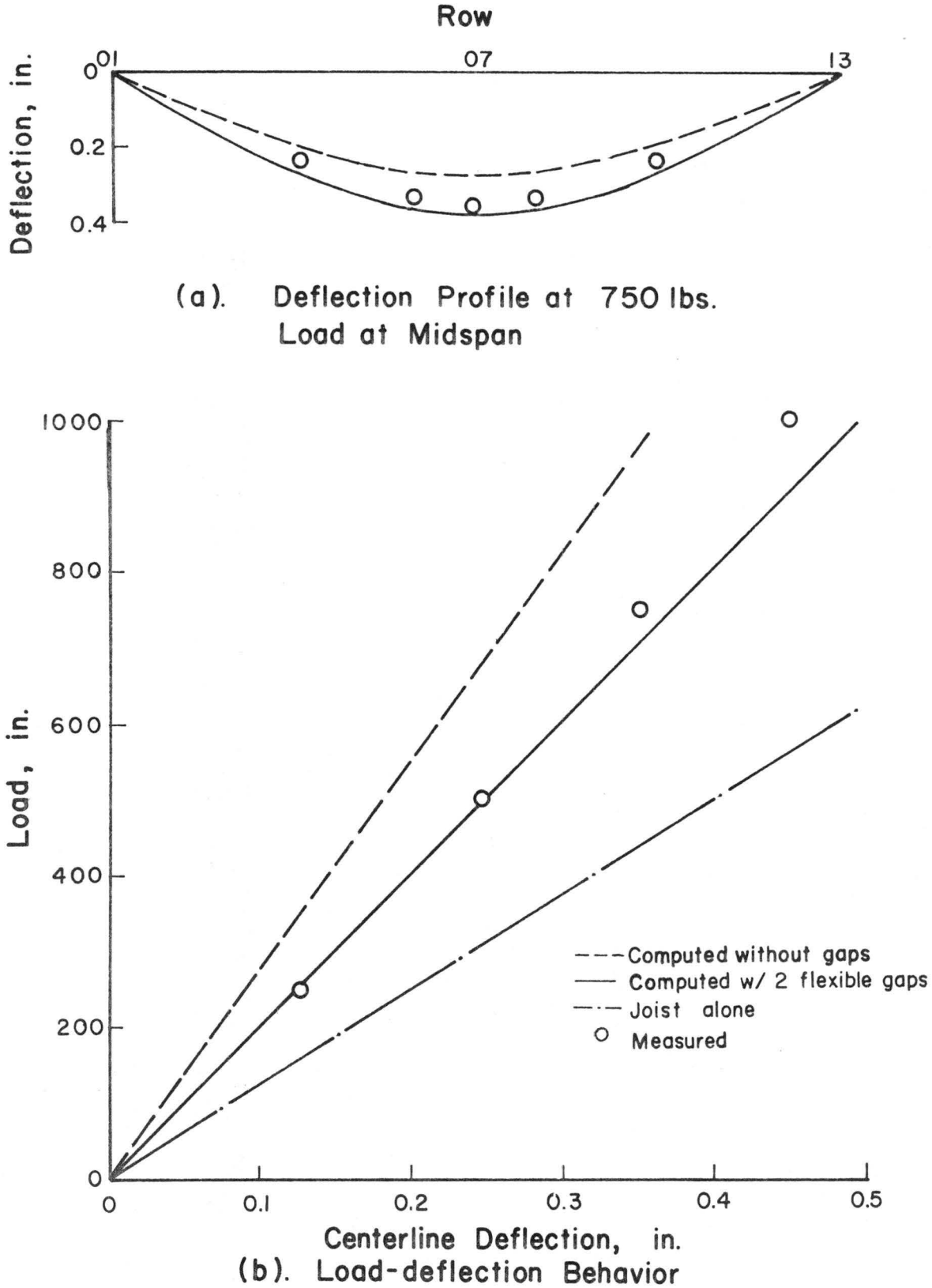

Figure E.18. Beam Verification - T8-8D16-1
JO2 with Butted T&G Joints

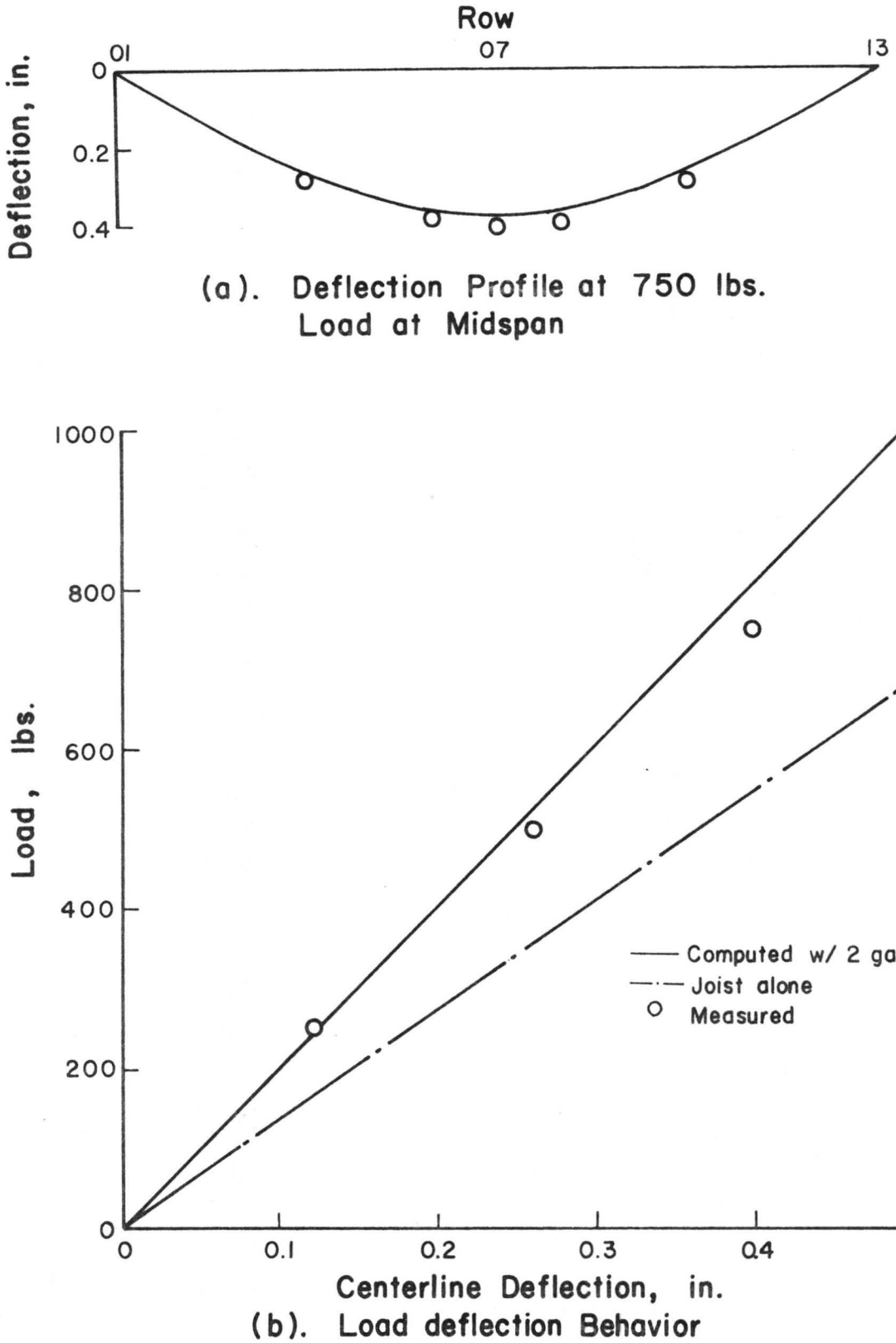

Figure E.19. Beam Verification - T8-8D16-1
J01 with Gaps

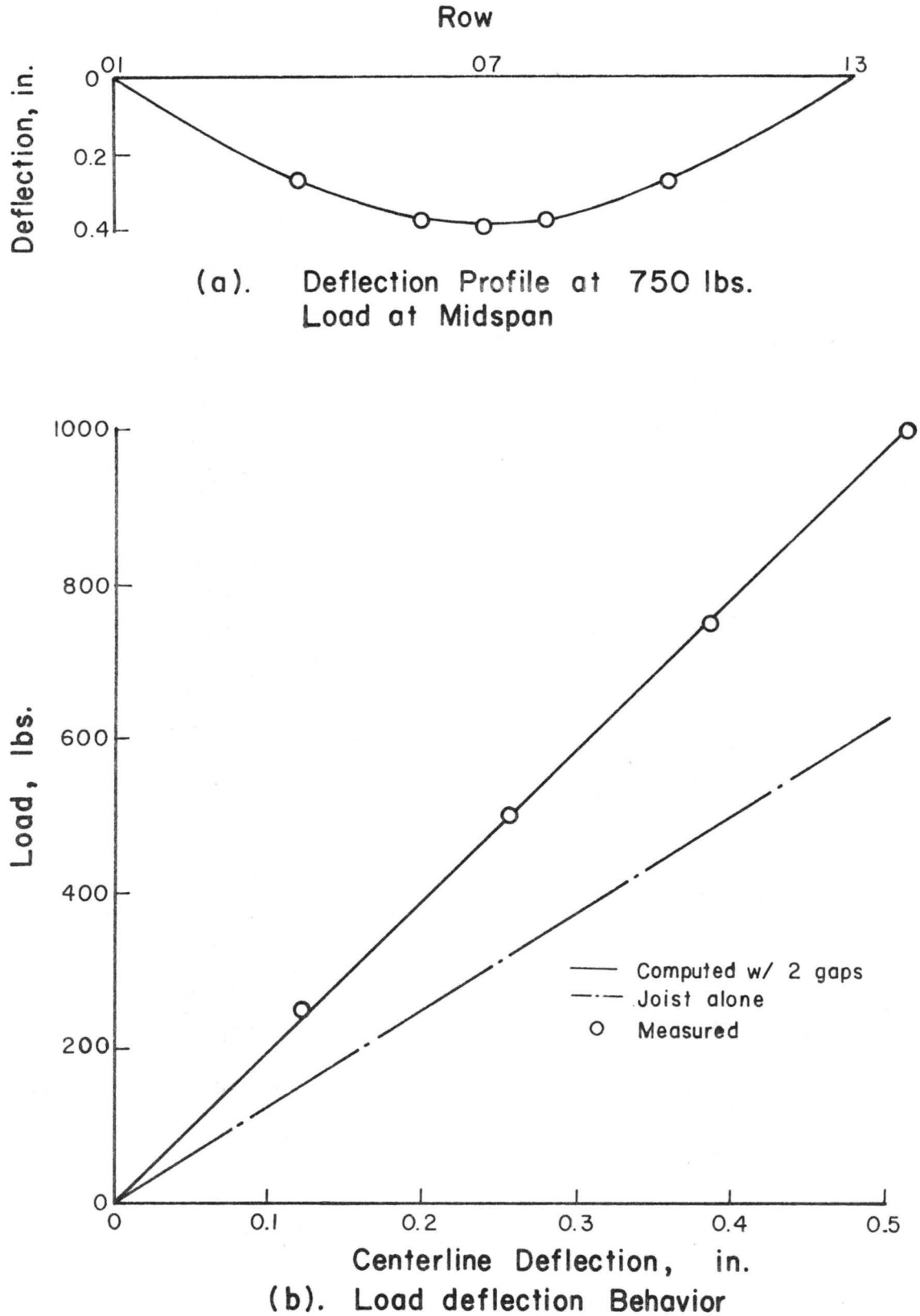

Figure E.20. Beam Verification - T8-8D16-1
JO2 with Gaps

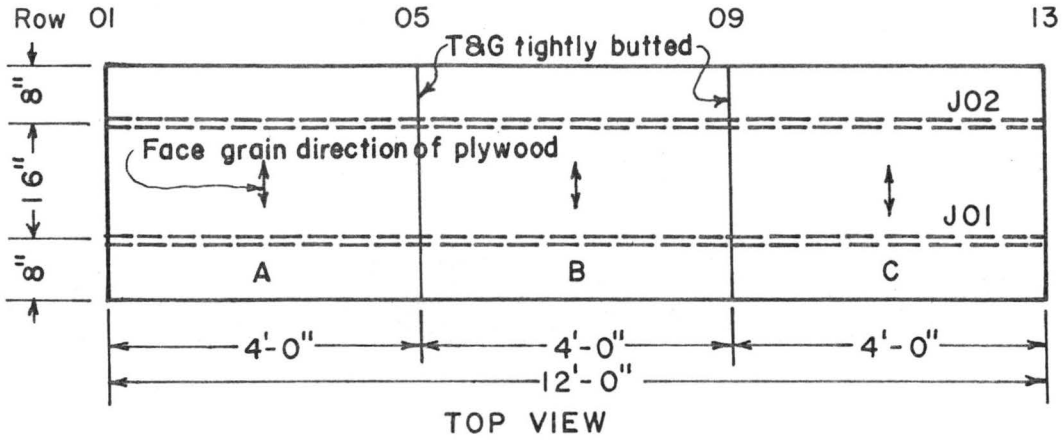

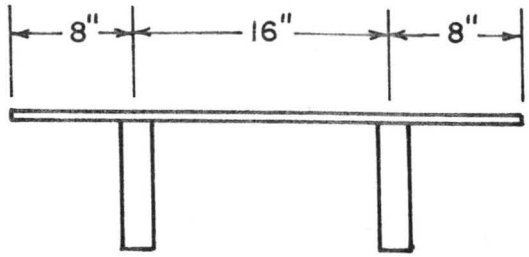

Description of specimen:

Joist: 2x8 Douglas fir

J01	DW-S-08-12	$E = 2.269 \times 10^6$ psi
J02	DW-S-08-05	$E = 2.566 \times 10^6$

Sheathing: 3/4" D.F. Plywood

A	DP-34-18	$E_{\perp} = 5.352 \times 10^5$ psi
B	DP-34-18	$E_{\perp} = 5.352 \times 10^5$ psi
C	DP-34-18	$E_{\perp} = 5.352 \times 10^5$ psi

Connector: Franklin Construction Adhesive

Sheathing Joints: T&G tightly butted

Slip Modulus: $k = 16{,}000$ lb/in^2

Test sequence

1. Loaded at row 07 with $\Delta P = 500$ lbs up to $P = 2500$ lbs
2. Repeated test 1 for five times
3. Cut gaps at rows 05 and 09; reloaded same as in 1
4. Gaps filled with wood strip; repeated test 1
5. Gaps filled; repeated test 1 up to $P = 4000$ lbs
6. Test to failure: P at row 07; J02 cracked and completely failed at $P = 10{,}000$ lbs.
7. Test to failure for single T, J01 failure load = 5000 lbs

Fig. E.21 Configuration and Properties of Specimen T9-8D16-1

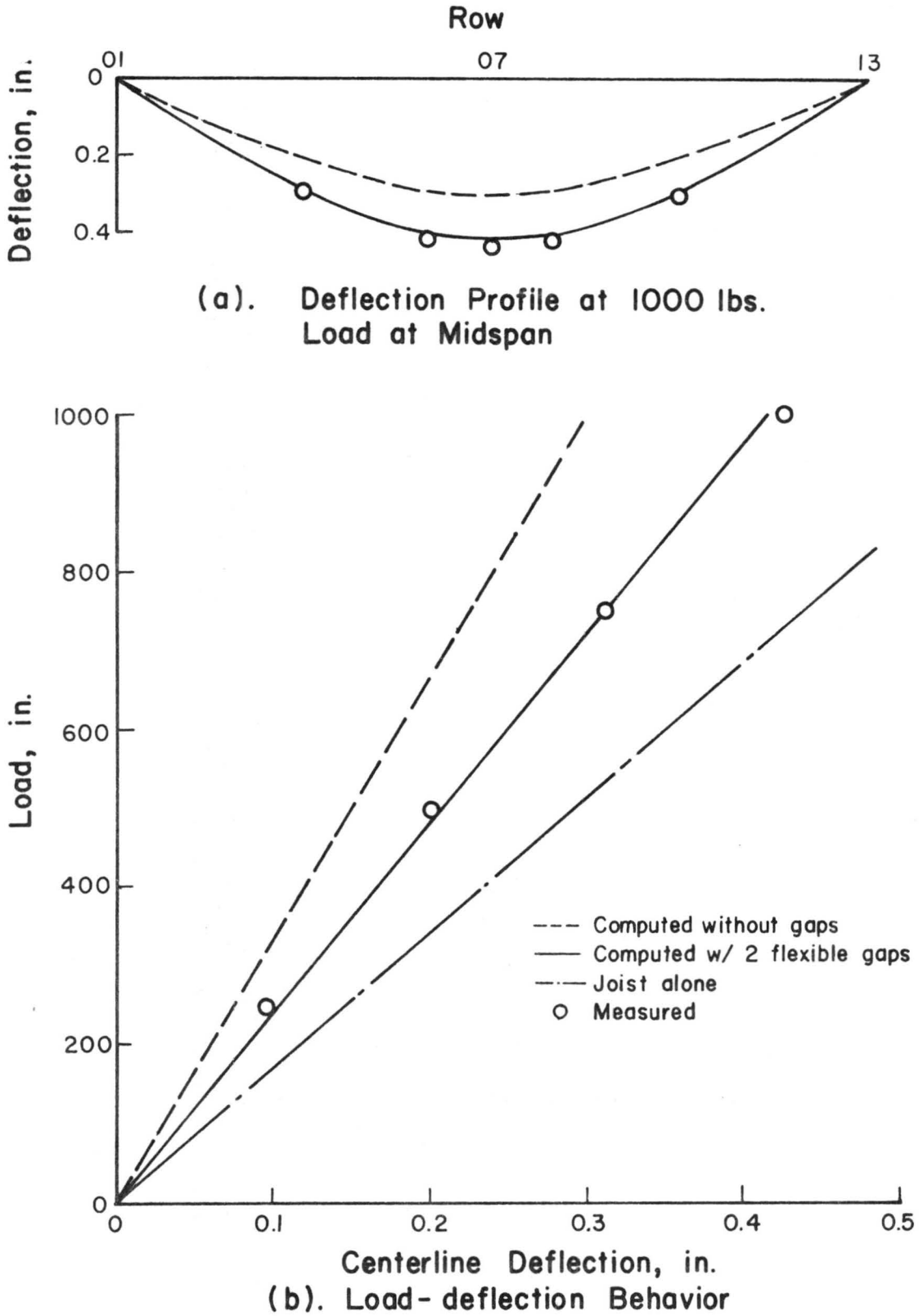

Figure E.22. Beam Verification - T9-8D16-1
J01 with Butted T&G Joints

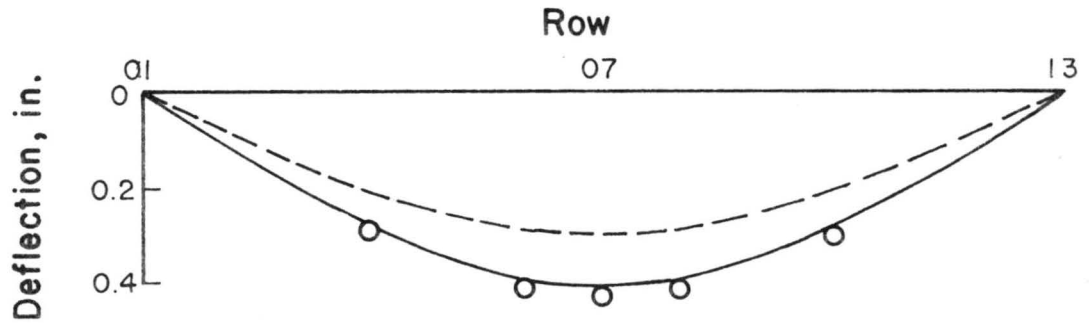

(a). Deflection Profile at 1000 lbs. Load at Midspan

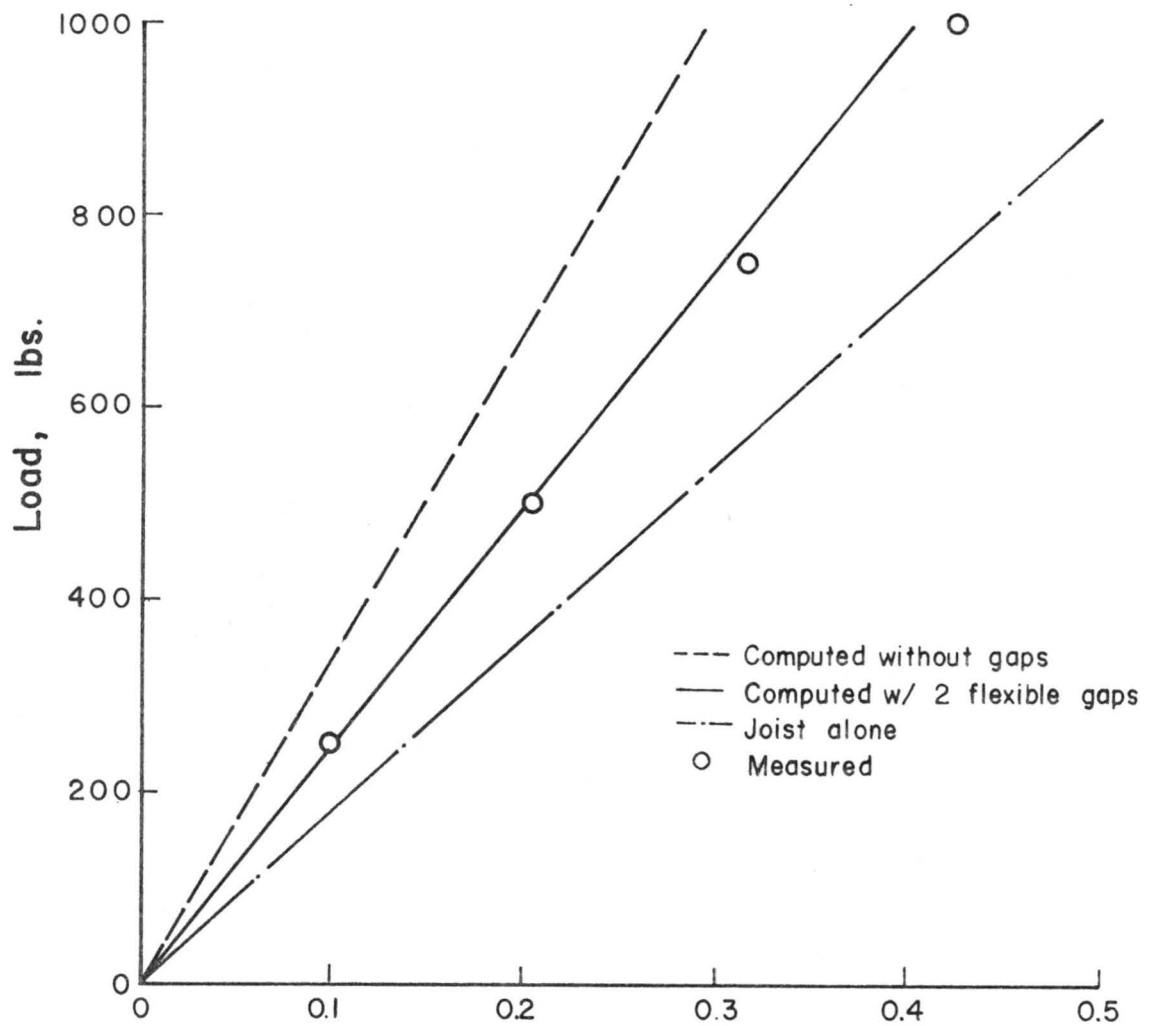

(b). Load-deflection Behavior

Figure E.23. Beam Verification - T9-8D16-1 JO2 with Butted T&G Joints

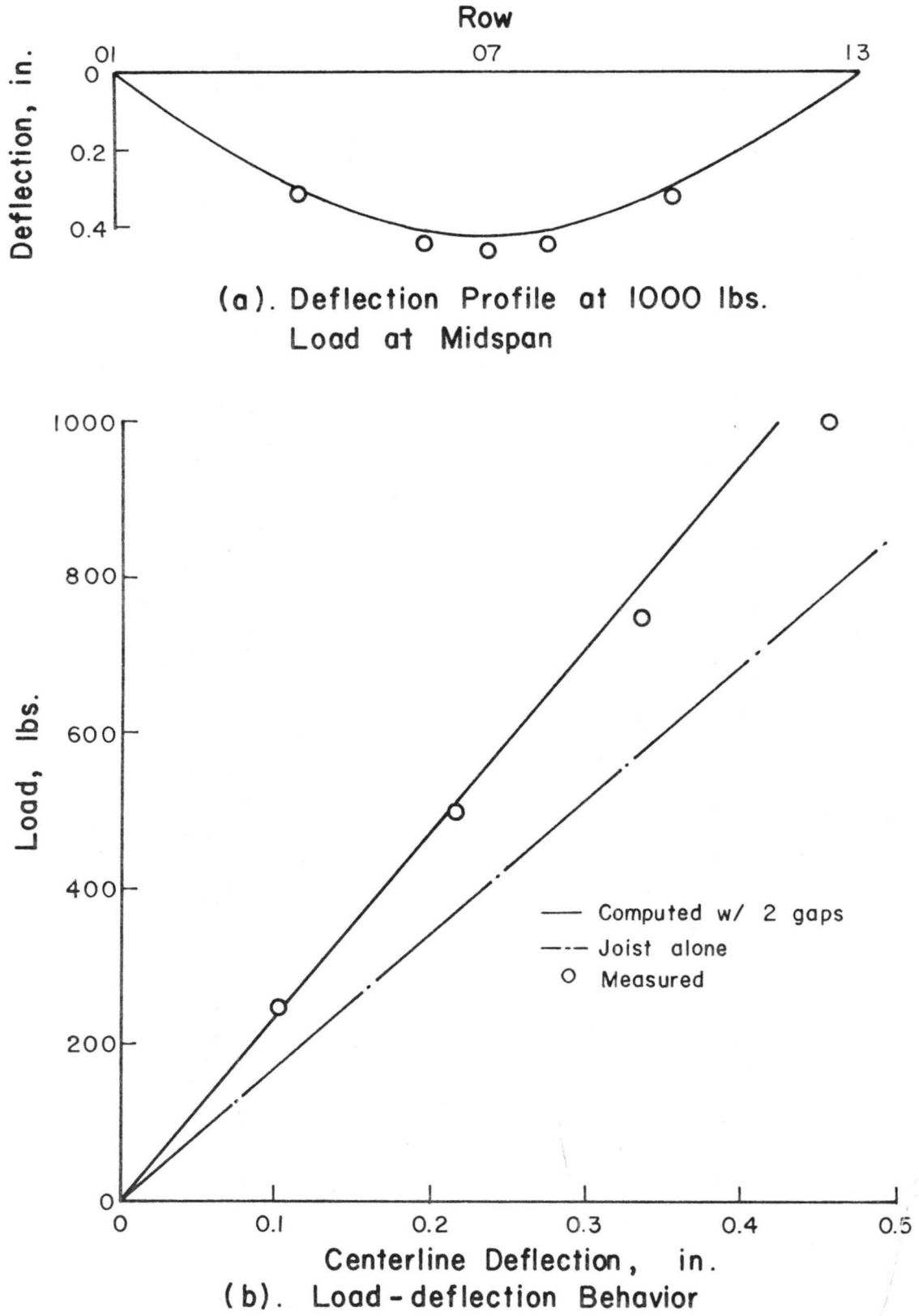

Figure E.24. Beam Verification - T9-8D16-1
J01 with Gaps

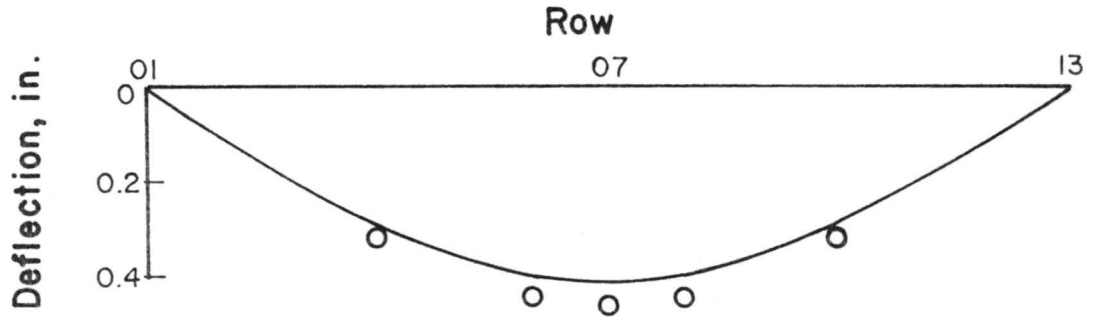

(a). Deflection Profile at 1000 lbs. Load at Midspan

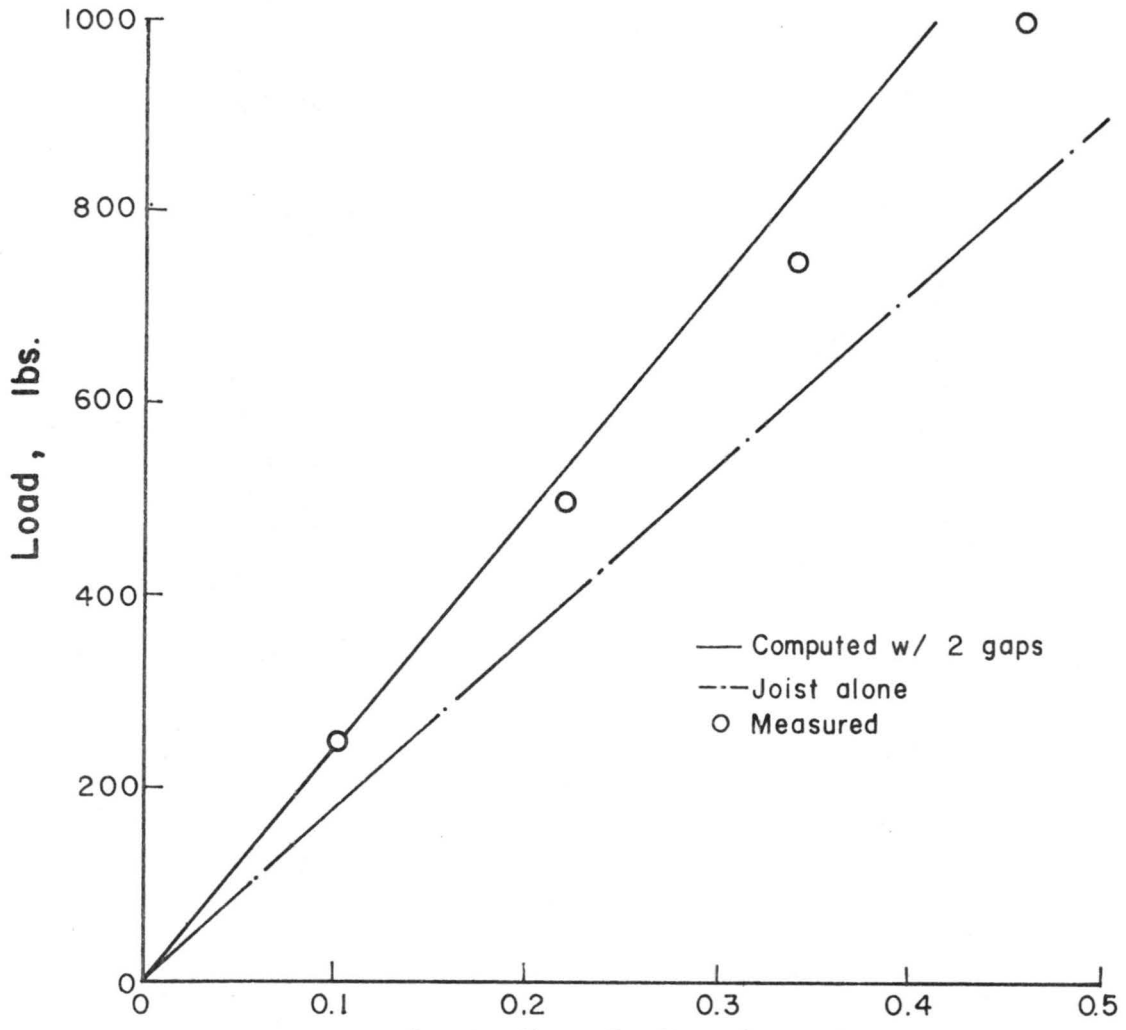

(b). Load-deflection Behavior

Figure E.25. Beam Verification - T9-8D16-1 J01 with Gaps

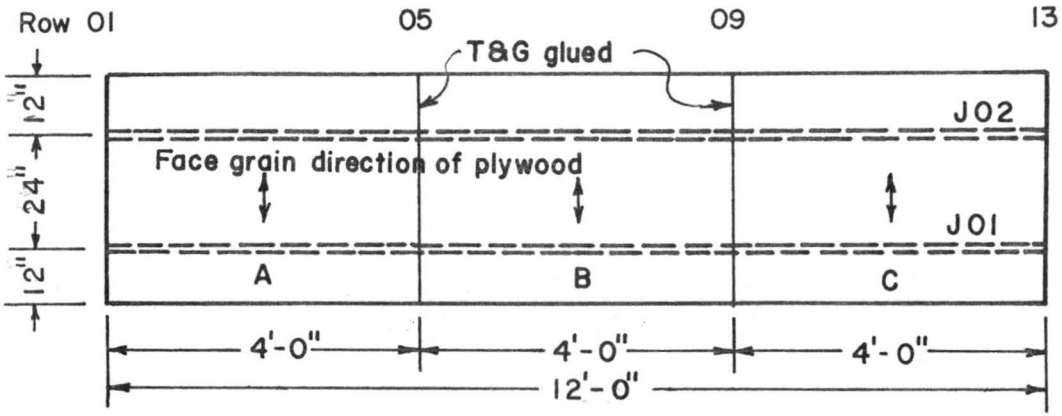

TOP VIEW

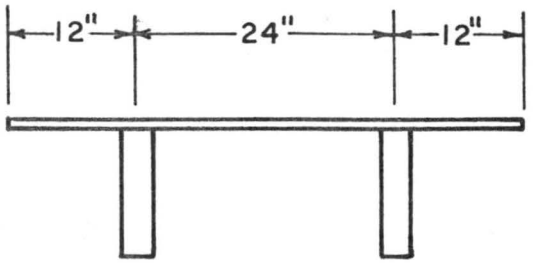

CROSS SECTION

Description of specimen:

Joist: 2x12 Engelmann spruce

J01	EC-S-12-05	$E = 1.269 \times 10^6$ psi
J02	EC-S-12-04	$E = 1.261 \times 10^6$

Sheathing: 3/4" D.F. Plywood

A	DP-34-10	$E_\perp = 5.463 \times 10^6$ psi
B	DP-34-13	$E_\perp = 5.516 \times 10^6$
C	DP-34-13	

Connector: 8-d common nails spaced at 8"

Sheathing Joints: glued T & G

Slip Modulus: k = 30,000 lb/in

Test sequence

1. Loaded at row 07 with ΔP = 1000 lbs up to P = 4000 lbs. Repeated three times
2. Cut gaps at rows 05 and 09, loaded at row 07 with ΔP = 500 up to P = 2000 lbs. Repeated twice.
3. Cut gaps at 2-foot intervals and loaded as in 2
4. Cut gaps at 1 foot intervals and loaded as in 2
5. Cut gaps at 6 in intervals and loaded as in 2 but P_{max} = 3000 lbs
6. Test to failure: loaded at row 07; both joists failed at P = 5500 lbs.

Fig. E.26 Configuration and Properties of Specimen T10-12E24-1

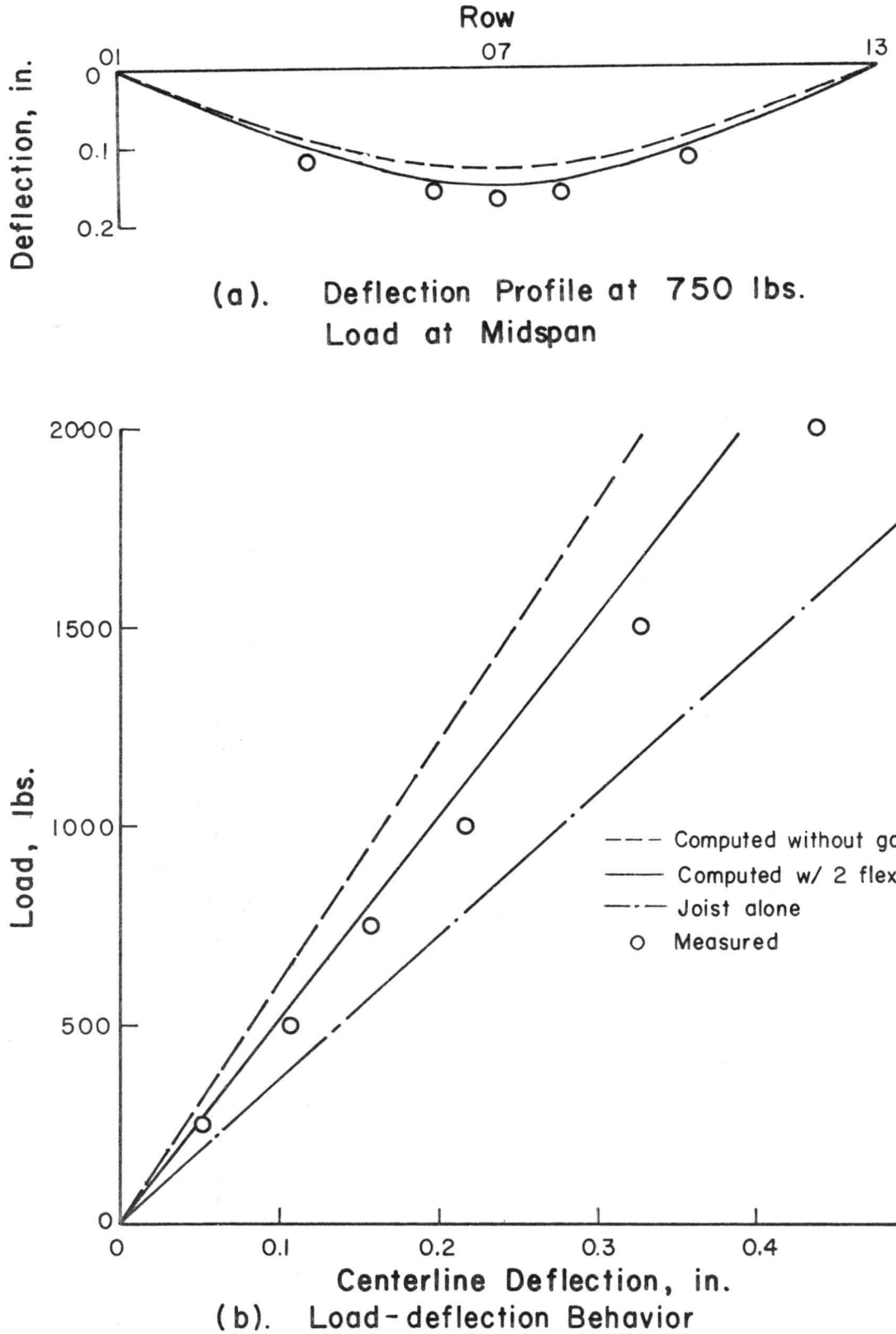

Figure E.27. Beam Verification - T10-12E24-1
J01 with Glued T&G Joints

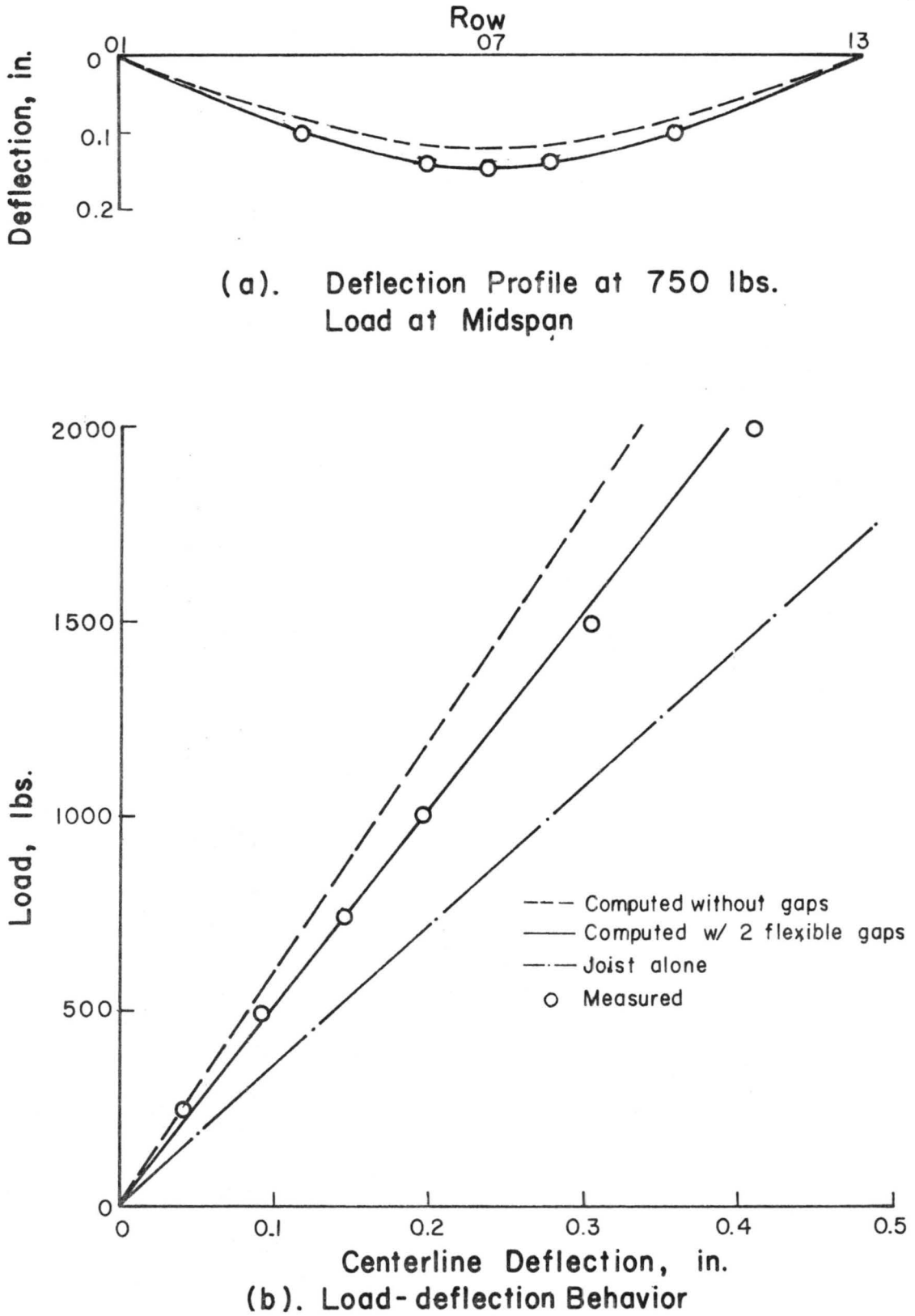

Figure E.28. Beam Verification - T10-12E24-1
J02 with Glued T&G Joints

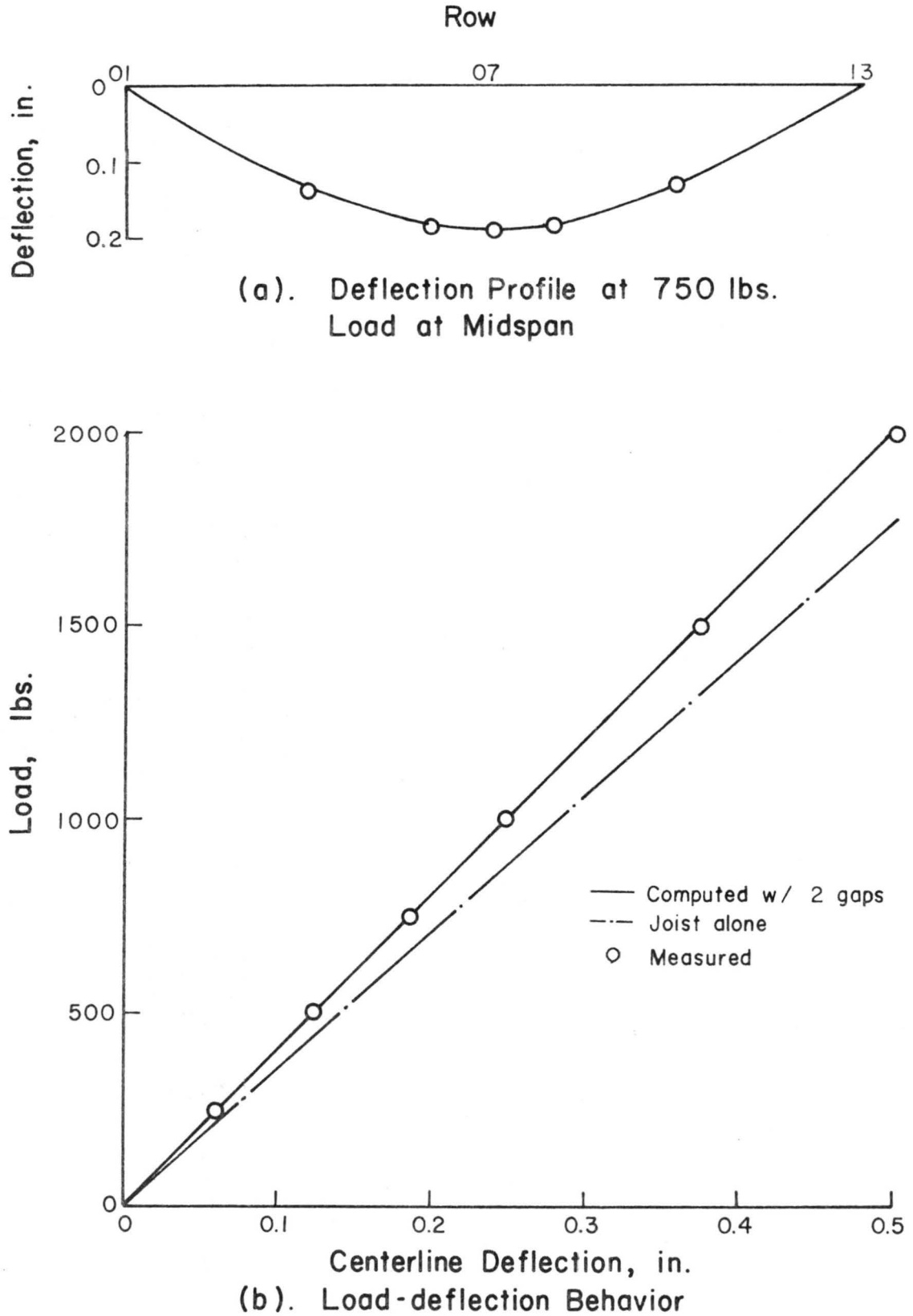

Figure E.29. Beam Verification - T10-12E24-1
J01 with Gaps

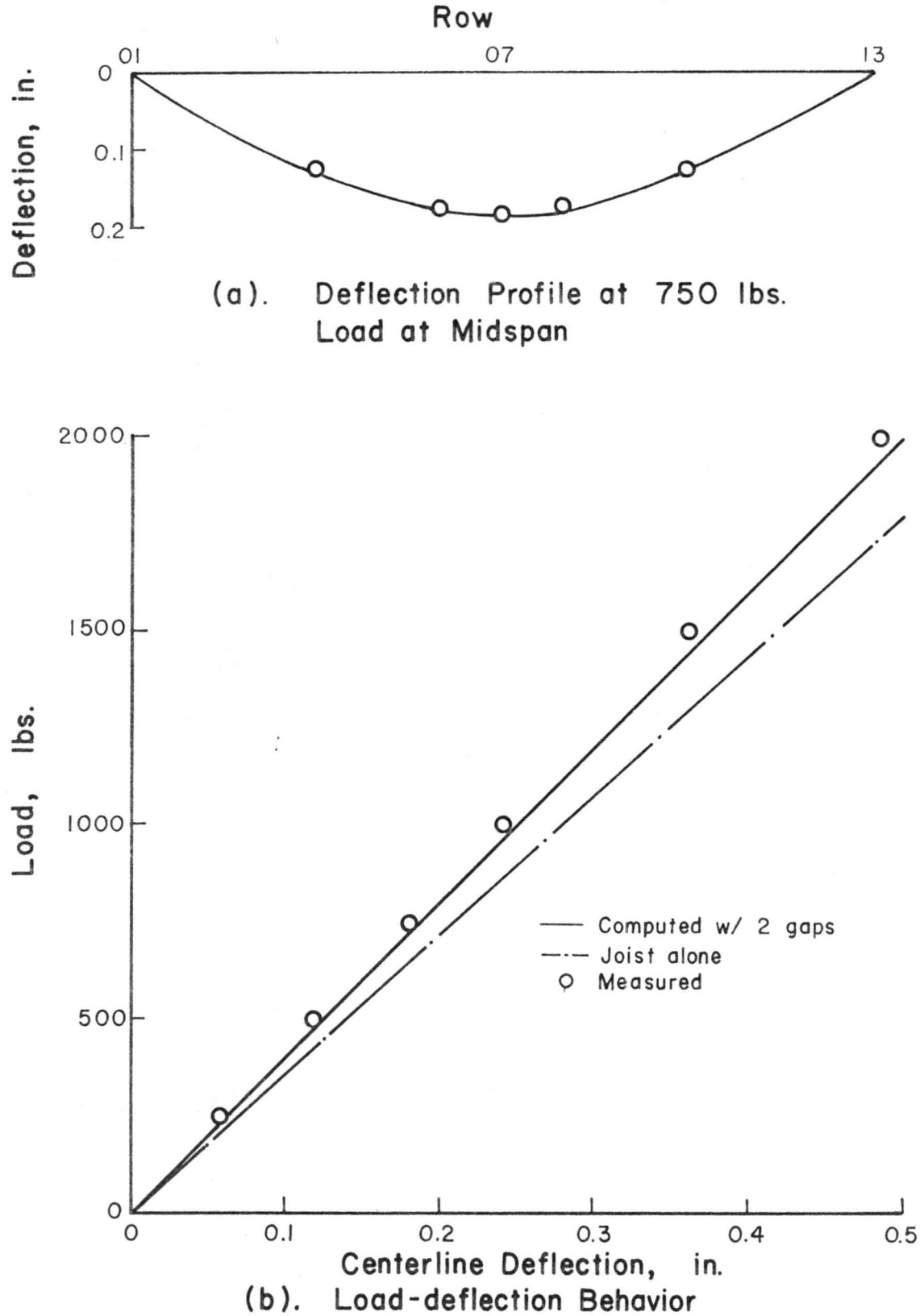

Figure E.30. Beam Verification - T10-12E24-1
J02 with Gaps

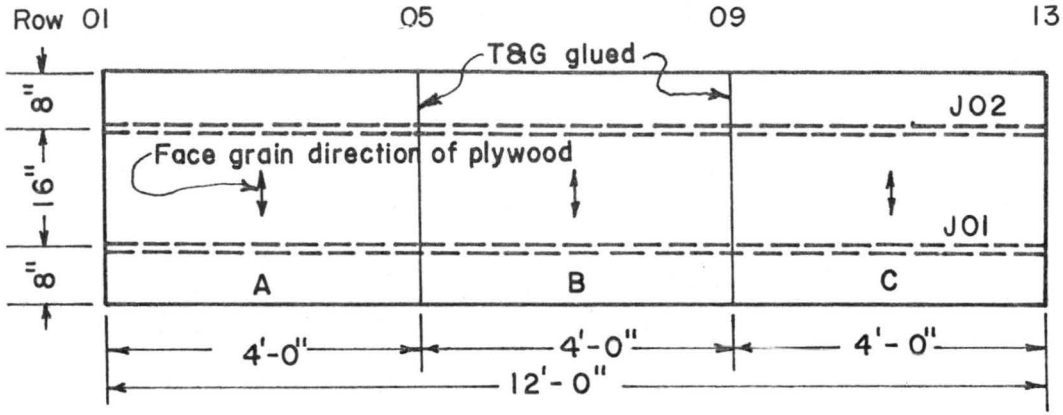

TOP VIEW

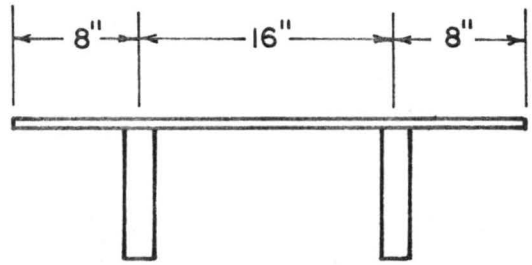

CROSS SECTION

Description of specimen:

Joist: 2x8 Douglas fir

J01	DW-N-08-52	$E = 0.975 \times 10^6$ psi
J01	DW-N-08-47	$E = 1.088 \times 10^6$

Sheathing: 3/4" D.F. Plywood

A	DP-34-8	$E_{\perp} = 5.326 \times 10^5$ psi
B	DP-34-8	$E_{\perp} = 5.326 \times 10^5$ psi
C	DP-34-8	$E_{\perp} = 5.326 \times 10^5$ psi

Connector: Franklin Construction Adhesive

Sheathing Joints: glued T&G

Slip Modulus: $k = 16{,}000$ lb/in^2

Test sequence

1. Loaded at row 07 with $\Delta P = 250$ lb up to $P = 1500$ lb. Repeated twice
2. Cut gap at midspan and loaded at row 07 with $\Delta P = 250$ up to $P = 1000$ lbs
3. Loaded at row 05 with $\Delta P = 250$ up to $P = 1250$ lbs
4. Test to failure: loaded at row 07 with $\Delta P = 500$ up to $P = 1500$ lbs.; then $\Delta P = 250$ up to failure. J01 failed at $P = 3750$ lbs.

Fig. E.31 Configuration and Properties of Specimen T11-8D16-1

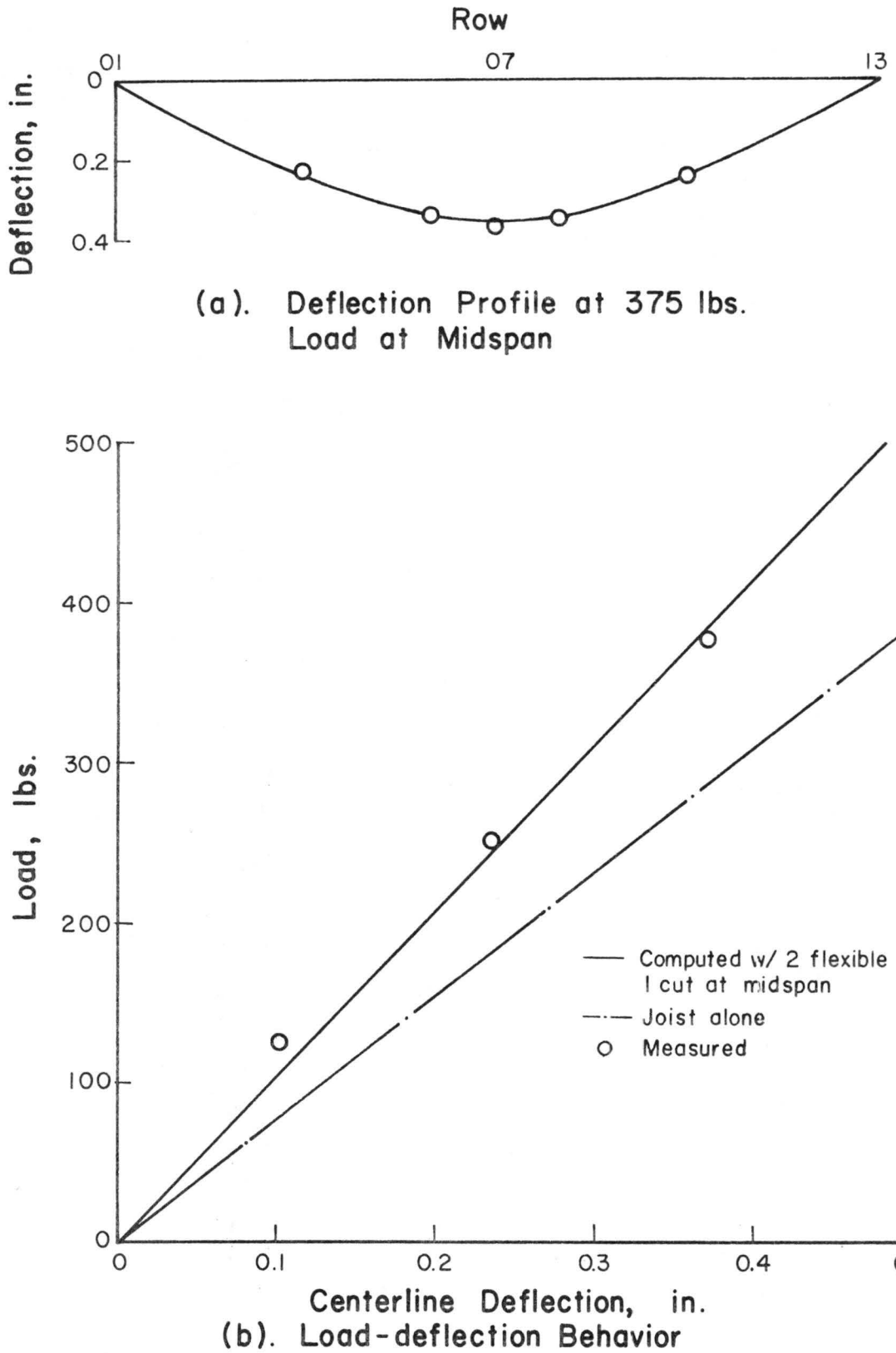

Figure E.32. Beam Verification - T11-8D16-1 J01

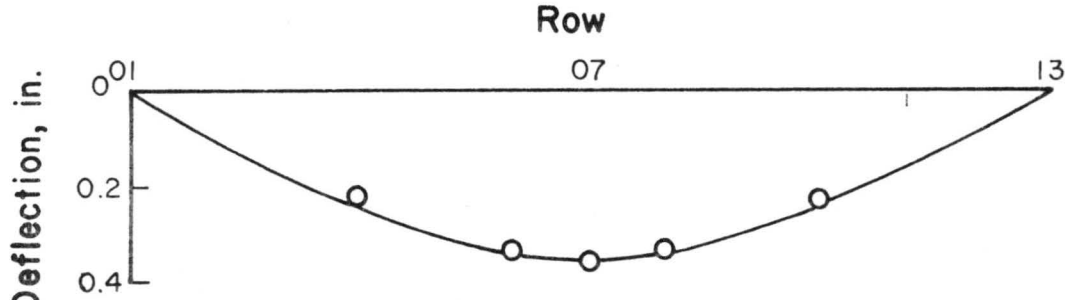

(a). Deflection Profile at 375 lbs. Load at Midspan

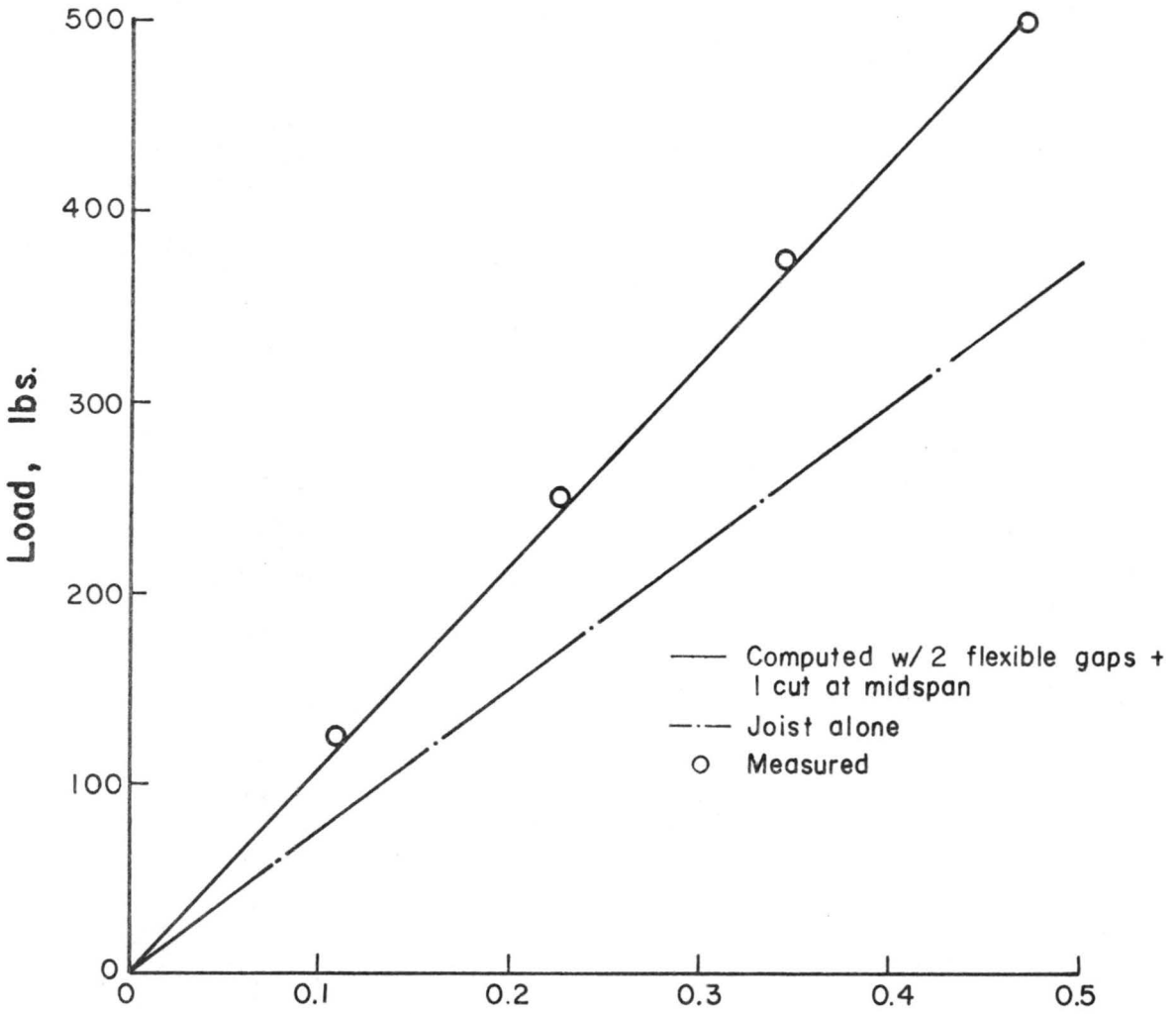

(b). Load-deflection Behavior

Figure E.33. Beam Verification - T11-8D16-1 J02

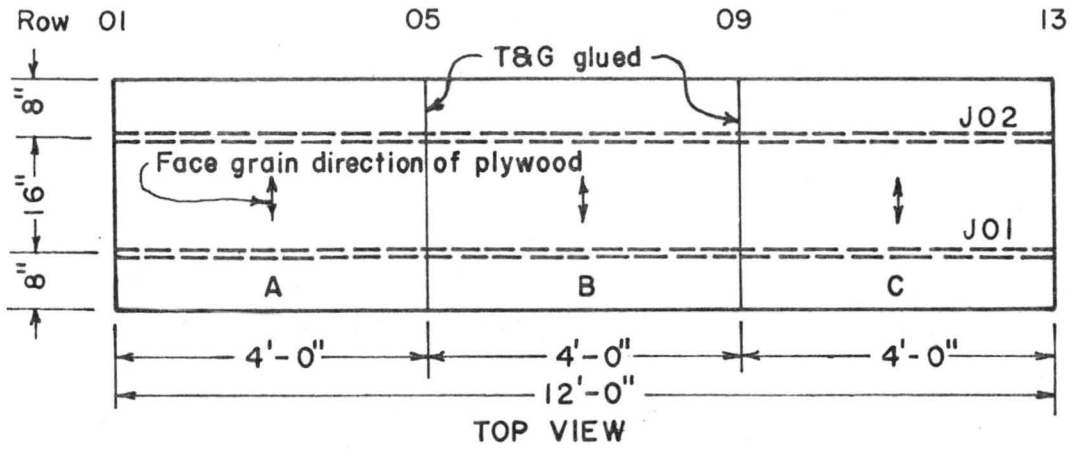

TOP VIEW

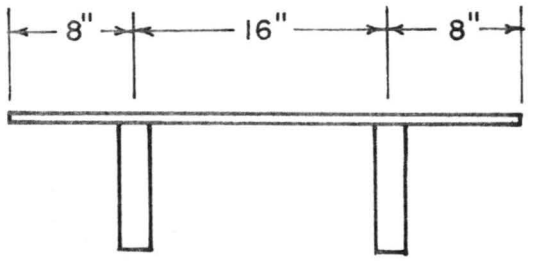

CROSS SECTION

Description of specimen:

Joist: 2x8 Douglas fir

J01	DW-N-08-51	$E = 1.249 \times 10^6$ psi
J02	DW-N-08-55	$E = 1.261 \times 10^6$

Sheathing: 3/4" D.F. Plywood

A	DP-34-12	$E_\perp = 5.581 \times 10^5$ psi
B	DP-34-12	$E_\perp = 5.581 \times 10^5$ psi
C	DP-34-12	$E_\perp = 5.581 \times 10^5$ psi

Connector: 8-d common nails spaced at 6"

Sheathing Joints: T&G glued

Slip Modulus: k = 38,000 lb/in

Test sequence

1. Loaded at row 07 with ΔP = 250 lb up to P = 1250 lbs. Repeated three times.
2. Cut gap at row 07 and tested as in 1
3. Cut gaps at rows 05 and 09 (total 3 cuts), loaded at row 07 with ΔP = 250 lb up to P = 1000 lbs
4. Loaded at rows 03 and 04 with center gap filled; P_{max} = 1000 lbs
5. Cut gaps at 2-foot intervals and loaded as in 3
6. Cut gaps at 1-foot intervals and loaded at row 07 with P = 750 lbs
7. Cut gaps at 6 in intervals and loaded as in 6.

Fig. E.34 Configuration and Properties of Specimen T12-8D16-1

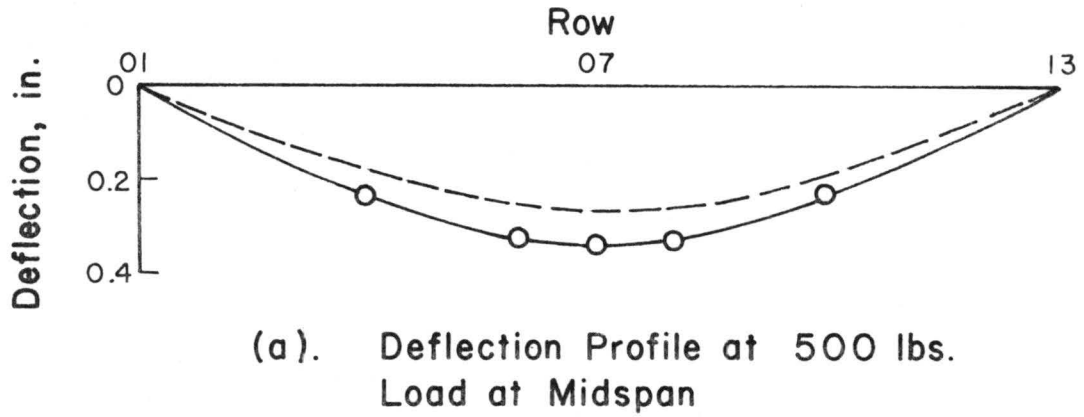

(a). Deflection Profile at 500 lbs. Load at Midspan

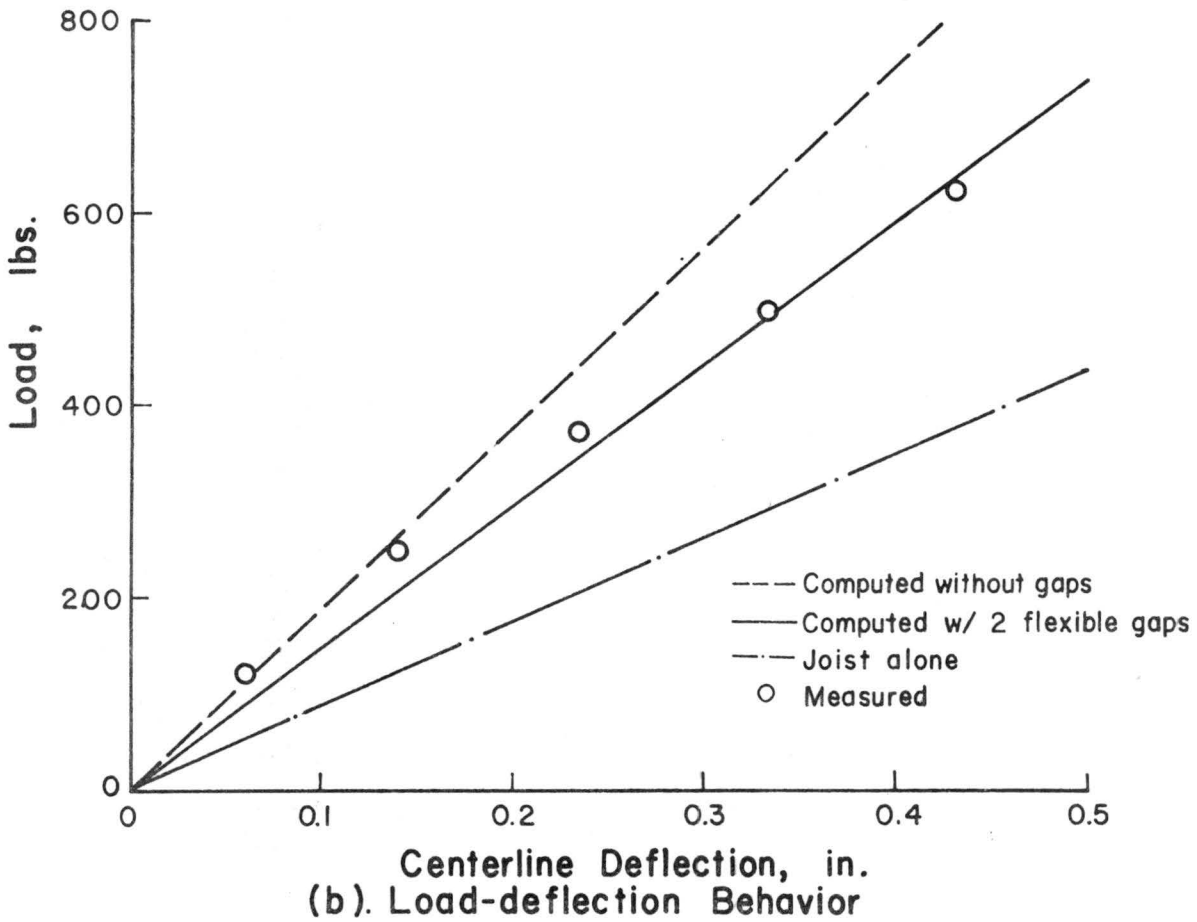

(b). Load-deflection Behavior

Figure E.35. Beam Verification - T12-8D16-1 J01 with Glued T&G Joints

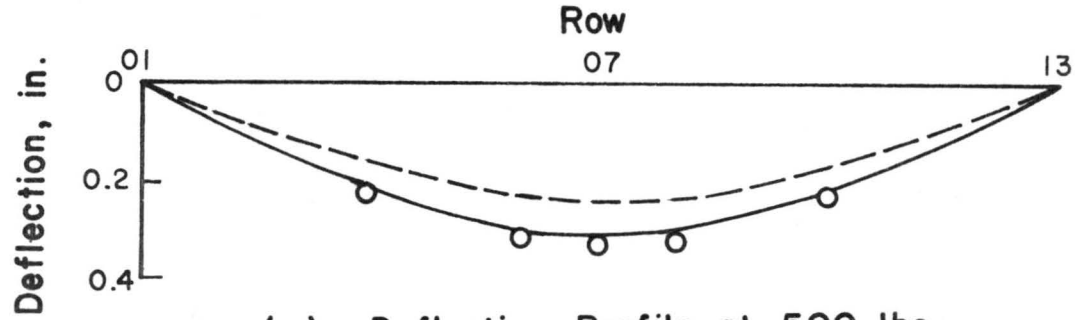

(a). Deflection Profile at 500 lbs. Load at Midspan

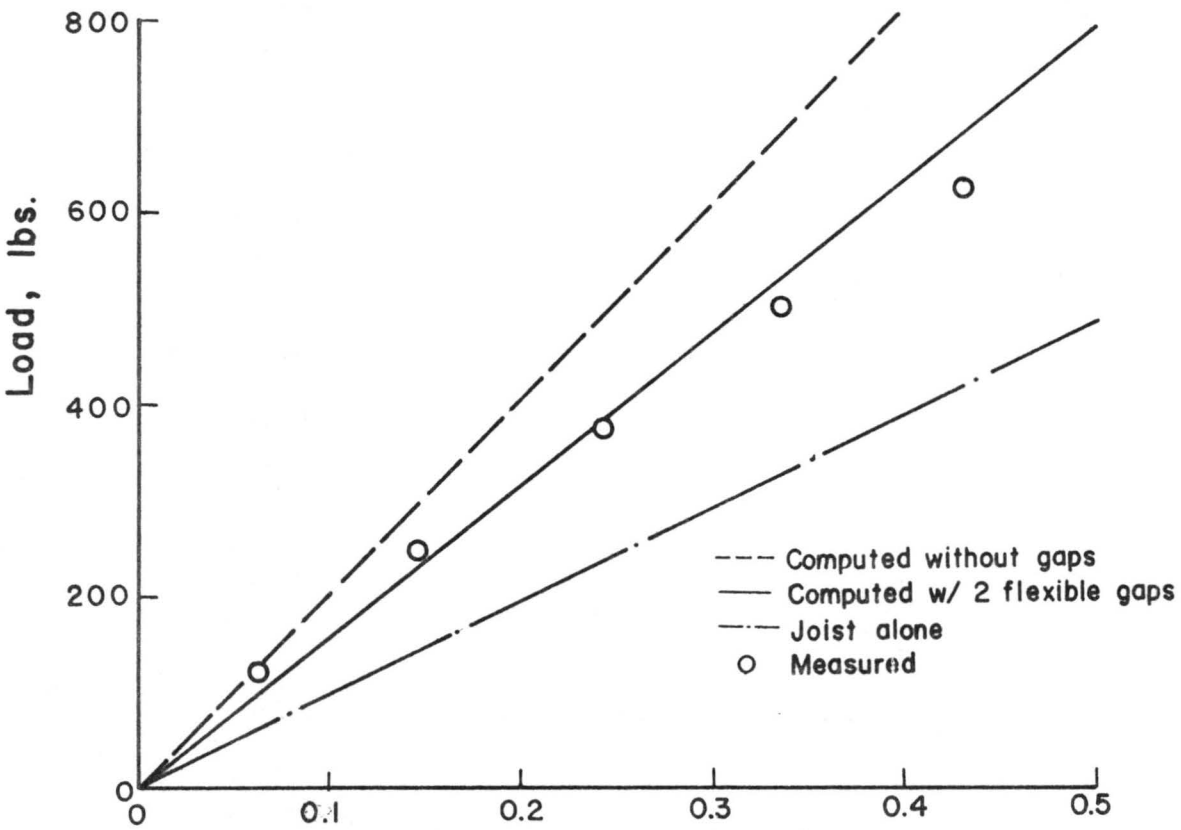

(b). Load-deflection Behavior

FIGURE E.36 BEAM VERIFICATION — T12-8D16-1 J02 WITH GLUED T&G JOINTS

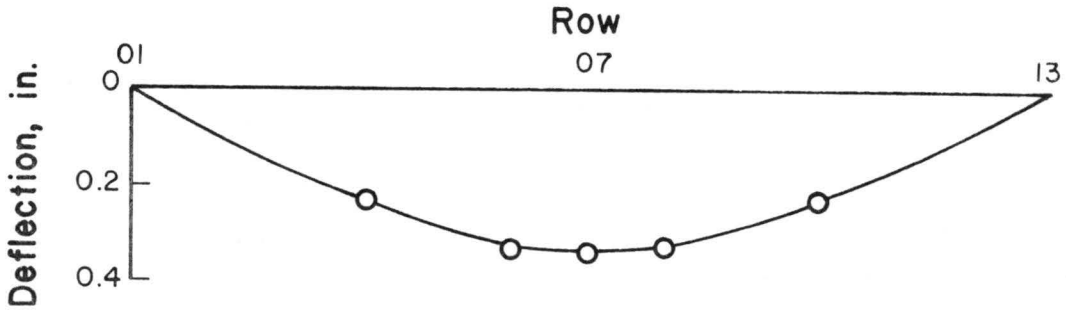

(a). Deflection Profile at 500 lbs. Load at Midspan

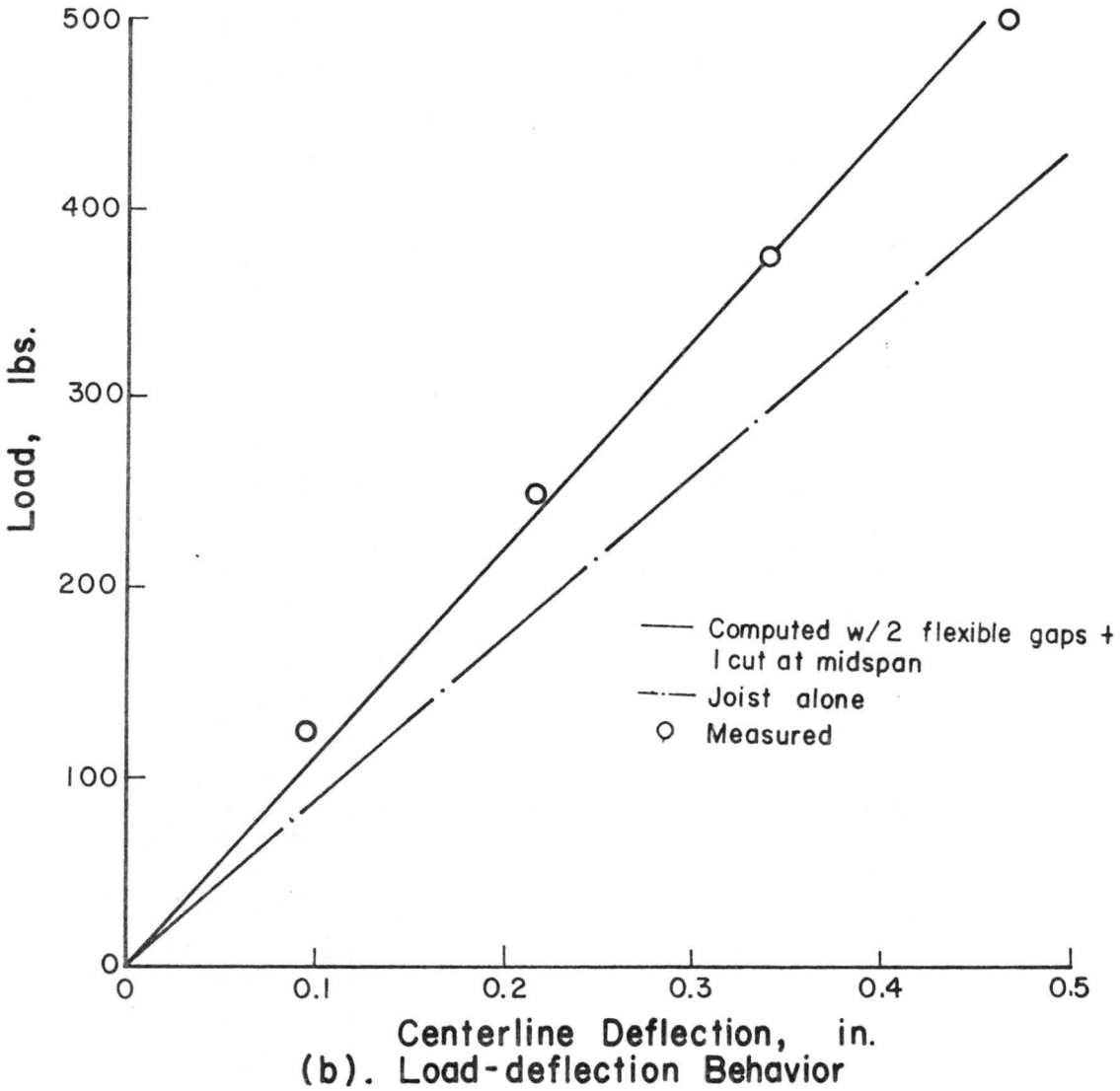

(b). Load-deflection Behavior

Figure E.37. Beam Verification - T12-8D16-1 JO1 with Gap

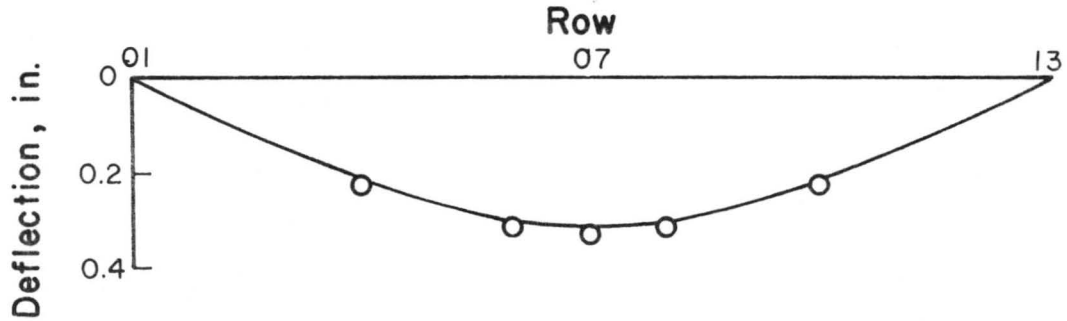

(a). Deflection Profile at 500 lbs. Load at Midspan

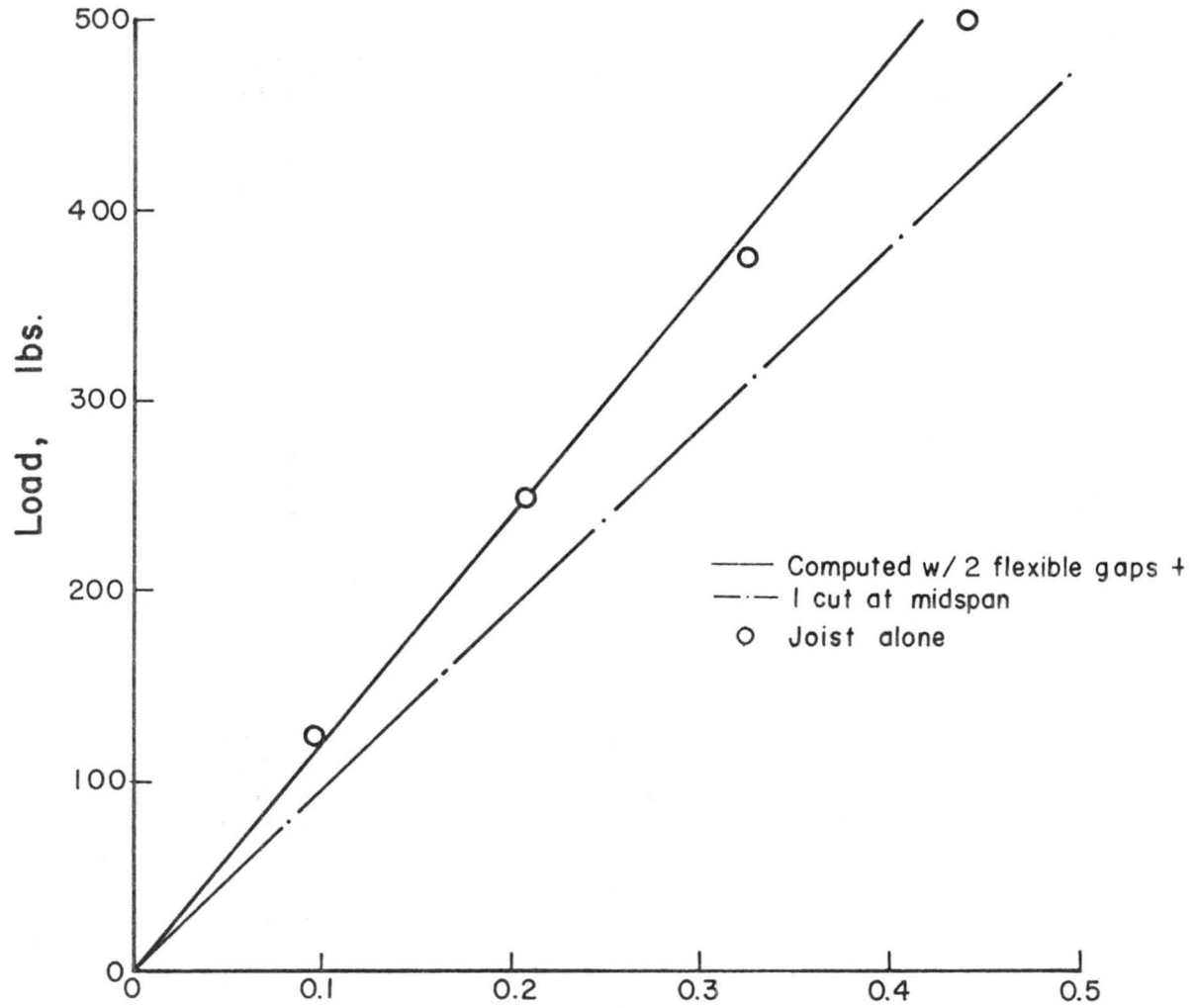

(b). Load-deflection Behavior

Figure E.38. Beam Verification - T12-8D16-1
JO2 with Gap

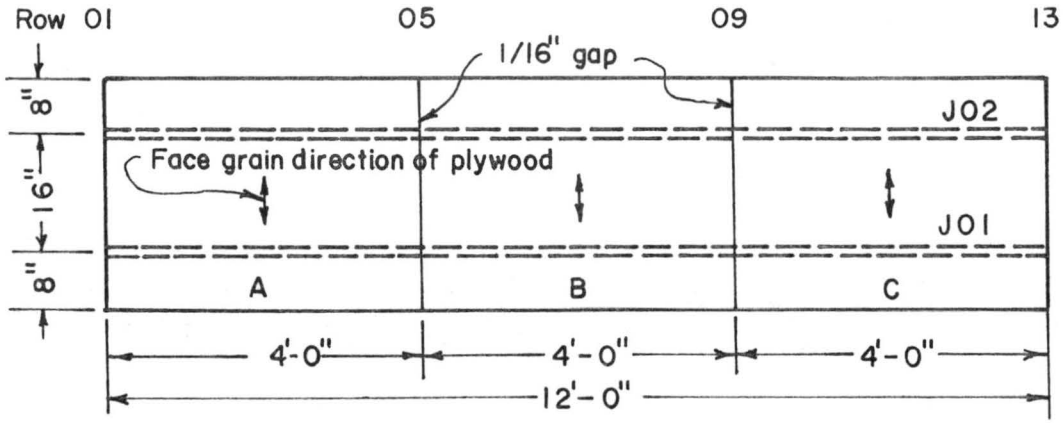

TOP VIEW

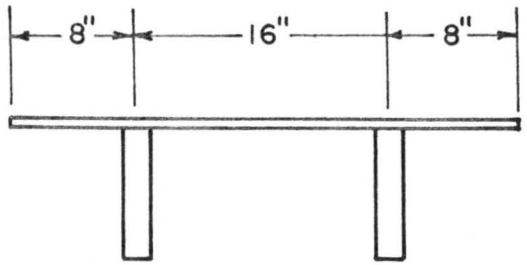

CROSS SECTION

Description of specimen:

Joist: 2x8 Douglas fir

J01	DW-N-08-21	$E = 1.342 \times 10^6$ psi
J02	DW-N-08-49	$E = 1.077 \times 10^6$

Sheathing: 3/4" E.S. Plywood

A	EP-58-28	$E_{\perp} = 4.323 \times 10^5$ psi
B	EP-58-28	$E_{\perp} = 4.323 \times 10^5$ psi
C	EP-58-28	$E_{\perp} = 4.323 \times 10^5$ psi

Connector: 8-d common nails spaced at 4"

Sheathing Joints: T&G with 1/16" gaps

Slip Modulus: k = 35,000 lb/in

Test sequence

1. Loaded at row 07 with ΔP = 250 up to P = 1000 lbs. Repeated twice.
2. Cyclic loading with load from 20 to 800 lbs. Ramp function with T = 80 sec., sustained for 850 cycles
3. Cyclic loading with load from 0 to 800 lbs. Ramp function with T = 40 sec., sustained for 750 cycles
4. Loaded at 07 with ΔP = 100 up to P = 1500 lbs.

Fig. E.39 Configuration and Properties of Specimen T13-8D16-1

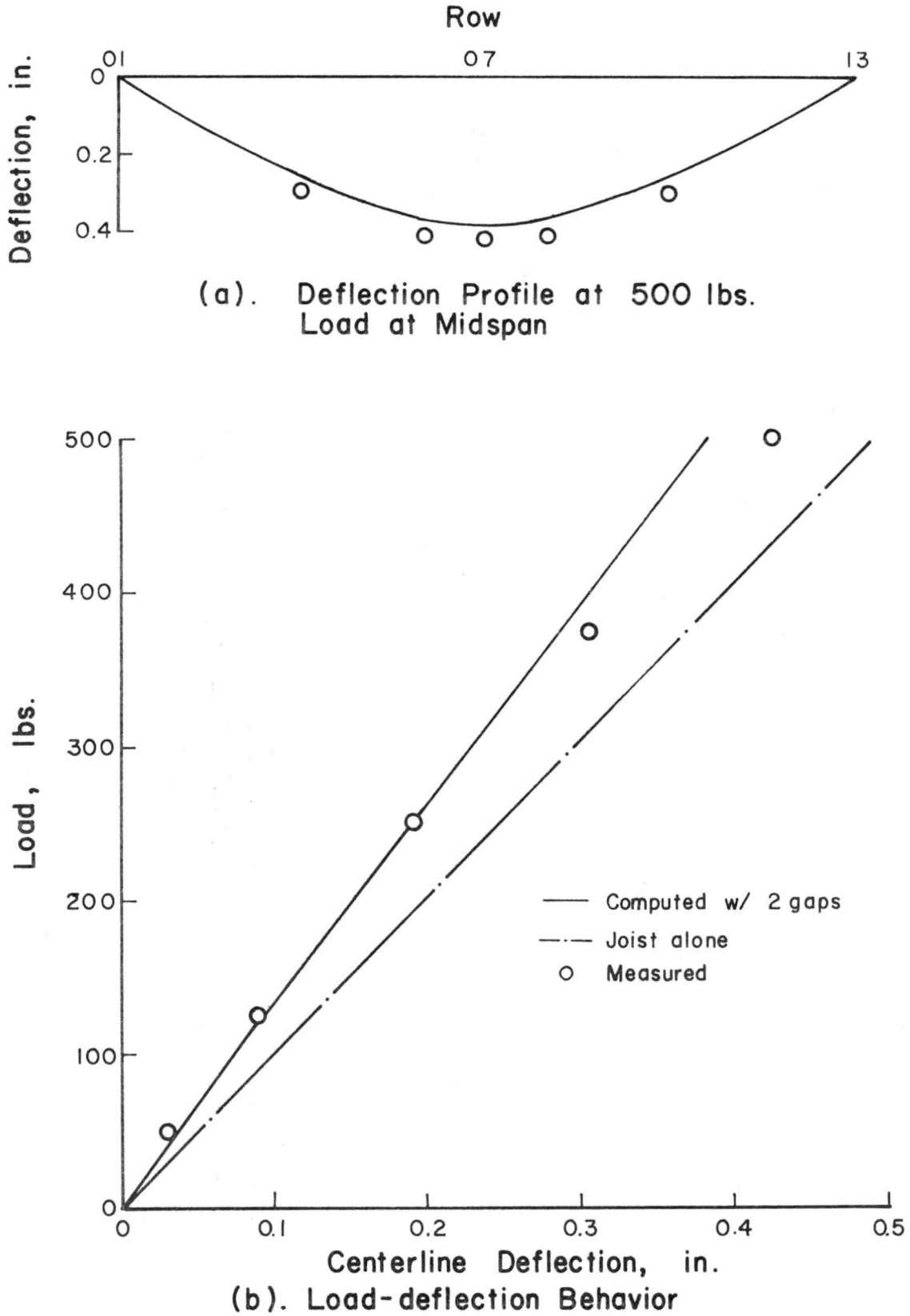

Figure E.40. Beam Verification - T13-8D16-1
J01 with Gaps

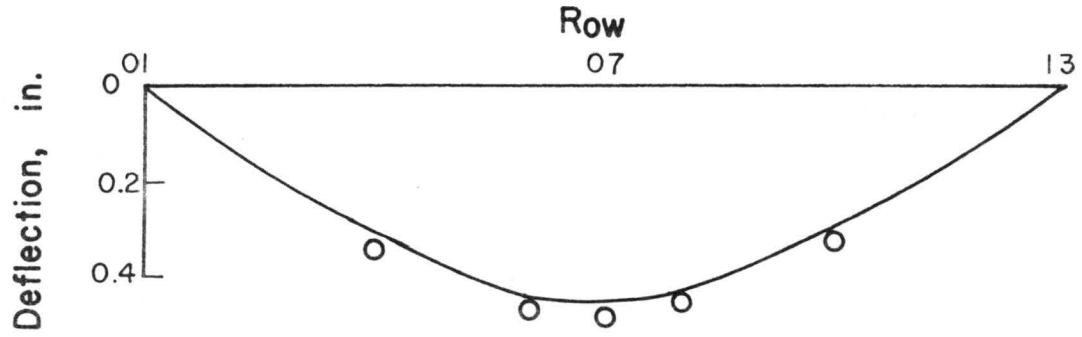

(a). Deflection Profile at 500 lbs. Load at Midspan

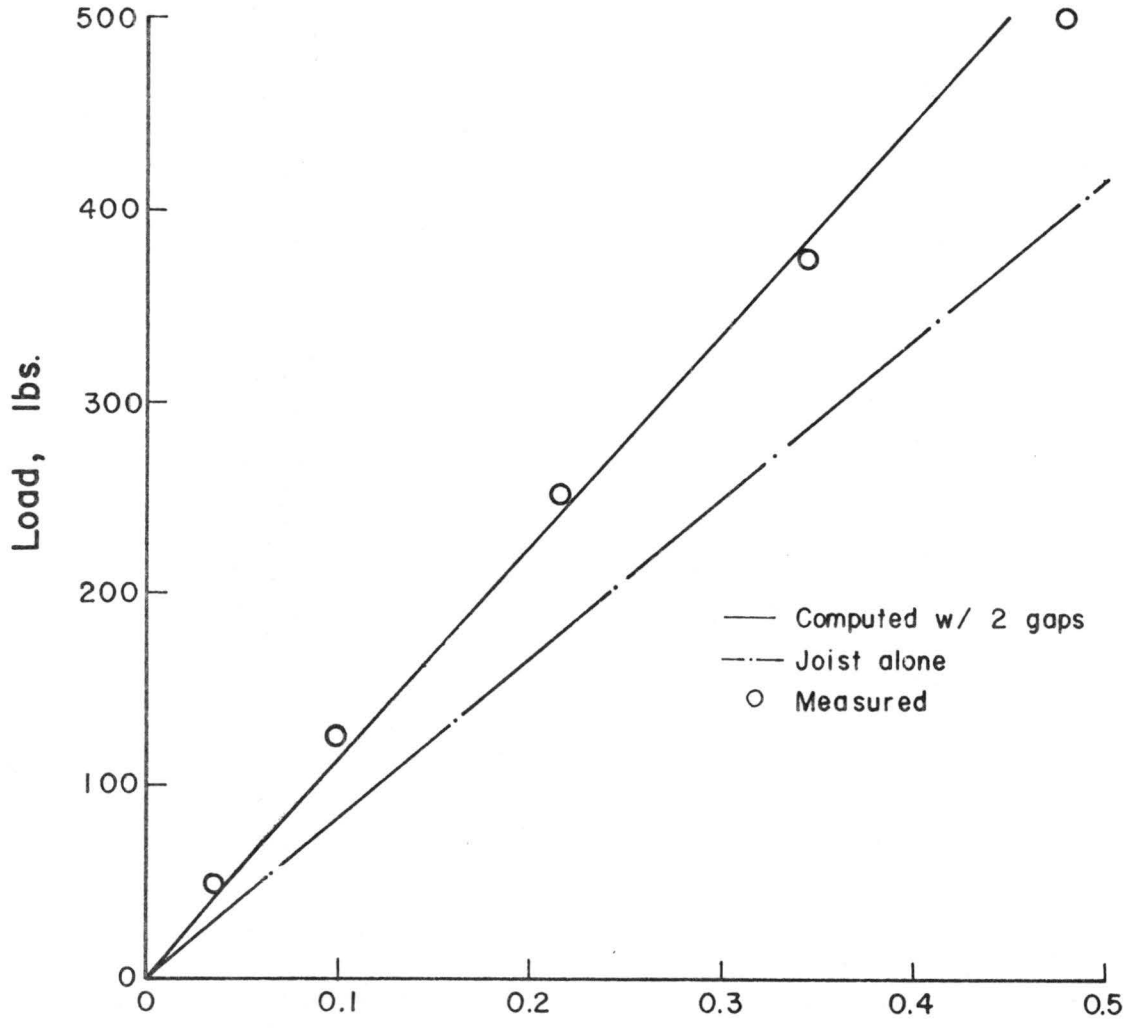

(b). Load-deflection Behavior

Figure E.41. Beam Verification - T13-8D16-1 JO2 with Gaps

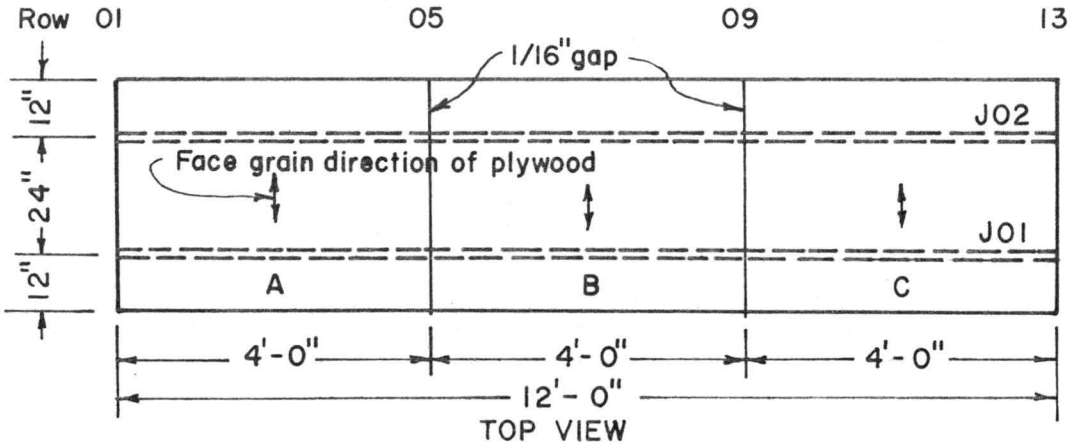

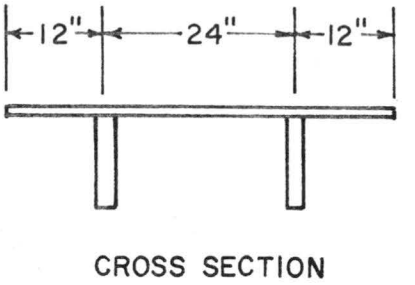

Description of specimen:

Joist: 2x12 Douglas fir

J01	DW-S-12-21	$E = 1.883 \times 10^6$ psi
J01	DW-S-12-23	$E = 1.715 \times 10^6$

Sheathing: 1/2" D.F. Plywood

A	DP-12-02	$E_{\perp} = 2.563 \times 10^5$ psi
B	DP-12-02	$E_{\perp} = 2.563 \times 10^5$ psi
C	DP-12-03	$E_{\perp} = 2.236 \times 10^5$ psi

Connector: 8-d common nails spaced at 8"

Sheathing Joints: left with 1/16" gaps

Slip Modulus: k = 30,000 lb/in

Test sequence

1. Loaded at row 07 with $\Delta P = 250$ up to $P = 1500$ lbs
2. Loaded at row 05 with loads same in 1
3. Loaded at row 03 with loads same in 1
4. Loaded at row 07 with P up to 2000 lbs.

Fig. E.42 Configuration and Properties of Specimen T14-12D24-1

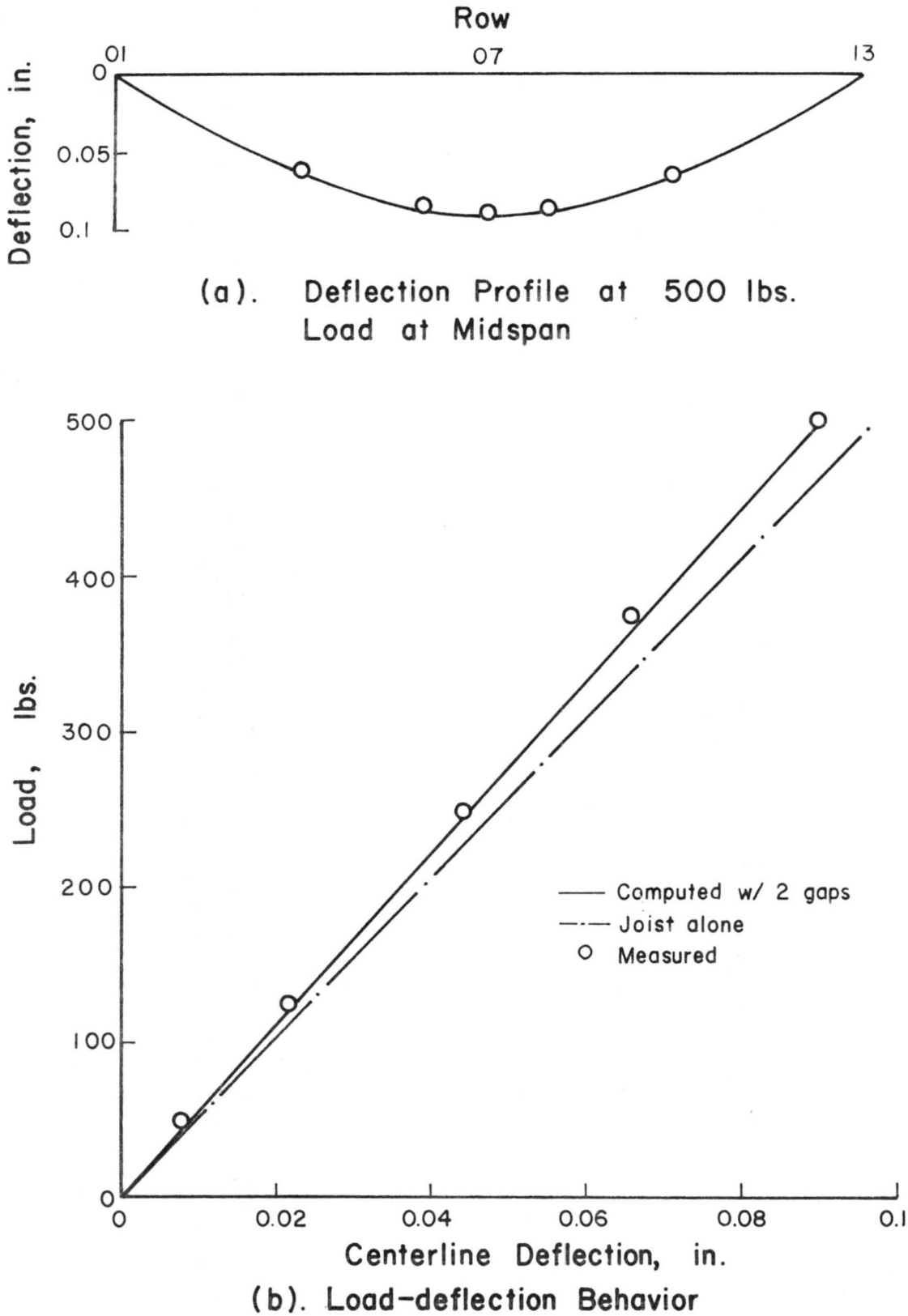

Figure E.43. Beam Verification - T14-12D24-1
J01 with Gaps

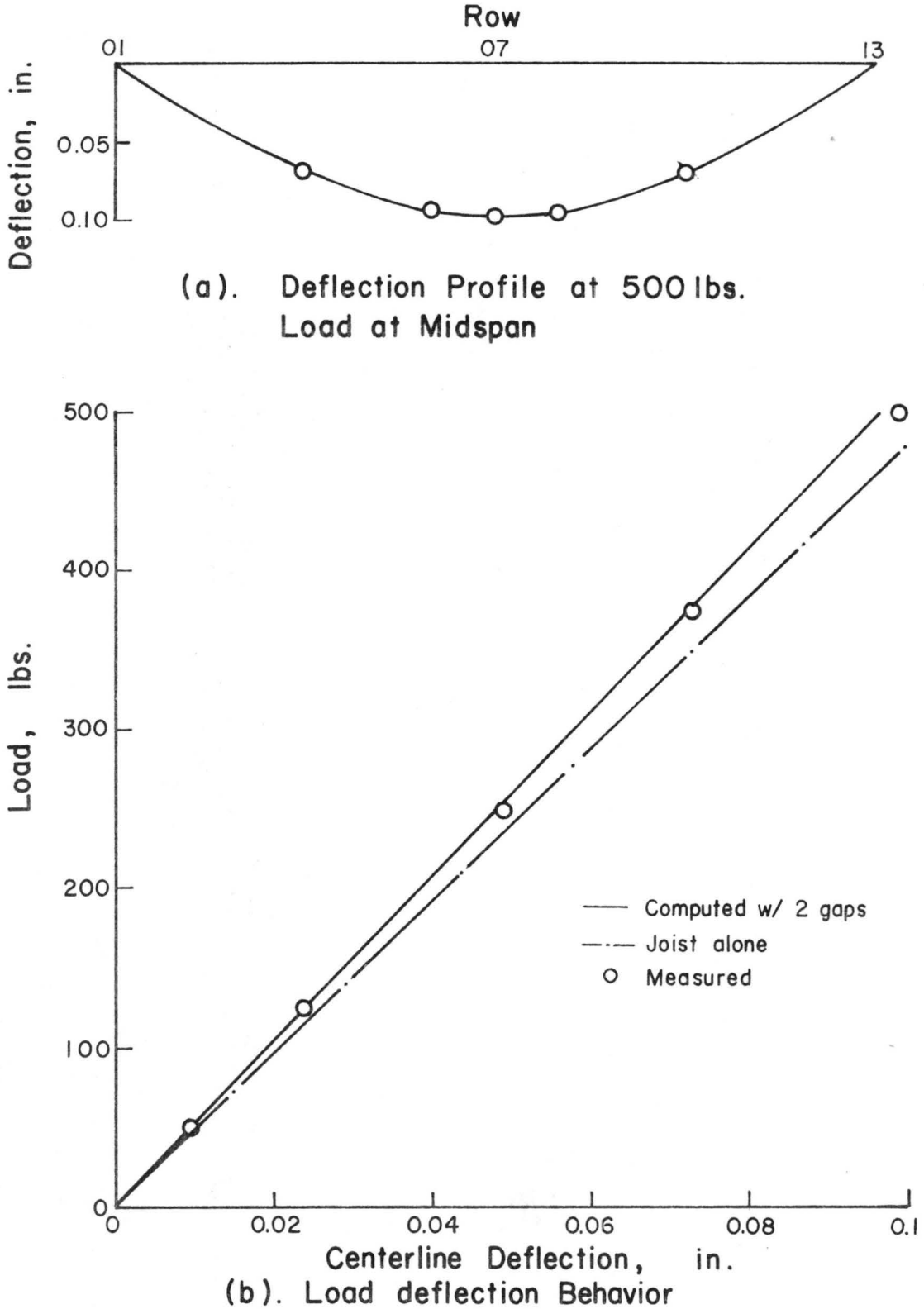

Figure E.44. Beam Verification - T14-12D24-1
J02 with Gaps

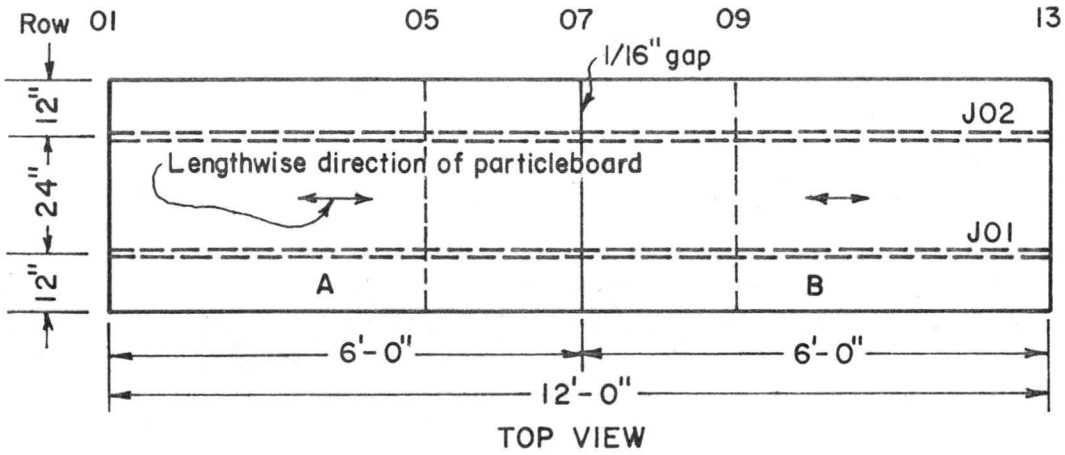

TOP VIEW

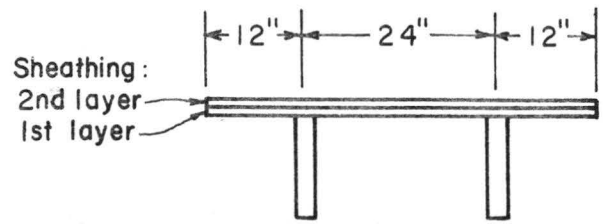

CROSS SECTION

Description of specimen:

Joist: 2x12 Douglas fir (see T14-12D24-1)

Sheathing: 1st layer (see T14-12D24-1)
2nd layer 1/2" particleboard

A	DB-12-20	$E_{\perp} = 5.837 \times 10^5$ psi
B	DB-12-19	$E_{\perp} = 5.782 \times 10^5$

Connector: 1st layer (see T14-12D24-1)
2nd layer 6d cement-coated nails spaced at 8"

Sheathing Joint: 1/16" gap

Slip Modulus: k = 4500 lb/in (2nd layer)
k = 60,000 lb/in (1st layer)

Test sequence

1. Loaded at row 07 with ΔP = 250 to P = 500 and ΔP = 500 up to P = 2500 lbs
2. Loaded at row 05 with loads same in 1
3. Loaded at row 03 with loads same in 1
4. Test to failure: loaded at row 07 with ΔP = 500. J01 cracked at P = 12500 lbs and J02 failed at P = 14,000 lbs.

Fig. E.45 Configuration and Properties of Specimen T14-12D24-2

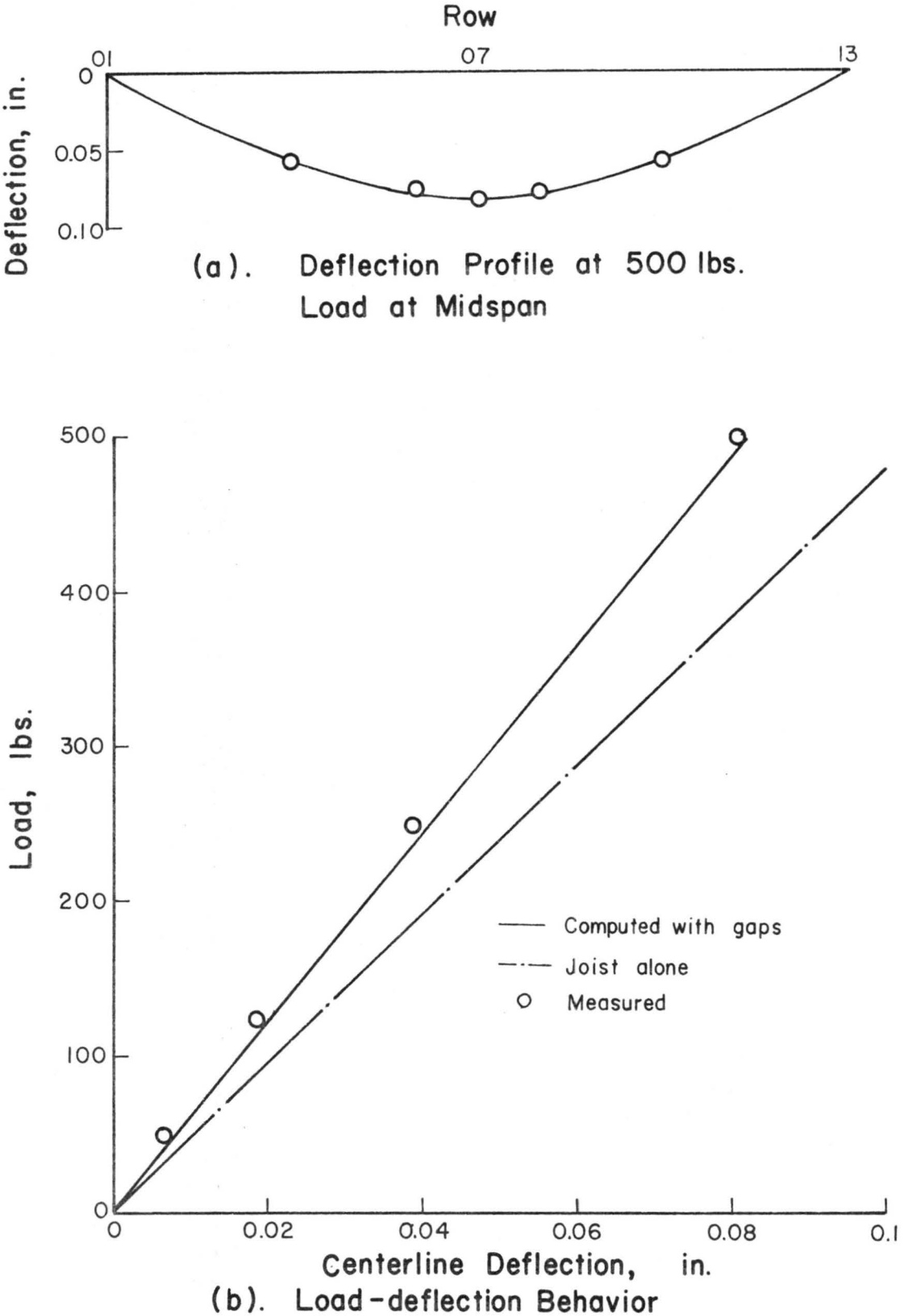

Figure E.46. Beam Verification - T14-12D24-2 J02 with Gaps

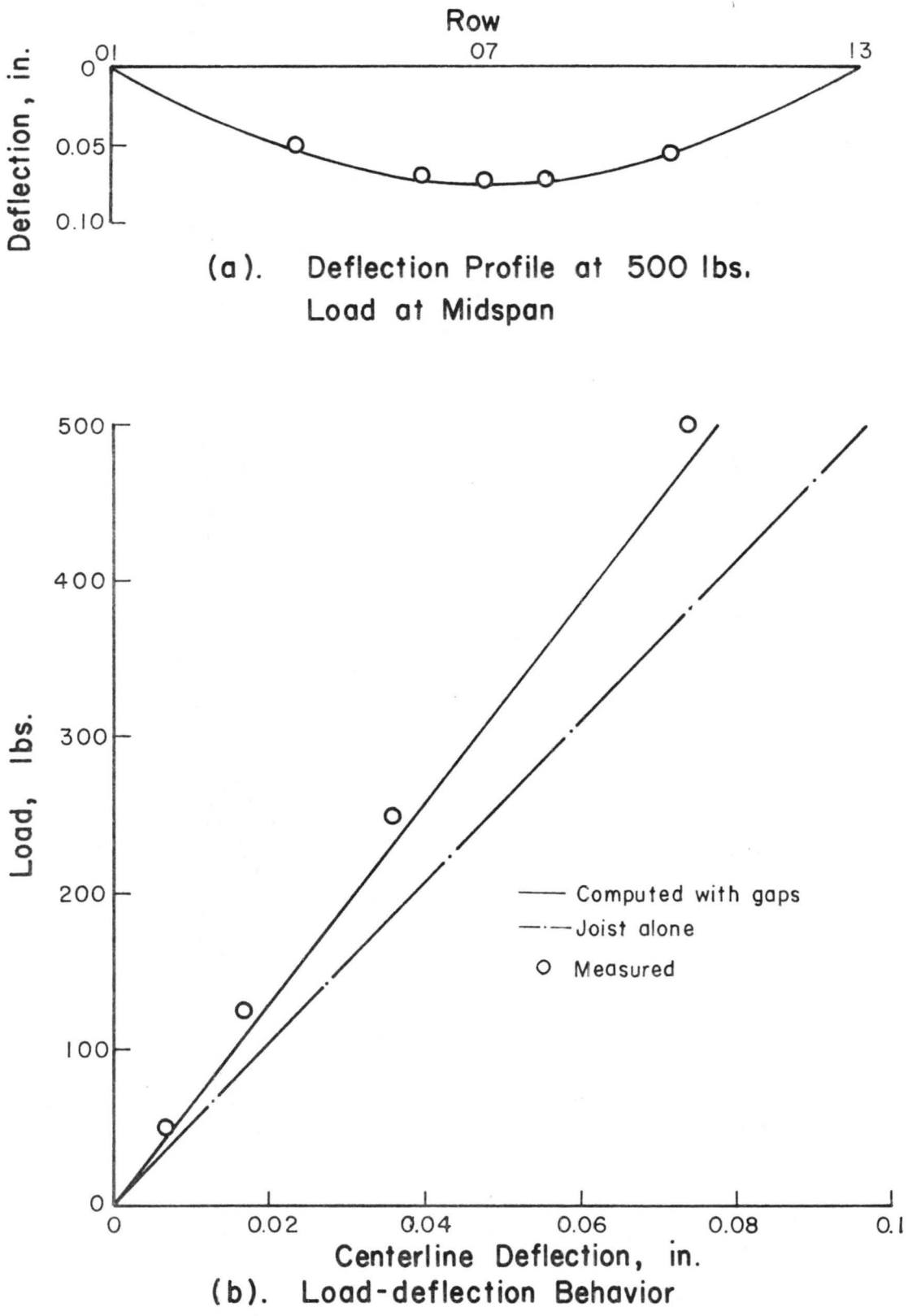

Figure E.47. Beam Verification - T14-12D24-2 J01 with Gaps

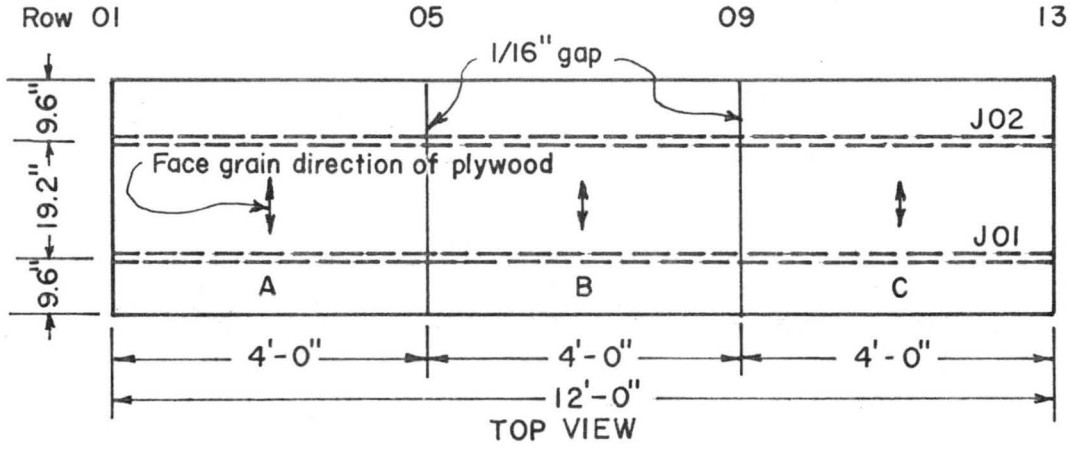

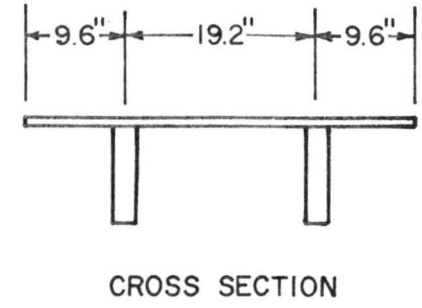

Description of specimen:

Joist: 2x8 Engelmann spruce

J01	EK-S-08-01	$E = 1.191 \times 10^6$ psi
J02	EK-S-08-09	$E = 1.151 \times 10^6$

Sheathing: 1/2" E.S. Plywood

A	EP-12-03	$E_{\perp} = 2.221 \times 10^5$ psi
B	EP-12-02	$E_{\perp} = 2.157 \times 10^5$
C	EP-12-02	

Connector: 8-d common nails spaced at 8"

Sheathing Joints: left with 1/16" gaps

Slip Modulus: k = 18,000 lb/in

Test sequence

1. Loaded at row 07 with $\Delta P = 250$ up to $P = 750$ lbs
2. Repeated 1 with $\Delta P = 100$ up to $P = 600$ lbs
3. Loaded at row 05 with $\Delta P = 100$ up to $P = 700$ lbs
4. Loaded at row 03 with loads same in 2.

Fig. E.48 Configuration and Properties of Specimen T15-8E19.2-1

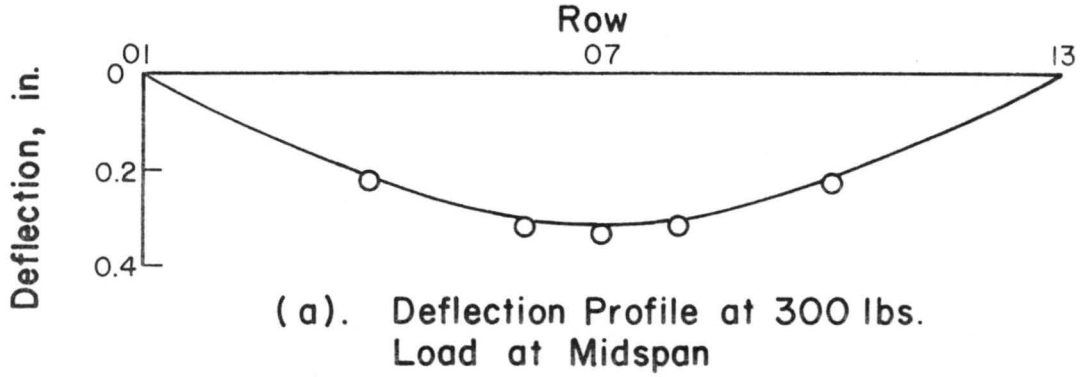

(a). Deflection Profile at 300 lbs. Load at Midspan

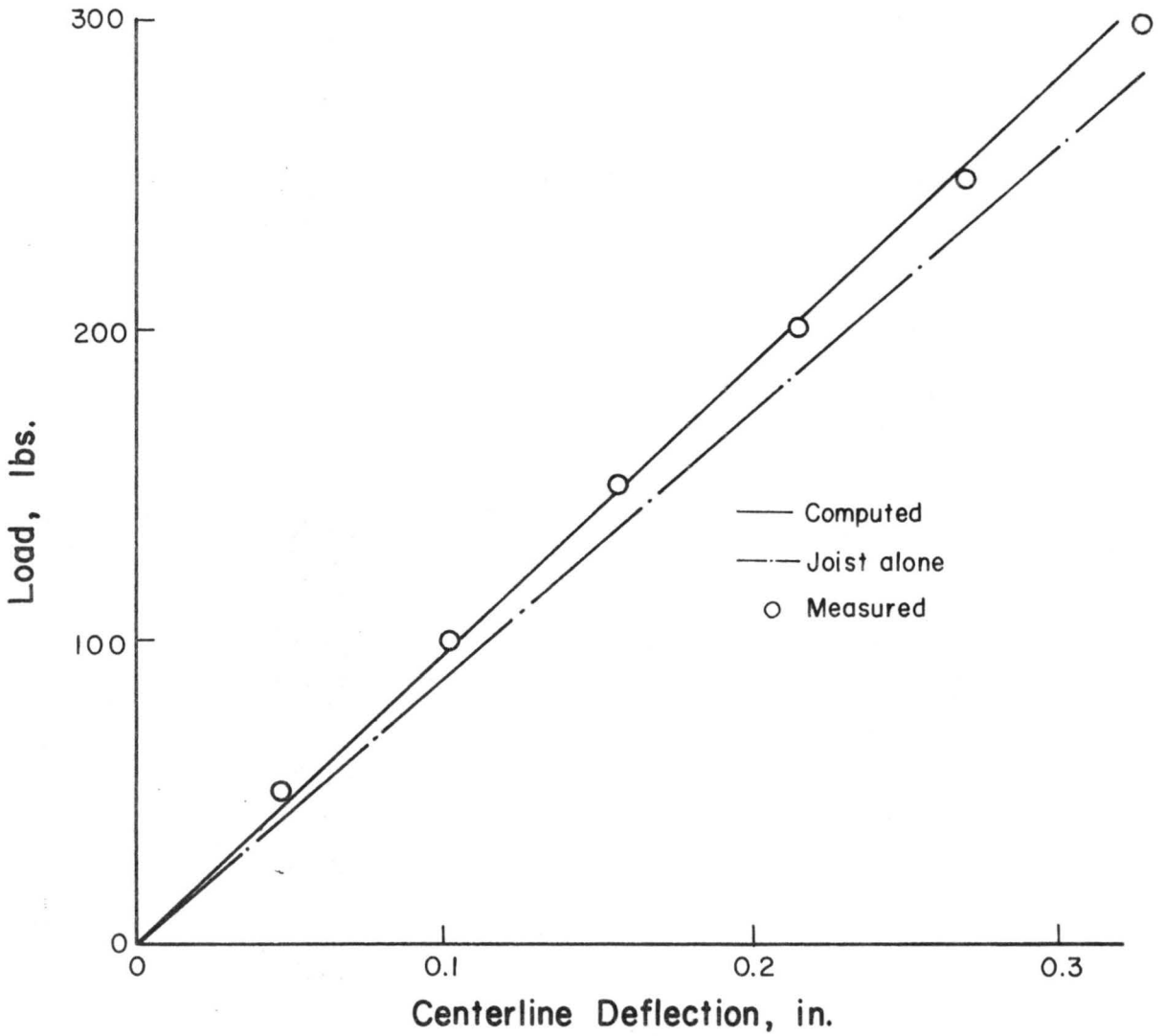

(b). Load-deflection Behavior

FIGURE E.49 BEAM VERIFICATION – T15-8E19.2-1 JOI WITH GAPS

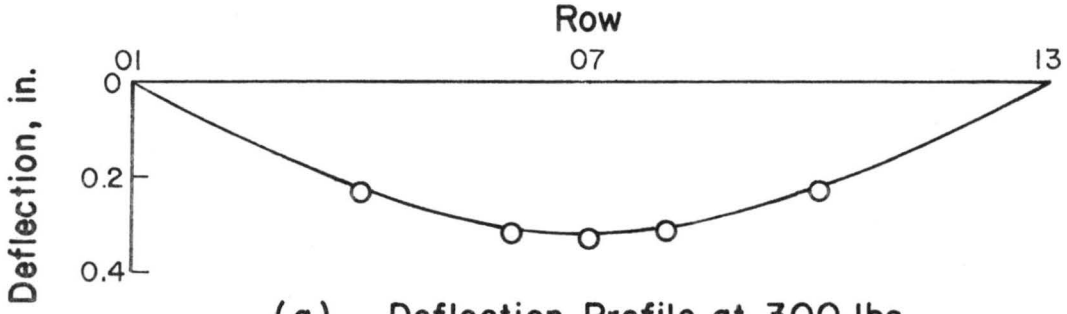

(a). Deflection Profile at 300 lbs. Load at Midspan

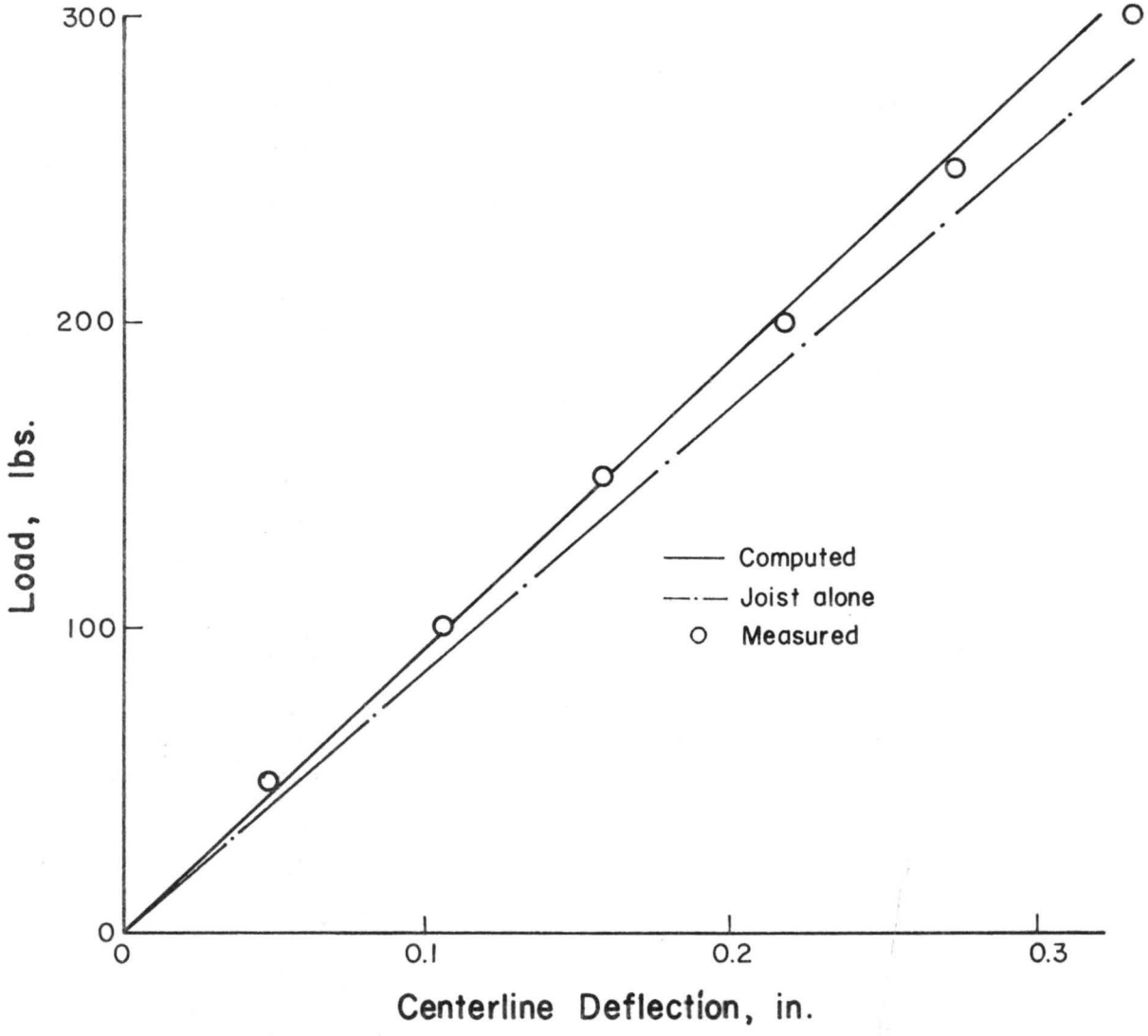

(b). Load-deflection Behavior

FIGURE E.50 BEAM VERIFICATION- T15-8E19.2-1 J02 WITH GAPS

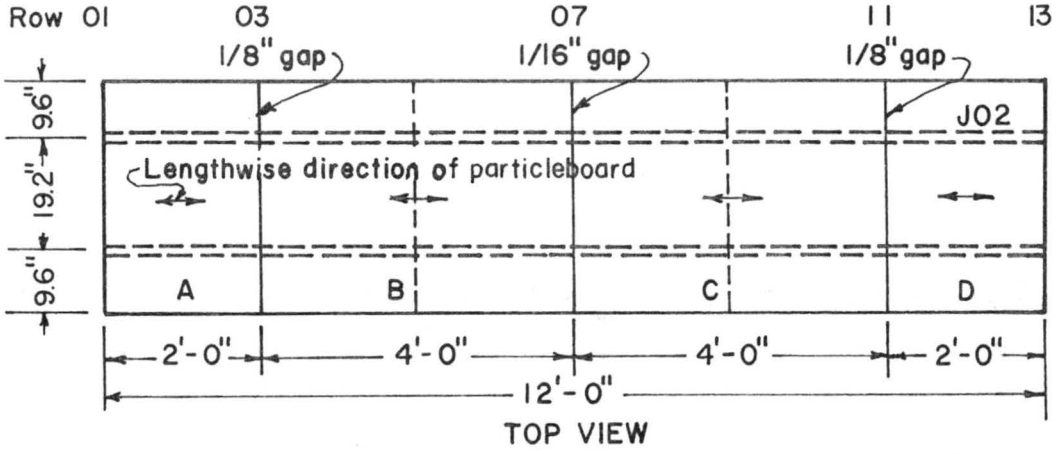

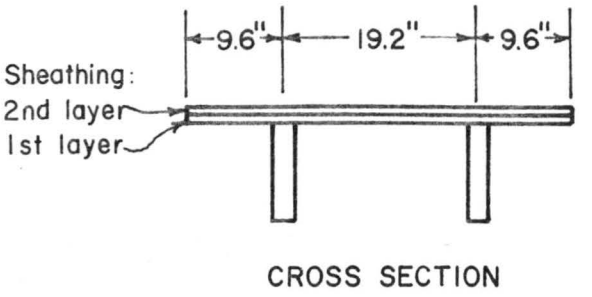

Description of specimen:

Joist: 2x8 Engelmann spruce (see T15-8E19.2-1)

Sheathing: 1st layer (see T15-8E19.2-1)
2nd layer 1/2" particleboard

A	DB-12-20	$E_{\perp} = 5.837 \times 10^5$ psi
B	DB-12-21	$E_{\perp} = 5.447 \times 10^5$
C	DB-12-21	$E_{\perp} = 5.447 \times 10^5$
D	DB-12-19	$E_{\perp} = 5.782 \times 10^5$

Connector: 1st layer (see T15-8E19.2-1)
2nd layer 6-d cement-coated nails spaced at 6"

Sheathing Joints: left with 1/16" and 1/8" gaps

Slip Modulus: k = 5000 lb/in (2nd layer)
k = 45,000 lb/in (1st layer)

Test sequence

1. Loaded at row 07 with ΔP = 100 up to P = 800 lbs
2. Loaded at row 05 with ΔP = 200 up to P = 1000 lbs
3. Loaded at row 03 with loads same in 2
4. Test to failure: loaded at row 07 with ΔP = 500. J01 failed at P = 4500 lbs.

Fig. E.51 Configuration and Properties of Specimen T15-8E19.2-2

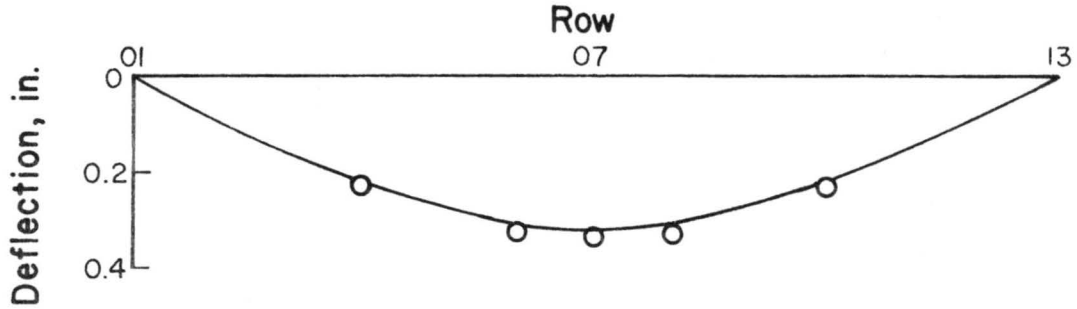

(a). Deflection Profile at 400 lbs. Load at Midspan

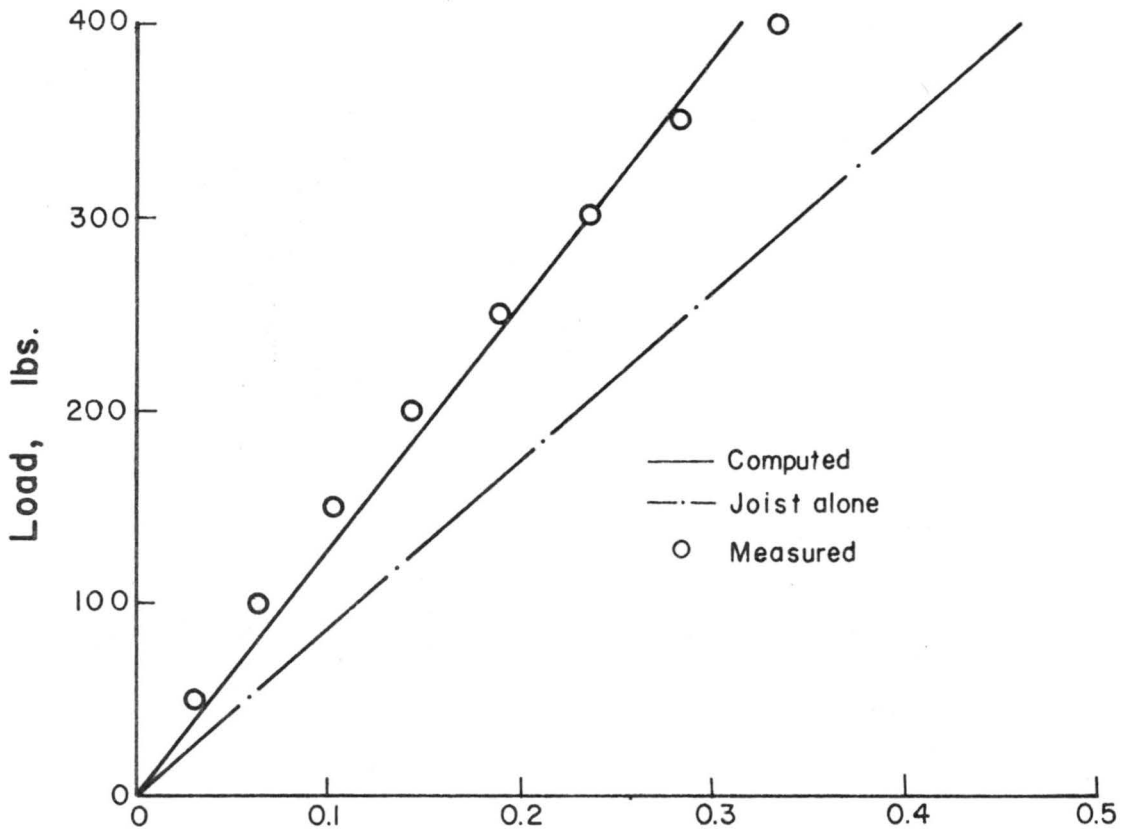

(b). Load-deflection Behavior

Figure E.52. Beam Verification - T15-8E19.2-2 J01 with Gaps

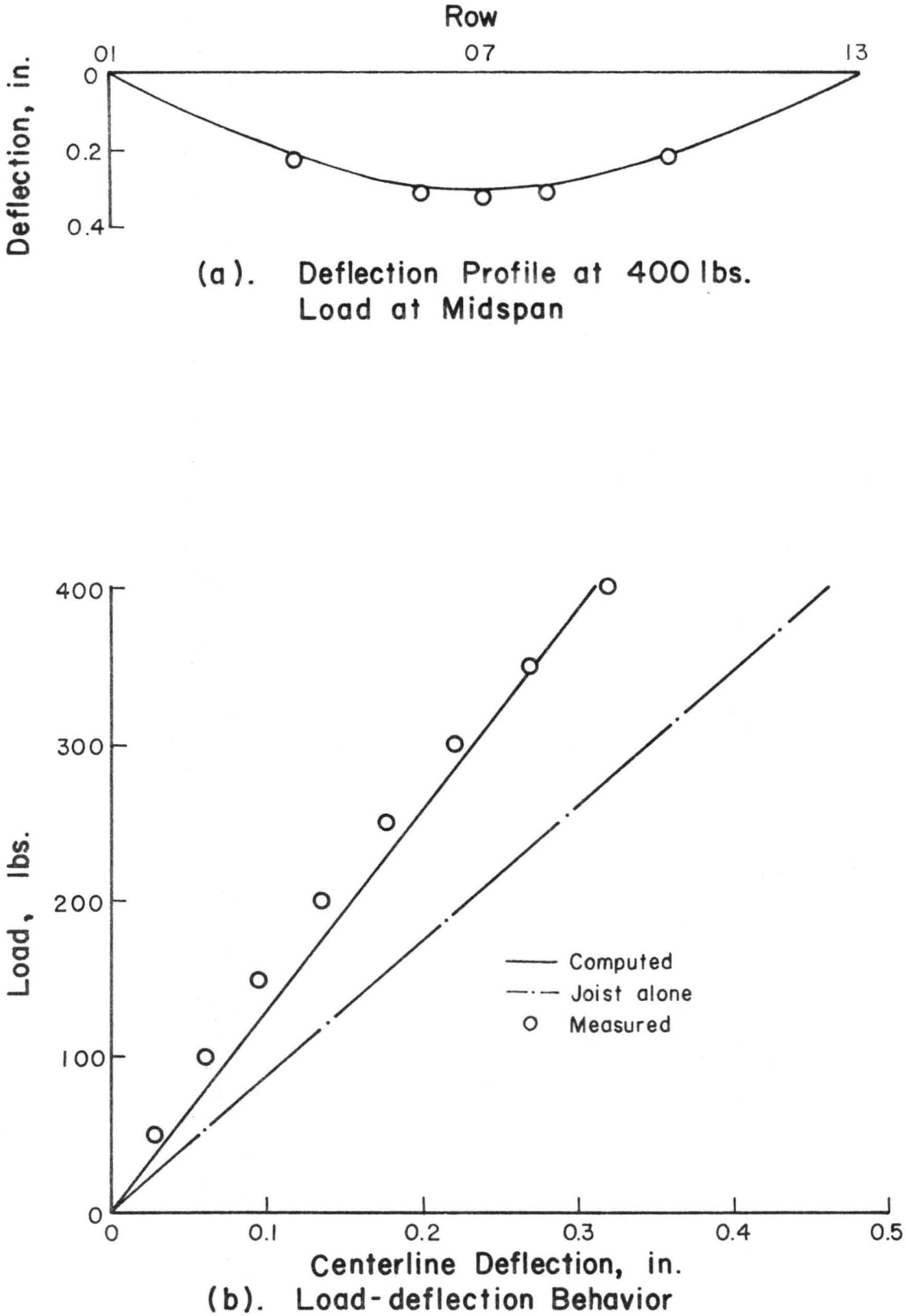

Figure E.53. Beam Verification - T15-8E19.2-2 J02 with Gaps

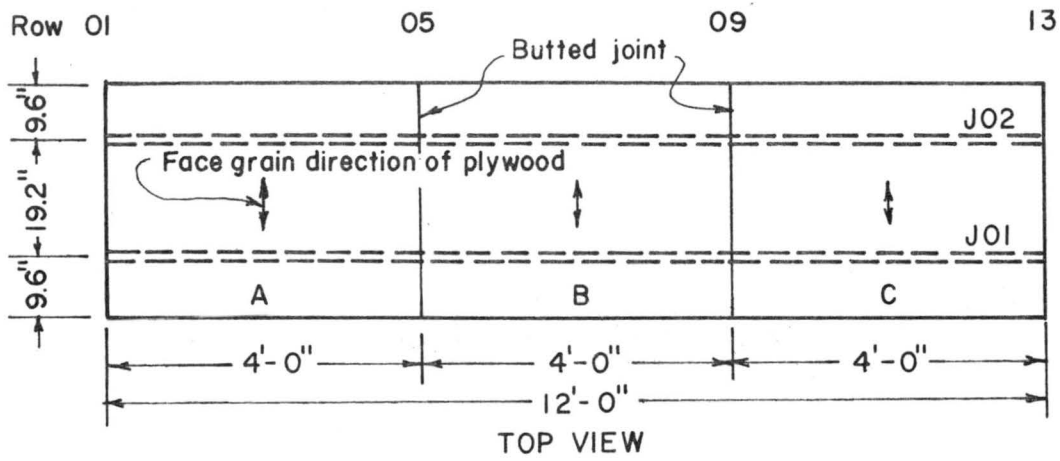

TOP VIEW

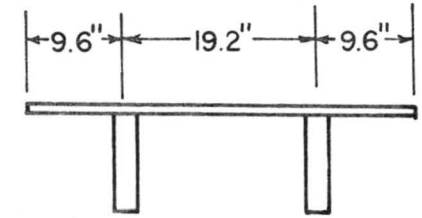

CROSS SECTION

Description of specimen:

Joist: 2x8 Engelmann spruce

J01	EC-S-08-06	$E = 1.410 \times 10^6$ psi
J02	EK-N-08-13	$E = 1.276 \times 10^6$

Sheathing: 1/2" E.S. Plywood

A	EP-12-04	$E_{\perp} = 2.287 \times 10^5$ psi
B	EP-12-04	$E_{\perp} = 2.287 \times 10^5$ psi
C	EP-12-03	$E_{\perp} = 2.157 \times 10^5$ psi

Connector: 8-d common nails spaced at 8"

Sheathing Joints: tightly butted

Slip Modulus: k = 18,000 lb/in

Test sequence

1. Loaded at row 07 with $\Delta P = 200$ up to P = 800 lbs
2. Loaded at row 05 with loads same in 1
3. Loaded at row 03 with loads same in 1.

Fig. E.54 Configuration and Properties of Specimen T16-8E19.2-1

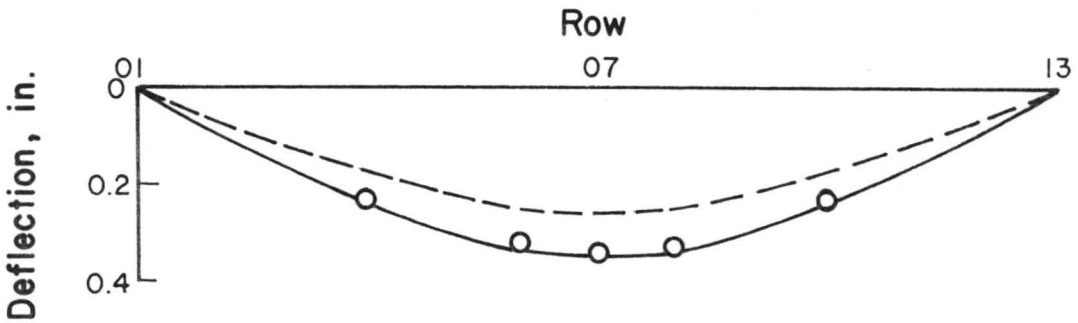

(a). Deflection Profile at 400 lbs. Load at Midspan

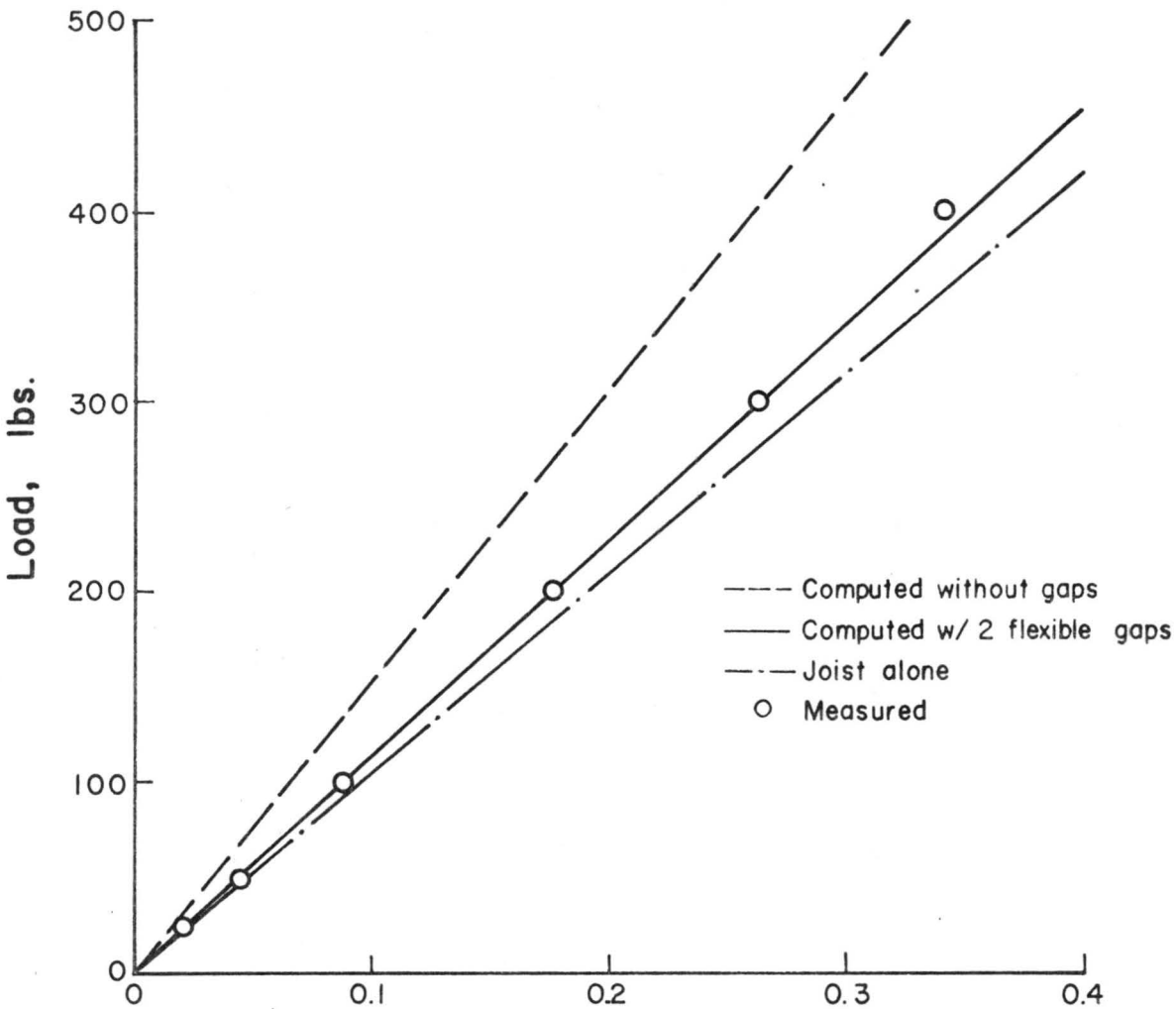

(b). Load-deflection Behavior

Figure E.55. Beam Verification - T16-8E19.2-1
JO1 with Butted Joints

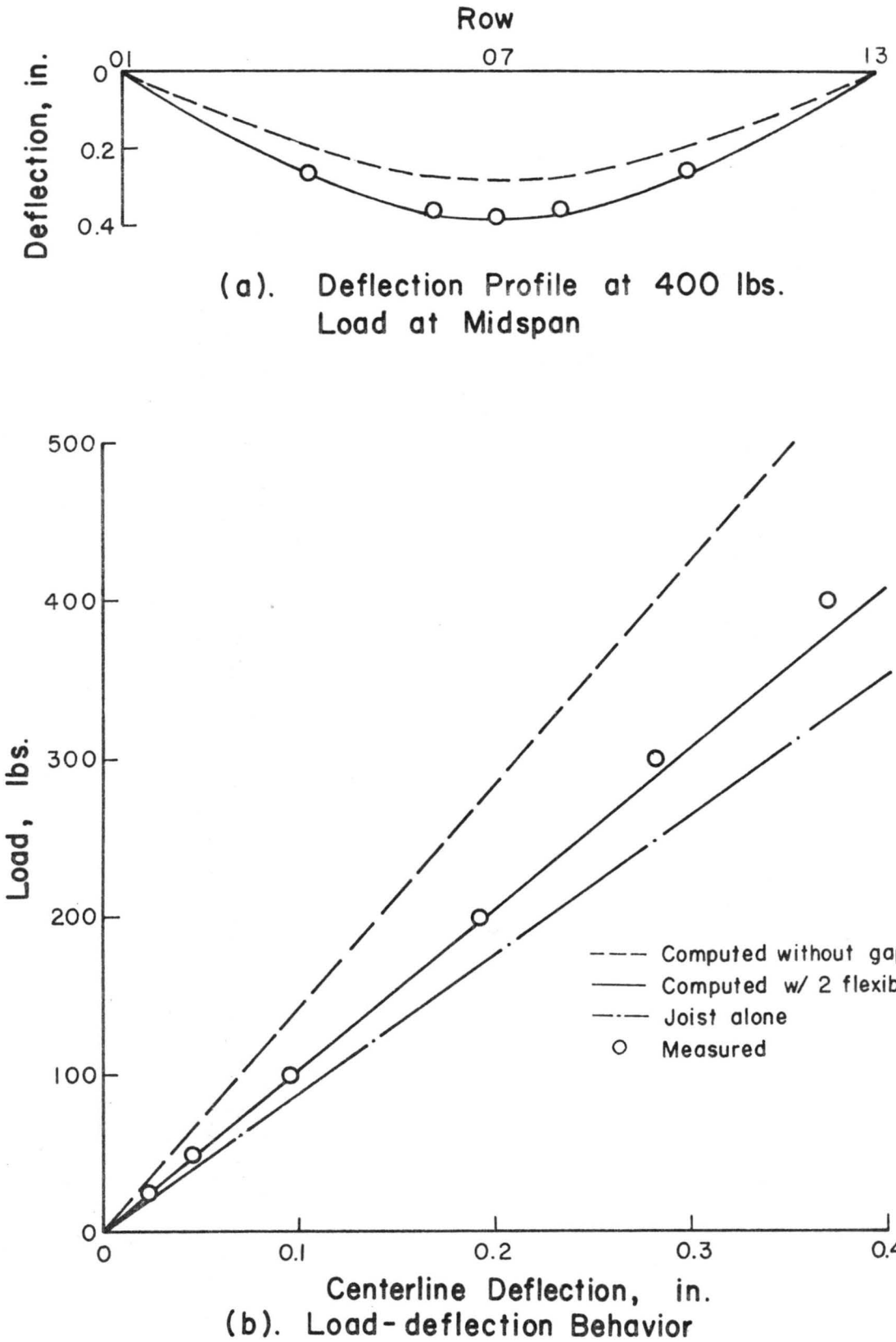

Figure E.56. Beam Verification - T16-8E19.2-1
J02 with Butted Joints

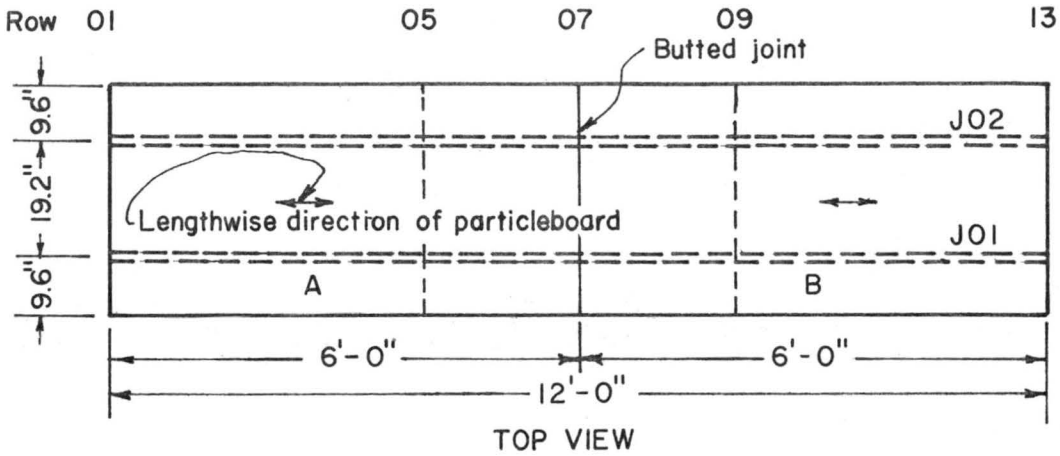

TOP VIEW

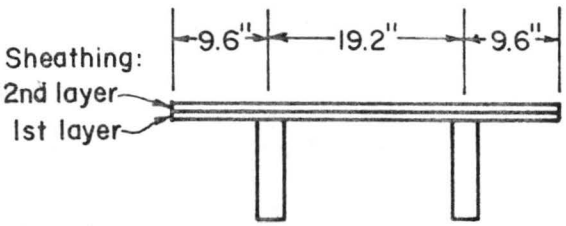

CROSS SECTION

Description of specimen:

Joist: 2x8 E.S. (see T16-8E19.2-1)

Sheathing: 1st layer (see T16-8E19.2-1)
2nd layer 1/2" particleboard

A	DB-12-10	$E_{\perp} = 4.869 \times 10^5$ psi
B	DB-12-07	$E_{\perp} = 4.486 \times 10^5$

Connector: 1st layer (see T16-8E19.2-1)
2nd layer 6-d common nails
spaced at 8", 2 rows per joist
(Nails not driven into joist)

Sheathing Joint: tightly butted

Slip Modulus: k = 3500 lb/in (2nd layer)
k = 18,000 lb/in (1st layer)

Test sequence

1. Loaded at row 07 with $\Delta P = 200$ up to $P = 1000$ lbs
2. Loaded at row 05 with loads same in 1
3. Loaded at row 03 with loads same in 1
4. Test to failure: loaded at row 07 with $\Delta P = 500$, J02 failed at $P = 3400$ lbs.

Fig. E.57 Configuration and Properties of Specimen T16-8E19.2-2

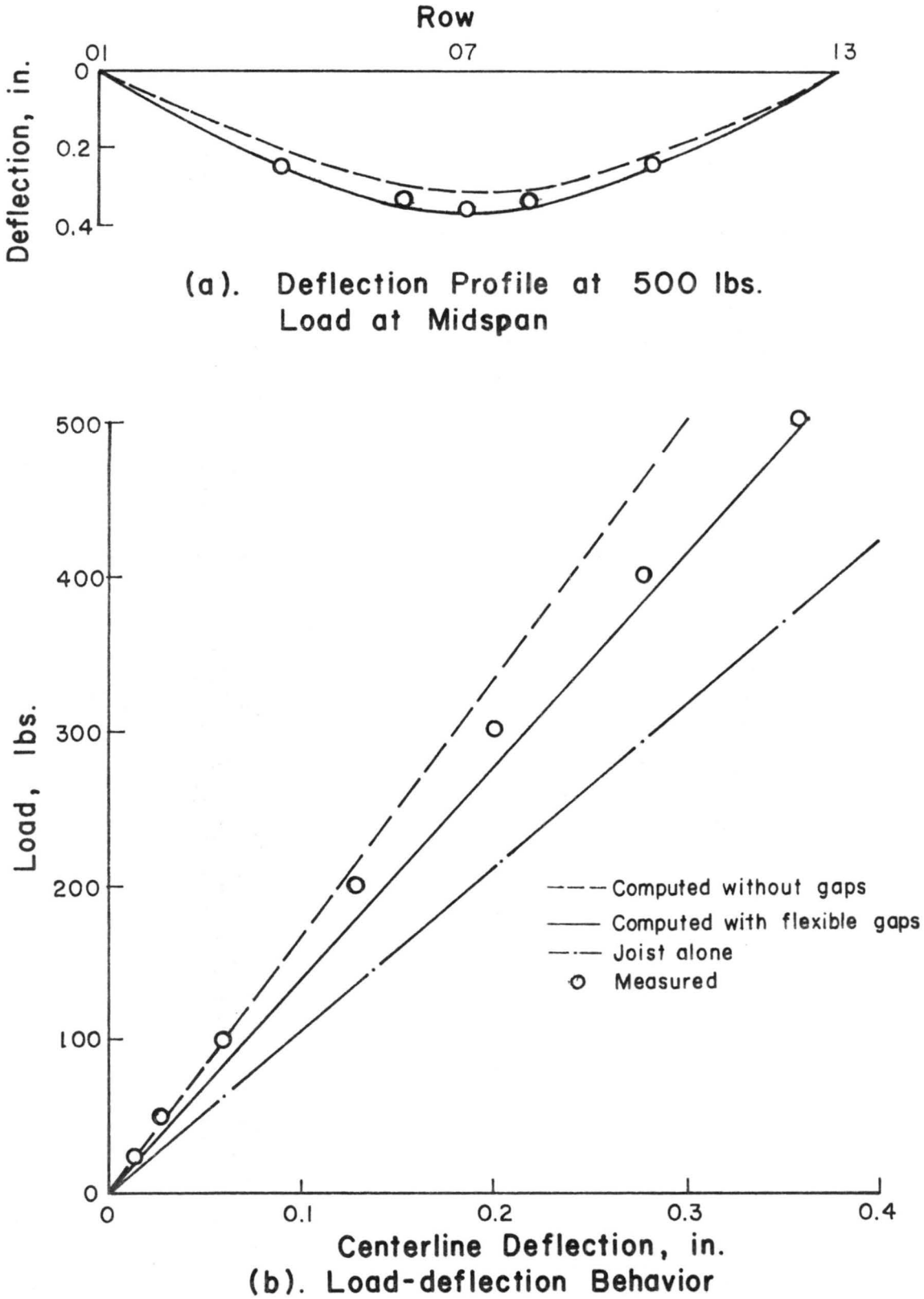

Figure E.58. Beam Verification - T16-8E19.2-2 JO1 with Butted Joints

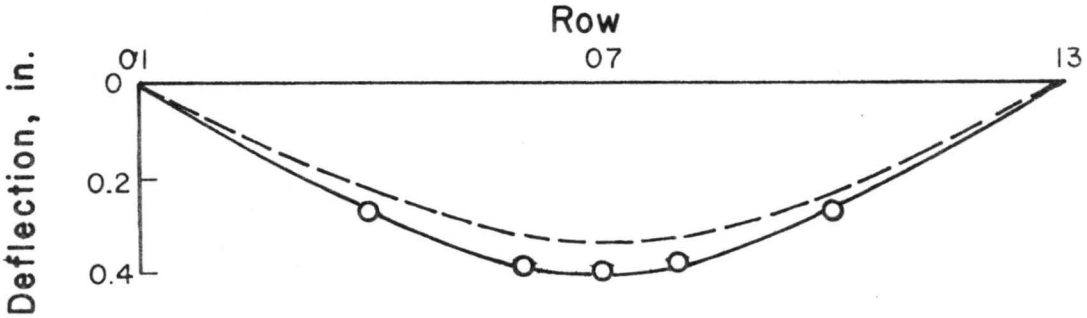

(a). Deflection Profile at 500 lbs. Load at Midspan

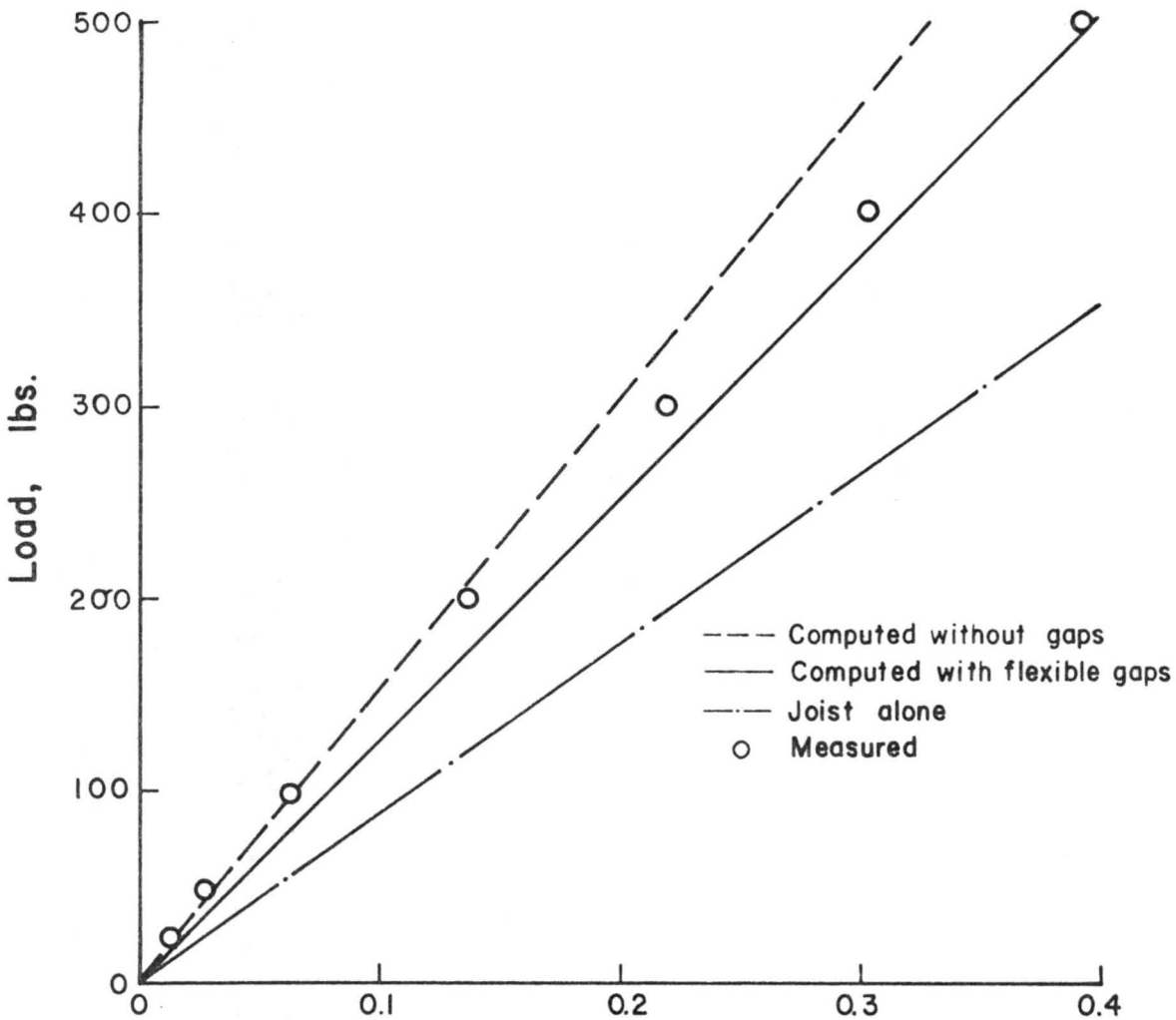

(b). Load-deflection Behavior

Figure E.59 Beam Verification-T16-8E19.2-2 J02 with Butted Joints

APPENDIX F

FORMULATION OF THE FINITE ELEMENT SOLUTION TECHNIQUE

APPENDIX F FORMULATION OF THE FINITE ELEMENT SOLUTION TECHNIQUE

To formulate the finite element solution technique for the mathematical model, the beam is divided into a series of one dimensional elements as shown in Fig. F.1. For each element of the beam, the deflection y_i and the axial displacement u_i are approximated by polynomials in x. Piecewise linear approximating functions are used for the axial deformation and a cubic approximating function is used for deflection.

The potential energy for any element, considering the contributions from external load, bending, axial deformations, and interlayer slip, is approximated in terms of the nodal point values for y, dy/dx, and u. The variation of the potential energy for a single element can be placed in the following form, where J_i represents the sum of all the potential energy terms for the i^{th} element:

$$\delta J_i = \{\delta s\}_i^T [k] \{s\}_i - \{\delta s\}_i^T \{f\}_i \qquad (F.1)$$

where $\{s\}_i$ = matrix combining all the generalized displacements for y, dy/dx, u,

$\{k\}_i$ = stiffness matrix for element i, and

$\{f\}_i$ = matrix combining all generalized external force corresponding to s .

By direct summation of element matrices, the total variation of potential energy leads to the general equilibrium equation

$$[K] \{S\} = \{F\} \qquad (F.2)$$

where $[k]$, $\{S\}$, and $\{F\}$ are the system equivalent of $[k]_i$, $\{s\}_i$ and $\{f\}_i$.

The nodal point deflection y_i, slope dy/dx, and axial displacement u_i are obtained by solving Eq. (F.2) for S .

The flow diagram contained in Fig. F.2 depicts the computational procedure utilized by a computer program written by Thompson (27) using this finite element method based on the mathematical model to compute the nodal point deflection. A CDC 6400 65 core computer system and peripheral equipment provided the necessary computational capacity.

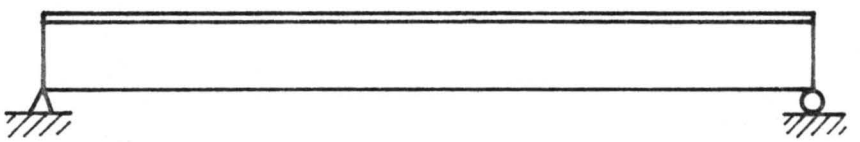

T-beam Configuration

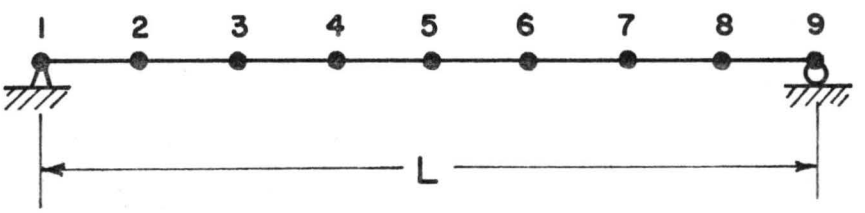

Node Point Division

FIGURE F.1 FINITE ELEMENT REPRESENTATIONS

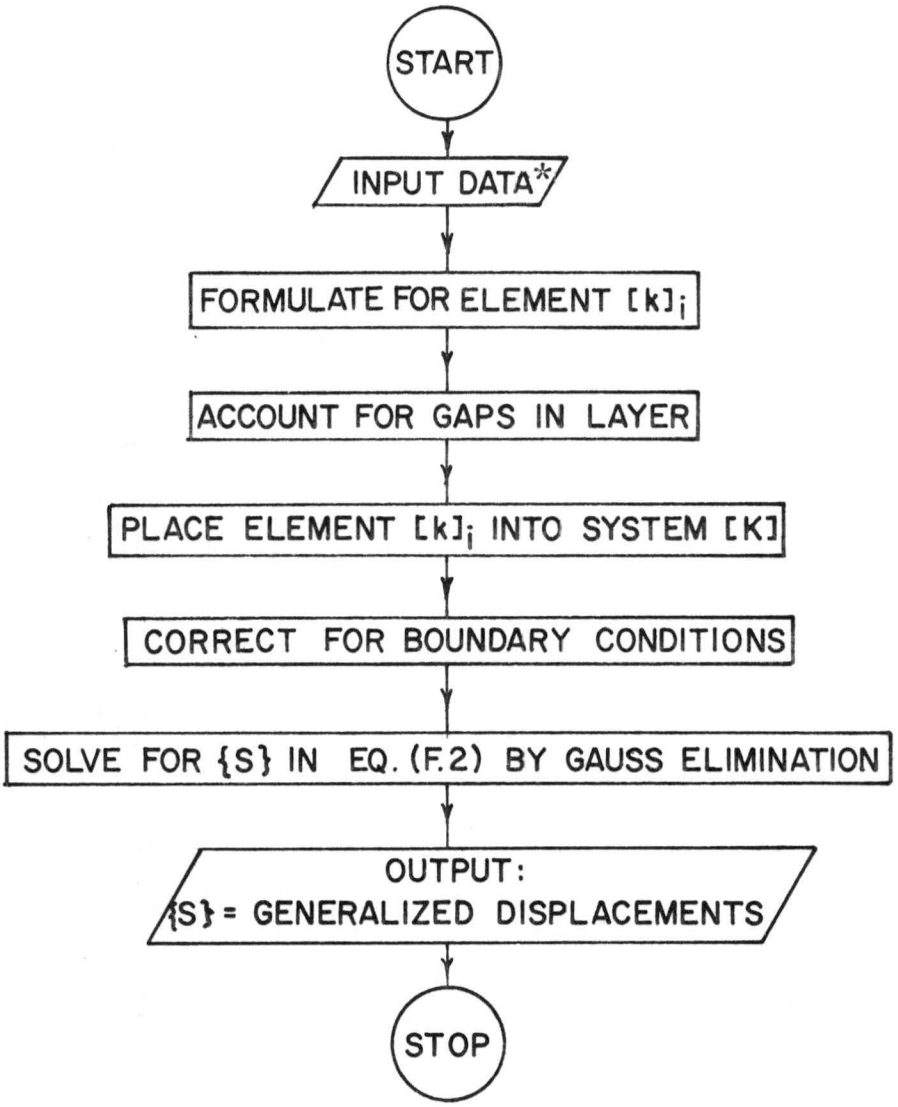

* Input data includes number of elements, layers, and gaps; modulus of elasticity values in bending and axial loading for each layer; dimensions of each layer and nodal point coordinates; connector slip modulus, spacing, and number of rows; load level and location.

FIGURE F.2 FLOW DIAGRAM

APPENDIX G

CONVERSION FACTOR FOR PLYWOOD MODULUS OF ELASTICITY

APPENDIX G CONVERSION FACTOR FOR PLYWOOD MODULUS OF ELASTICITY

Because of the orthotropic nature of wood and the orthogonal orientation of the adjacent plies of the plywood, the mechanical properties in the two principal directions are different. A transformed cross section must be used to determine the area and moment of inertia of the plywood in each direction. A parameter, k*, which converted the gross modulus of elasticity values valid for bending to gross modulus of elasticity values valid for axial load can be determined. The computation of k* is presented below, along with the k* values for various plywood species and thicknesses are listed in Table G.1.

$$\therefore \quad (E_{gr})_b I_{gr} = (E_t)_b I_{tr}$$

$$(E_{gr})_b = \frac{(E_t)_b I_{tr}}{I_{gr}}$$

$$(E_t)_b = \frac{(E_{gr})_b I_{gr}}{I_{tr}}$$

and

$$(k^*(E_{gr})_b)A_{gr} = \frac{(E_{gr})_b I_{gr}}{I_{tr}} A_{tr} = (e_{gr})_a A_{gr}$$

$$\therefore \quad k^* = \frac{I_{gr} A_{tr}}{I_{tr} A_{gr}}$$

where

$(E_{gr})_a$ = MOE for axial load based on gross dimension of the material,

$(E_{gr})_b$ = MOE for bending based on gross dimension of the material,

I_{gr} = the moment of inertia of the material based on gross dimension,

A_{gr} = gross cross section of the material,

E_t = true MOE of the material based on the transformed section,

I_{tr} = moment of inertia based on the transformed section,

A_{tr} = transformed cross section area.

It is to be noted that the transformed cross section is based on the veneer in which the grain direction is subjected to bending.

Table G.1 Conversion Factor for Plywood

Plywood Species	Nominal Thickness in	Face grain Direction	A_{tr} in^2	A_{gr} in^2	I_{tr} in^4	I_{gr} in^4	k*
Douglas fir	1/2	⊥	3.060	6.0	0.0183	0.125	3.4836
	1/2	∥	3.060	6.0	0.1072	0.125	0.5947
	3/4	⊥	4.563	9.0	0.1301	0.422	1.6445
	3/4	∥	4.435	9.0	0.2682	0.422	0.7754
Engelmann	1/2	⊥	2.641	6.0	0.0120	0.125	4.585
Spruce	1/2	∥	2.641	6.0	0.0781	0.125	0.7045
	3/4	⊥	2.728	9.0	0.0794	0.422	1.6110
	3/4	∥	3.998	9.0	0.2105	0.422	0.8906

⊥ = face grain perpendicular to direction of bending
∥ = face grain parallel to direction of bending

APPENDIX H

DATA FROM T-BEAM WITH MANUFACTURED JOISTS

APPENDIX H

DATA FROM T-BEAM WITH MANUFACTURED JOISTS

Table H.1. Properties of Manufactured Specimens

Specimen No.	Span length in	Joist Properties			Flange Properties**				Connector Properties		
		h in.	b[1] in.	E_{gr}[2] psi	t in.	b in.	E_{gr} psi	k*	Type	Estimated k lb/in.	Spacing of Nails
1	284	20	.936	1.448×10^6	.594	12	400,000	1.054	Nailed (8-d)	21600	12"
2	284	20	.936	1.575×10^6	.594	12	400,000	1.054	Glue-Nailed	35000	12
3	284	20	.936	1.511×10^6	.594	12	400,000	1.054	Glue-Nailed	35000	12
4	284	20	.936	1.623×10^6	.594	12	400,000	1.054	Glue-Nailed	35000	12
5	188	10	1.513	1.509×10^6	.594	12	400,000	1.054	Nailed (8-d)	26300	12
6	188	10	1.513	1.358×10^6	.594	12	400,000	1.054	Glue-Nailed	35000	12
7	188	10	1.513	1.509×10^6	.594	12	400,000	1.054	Glue-Nailed	35000	12
8	188	10	1.513	1.571×10^6	.594	12	400,000	1.054	Glue-Nailed	35000	12
9	92	10	1.513	$.916 \times 10^6$	.594	12	400,000	1.054	Glue-Nailed	35000	12
10	92	10	1.513	$.816 \times 10^6$	.594	12	400,000	1.054	Glue-Nailed	35000	12

Notes: 1. b calculated to make equivalent transformed I correct for h given.
2. Calculated from P-Δ plots provided for loading of joist assembly only.

**Properties based on three tests of plywood flange material, values assumed similar for all specimens.

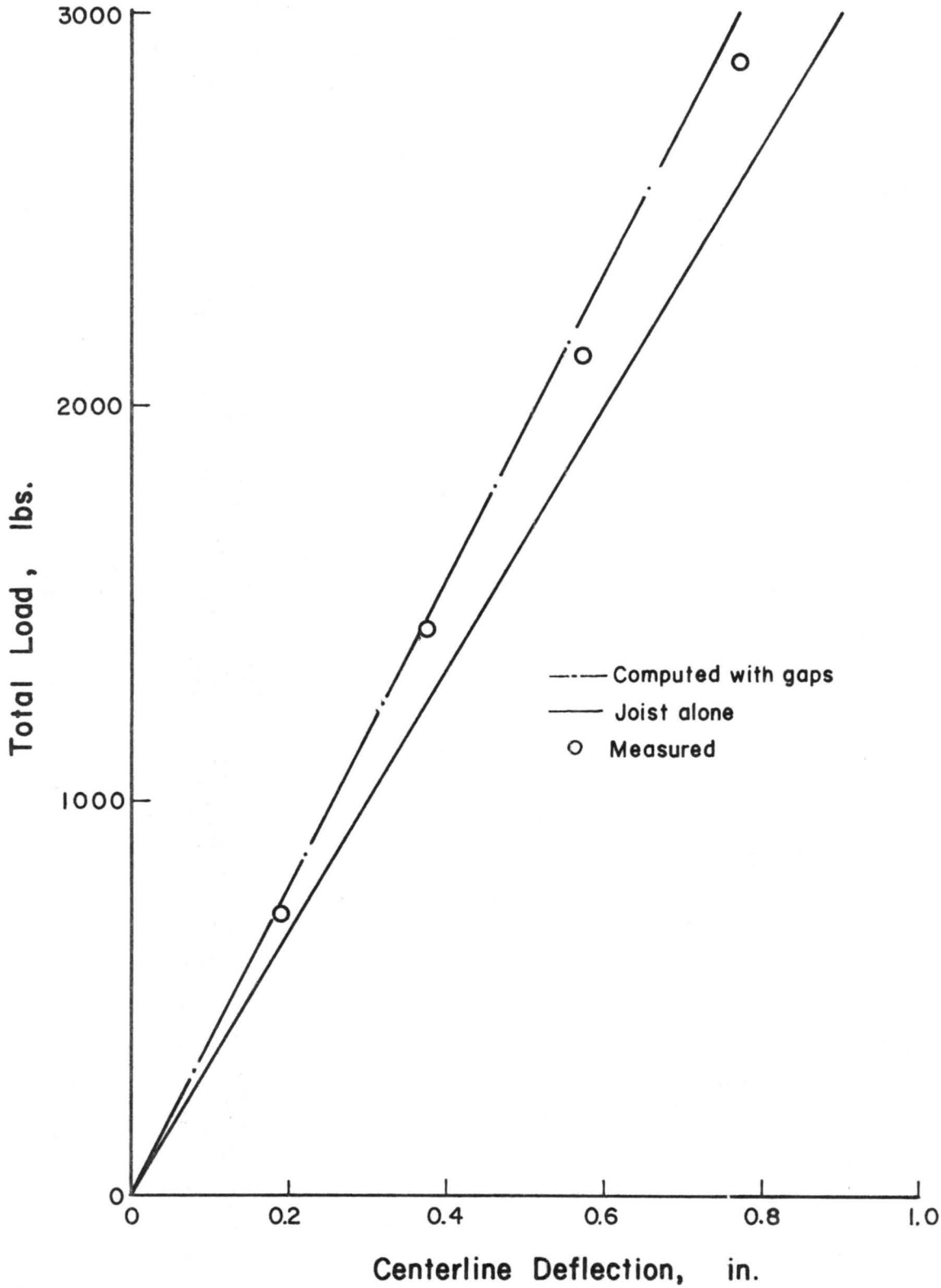

Figure H.1. Beam Verification - Manufactured Joist No. 2 (glue-nailed specimen).

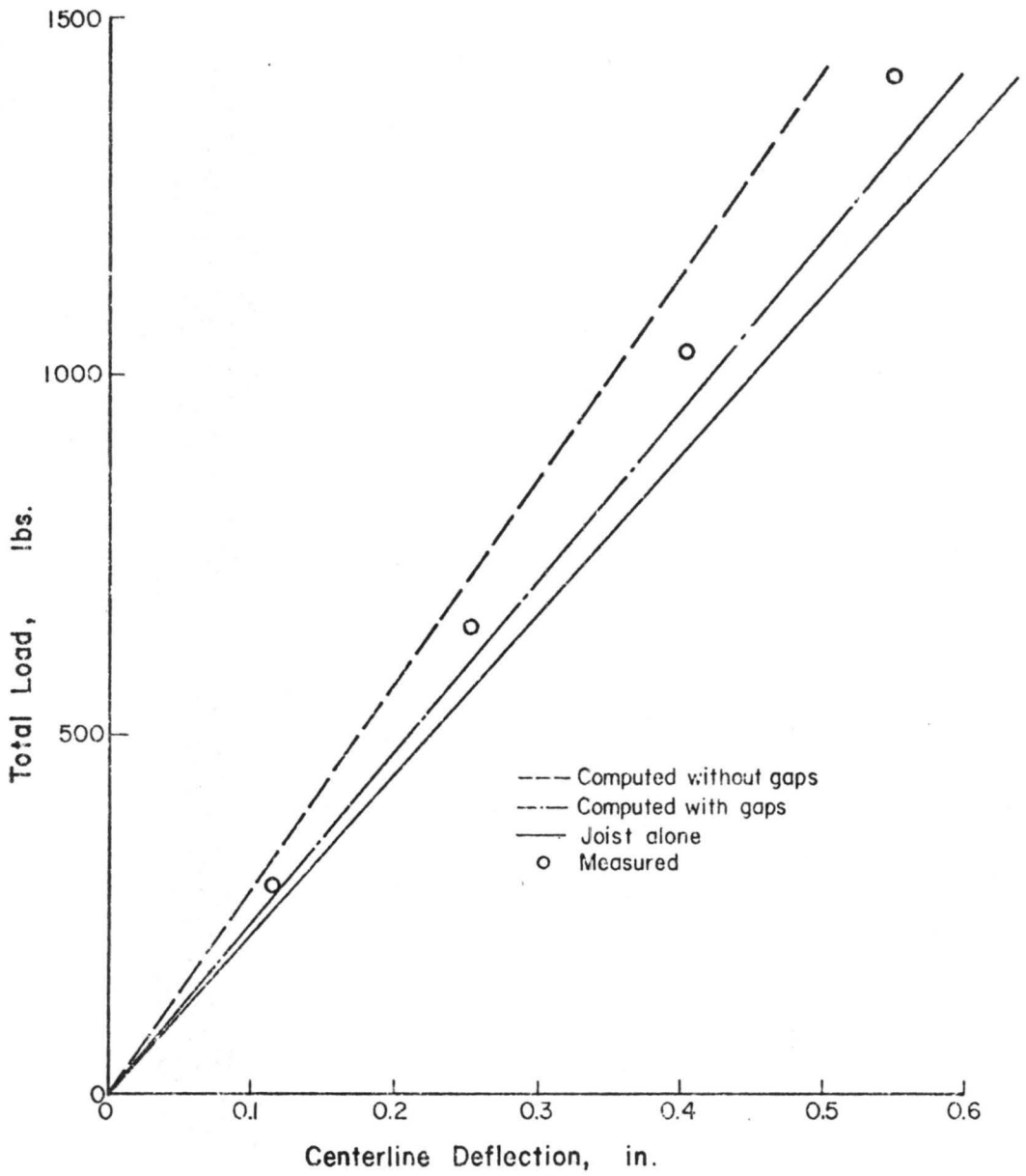

FIGURE H.2 BEAM VERIFICATION – MANUFACTURED JOIST NO. 5 (NAILED SPECIMEN)

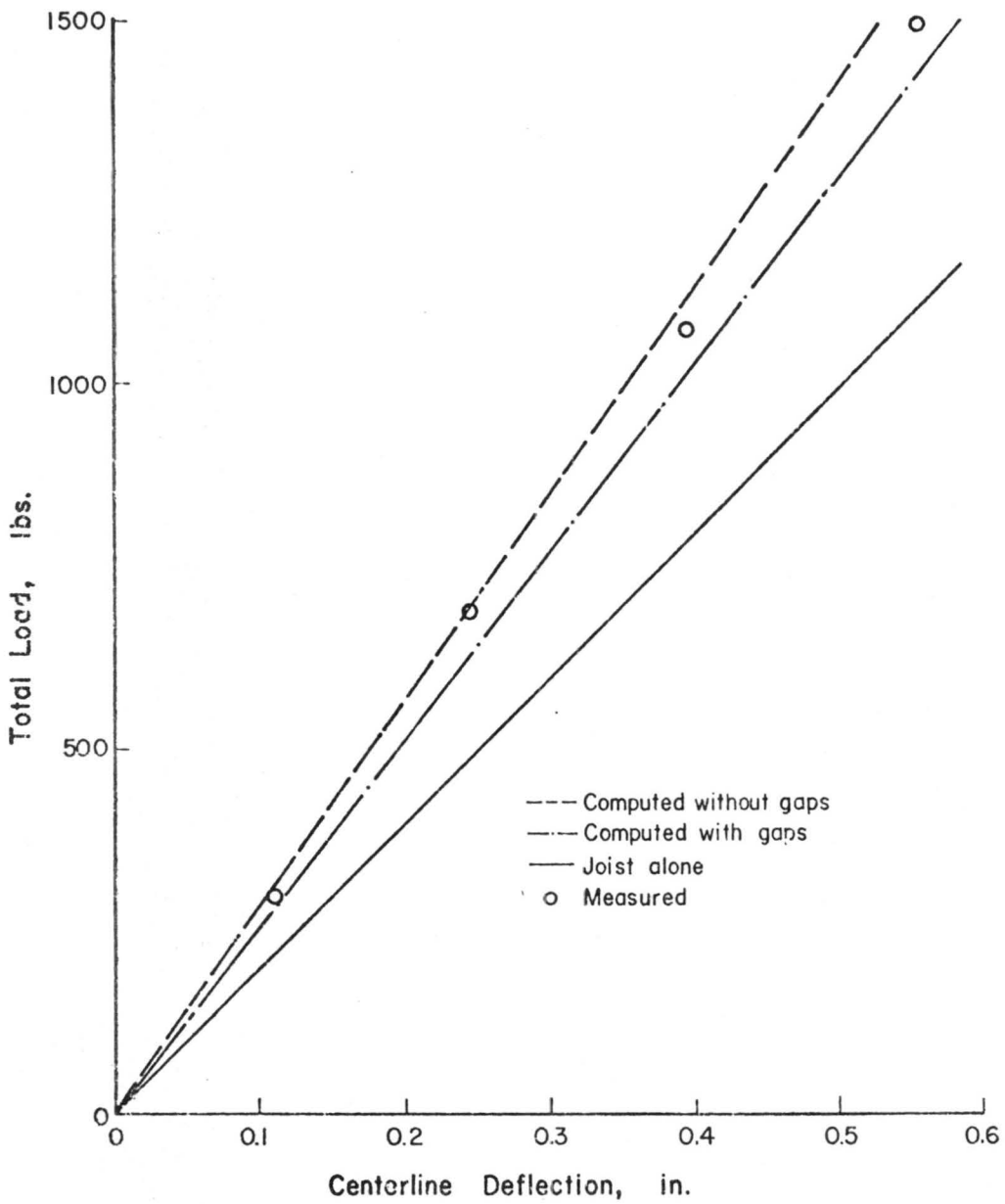

FIGURE H.3 BEAM VERIFICATION - MANUFACTURED JOIST NO. 6 (GLUE-NAILED SPECIMEN)

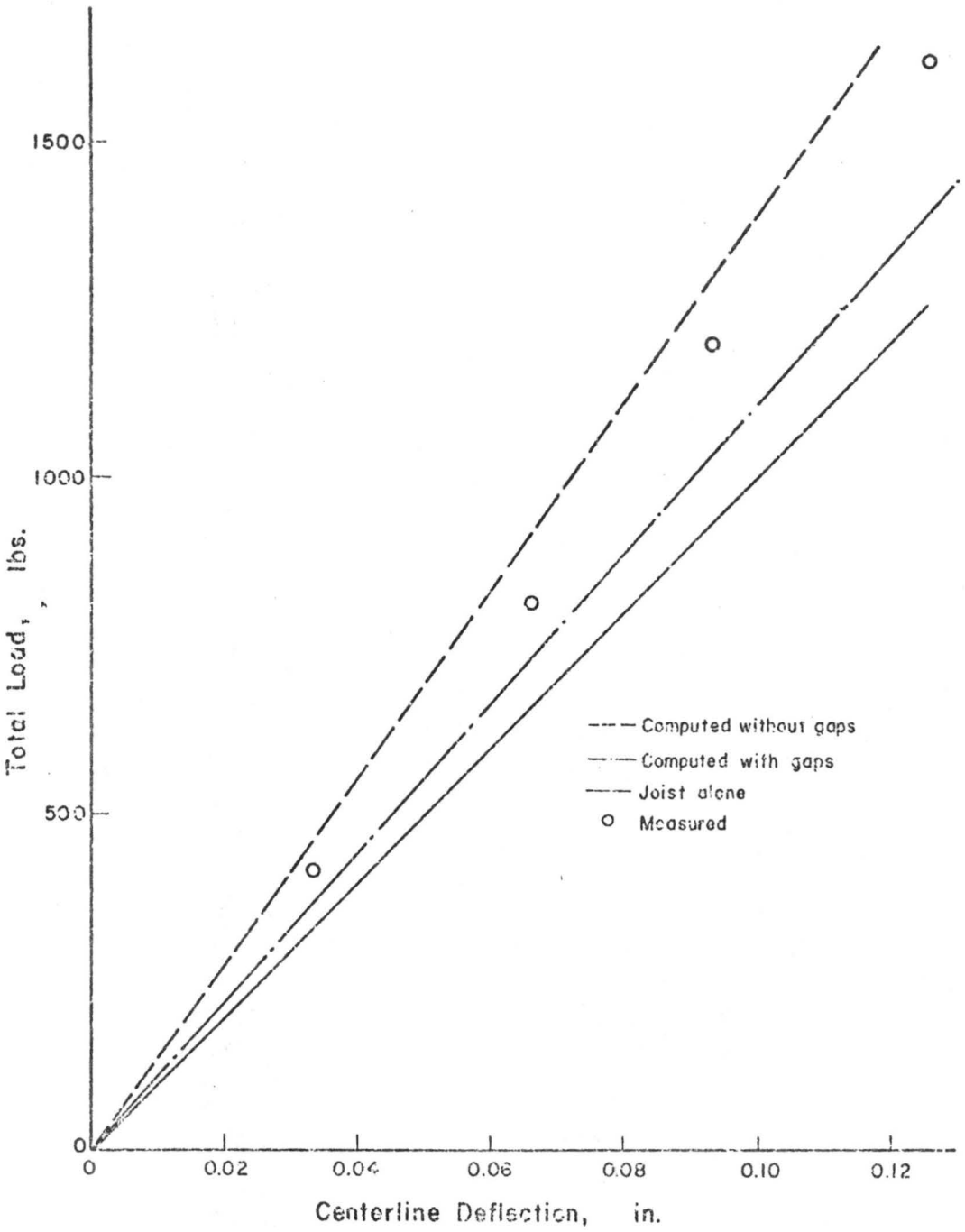

FIGURE H.4 BEAM VERIFICATION - MANUFACTURED JOIST NO. 10 (GLUE-NAILED SPECIMEN)